

**IDENTIFICATION OF REGULATORY PATHWAYS  
CONTROLLING HISTONE H3.3 DEPOSITION IN THE  
CENTRAL NERVOUS SYSTEM (CNS)**

LIANG, QINGYI

This dissertation is submitted to University College London for the  
examination of Doctor of Philosophy

University College London, 2019

## **DECLARATION**

I, Qingyi Liang, confirm that the work presented in this thesis is my own. Information derived from other sources and any collaborative contributions have been clearly indicated and acknowledged in the thesis.

## **ACKNOWLEDGEMENTS**

I am grateful for Professor Paolo Salomoni for having me as his PhD student, and giving me the opportunity to work on this project. I thank him for believing in me, his guidance and mentoring of me throughout my research period and thesis writing. I am exceptionally grateful for him bringing me to his laboratory in Germany in the third year of my study, so that I could continue working on my project. His continuous supervision, support and advice throughout my time in his laboratory has helped me to become a more confident and independent scientist.

I would like to thank my University for having me as one of the research students on campus, and I am honoured to be part of this large and brilliant community for the past five years. I would like to express my gratitude to my graduate tutors, Dr Julie Olszewski and Dr Adam Paige, for their continuous support during my PhD study at the UCL Cancer Institute. A special thank you to Dr Paige for his support during my final year of thesis writing. I am also grateful for Professor Alasdair Gibb without whom I would not have initiated my postdoctoral studies at UCL.

I would like to thank Professor Antonella Riccio, my secondary supervisor, and Dr Pablo Rodriguez-Viciano for their valuable advice and feedback on my upgrade viva.

I greatly appreciate our collaborators for all their help on the project. Many thanks to Dr Marco Gaspari and his group at University of Catanzaro in Italy for sharing their valuable knowledge on Mass Spectrometry (MS), and all their help on MS analysis for the potential Daxx-interacting partners. I am deeply thankful to Dr David Michod for letting me use his laboratory and work with his PhD student Stefanie Meier on the visualisation assay project. Many thanks to Professor Richard Jenner and Dr Lenka Skalska for their support on the iCLIP experiments. I would also like to thank Dr Steen Ooi and Dr Nancy Stathopoulou for their kind suggestions and support on improving the immunoprecipitation protocol. A special thanks to Dr Philip Denner and Dr Dominik Stappert from the LAT at DZNE for their support on the high content screening set-up. Thank you, Dr Stappert, for your patience on my endless questions on operating the robotised automation platform.

I am deeply thankful to all the past members from Samantha Dickson Brain Cancer Unit. Even though we are not working together anymore, I cherish the memories of the group colleagues that I worked with in the laboratory. I would like to thank Dr Aikaterini Lampada, who showed me how hard PhD students should work to obtain good outcomes. Thank you for teaching me all the tricks to perform a good immunoblotting, while casually drinking double espressos from the M&M green mug. I would like to thank Dr Julia Hofmann for all her help during my PhD project, especially during my stay in the German laboratory. I would always remember how you fast-type emails using only one finger. Special thanks to Dr Deli A, for being a fun lab-mate and my desk-neighbour for two years. The dark chocolates you brought always lit up my day. I would like to express my gratitude to all the post-doctorates in the lab, Dr Ketty Kessler, Dr Valeria Amodeo, Dr Manav Pathania, Dr Sara Bianco, for all their patient guidance and support during my PhD. I thank Nicola Maestro for his kind help and support and the enjoyable memories. I would like to thank Dr Susanne Scheipl, Dr Lucia Cottone, Dr Ana Paula Leite, Aditya Shroff, Teresa Sposito and Natalia Izotova for the time we spent together and the fun moments we created. Finally, I would like to thank my colleagues from the group at DZNE, Germany, Dr Pirasteh Pahlavan, Dr Jenny Russ, Dr Simona Maida, and Manon Chevallot for spending a short but joyful period together.

I am grateful for having the love and support of my family: mum, dad, grandma, grandpa, aunt Wendi, uncle Jinghua, cousin Tengyu, cousin Qian, and all other members. Thank you all for believing in me and continuously supporting my study and dreams. Thank you, mum, for always being on my side and praying for me so far away from the other side of the earth. Last but by no means least, I would like to thank James, my fiancé, for your unreserved love, understanding and support throughout my smooth and difficult times. Thank you for always being there for me, with your heart and your presence.

Thank you all for your support throughout my study. I would not have been possible to become the person I am now without any of you being there for me.

***To my beloved parents and fiancé***

## HIGHLIGHTS

- A platform for imaging histone 3.3 (H3.3) *de novo* loading in differentiated Neuro2a neuroblastoma cells was developed, which is suitable for testing candidate modulators of H3.3 loading in cells as well as for high-content screens. This has implications for identifying novel modulators of H3.3 loading in the context of brain pathological states and ageing.
- A co-immunoprecipitation (co-IP) protocol for identifying interacting partners of the histone chaperone Daxx (death domain–associated protein 6) was developed in mouse cortical neural progenitor cells.
- Nr2c2 (nuclear receptor subfamily 2 group C member 2; Tr4, testicular orphan nuclear receptor 4) and Cpsf2 (cleavage and polyadenylation specificity factor 2) were identified as novel Daxx interaction partners, linking Daxx to transcription and polyadenylation regulation.

## ABSTRACT

Studies have implicated the importance of the histone H3 variant H3.3 in chromatin remodelling and transcriptional regulation in the central nervous system (CNS). Gain-of-function mutations affecting H3.3 and its loading machinery have been recently identified in glioblastoma multiforme (GBM) and other tumours. Moreover, H3.3 accumulates on chromatin during ageing and plays significant roles in ageing-related signalling pathways, as recently demonstrated in the context of *Caenorhabditis elegans*. Given H3.3 involvement in human neoplasia and ageing, there is a need to better understand how H3.3 loading is regulated in cells and how pharmacological intervention could be used to either augment or suppress its incorporation.

Loss-of-function mutations of H3.3 chaperone DAXX (death domain-associated protein 6) lead to chromatin instability and alternative lengthening of telomeres (ALT), correlating with a variety of cancers including GBM and pancreatic neuroendocrine tumours (pNETs). Studying DAXX interactome would improve our knowledge on its novel cellular functions involved in normal biological processes as well as tumorigenesis.

During my PhD project, I developed an H3.3 visualisation platform based on Halo-Tag technology in Neuro2a cells (a neuroblastoma cell line). The Halo-Tag visualisation assay was developed via leading-edge robotised automation, rendering it suitable for high-content/drug screening. I also established a FLAG-Daxx affinity purification system in mouse neural progenitor cells (NPCs). Mass spectrometry of FLAG-Daxx affinity purification revealed two novel Daxx-interacting partners, Nr2c2 (nuclear receptor subfamily 2 group C member 2; Tr4, testicular orphan nuclear receptor 4) and Cpsf2 (cleavage and polyadenylation specificity factor 2), which were verified by protein immunoblotting.

Overall, this study provides: i) a new tool for discovery science efforts aimed at identifying novel actionable regulators of H3.3 deposition in cells in the context of neoplastic disease and ageing, and ii) a basis for further investigation of mechanisms regulating histone variant loading in the nervous system.

## **Impact Statement**

Paediatric glioblastomas (pGBM) are the leading causes of cancer-related death in children. Current understanding of the biological mechanisms is limited, and no effective treatment has been developed so far. Brain tumour (GBM is the commonest class of brain tumours) survival remains low, and has changed little in over a generation. Cancer Research UK have made brain tumours a strategic priority as one of the four “cancers of unmet need”.

Accordingly, comprehensive research is urgently needed for advancing knowledge of the molecular mechanisms underlying pGBM pathogenesis. Epigenetic reprogramming can be modulated via histone modification and histone variants exchange in the chromatin.

This research was performed to address a number of key questions, i.e. how dysfunctional H3.3 and its loading machinery (chaperone DAXX) contributes to tumourigenesis, and more specifically, to define the molecular changes underlying the H3.3 alterations, and how it relates to changes in pGBM pathogenesis, with implications for other tumours and disorders. The findings promise to reveal functional associations between H3.3 and its chaperone DAXX, and aid better understanding of the fundamental mechanisms of chromatin structure and transcription organisation. Furthermore, it could exert key effects on developing novel biomarkers with diagnostic value as well as new therapeutic targets.

# TABLE OF CONTENTS

LIST OF FIGURES .....	14
LIST OF TABLES.....	16
LIST OF ABBREVIATIONS.....	17
1. Introduction.....	23
1.1 Histones, histone modification and functions .....	23
1.1.1 H3 variants .....	24
1.1.1.1 Modifications on H3 .....	25
1.1.1.2 Functions of canonical and variant H3 .....	26
1.1.2 Linker histone H1 .....	29
1.1.2.1 Modifications on H1 .....	29
1.1.2.2 Functional studies on H1 .....	31
1.1.3 H2A/H2B variants.....	32
1.1.3.1 Modifications on H2A/H2B .....	32
1.1.3.2 H2A/H2B functions .....	33
1.1.4 H4.....	35
1.1.4.1 Modifications on H4 .....	35
1.1.4.2 H4 functions .....	35
1.2 H3.3 chaperones and other chromatin remodelling factors.....	36
1.2.1 HSP, NASP, ASF1 and HAT1 .....	36
1.2.2 DAXX/ATRAX complex.....	37
1.2.3 HIRA/UBN-1/CABIN-1 complex .....	40
1.2.4 The PRCs.....	40
1.2.5 ATP-dependent chromatin-remodelling factors .....	42
1.2.5.1 BRG1 and BRM.....	42
1.2.5.2 The CHDs .....	43
1.3 H3.3 and chaperone DAXX in neurodevelopment, ageing and disease .	44
1.3.1 H3.3.....	44
1.3.1.1 H3.3 in neurodevelopment, brain homeostasis and ageing.....	44
1.3.1.2 H3.3 in brain and bone tumours .....	45
1.3.2 The H3.3 chaperone DAXX .....	47
1.3.2.1 DAXX as a transcriptional regulator .....	47
1.3.2.2 DAXX in apoptosis and ageing .....	48
1.3.2.3 DAXX and tumourigenesis .....	48

1.3.2.4 DAXX and PML-NBs .....	49
1.4 Outstanding questions, hypotheses and aims.....	50
1.5 Aims .....	51
1.6 Project Scheme .....	52
2. Material and Methods .....	54
2.1 Materials .....	54
2.1.1 Plasmids.....	54
2.1.2 Primers .....	55
2.1.2.1 PCR.....	55
2.1.2.2 Real-time PCR (qPCR).....	55
2.1.3 NPCs and cell lines.....	55
2.1.4 Antibodies .....	56
2.1.4.1 Antibodies for immunoblotting (western blotting) .....	56
2.1.4.2 Antibodies for immunofluorescence (IF).....	57
2.1.5 siRNA oligonucleotides.....	57
2.1.6 Materials for immunoprecipitation (IP).....	58
2.1.7 Buffer Recipes .....	58
2.2 Methods .....	59
2.2.1 Molecular biology .....	59
2.2.1.1 Cloning (restriction enzyme digestion and ligation).....	59
2.2.1.2 Transformation.....	60
2.2.1.3 Miniprep, sequencing, and Maxiprep .....	60
2.2.2 Cell culture .....	61
2.2.2.1 Calcium phosphate transfection for virus particle production ...	61
2.2.2.1.1 Lentiviral production .....	61
2.2.2.1.2 Lentivirus titration (pHIV-dTomato and FLAG-Daxx-pHIV-dTomato) for dTomato expression.....	62
2.2.2.1.3 Lentivirus transduction (pHIV-dTomato and FLAG-Daxx-pHIV-dTomato) in NIH3T3 cells and NPCs and cell sorting .....	63
2.2.2.1.4 Lentivirus titration (H3.3-HaloTag-pLenti-PGK-Neo-DEST w531-1 and dH3-HaloTag-pLenti-PGK-Neo-DEST w531-1) for neomycin expression .....	64
2.2.2.1.5 Lentivirus transduction (H3.3-HaloTag-pLenti-PGK-Neo-DEST w531-1 and dH3-HaloTag-pLenti-PGK-Neo-DEST w531-1) in Neuro2a cells and cell sorting.....	64
2.2.3 Biochemistry .....	65

<b>2.2.3.1 Immunoprecipitation (IP)</b> .....	65
<b>2.2.3.1.1 IP optimisation I</b> .....	65
<b>2.2.3.1.2 IP optimisation II</b> .....	65
<b>2.2.3.1.3 IP optimisation III</b> .....	66
<b>2.2.3.1.4 IP optimisation IV</b> .....	67
<b>2.2.3.1.5 IP optimisation V</b> .....	68
<b>2.2.3.1.6 ‘Mock’ IP optimisation V with different protease and phosphatase inhibitors</b> .....	70
<b>2.2.3.1.7 IP optimisation V with dithiothreitol (DTT)</b> .....	70
<b>2.2.3.1.8 Modified IP optimisation V for reduced background and specificity of co-IP proteins</b> .....	70
<b>2.2.3.1.9 IP optimisation VI</b> .....	71
<b>2.2.3.1.10 IP optimisation VII (non-denaturing buffer)</b> .....	73
<b>2.2.3.2 MS sample preparation</b> .....	74
<b>2.2.3.3 siRNA transfection and immunoblotting of Daxx, Hira and Gapdh</b> .....	75
<b>2.2.3.4 Immunoblotting (western blotting)</b> .....	76
<b>2.2.3.4.1 Gel electrophoresis, protein transfer and primary antibody incubation</b> .....	76
<b>2.2.3.4.2 Transfer</b> .....	77
<b>2.2.3.4.3 Immunoblotting</b> .....	78
<b>2.2.3.5 Silver staining</b> .....	78
<b>2.2.3.6 Coomassie staining</b> .....	79
<b>2.2.3.7 iCLIP</b> .....	79
<b>2.2.3.8 Immunofluorescence (IF)</b> .....	80
<b>2.2.3.9 Chromatin extraction for HaloTag and histone proteins</b> .....	81
<b>2.2.4 Function assay: HaloTag imaging assay</b> .....	82
<b>2.2.4.1 H3.3/dH3-HaloTag Lipofectamine transfection on HEK293T cells and HaloTag live imaging</b> .....	82
<b>2.2.4.2 Preliminary examinations of the HaloTag imaging assay</b> .....	82
<b>2.2.4.3 Cell number and plate coating for high-content screens</b> .....	83
<b>2.2.4.4 Mitotic index (pH3 staining) with automated platform</b> .....	83
<b>2.2.4.5 EdU staining on differentiated versus G1-inhibited Neuro2a cells</b> .....	84

2.2.4.6	Batch preparation of H3.3-HaloTag and dH3-HaloTag overexpression Neuro2a cells for high-content screens .....	85
2.2.4.7	H3 deposition on H3.3-HaloTag and dH3-HaloTag overexpression Neuro2a cells: High-content screening setup with automated technologies .....	85
2.2.4.8	qPCR of siRNA-transfected Neuro2a cells.....	86
<b>3.</b>	<b>Visualisation of H3.3 Loading for High-content Screening.....</b>	<b>89</b>
<b>3.1</b>	<b>Background .....</b>	<b>89</b>
3.1.1	Visualisation of H3.3 loading .....	89
3.1.2	High-content screening analysis .....	89
3.1.3	Neuro2a cells and their differentiation .....	89
3.1.4	HaloTag system and H3.3 deposition .....	90
3.1.5	Quench-chase-pause analysis.....	91
<b>3.2</b>	<b>Results .....</b>	<b>92</b>
3.2.1	Construction of expression vectors (H3.3/dH3-HaloTag and H3.3/dH3-pLenti-PGK-Neo-DEST) .....	92
3.2.2	H3.3/dH3-HaloTag Lipofectamine transfection on HEK293T cells, and HaloTag live imaging.....	93
3.2.3	H3.3-HaloTag and dH3-HaloTag overexpression in Neuro2a cells... ..	93
3.2.4	Neuro2a cell differentiation and growth arrest .....	94
3.2.5	H3.3 and dH3 loading in Neuro2a cells: HaloTag fluorescence imaging assay .....	96
3.2.6	Establishment of H3.3 deposition assay for high-content compound/drug screening.....	99
3.2.7	Single downregulation of Hira and Daxx with RNAi .....	105
3.2.8	Hira and Daxx double downregulation with RNAi .....	107
<b>3.3</b>	<b>Discussion.....</b>	<b>111</b>
3.3.1	HaloTag imaging assay for H3.3 deposition .....	111
3.3.1.1	Generation of H3.3/dH3-HaloTag overexpression Neuro2a cells .....	111
3.3.1.2	RA differentiation of Neuro2a cells.....	111
3.3.1.3	Quench-chase-pause assay.....	111
3.3.1.4	Canonical H3 deposition.....	112
3.3.2	Downregulation of Hira and Daxx .....	113
<b>4.</b>	<b>H3.3 Chaperone Binding Partners in NPCs.....</b>	<b>116</b>
<b>4.1</b>	<b>Background .....</b>	<b>116</b>

4.1.1 Choice of model: neural progenitor cells.....	116
4.1.2 Identifying H3.3 regulatory pathways in neural cells .....	116
4.1.3 Mass spectrometry .....	117
<b>4.2 Results .....</b>	<b>118</b>
4.2.1 Generating FLAG-Daxx and FLAG-Daxx-pHIV-dTomato constructs, and FLAG-Daxx overexpression in NPCs .....	118
4.2.2 Initial optimisation of FLAG-IP in FLAG-Daxx overexpression mNPCs .....	121
4.2.2.1 Optimisation I (IP on whole cell lysate).....	121
4.2.2.2 Optimisation II (IP of nuclear extracts with high-salt buffer) .....	123
4.2.2.3 Optimisation III (IP of nuclear extracts with pre-clearing, low-salt buffer and stringent washes).....	125
4.2.2.4 Optimisation IV (IP with 300mM salt washing buffer) .....	127
4.2.3 Optimised FLAG-IP in FLAG-Daxx-overexpression mNPCs and MS analysis .....	129
4.2.3.1 FLAG-IP of the nuclear extract of FLAG-Daxx overexpression mNPCs (Optimisation V protocol) .....	129
4.2.3.2 Mass spectrometry analysis .....	131
4.2.3.3 Validation of top hits Net1, Nr2c2 and Cpsf2 .....	133
4.2.4 Attempts to optimise IP.....	134
4.2.4.1 Protein degradation and oxidative stress .....	134
4.2.4.2 Background reduction.....	136
4.2.4.3 Optimisation VI (Elution with FLAG peptides) .....	138
4.2.4.4 Optimisation VII (IP with non-denaturing buffer) .....	139
4.2.5 Candidate approach .....	143
4.2.5.1 Analysis of candidate chromatin regulators for their ability to interact with Daxx .....	143
4.2.5.2 iCLIP: Daxx association with RNA .....	144
<b>4.3 Discussion.....</b>	<b>146</b>
4.3.1 Daxx binding partners in mNPCs: Identifying the best FLAG-Daxx IP protocol .....	146
4.3.2 Mass Spectrometry analysis and Daxx interaction candidates.....	147
4.3.2.1 Net1 (PSM ratio score 42.72).....	148
4.3.2.2 Nr2c2 (PSM ratio score 40.94).....	149
4.3.2.3 Cpsf2 (PSM ratio score 32.76).....	150
4.3.3 Graphical representation of LC-MS/MS results .....	151

4.3.4 Further optimisations of FLAG-Daxx IP .....	152
4.3.5 Candidate approach (immunoblotting and iCLIP) .....	153
5 Conclusions and Future Research .....	155
5.1 Conclusions.....	155
5.2 Future research .....	157
Bibliography.....	158
Appendix I: Identified proteins from MS with PSM ratio $\geq 4.0$ .....	180

## LIST OF FIGURES

Figure 1. 1: The chromatin folding hierarchy and nucleosome structure. ....	23
Figure 1. 2: Sequence alignment of human histone H3 variants. ....	26
Figure 1. 3: Nuclear import of canonical and variant H3 in humans. ....	37
Figure 1. 4: Deposition complexes mediate H3.3 chromatin assembly. ....	39
Figure 1. 5: Two groups of chromatin remodelling complexes. ....	42
Figure 1. 6: Potential effects of H3.3 mutations in the tumourigenic process of paediatric high-grade gliomas. ....	47
Figure 3. 1: The HaloTag imaging platform. ....	91
Figure 3. 2: HaloTag imaging platform of H3.3 deposition into the nucleosome. .....	92
Figure 3. 3: H3.3- and dH3-HaloTag construct. ....	92
Figure 3. 4: HEK293T HaloTag live cell imaging. ....	93
Figure 3. 5: Chromatin extraction and IF of H3.3-HaloTag– and dH3-HaloTag– transduced Neuro2a cells. ....	94
Figure 3. 6: Neuro2a cell differentiation and pH3 expression. ....	95
Figure 3. 7: HaloTag IF of quench-chase-pause in H3.3/dH3-HaloTag overexpression Neuro2a cells. ....	97
Figure 3. 8: HaloTag IF of quench-chase-pause in H3.3/dH3-HaloTag overexpression Neuro2a cells (duplicate). ....	99
Figure 3. 9: <i>In vitro</i> HaloTag expression in transduced Neuro2a cells, and the HaloTag imaging assay. ....	100
Figure 3. 10: Analysis of cell growth arrest and EdU staining. ....	101
Figure 3. 11: H3.3/dH3-HaloTag deposition assay in differentiated Neuro2a cells. The quench-chase-pause assay visualises and quantifies H3.3/dH3 eviction and incorporation from and into the chromatin. ....	104
Figure 3. 12: <i>Hira</i> siRNA downregulation in the H3.3/dH3-HaloTag overexpression Neuro2a cells. ....	106
Figure 3. 13: <i>Daxx</i> siRNA downregulation in H3.3/dH3-HaloTag overexpression Neuro2a cells. ....	107
Figure 3. 14: <i>Daxx</i> and <i>Hira</i> siRNA downregulation in H3.3/dH3-HaloTag overexpression Neuro2a cells. ....	108
Figure 3. 15: <i>Hira</i> siRNA downregulation in H3.3/dH3-HaloTag overexpression Neuro2a cells. ....	109

Figure 3. 16: <i>Daxx</i> and <i>Hira</i> siRNA downregulation in H3.3/dH3-HaloTag overexpression Neuro2a cells.....	110
Figure 4. 1: Schematic presentation of the DAXX domain map. ....	117
Figure 4. 2: NIH3T3 lentiviral transduction, and IF of FLAG/Daxx expression. ....	119
Figure 4. 3: FLAG/Daxx overexpression in NIH3T3 cells and the transduction of mNPCs. ....	120
Figure 4. 4: Immunoblotting and silver staining analyses of FLAG IP by Optimisation I on whole cell lysate. ....	122
Figure 4. 5: Immunoblotting and silver staining of FLAG IP from Optimisation II of nuclear extracts. ....	124
Figure 4. 6: Immunoblotting and silver staining of FLAG IP from Optimisation III. ....	126
Figure 4. 7: Immunoblotting and silver staining of FLAG IP from Optimisation IV. ....	128
Figure 4. 8: Immunoblotting and silver staining of FLAG IP with Optimisation V. ....	130
Figure 4. 9: Validation of Net1, Nr2c2 and Cpsf2. ....	133
Figure 4. 10: Protein degradation and oxidative stress. ....	135
Figure 4. 11: Reduction of the background and specificity of co-IP proteins.. ....	137
Figure 4. 12: Immunoblotting of FLAG IP from Optimisation VI. ....	138
Figure 4. 13: Immunoblotting of FLAG IP from Optimisation VII on HEK293T cells eluted with FLAG peptides followed by Laemmli buffer. ....	140
Figure 4. 14: Immunoblotting and silver staining of FLAG IP from Optimisation VII eluted with FLAG peptides and Laemmli buffer. ....	142
Figure 4. 15: Co-IP (candidate approach). ....	143
Figure 4. 16: FLAG iCLIP on FLAG-Daxx- and EV-transduced mNPCs. ....	145
Figure 4. 17: MS analysis identified candidates Daxx-associated proteins with PSM ratio $\geq 4.0$ (STRING). ....	151

## LIST OF TABLES

Table 2. 1 Plasmids.....	54
Table 2. 2 Primers for PCR. ....	55
Table 2. 3 Primers for qPCR.....	55
Table 2. 4 Primary antibodies for western blotting.....	56
Table 2. 5 Secondary antibodies for western blotting. ....	56
Table 2. 6 Primary antibodies for immunofluorescence studies.....	57
Table 2. 7 Secondary antibodies for immunofluorescence studies.....	57
Table 2. 8 siRNA oligonucleotides. ....	57
Table 2. 9 Materials for immunoprecipitation.....	58
Table 2. 10 Quantity of protein for immunoblotting analyses.....	76
Table 2. 11 Quantity of protein for silver staining.....	79
Table 4. 1: Identified proteins from MS with PSM ratio $\geq 10.0$ .....	132
Table 4. 2: Identified Daxx-associated proteins with PSM ratio $\geq 4.0$ (STRING: Known and Predicted Protein–Protein Interactions).....	148

## LIST OF ABBREVIATIONS

53BP1	p53-binding protein 1
A (amino acid)	Alanine
ALT	Alternative lengthening of telomeres
APL	Acute promyelocytic leukaemia
ASF1	Anti-silencing function 1
ATM	Ataxia telangiectasia mutated
ATP	Adenosine triphosphate
ATRX	Alpha thalassemia/mental retardation syndrome x-linked
BAF	Barrier-to-autointegration factor
bp	Base pairs
BRDs	Bromodomains
C (amino acid)	Cysteine
CABIN1	Calcineurin-binding protein 1
CAF-1	Chromatin assembly factor 1
CDK8	Cyclin-dependent kinase 8
CentH3	Centromere specific histone 3
CENP-A	Histone H3-like centromeric protein A
CFI	Cleavage factor I
CFII	Cleavage factor II
CHD	Chromodomain-helicase-DNA-binding protein
ChIP	Chromatin immunoprecipitation
CNS	Central nervous system
Co-IP	Co-immunoprecipitation
COMPASS	Complex proteins associated with Set1
CPSF2	Cleavage and polyadenylation specificity factor 2
CREST	Calcium-responsive transactivator
Cul4A	Cullin-4A
DAXX	Death domain-associated protein 6
dH1	<i>Drosophila</i> H1

dH3	<i>Drosophila</i> H3
DIPG	Diffuse intrinsic pontine gliomas
DLBCL	GCB-type diffuse large B-cell lymphoma
DLP	DAXX-like protein
DNA	Deoxyribonucleic acid
Dot1	Disrupter of telomere silencing protein 1
DSB	Double-Strand Break
DSC	DNA synthesis–coupled
DSI	DNA synthesis–independent
E (amino acid)	Glutamic acid
E(Z)	Enhancer of zeste
ECL	Enhanced chemiluminescence
esBAF	Embryonic stem cell BAF
ESCs	Embryonic stem cells
EV	Empty vector with no protein overexpressed
EZH1/2	Enhancer of zeste homolog 1/2
FACS	Fluorescence-activated cell sorting
FACT	Facilitates chromatin transcription
FBS	Fetal bovine serum
FL	Follicular lymphoma
FLAG-DAXX	FLAG-DAXX overexpression
G (amino acid)	Glycine
G1/G2 phase	Gap 1/GAP 2 phase
GBM	Glioblastoma multiforme
GC	Germinal centre
H (amino acid)	Histidine
H1	Histone 1
H2	Histone 2
H2a.Bbd or H2A.B	H2A Barr body deficient
H2AK119ub	Monoubiquitylates Lys119/H2A

H2BFWT or H2B.W	Histone H2B type WT
H3	Histone 3
H3.3	Histone 3.3
H3T/H3.4	Histone 3.4
H4	Histone 4
HAT1	Histone acetyltransferase 1
HD	Huntington's disease
HDAC	Histone deacetylase
HIRA	Histone regulator A
HMTs	Histone methyltransferases
HP1	Heterochromatin Protein 1
HSP	Heat shock proteins
I (amino acid)	Isoleucine
iCLIP	Individual-nucleotide resolution cross-linking and immunoprecipitation
IEGs	Immediate early genes
IF	Immunofluorescence
INO80	Inositol requiring 80
IP	Immunoprecipitation
K (amino acid)	Lysine
KDa	Kilodaltons
L (amino acid)	Leucine
M (amino acid)	Methionine
MDD	Major depressive disorder
ml	Millilitre
mM	Millimolar
MS	Mass spectrometry
NAc	Nucleus accumbens
Nano LC-MS/MS	Nanoscale liquid chromatography coupled to tandem mass spectrometry
NASP	Nuclear autoantigenic sperm protein

nBAF	Neuron BAF complex
ND10	Nuclear domain 10
NET1	Neuroepithelial cell transforming 1
NLS	Nuclear localisation signal
nm	Nanometre
npBAF	Neural progenitor BAF complex
NPC	Neural progenitor cells
NR2C2 (TR4)	Nuclear receptor subfamily 2 group C member 2 (testicular orphan nuclear receptor 4)
NuRD	Nucleosome remodelling and deacetylase
NURF	Nucleosome remodelling factor
PAF1	Polymerase associated factor 1
PAP	Poly(A) polymerase
PBS	Phosphate-buffered saline
PcG	Polycomb group
Pen/Strep	Penicillin/Streptomycin
pGBM	Paediatric glioblastoma multiforme
pH3	phosphorylated Histone 3
PHD	Plant homeodomain
PKA	Protein kinase A
PML- RAR $\alpha$	PML-retinoic acid receptor $\alpha$
PML-NBs	Promyelocytic leukaemia protein nuclear bodies
pNETs	Pancreatic neuroendocrine tumours
PODs	PML oncogenic domains
PRC	Polycomb repressive complex
PSM	Peptide-spectrum matches
PTMs	Post-translational modifications
R (amino acid)	Arginine
RE	regulatory element
Rho GEFs	Rho guanine nucleotide exchange factors
RING1A/1B	Ring finger protein 1A/1B

RNA	Ribonucleic acid
RNA Pol II	RNA polymerase II
RNAP	RNA polymerase
rRNA	Ribosomal RNA
S (amino acid)	Serine
S phase	Synthesis phase
Ser2P/5P	Phospho-Ser2/5
Spt6/16	FACT complex subunit SPT6/16
SSRP1	Structure specific recognition protein 1
SUZ12	Suppressor of zeste 12 protein homolog
SWI/SNF	Switching defective/Sucrose nonfermenting
T (amino acid)	Threonine
TFIID	Transcription Factor II D
TIP60/KAT5	60 kDA Tat-interactive protein/ Histone acetyltransferase KAT5
TRP53	Transformation related protein 53
TrxG	Trithorax group
TSH2B	Testis-specific histone H2B
TSS	Transcription start sites
ubH2B	Ubiquitin H2B
UBN1	Ubinuclein-1
V (amino acid)	Valine
W (amino acid)	Tryptophan
Xist	X-inactive specific transcript
Y (amino acid)	Tyrosine
ZMYND8	Zinc finger MYND-type containing 8
$\gamma$ -H2A.X	Phosphor-H2A.X
$\mu$ l	Microlitre
$\mu$ M	Micromolar

# **Chapter 1**

## **Introduction**

# 1. Introduction

## 1.1 Histones, histone modification and functions

In eukaryotic cells, genetic information is stored in the form of deoxyribonucleic acid (DNA) molecules, that are tightly packed into a large nucleoprotein complex named chromatin. The basic unit of chromatin is the nucleosome, which consists of approximately 147-bp DNA wrapped about 1.75 times around a histone octamer. Each octamer contains two copies of the following core histones H2A, H2B, H3, H4, and the linker histone H1 (Luger *et al.* 1997, Widom 1998). Each core histone is composed of a histone fold structure with a flexible amino-terminal tail. The nucleosomes are formed at periodic intervals and connected by 10–70-bp linker DNA (Mei *et al.* 2017), forming a structure resembling ‘beads-on-a-string’. The linker histone H1 is essential for nucleosome compaction into an advanced-order chromatin structure. The composite of the nucleosome and a linker histone is the chromatosome. The chromatosome particles form short-range inter-nucleosomal interactions, which further organise into long-range fibre–fibre interactions (Figure 1. 1).

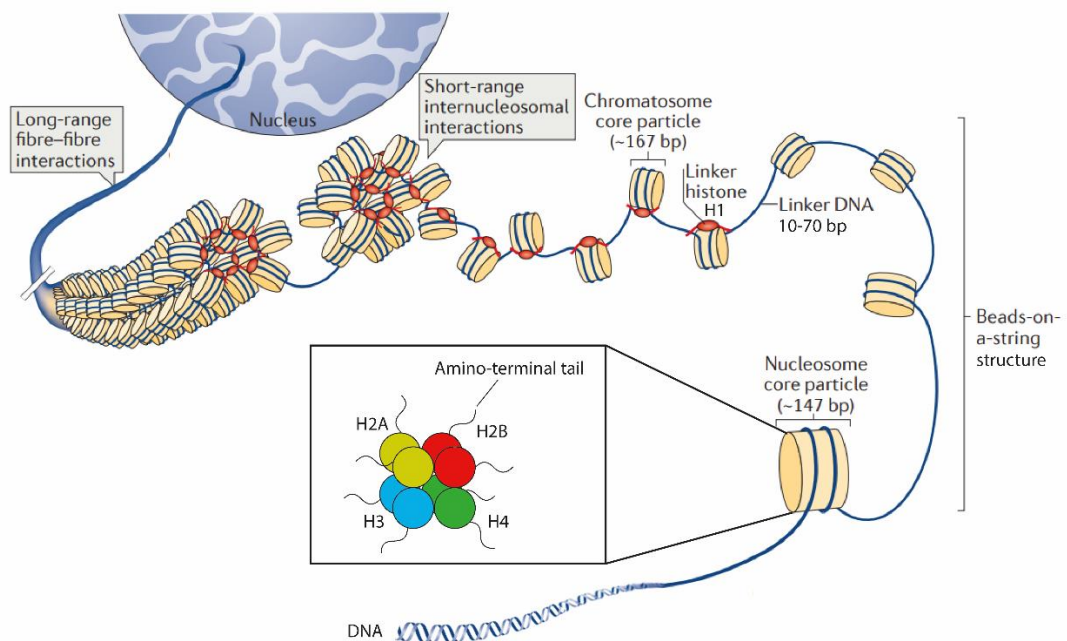


**Figure 1. 1: The chromatin folding hierarchy and nucleosome structure.** DNA in eukaryote cells is stored in the nucleus through histone-dependent interactions, including the formation of the nucleosome core particle, beads-on-a-string arrangement of nucleosomes, the chromatosome core particle, and the association of individual fibres, which eventually produces tertiary structures. **Bottom box:** An illustration of human core histone variants H2A (yellow), H2B (red), H3 (blue) and H4 (green). (Figure modified based on Fyodorov *et al.*, 2017.)

During nervous system development and maintenance, gene expression regulation is modulated not only via the transcriptional machinery (i.e. regulatory signals between gene-specific activators and RNA polymerase II [RNA Pol II]–mediated transcription) (Kornberg 2005), but is also controlled by epigenetic mechanisms including DNA methylation, histone modifications, nucleosome and chromatin remodelling, and non-coding RNA-mediated regulatory mechanisms (Wu and Sun 2006, Feng *et al.* 2007).

Among these epigenetic regulatory processes, nucleosome remodelling and deposition on chromatin has emerged as critically important for DNA-based processes such as transcription and repair (Ray-Gallet and Almouzni 2010). Histone exchange is one mechanism used by the cell to remodel chromatin, which involves the removal of parts (histones) or the entirety of the nucleosome, followed by replacement with newly synthesised histones, which could be the same or different histone variant (Venkatesh and Workman 2015). Majority of histones are synthesised at the S phase and they deposit immediately after the replication fork, these are referred to as canonical histones. On the other hand, histone variants are replacement histones that are expressed throughout the cell cycle and can be deposited onto the chromatin, independent of DNA replication. Histone exchange can be modulated by the enzymes involved in histone post-translational modifications (PTMs), energy-dependent chromatin remodellers, as well as histone chaperones (Venkatesh and Workman 2015). Histone replacements of canonical histones by their histone variants have many implications for the composition, structure and function of different genomic regions. For example, it can modulate the accessibility of a particular genomic region to RNA Pol II, thus facilitating or restricting transcription of a given gene (Venkatesh and Workman 2015). Notably, the deposition of histones and their variants is considered significant to establishing and/or maintaining epigenetic information and nucleosome positioning, as well as the chromatin structure.

### **1.1.1 H3 variants**

Depending on the timing of production and incorporation into the chromatin, H3 can be divided into two subgroups: canonical and variants. The canonical histones H3.1 and H3.2 are expressed limitedly in the S phase (synthesis

phase), and form the main supply of H3 during the DNA-replication period. The incorporation of these histones takes place in a DNA synthesis–coupled (DSC) manner. On the other hand, H3.3 is a replacement histone, and is expressed throughout the cell cycle. Unlike the canonical histones, H3.3 is deposited into the chromatin in a DNA synthesis–independent (DSI) manner (Tagami *et al.*, 2004; Szenker, Ray-Gallet and Almouzni, 2011). Another variant, centromere-specific histone 3 (CenH3), is also grouped as a replacement variant, and is found highly enriched at centromeres.

H3.4 (also known as H3T) and H3.5 are highly expressed in human testis. H3.4 is incorporated genome-wide at late meiosis or early spermiogenesis, and also forms a small proportion in the chromatin of somatic cells (Tachiwana *et al.* 2010). H3.5 is specifically expressed in the seminiferous tubules of human testis, and can potentially replace the essential functions of H3.3 in cell growth (Schenk *et al.* 2011). In addition, H3.Y histones, including H3.Y.1 and H3.Y.2, are primate-specific H3 variants. They accumulate preferentially at the transcription start sites (TSS) (Tachiwana *et al.* 2010).

#### **1.1.1.1 Modifications on H3**

The PTMs on the core histones determine epigenetic gene expression. How the histone amino terminals are modified in the nucleosome determines the dynamic gene transitions being between transcriptionally active or silent (Jenuwein and Allis 2001). The H3 variants are responsible for chromatin organisation in the nucleus. Although their protein codes differ by a few amino acids (Figure 1. 2), the expression and PTM patterns of H3 and its variants vary considerably. Some genetic transcription silencing is carried out via the H3 methylation. H3 methylation at lysine (K) 27 and/or K9 is usually mediated by the enhancer of zeste [E(Z)], a polycomb-group (PcG) transcriptional repressor, followed by binding of the PcG proteins or recognition of the heterochromatin proteins (Czermin *et al.* 2002, Grewal and Elgin 2002, Müller *et al.* 2002, Ringrose and Paro 2004).

H3.1 is enriched with PTMs associated with genetic activation, for example, H3.1/K14 acetylation. It can also be dimethylated at K9, which is associated with genetic silencing. H3.2 can be dimethylated and trimethylated at K27, which are the markers of repression associated with gene silencing and

facultative heterochromatin formation. Unlike metazoans, *Drosophila* contains only one type of canonical H3, i.e. H3.2, which accumulates at transcriptionally silenced gene regions. H3.3 can be hyperacetylated and dimethylated at K36 and K79, which associates with transcriptionally active gene loci (Hake *et al.* 2006). Upon transcriptional activation, the canonical H3 in the chromatin is replaced by H3.3, and the H3.3 is dimethylated or trimethylated at K4 (Hödl and Basler 2009).

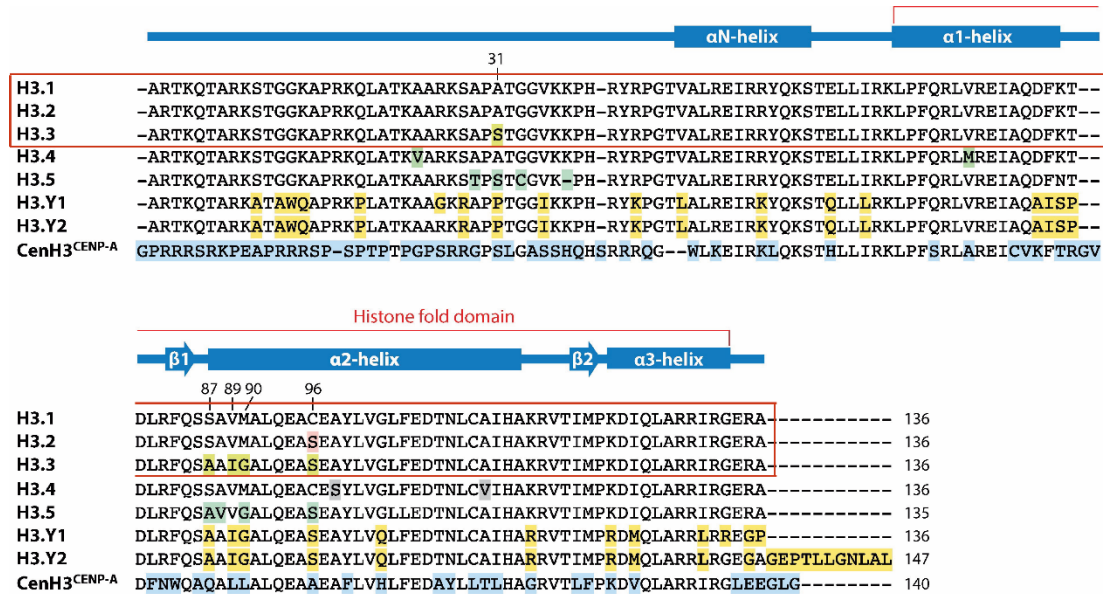


**Figure 1. 2: Sequence alignment of human histone H3 variants.** Red box highlights the sequence of canonical H3 and H3.3. Important residues of H3.3 distinct from H3.1: S31/A31, A87/S87, I89/V89, G90/M90 and S96/C96 are indicated and highlighted in yellow. S: serine. A: alanine. I: isoleucine. V: valine. G: glycine. M: methionine. C: cysteine. (Figure modified based on Szenker, Ray-Gallet and Almouzni, 2011.)

### 1.1.1.2 Functions of canonical and variant H3

Sequence analysis and single mutation studies have shown that the amino acid residues S31, A87, I89 and G90 (in H3.3) or A31, S87, V89 and M90 (in H3.1/H3.2) in the histone folding domain are responsible for the differences in H3 variant deposition. Notably, the three-amino acid–mutated H3.1 with the A31, A87, I89 and G90 sequence undergoes both replication-dependent and replication-independent deposition into the chromatin. It has also been demonstrated that the combination of residues A31, S87, V89 and M90 in the canonical H3 is necessary for restricting its DNA replication–independent assembly into the chromatin (Ahmad and Henikoff 2002).

Chromatin immunoprecipitation (ChIP) analyses have shown that H3.3 is also associated with transcriptionally active gene regions. In detail, H3.3 specifically incorporates into the gene bodies of the transcribed genes (Daury *et al.* 2006), while also being enriched at the promoter region at transcriptionally active genes (Chow *et al.* 2005). H3.3 deposition at the transcribed genes remains as an extended post-transcriptional marker, even when the genes are inactivated (Tamura *et al.* 2009). Moreover, genome-wide profiling of embryonic stem cells (ESCs) has demonstrated that H3.3 is enriched at the promoters of developmentally regulated genes, which are typically silenced or transcribed at low levels (Goldberg *et al.* 2010). This indicates that H3.3 might not be required for active transcription, but instead might be necessary for establishing a chromatin landscape allowing proper gene expression (via polycomb repressive complex 2 [PRC2] recruitment) upon differentiation (Banaszynski *et al.* 2013).

H3 histones and its variants contribute to structural differences on individual nucleosomes, nucleosomal arrays, as well as advanced-order chromatin domains, regardless of the impact of PTMs on the variants (Hake and Allis 2006). These potential H3 functions take place via the amino acid cysteine (C). C110 is encoded at the H3 core region, and this distinguishes H3 from the other histones. Cysteines can form disulphide bonds under oxidative conditions, and are involved in homotypic or heterotypic protein dimerisation and oligomerisation (Hake and Allis 2006). Under oxidising conditions, the H3/C110 stabilises the H3-H4 tetramer by forming a disulphide bond with the other H3 within the same nucleosome (Luger *et al.* 1997). This finding is supported by the study by Banks and Gloss's laboratory, where mutated C110E (cysteine 110 to glutamic acid) led to the destabilisation of H3-H3 hydrophobic 4-helix bundle tetramer interface (Banks and Gloss 2004). Moreover, the canonical histone H3.1 contains C96, and H3.1/C96 forms a disulphate bond with other H3.1 histones in the neighbouring nucleosomes (Luger *et al.* 1997). The disulphate bond formation between the neighbouring nucleosomes contributes to the chromatin condensation involved in heterochromatin and transcription repression.

H3 variants are also involved in epigenetic memory, where epigenetic information is passed down to the next-generation daughter cells. H3.3

incorporation occurs at both genic and intergenic regulatory regions. In *Drosophila melanogaster*, the cellular memory is maintained at the homeotic gene clusters by non-coding DNA, which regulates the transcription of the cis-regulatory elements. Interestingly, peaks of H3 replacement by H3.3 have been observed in the cis-regulatory domains. Such replacement peaks have also been observed at nuclease-hypersensitive sites, PcG and trithorax group (trxG) protein-binding sites, as well as at nucleosome depletion sites (Ringrose and Paro 2004, Mito *et al.* 2007).

Research on H3.3 has demonstrated its important roles in development and lifespan, which is conserved among species. In *D. melanogaster*, H3.3 deletion leads to reproduction deficiency, including low viability and sterility, in both females and males (Hödl and Basler 2009). Moreover, in *C. elegans*, H3.3 deficiency affects the insulin/IGF-1 signalling/lifespan-extending signalling pathways and leads to shortened longevity (Piazzesi *et al.* 2016). In vertebrates such as *Xenopus laevis*, downregulated H3.3 results in defects at the late gastrointestinal formation stage (Szenker *et al.* 2012). In mice and humans, H3.3 histones are encoded by two genes, *H3f3a* and *H3f3b*. *H3f3a* mutation or loss results in post-natal lethality, growth rate reduction, neuromuscular deficiency as well as copulatory activity reduction in males (Couldrey *et al.* 1999). On the other hand, *H3f3b* deletion in mice results in growth deficiency and death at birth. *H3f3b* heterozygous mice do not die, but have reduced growth rates, as well as male sterility (Tang *et al.* 2015).

Canonical and variant H3 histones have distinct chromatin incorporation machineries. The deposition of H3.1 is chaperoned by the chromatin assembly factor 1 (CAF-1) complex (Hoek and Stillman 2003). As the loss of CAF-1 leads to DNA replication and S phase progression deficiency, it has been suggested that CAF-1 plays critical roles in cell proliferation. CAF-1 binds to HP1 (the fundamental unit of heterochromatin packaging) at its chromoshadow domain, a protein domain distantly related to the chromodomain. CAF-1 comprises several subunits, including p150, p60, and p48. CAF-1 downregulation in *Drosophila* leads to reduction in H3K9 methylation (a marker of transcriptional repression) at the pericentric heterochromatin, and reduced effectiveness in recruiting HP1 to the chromocentres of polytene chromosomes (Huang *et al.* 2010). In *X. laevis*,

deletion of the p150 subunit resulted in defective nuclear organisation as well as impaired cell cycle progression (Quivy *et al.* 2001). In human cells, CAF-1 is required for efficient cell cycle progression, while its loss causes accumulation in the S phase. The chromatin incorporation machineries of H3.3 are discussed in Section 1.2 below.

### **1.1.2 Linker histone H1**

The linker histone H1 family members are a fundamental element of chromatin, as they bind to the nucleosomal core particle around the DNA entry and exit sites (Hergeth and Schneider 2015). H1 is essential for stabilising nucleosome and advanced-order chromatin structures. In humans and mice, 11 H1 variants have been reported, consisting of 7 somatic subtypes: H1<sup>o</sup>, H1.1–H1.5, and H1x, 3 testis-specific subtypes: H1t, H1T2 and HILS1, and one oocyte-specific subtype: H1oo (Fyodorov *et al.* 2017).

The somatic subtypes H1.1–H1.5 are broadly expressed in different cell types, presenting a DNA synthesis–dependent manner, with peak expression at S phase (FMarzluff 2005). In the histone gene cluster, these variants are encoded along with the core histone genes H2A/B, H3 and H4 (Hall and Cole 1986, Albig and Doenecke 1997). Significantly, genetic origin study has shown that the core histone genes originated from archaeobacteria, while the linker histone genes originated from eubacteria (Kasinsky *et al.* 2001).

Unlike the other somatic subtypes, H1<sup>o</sup> and H1x are expressed throughout the cell cycle (Hergeth and Schneider 2015). Study of mouse GBM cells has indicated a correlation between increased H1<sup>o</sup> expression and DNA replication inhibition (Hall and Cole 1986). It has also been proposed that H1<sup>o</sup> and H1x are replacement histones for the somatic H1 variants in terminally differentiated or quiescent cells, and they are differentially regulated and may have different functions (Hall and Cole 1986, Happel *et al.* 2005, Hergeth and Schneider 2015).

#### **1.1.2.1 Modifications on H1**

Similar to the core histones, the linker histones are subjected to various PTMs. These PTMs can be found in the globular domain as well as in the tail of H1. The globular domain PTMs are highly conserved among the somatic H1 variants, but vary substantially at the histone tails. This indicates that different

H1 variants could correspond to distinct cellular functions. In human and mouse cells, the level of phosphorylated H1 is lowest in the G1 phase, increasing in the S and G2 phases, and eventually peaking at metaphase (Fyodorov *et al.* 2017).

Daujat *et al.* discovered that heterochromatin protein 1 (HP1), an essential heterochromatin component, specifically recognises and binds to methylated H1.4/K26. Yet, the simultaneous phosphorylation of H1.4/S27 (serine 27) prevents the binding of K26 to HP1 (Daujat *et al.* 2005). Mass spectrometry analysis has revealed that protein kinase A (PKA)-mediated H1.4/S35 phosphorylation dissociates H1.4 from mitotic chromatin, suggesting a functional role of H1.4 in mitotic chromatin compaction (Chu *et al.* 2011). Moreover, the work by Zheng *et al.* on HeLa cells has implied that location-specific H1.4/S187 phosphorylation promotes glucocorticoid nuclear hormone receptor-mediated DNA transcription (Zheng *et al.* 2010).

A functional study has shown that the phosphorylation of H1 variants H1.2 and H1.5 at S172 are colocalised to DNA replication and transcription sites (Talasza *et al.* 2009). That study has also shown that the two variants may be phosphorylated in different forms localising at various regions of the chromatin, indicating their distinct function in the cell cycle. Furthermore, the H1.2/T146 (threonine 146) phosphorylation may enhance p53 transcription activity by dissociating itself from p53, therefore triggering the p53-dependent DNA damage response pathways such as apoptosis (Kim *et al.* 2012).

H1 can also bear other PTMs, for example, methylation, acetylation, citrullination, and ubiquitylation. As stated above, HP1 is recruited via the methylation of H1.4/K26, leading to heterochromatin formation and gene silencing (Daujat *et al.* 2005). As the sole variant linker histone in *D. melanogaster*, *Drosophila* H1 (dH1) is methylated at K27. Interestingly, dH1/K27 accumulates at the pericentromeric heterochromatin during metaphase, and this potentially contributes to heterochromatin organisation (Bonet-Costa *et al.* 2012). Furthermore, a functional characterisation study on H1 acetylation from Kamieniarz's group has shown that H1.4/K34 acetylation is mediated by the histone acetyltransferase GCN5, and it is enriched at the promoter region of transcriptionally active genes. GCN5 activates gene transcription in H1.4K34ac-rich regions via acetylation of the histone, and thus

increases H1.4 mobility and facilitates the mediation of transcription factor II D (TFIID) recruitment (Kamieniarz *et al.* 2012).

### 1.1.2.2 Functional studies on H1

Although the functions of linker histone H1 and its variants have not been fully understood, current findings have suggested a number of fundamental roles for H1, including chromatin organisation, gene regulation and protein interaction.

Depletion of H1 in *D. melanogaster* leads to significant alterations in chromatin structure and loss of chromatin banding. It also results in near full abrogation of the repressive H3K9me2 marker, as well as the replacement of the single chromocentre by multiple HP1 foci (Lu *et al.* 2009). Triple depletion of H1 in mouse embryonic stem cells led to pericentric chromocentre clustering and the de-repression of major satellites, indicating the roles of H1 in heterochromatin structural maintenance (Cao *et al.* 2013). Furthermore, the extensive reduction of H1 in mice embryos led to global shortening of the spacing between nucleosomes (Fan *et al.* 2003).

In addition, H1 *in vivo* depletion in *D. melanogaster* and mouse embryo has also revealed its regulation in specific gene expression (Vujatovic *et al.* 2012). RNAi downregulation of dH1 upregulates inactive genes, predominantly in heterochromatin, whereas reduced dH1 expression corresponds to the downregulation of active genes in euchromatin (Vujatovic *et al.* 2012). Vujatovic and colleagues demonstrated that dH1 regulates genetic expression in a structurally organised manner.

In mouse embryos, the lack of three H1 subtypes resulted in death by mid-gestation, whereas reduced embryo size was observed in mice void of five of the six H1 alleles (Fan *et al.* 2003). These findings show that the total amount of H1 is critical for proper embryonic development.

In addition to direct regulation of gene expression and chromatin architecture, H1 subtypes also interact with proteins including transcriptional activators and repressors. Kim *et al.* demonstrated that H1.2 binds to the cullin-4A (Cul4A) E3 ubiquitin ligase and polymerase associated factor 1 (PAF1) elongation complexes, promotes the induction of H4K31 ubiquitination, and leads to the methylation of H3K4 and H3K79, thus initiating target gene transcription.

Moreover, H1.2 located at actively transcribed target loci recognises and binds to the phosphorylated RNA Pol II Ser2, and it further retains the transcriptional activation by recruiting Cul4A and PAF1 (Kim *et al.* 2013).

### **1.1.3 H2A/H2B variants**

Eight variants of H2A have been identified in human somatic cells: H2A.X, H2A.Z.1, H2A.Z.2.1, H2A.Z.2.2, H2A Barr body–deficient (H2a.Bbd or H2A.B), macroH2A1.1, macroH2A1.2 and macroH2A2. Additionally, two testis-specific variants of H2B: H2B type WT (H2BFWT or H2B.W) and testis-specific histone H2B (TSH2B), have been identified.

#### **1.1.3.1 Modifications on H2A/H2B**

H2A.Z is the most conserved H2A variant between species (Jackson *et al.* 1996). Although H2A.Z is a H2A variant, its core region sequence differs significantly from that of its canonical histone H2A. In addition, H2A.Z is preferentially associated with actively transcribed chromatin (Stargell *et al.* 1993), and marks important regulatory genomic regions including core promoters (Gatta and Mantovani 2011). Genome-wide analysis data have mapped H2A.Z downstream of TSS, and it is enriched in cell cycle promoters (Gatta and Mantovani 2011).

Mammalian H2A.Z can carry a variety of PTMs, including acetylation, monoubiquitylation and methylation at its lysine loci. H2A.Z acetylation is reportedly crucial for gene transcriptional activation. In *Saccharomyces cerevisiae*, H2A.Z acetylation correlates with global gene activity; whereas in chicken, it is enriched at the 5' terminus of active genes.

H2A.X represents 2–25% of the mammalian H2A histone. It contains S139 located 4 amino acids away from the C-terminal end, which is phosphorylated when DNA experiences a double-strand break (DSB). In detail, phosphor-H2A.X (i.e.  $\gamma$ -H2A.X) accumulates around the DNA damage lesion and results in further recruitment of DNA repair proteins and checkpoint factors to the DSB site (MacAlpine and Almouzni 2013).

MacroH2A comprises a domain homolog to histone H2A, as well as a large unique non-histone C-terminal ligand-binding domain. The binding domain contains a segment that resembles a leucine zipper and is involved in the

dimerisation of transcription factors, suggesting its role in interaction with other nuclear proteins (Pehrson and Fried 1992).

Less is known about the regulation of H2B modifications. Genome-wide analysis by Minsky *et al.* has shown that, H2B/K120 mono-ubiquitination corresponds with DNA transcription in active genes (Minsky *et al.* 2008). However, other studies have reported conflicting results. Gatta and Mantovani demonstrated that ubH2B could only be found in the regions of transcribed cell cycle genes, while H2B/K120 acetylation is found in transcriptionally repressed genes (Gatta and Mantovani 2010). In addition, H2B/S14 phosphorylation has been found in human cells undergoing programmed apoptosis, and corresponds with the cellular process that regulates the chromatin condensation during apoptosis (Cheung *et al.* 2003). Notably, the PTMs on H2B can facilitate the PTMs of another histone. For example, the mono-ubiquitination of H2BK123 is necessary for trimethylation by the methyltransferases, such as COMPASS (complex proteins associated with Set1) and Dot1 (disrupter of telomere silencing protein 1), of H3K4 and H3K79 (Nakanishi *et al.* 2009).

#### **1.1.3.2 H2A/H2B functions**

H2A.Z is enriched at the transcription initiation sites in the promoters of both active and inactive genes. H2A.Z accumulation on the chromatin is generated upon DNA deposition signalling as well as acetylation of the histone tail (Raisner and Madhani 2006). Meneghini *et al.* have revealed that H2A.Z contributes to the prevention of the silent heterochromatin spreading by placing itself as an obstructor at promoter sites (Meneghini *et al.* 2003). In addition, H2A modulates chromatin stabilisation by replacing itself with a H2A variant histone. In detail, the H3 three hydrogen bonds in the nucleosome are lost upon H2A (Glycine 104 [G104]) replacement by H2A.Z (G106), as the (H3-H4)<sub>2</sub> tetramer docking domain in the H2A differs from its variants, leading to a less stable chromatin structure (Luger *et al.* 2000).

Studies have suggested that H2A.Z may interact with the nuclear proteins associated with cancer. Histidine (H) 112 on the surface of the H2A.Z histone octamer binds to a manganese ion that is partly stabilised by H114, and this potentially provides a unique interaction interface for nuclear proteins. The

presence of H2A.Z in the H2A.Z-H2B dimers in the nucleosome unit may also be necessary for its interaction with adjacent H4 tails or non-histone protein factors (Raisner and Madhani 2006).

H2A.Z has also been suggested to have effects on cancer progression. Valdés-Mora *et al.* have implicated that H2A.Z might be involved in genetic expression de-regulation and tumour progression in prostate cancer, and the increased level of global H2A.Z acetylation correlates with poorer prognosis (Valdés-Mora *et al.* 2017). That study involved a model of prostate cancer progression, where the gain of acetylation in the H2A.Z-containing nucleosomes promotes the transcription of oncogenes at their promoters, whereas the loss of H2A.Z acetylation silences tumour suppressor genes via genome transcription inactivation. Specifically, H2A.Zac-containing nucleosomes flank the androgen receptor genes, initiating the formation of nucleosome-free regions and activating the production of androgen receptor enhancer RNAs in response to the androgen treatment, resulting in a reduced androgen level and a poorer prognosis.

macroH2A1 protein, another H2A variant, is preferentially concentrated in the inactive X chromosome (Costanzi and Pehrson 1998). The high concentration of macroH2A-containing nucleosomes in the inactive X chromosome assists the formation of a distinct chromatin structure for transcriptional silencing, via its interaction with other inactive X chromosome components such as the chromosome-coating RNA X-inactive specific transcript (Xist).

Creppe *et al.* have demonstrated an important role of macroH2A1 in coordinating between self-renewal and differentiation in embryonic and adult stem cells (Creppe *et al.* 2012). Specifically, the proper differentiation gene activation processes are disrupted in mouse embryonic stem cells that lack *macroH2A*, and this in turn leads to the limited differentiation capacity of the cells. Cells lacking the *macroH2A1* gene have also shown incomplete suppression of the pluripotency genes, as well as the formation of defective embryoid bodies (Creppe *et al.* 2012). The study has also implicated that, in primary human keratinocytes, the *macroH2A1* expression level is negatively related to the cells' self-renewal capacity and pluripotent compartment.

MacroH2A might also function as a tumour suppressor. Biopsy studies on human breast and lung tumours have shown inverse expression levels of

macroH2A1.1 and macroH2A2 in response to tumour cell proliferation (Sporn *et al.* 2009). In low malignant melanoma, knockdown of the macroH2A1 and macroH2A2 proteins increased cell proliferation and migration significantly *in vitro*, and boosted tumour growth and metastasis *in vivo*. By contrast, restoration of the expression of macroH2A isoforms reoccurred the malignant phenotypes through CDK8 regulation (Kapoor *et al.* 2010). Similar results were observed during the proliferation-suppressing restoration in lung and cervical cancer cells, where significant low expression of macroH2A1.1 was present before the rescue (Novikov *et al.* 2011).

#### **1.1.4 H4**

H4 is one of the four core histones composing the nucleosomes, and the only one with no existing variants. Similar to H3.3, H4 is expressed throughout the cell cycle (Kamakaka and Biggins 2005).

##### **1.1.4.1 Modifications on H4**

H4 is involved in the activation of transcriptionally active regions. H4 can be acetylated by histone lysine acetyltransferases (HATs) at K16. HATs are enriched in the transcriptionally active regions of the chromatin. They mark the active enhancers and modulate chromatin organisation (Taylor *et al.* 2013, Dhar *et al.* 2017). Lysine acetylation at the H4 tail region neutralises the positive charge on the histones, thereby reducing the interactions between the histone and DNA. It also results in reduced binding with the neighbouring inter-nucleosomes, thus leading to chromatin de-condensation.

H4 acetylation also generates binding sites for chromatin proteins carrying bromodomains (BRDs). BRDs are acetyl-lysine readers, and are involved in transcriptional regulation and DNA repair. The binding of the BRD proteins at the acetylated sites would further assemble other complexes, including HDAC, and transcriptional co-activators to the gene sites for transcriptional activation. H4 can be methylated at arginine (R) 3 by the methyltransferase PRMT1. H4/R3 methylation is required for establishing and maintaining the active chromatin structures and gene expression (Huang *et al.* 2005).

##### **1.1.4.2 H4 functions**

H4 responds to and is involved in the repair of DSBs (Dhar *et al.* 2017). In detail, when the cell detects DSBs in the DNA, it creates a repressive

environment at the chromatin site with the repressor complexes HP1 and H3K9 methyltransferases. During this process, H4 is associated with the acidic patch on the adjacent nucleosome. Once the repressor complexes leave the DNA, H4 is acetylated by TIP60, through which the internucleosomal bound is weakened and the damaged chromatin is opened. Following H4 acetylation, 53BP1 is recruited to the DNA being repaired. It then mediates DSB repair by providing docking sites for BRD proteins like ZMYND8 and BRD4 that are crucial for DSB repair.

## **1.2 H3.3 chaperones and other chromatin remodelling factors**

The exchange of histone deposition involves a group of dedicated molecular complexes, the histone chaperones. Histone chaperones play significant roles in histone deposition in the chromatin dynamics.

### **1.2.1 HSP, NASP, ASF1 and HAT1**

HSP (heat shock proteins), NASP (nuclear autoantigenic sperm protein), ASF1 (anti-silencing function 1 protein) and HAT1 (histone acetyltransferase 1) are the general chaperones utilised by canonical and variant H3 during their deposition into the chromatin (Figure 1. 3).

Once they are newly synthesised in the cytosol, the H3 histones are coupled with the heat shock proteins, including HSC70 and HSP90, to prevent protein misfolding and degradation. When the histones reach the nuclear membrane, they are further coupled with the abundant general histone chaperones in the following sequence: NASP, HAT1, ASF1 and importin-4. NASP is crucial for stabilising the assembled H3/H4 dimers (Cook *et al.* 2011), as it exposes the H4 tail to HAT1 for K5/12 acetylation in the cytosol, which stabilises the H3/H4 heterodimers. The complex then associates with ASF1, interacts with importin-4 and transports the histone dimers into the nucleus (Campos *et al.* 2010). ASF1 coordinates the H3/H4 deposition pathways as well as the recycling of the evicted histones (Cook *et al.* 2011).

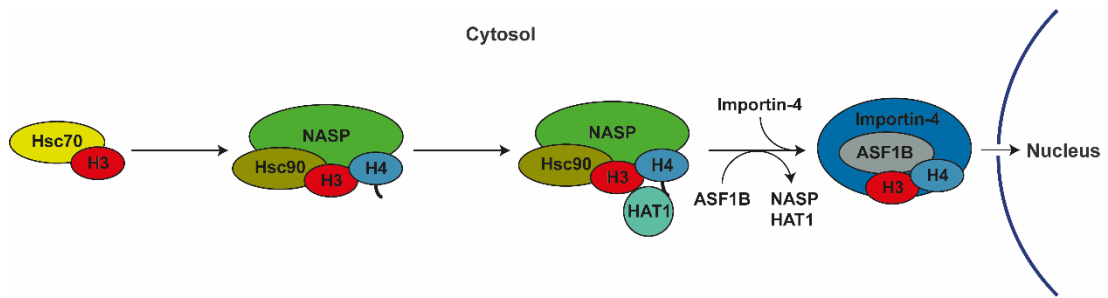


**Figure 1. 3: Nuclear import of canonical and variant H3 in humans.** H3 folding is first assisted by the Hsc70 chaperone at the ribosomal exit and transferred to Hsp90. Hsp90 assembles H3 into H3/H4 dimers along with NASP cochaperone. The NASP chaperone binds H3/H4 heterodimers and presents the H4 carboxyl domain to recruit HAT1. After H4 acetylation, the H3/H4 heterodimers are stabilised. The histones are transferred to ASF1B, which associates with importin-4 and transports the histones into the nucleus. (Figure generated based on Campos *et al.*, 2010.)

### 1.2.2 DAXX/ATRX complex

DAXX and the chromatin remodeller alpha thalassemia/mental retardation syndrome x-linked protein (ATRX) complex is a set of H3.3-specific chaperones. The DAXX/ATRX chaperone complex modulates H3.3 deposition at the pericentric heterochromatin and telomeres in a replication-independent manner (Drane *et al.* 2010, Goldberg *et al.* 2010) (Figure 1. 4). Studies by our group have demonstrated the involvement of DAXX in activity-dependent regulation of H3.3 loading at the immediate early genes (IEGs) in neurons (Michod *et al.* 2012) (Figure 1. 4). In detail, following membrane depolarisation upon neuronal activation, calcineurin dephosphorylates DAXX and thus facilitates the DAXX-dependent H3.3 deposition in IEGs, indicating a stimuli-induced gene transcription signalling pathway and a potential targetable H3.3 loading mechanism in the CNS.

DAXX interacts with ATRX as part of the histone chaperone complex. DAXX has intrinsic preference for H3.3 due to the specific amino acid AAIG motif in the histone folding domain. The association of the H3.3/H4 dimers and DAXX results in the uncoupling of the general histone chaperone ASF1 when the histone is produced and transferred into the nucleus (Lewis *et al.* 2010, Elsässer *et al.* 2012). ATRX is an ATP-dependent chromatin remodelling factor. It contains a PHD finger that binds H3K9me3/H3K4me0, and it is part of the switching defective/sucrose nonfermenting 2 (SWI2/SNF2)-related ATPase family involved in chromosome stability modification (Hargreaves and Crabtree 2011). ATRX is found crucial for H3.3 localisation specifically at the

pericentric heterochromatin and telomeres (Tang *et al.* 2004). In addition, The DAXX/ATRX chaperone complex deposits H3.3 into pericentric heterochromatin and telomeres by interacting with histone deacetylase II (HDACII, which is essential for transcriptional repression) and the chromatin associated protein Dek, where histone methyltransferases (HMTs) establish a repressive chromatin state (Hollenbach *et al.* 2002). The interaction between ATRX and non-coding RNAs regulates PRC2 function (Sarma *et al.* 2014). In detail, the inactivation of X chromatin requires the binding of ATRX to long non-coding chromosome-coating RNA Xist, thus promoting PRC2 repression activity and establishing the repressive chromatin.

Interestingly, H3.3 can also utilise other histone-specific chaperones for its own deposition. In detail, H3.3 can be associated with the H3.1-specific chaperone CAF-1 if both the H3.3 chaperones DAXX and HIRA are absent. This indicates a replication-dependent deposition pathway for H3.3 (Drane *et al.* 2010, Lewis *et al.* 2010).

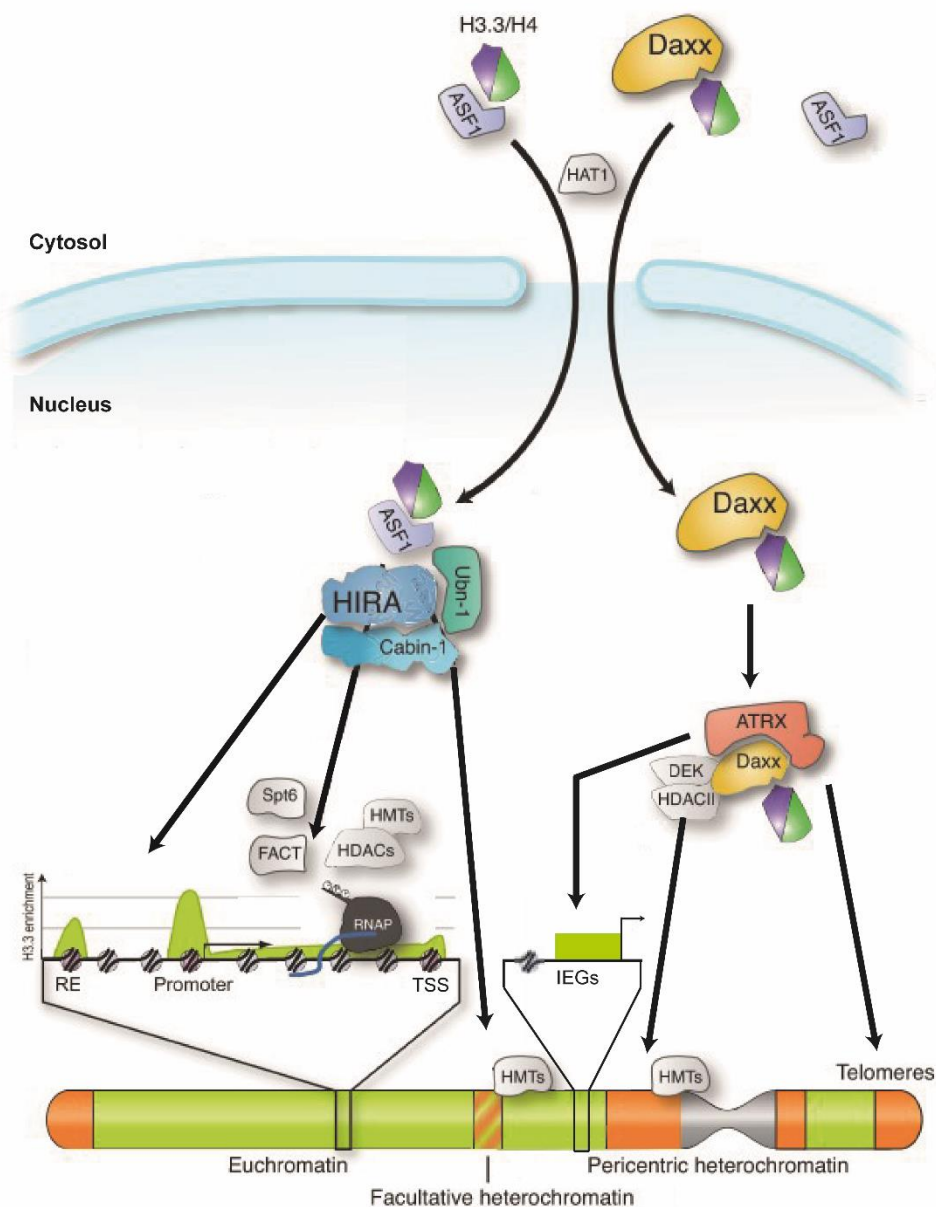


**Figure 1. 4: Deposition complexes mediate H3.3 chromatin assembly.** A model for the flow of histones from their synthesis in the cytosol to their target genomic regions in the nucleus. **Right:** Newly synthesised histones H3.3/H4 are chaperoned by ASF1 and a cytosolic pool of Daxx. HAT1 acetylates H4K5/K12 in the cytosol. Chaperone Daxx cooperates with ATRX and possibly other factors (Dek and HDACII) in depositing H3.3 into pericentric heterochromatin and telomeres. Daxx/ATRX also mediates deposition of H3.3 into immediate early genes (IEGs) at euchromatin in neuronal cells. **Left:** Newly synthesised H3.3/H4 are chaperoned by ASF1 into the nucleus and coupled with chaperone complex HIRA/Ubn1/Cabin-1. HIRA chaperone complex deposits histones at regulatory elements (REs), and at facultative heterochromatin in senescent cells. HIRA also mediates deposition of H3.3 at promoters, transcribed regions and transcription start sites (TSS), together with RNA polymerase (RNAP)-associated FACT (Spt16/SSRP1) and Spt6 histone chaperones. HMTs establish a repressive chromatin state. (Figure modified based on Elsaesser and Allis 2010.)

### 1.2.3 HIRA/UBN-1/CABIN-1 complex

HIRA is a H3.3-specific chaperone involved in the DSI nucleosome assembly into the transcribed regions, gene promoters as well as the regulatory elements (REs) localised in the euchromatin (Tagami *et al.* 2004, Goldberg *et al.* 2010) (Figure 1. 4). The HIRA deposition pathway is evolutionarily conserved (Rai *et al.* 2011, Ricketts *et al.* 2015). The HIRA histone chaperone complex associates with the general histone chaperone ASF1 and mediates the deposition of H3.3/H4 dimers. Ubinuclein-1 (UBN-1) is essential for the functional activity of the HIRA complex (Banumathy *et al.* 2009, Ray-Gallet *et al.* 2011). UBN-1 associates specifically with H3.3/H4 dimers by binding with H3.3/G90 through its Hpc2-related domain (Ricketts *et al.* 2015). CABIN-1 (calcineurin-binding protein 1), identified as another HIRA complex unit, is activated upon calcium signalling (Youn *et al.* 1999). Remarkably, CABIN-1 also mediates H3.3/H4 dimer assembly into facultative heterochromatin regions in senescent cells, in which HMTs help to establish a repressive chromatin state (Banumathy *et al.* 2009).

Furthermore, histone chaperones FACT (Spt16/SSRP1) and Spt6 are also involved in the HIRA-associated H3.3/H4 deposition into the transcribed regions. Their association to RNA polymerase (RNAP) contribute to histone exchange during DNA transcription (Elsaesser and Allis 2010).

The HIRA complex also interacts with Ser5P and Ser2P. These proteins are the initiation and elongation forms of RNA Pol II. The HIRA-RNA Pol II association mediates the enrichment of H3.3 in the transcribed regions, as well as at the promoter and downstream of the transcription start sites (TSS) (Ray-Gallet *et al.* 2011).

### 1.2.4 The PRCs

The PcG proteins are conserved chromatin factors that were first considered repressive regulators of *Hox* genes. They are involved in specifying cell identity along the anteroposterior axis of the body plan of *Drosophila* (McKenzie Duncan 1982). However, genome-wide mapping of PcG components in *D. melanogaster*, murine and human cells have revealed that these proteins bind many other genes in addition to the *Hox* genes, including

transcription factors involved in diverse cellular functions and developmental pathways (Boyer *et al.* 2006, Lee *et al.* 2006, Schwartz *et al.* 2006).

The PcG proteins form two major core complexes: PRC1 and PRC2. Polycomb-mediated gene silencing relies mostly on regulation of the chromatin structure through the PTMs of histones. Specifically, the PRC1 complex monoubiquitylates K119 on H2A (i. e. H2AK119ub) via its subunits, the ubiquitin ligases RING1A and RING1B. The H3.3 chaperone HIRA has been reported to interact with PRC2 in the H3.3 deposition at the promoters of developmentally regulated genes in mouse embryonic stem cells (Banaszynski *et al.* 2013). The PRC2 complex is also responsible for the dimethylation and trimethylation of K27 on H3 (H3K27me<sub>2/3</sub>) via its enzymatic subunits EZH1/2 (Margueron and Reinberg 2011). EZH2 is part of the PcG complexes PRC2 and PRC3, and a H3K27-specific methyltransferase. Importantly, the repressive marks H3K27me<sub>2</sub> and H3K27me<sub>3</sub> have been found in facultative heterochromatin where they mediate tissue-specific gene silencing (Margueron and Reinberg 2011).. SUZ12 is another component of the PRC2 and PRC3 complexes, and acts as a DNA binding factor directing the PRC proteins to specific sites in the genome (Gibbons 2005).

Importantly, polycomb proteins might promote or inhibit tumorigenesis through their HMT activity. The expression of PRC2 components is upregulated in cancers such as melanoma, lymphoma, and breast and prostate cancer (Yamaguchi and Hung 2014), while EZH2 is considered a marker for the aggressive stages of prostate and breast malignancies (Kleer *et al.* 2003, Deb *et al.* 2013). EZH2 overexpression promotes neoplastic transformation of normal prostatic cells and hyperplasia in breast epithelium, and is poor prognosis-associated. (Kleer *et al.* 2003, Deb *et al.* 2013), whereas its deletion leads to a significant reduction in cell proliferation (Bracken *et al.* 2003). Gain-of-function EZH2 mutation (Y641) drives the accumulation of H3K27me<sub>3</sub> and promotes lymphoid transformation in germinal centre (GC) derived B-cell lymphoma, including follicular lymphoma (FL) and GCB-type diffuse large B-cell lymphoma (DLBCL) (Zhou *et al.* 2015). Loss-of-function EZH2 mutations caused by frameshift or stop mutation premature chain termination is common in acute myeloid leukaemia (AML) and myelodysplastic syndromes (MDS) (Ernst *et al.* 2010). In addition, EZH2 loss-of-function

mutations in myeloid malignancies have been identified in Weaver syndrome, a human overgrowth condition, and the affected individuals may develop increased susceptibility to myeloid and/or other malignancies (Tatton-Brown *et al.* 2011). On the other hand, SUZ12 could function as an oncogene upon loss of its DNA-binding ability in PRC2, which leads to a disrupted gene expression pattern and further promotes proliferation and metastasis in human tumours, including ovarian cancer and non–small cell lung cancer (Zahnow and Baylin 2010, Li *et al.* 2012).

### 1.2.5 ATP-dependent chromatin-remodelling factors

ATP-dependent chromatin remodellers utilise the energy from ATP hydrolysis to drive a DNA translocase, resulting in sliding or eviction of the nucleosomes (Becker and Workman 2013). The chromatin remodelling complexes can be classified based on their catalytic subunits (ATPases), these include: the SWI/SNF complex, with core subunits Brg1 and Brm; and the nucleosome remodelling and deacetylase (NuRD) complex, with core subunit Mi-2 (chromodomain-helicase-DNA-binding protein 4, CHD4) (Figure 1. 5). During DNA transcription, the chromatin remodelling factors are involved in the replacement of the canonical histones as well as their variants (Henikoff *et al.* 2004).

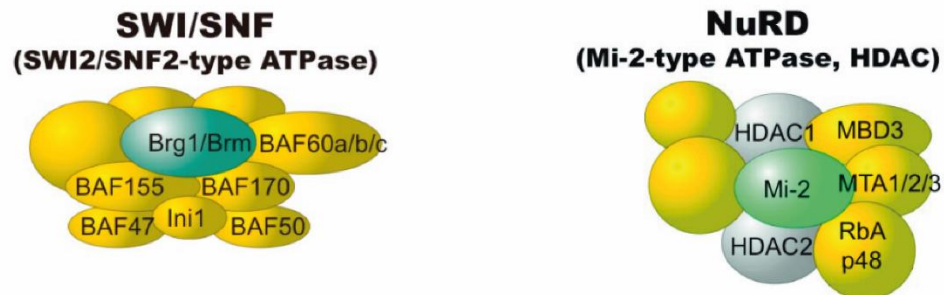


**Figure 1. 5: Two groups of chromatin remodelling complexes.** SWI/SNF complex with core subunits Brg1 and Brm; NuRD complex with core subunit Mi-2 (CHD4). (Figure modified based on Kato, Inoue, and Youn 2010.)

#### 1.2.5.1 BRG1 and BRM

The SNF2 subfamily is involved in gene regulation. In *S. cerevisiae*, 5% of the genes are modulated by SNF2, either for activation or repression (Sudarsanam *et al.* 2000). The mammalian homologues BRG1 and BRM both participate in the SWI/SNF chromatin remodelling complexes (Hohmann and Vakoc 2014).

The BRG1 and BRM subunits can be found in the BAF complex (SWI/SNF-A), the neural progenitor BAF (npBAF) complex and the neuron BAF (nBAF) complex (Olave *et al.* 2002, Becker and Workman 2013, Staahl and Crabtree 2013, Hohmann and Vakoc 2014); whereas the PBAF (SWI/SNF-B) complex and ESC BAF (esBAF) complex only contain BRG1 (Ho *et al.* 2009, Becker and Workman 2013).

It has been suggested that BRG1 and BRM contribute to various cancers as well as genetic modulation in the CNS. For example, reduced expression of Brg1 and Brm have been found in human non-small cell lung cancer (Reisman *et al.* 2003), whereas BRG1 plays essential roles in the maintenance and propagation of leukaemia (Buscarlet *et al.* 2014). BRG1 and calcium-responsive transactivator (CREST) form a complex in the active neurons, regulating promoter activation by orchestrating a calcium-dependent release of a repressor complex and recruitment of an activator complex. On the contrary, in resting neurons, the transcription of a proto-oncogene (*c-fos*) is inhibited by BRG1-dependent recruitment of a phospho-Rb-HDAC repressor complex (Qiu and Ghosh 2008).

Finally, BRG1 interacts with the H3.3 chaperone HIRA complex preferentially at the active promoters and enhancers (Pchelintsev *et al.* 2013). Its interaction with the HIRA complex might direct and modulate histone chaperone activity.

#### **1.2.5.2 The CHDs**

The CHD subfamily includes CHD1, CHD2, CHD3 and CHD4. The CHD proteins contain chromatin organisation modifier domains as well as DNA binding domains.

CHD1 is required for H3.3 HIRA associated-deposition into the male pronucleus during early embryonic development (Konev *et al.* 2007). Meanwhile, CHD2 knockdown *in vitro* prevents H3.3 deposition at the differentiation-dependent genes and inhibits myogenic gene activation (Harada *et al.* 2012). The same work also suggested that CHD2 may be associated with H3.3 chaperones (Harada *et al.* 2012). Furthermore, the H3.3 chaperone complex DAXX/ATRAX interacts with the epigenetic regulator HDACII (Hollenbach *et al.*, 2002), suggesting a potential histone exchange

pathway, where the chromatin remodelling complex take part in H3.3 deposition and eviction along with histone chaperones.

Moreover, CHD4 is the main component of the NuRD complex, and plays an important role in epigenetic control of transcriptional repression (Kehle *et al.* 1998). The two PHD zinc fingers in CHD4 are H3-binding modules. The PHD zinc fingers can bind H3 at its N-terminus, with one finger at H3 me-Lys and another at H3K9me3 (Mansfield *et al.* 2011). Moreover, the *Drosophila* hortholog of CHD3/CHD4, dMi-2, interacts with the D-Box repression domain of hunchback, a protein required for the repression of homeotic genes (Kehle *et al.* 1998). This ability of repressing homeotic genes can be abrogated by point mutations in the ATPase domains of Mi-2, demonstrating the importance of ATP-dependent remodelling in transcriptional repression.

### **1.3 H3.3 and chaperone DAXX in neurodevelopment, ageing and disease**

#### **1.3.1 H3.3**

##### **1.3.1.1 H3.3 in neurodevelopment, brain homeostasis and ageing**

Studies have suggested that H3.3 turnover may regulate transcriptional identity and plasticity in the CNS. In detail, H3.3 modulates the neuronal- and glial-specific genetic expression patterns in both embryonic and adult neurons (Michod *et al.* 2012, Maze *et al.* 2015). Moreover, H3.3 is enriched in the post-mitotic cells, and is crucial for maintaining and regulating chromatin organisation. In mice, H3.3 accumulates progressively in the somatic tissues and brain tissues with age, and reaches near complete replacement of its canonical H3.1 and H3.2 at the age of 18 months to 24 months (Maze *et al.* 2015, Tvardovskiy *et al.* 2017). Regardless of the H3.3 occupancy threshold, the H3.3-containing nucleosomes retain their dynamic turnover in adulthood and play essential roles in neuronal plasticity and cognition in a PTM-independent manner (Michod *et al.* 2012, Wenderski and Maze 2016).

H3.3 deficiency has been reported in several psychiatric disorders. In detail, H3.3 downregulation in mouse hippocampus results in impaired long-term memory, suggesting its significant function in cognition development. H3.3 expression levels are increased in the nucleus accumbens (NAc, part of the cognitive processing region related to motivation and reward) of human

patients with major depressive disorder (MDD). Moreover, the downregulation of H3.3 in mice presenting chronic social stress resulted in improved depressive-associated behaviours (Lepack *et al.* 2016). Last but not the least, it has been indicated that H3.3 protects against neurodegenerative disorders such as Huntington, Alzheimer and Parkinson disease, potentially through transcriptional silencing of the repetitive elements via its chromatin turnover in adult brain cells (Wenderski and Maze, 2016).

The study of Piazzesi and colleagues on H3.3 in *Caenorhabditis elegans* has shown a connection between H3.3 loss-of-function and impaired longevity (Piazzesi *et al.* 2016). In detail, the insulin/IGF-1 signalling pathway is one of the prominent lifespan pathways. In *C. elegans*, mutated IGF-1 gene *Daf-2* leads to increased health and elongated lifespan, and this process is mediated by the transcription factor *Daf-16*. In addition, *Daf-16* deletion completely abrogates the long-living phenotype, and loss of H3.3 in *C. elegans* with *Daf-2*–increased-lifespan results in reduced longevity. Piazzesi *et al.* provide insights into the H3.3-regulating, longevity-improving transcriptional programmes, suggesting the potential implications of H3.3 in the age-related processes.

#### **1.3.1.2 H3.3 in brain and bone tumours**

H3.3 is encoded by two genes: *H3F3A* and *H3F3B*, and has been implicated in human tumourigenesis. Driver mutations in the histone H3.3 variant (and to a lesser extent, the canonical H3) and/or its loading machinery have been identified in paediatric and adult glioblastoma multiforme (GBM) including diffuse intrinsic pontine gliomas (DIPG), giant-cell bone tumour and chondroblastoma (Khuong-Quang *et al.* 2012, Schwartzentruber *et al.* 2012, Sturm *et al.* 2012, Wu *et al.* 2012, Behjati *et al.* 2013).

The *H3F3A* gene is predominantly found mutated in brain tumours at two residues: the K27M (lysine 27 to methionine) mutation has been identified in paediatric thalamic and brainstem (and a small number of forebrain) GBM; G34R/V (glycine 34 to arginine/valine) has been found in cerebral hemisphere paediatric and young adolescent patients with GBM (Khuong-Quang *et al.* 2012, Schwartzentruber *et al.* 2012, Sturm *et al.* 2012, Wu *et al.* 2012) (Figure 1. 6). These two sets of mutations are associated with distinct transcription

and DNA methylation changes, and often co-exist with mutated p53 (Khuong-Quang *et al.* 2012, Yuen, Benjamin T. K. 2013).

The presence of H3.3 mutations in paediatric brain tumours suggests a possible role of this mutation during early brain development, especially in altering the NPC fate in a potential region-specific fashion (brainstem vs forebrain). In paediatric DIPG, K27M mutation is predominantly found in H3.3 and in H3.1 (Wu *et al.* 2012, Saratsis *et al.* 2014). Mechanistically, H3.3<sup>K27M</sup> mutation inhibits H3K27 trimethylation and leads to a global reduction in H3K27me3 levels (a repressive histone marker) and to neoplastic transformation (Bender *et al.* 2013, Lewis *et al.* 2013, Kallappagoudar *et al.* 2015). Epigenetically, H3K27 is an important target of the PRC2 complex (Kallappagoudar *et al.* 2015). In H3.3<sup>K27M</sup> mutants, PRC2 activities are blocked by the H3.3<sup>K27M</sup> peptide (Lewis *et al.* 2013, Venneti *et al.* 2013, Brown *et al.* 2014), possibly via stable binding to the PRC2 subunit EZH2 (Chan *et al.* 2013, Lewis *et al.* 2013). Pathania *et al.* recently reported that the combination of H3.3<sup>K27M</sup> mutation and Trp53 (transformation related protein 53) loss in mouse embryo leads to high-grade tumour lesions (Pathania *et al.* 2017). Their data also support an embryonic origin of the H3.3<sup>K27M</sup>-driven tumourigenesis.

The mechanisms underlying the function of H3.3<sup>G34R/V</sup> mutations in GBM remain unclear, and is under ongoing investigation by the Salomoni group jointly with Jabado's group in Montreal, Canada. So far, it has been suggested the H3.3<sup>G34R/V</sup> mutation alters H3K36me3 levels, thus disrupting gene expression and potentially leading to neoplasm (Lindroth and Plass 2013, Bano *et al.* 2017).

Finally, mutations in *H3F3A* as well as *H3F3B* have also been suggested to drive bone tumours. The H3.3<sup>G34W/L</sup> (glycine 34 to tryptophan/leucine) mutations of *H3F3A* have been predominantly found in giant cell tumour of bone, while K36M mutation in *H3F3B* characterises the chondroblastomas (Behjati *et al.* 2013).

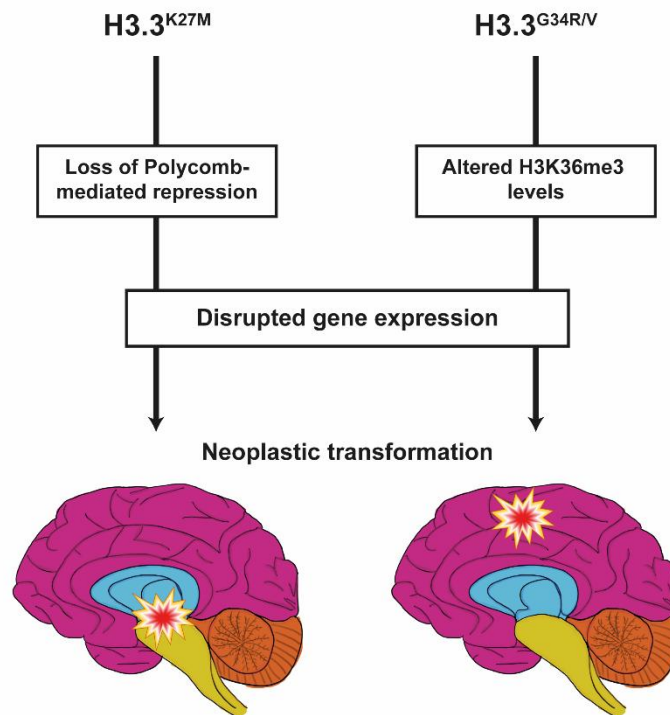


**Figure 1. 6: Potential effects of H3.3 mutations in the tumourigenic process of paediatric high-grade gliomas.** The H3.3<sup>K27M</sup> mutation blocks the polycomb-mediated target genes repression, and results in the development of glioma in the thalamus and the brainstem. The H3.3<sup>G34R/V</sup> mutation decreases H3K36 trimethylation, disrupts normal gene expression, and promotes the formation of paediatric glioblastomas in the cortex.

### 1.3.2 The H3.3 chaperone DAXX

#### 1.3.2.1 DAXX as a transcriptional regulator

DAXX is an inhibitor of Pax3, a member of the homeodomain family of transcription factors, by interacting with the protein and repressing its transcriptional activity (Hollenbach *et al.* 1999). This indicates that DAXX not only represses basal transcription, but also inhibits transcriptional activation by interacting with the DNA-binding transcription factors.

On the other hand, DAXX regulates events such as chromosome segregation and mitotic progression during interphase via interaction with centromere protein C (CENP-C) (Pluta *et al.* 1998). In addition, DNA methyltransferase 1 has been identified as another Daxx-interacting protein in mice, indicating the involvement of Daxx in gene silencing (Michaelson *et al.* 1999). Notably, similar embryonic lethality phenotypes have been found in mice lacking Daxx or DNA methyltransferase 1 (Li *et al.* 1992, Hollenbach *et al.* 2002). Furthermore, it has been suggested that promyelocytic leukaemia protein

(PML) interacts with DAXX *in vivo*, where they are localised at the PML nuclear bodies (PML-NBs), thus inhibiting DAXX transcriptional repression activity (discussed in Section 1.3.2.4).

### **1.3.2.2 DAXX in apoptosis and ageing**

DAXX was first identified as a member of an apoptosis pathway, as it modulates the cytosolic domain of Fas by activating its downstream c-Jun NH<sub>2</sub>-terminal kinase (JNK) signalling pathway through its interaction with apoptosis signal-regulating kinase 1 (ASK1). DAXX overexpression in human cells results in the activation of Fas and in the increased apoptosis response (Chang *et al.* 1998). In mice, Daxx knockout and deficiency lead to extensive apoptosis and embryonic lethality (Michaelson *et al.* 1999), suggesting a pro-survival role during development.

In *D. melanogaster*, the DAXX homolog protein DLP (DAXX-like protein) is involved in regulating the transcription of the pro-apoptotic gene *Ark*, and it interacts with Dmp53 (p53 homolog in mammals) and affects longevity (Bodai *et al.* 2007). In detail, DLP binds to Dmp53 at its C-terminus, and mutant DLP fails to interact with Dmp53 and leads to Dmp53 overexpression. This indicates a gene suppressor function of DAXX on the *Drosophila* p53.

### **1.3.2.3 DAXX and tumorigenesis**

Both the DAXX and ATRX proteins have been reported mutated in various tumours, including glioma, pancreatic neuroendocrine tumours (pNETs) and neuroblastoma (Heaphy *et al.* 2011, Cheung *et al.* 2012, Liu *et al.* 2014). The majority of ATRX/DAXX mutations are loss-of-function mutations, and are associated with chromosome instability and the alternative lengthening of telomeres (ALT) (Heaphy *et al.* 2011, Liu *et al.* 2014).

*In vivo* study on mice model of Atrx-deficient glioblastoma has shown that lack of Atrx is associated with reduced survival rate, and is linked to an increased mutation rate at the single-nucleotide variant level (Koschmann *et al.* 2016). Moreover, in mouse tumours, Atrx deficiency results in impaired non-homologous end joining (NHEJ), which is involved in repairing DNA DSB (Koschmann *et al.* 2016).

In addition, DAXX overexpression is linked to oncogenic effects on ovarian surface epithelial cells by interacting with PML and promoting the

transformation capacity and resistance to radiotherapy (Pan *et al.* 2013). Moreover, studies on DAXX expression in patients with oesophageal squamous cell carcinoma (ESCC) have revealed increased DAXX expression levels correlate directly with the patient survival rate (Ko *et al.* 2018).

#### **1.3.2.4 DAXX and PML-NBs**

The PML-NBs, also known as PML oncogenic domains (PODs) and nuclear domain (ND10), are recognised as tumour suppressors. It forms a multi-protein structure to accumulate proteins for PTMs. It also mediates the nuclear events responding to cellular stresses, including DNA damage, apoptosis, senescence and angiogenesis (Bernardi and Pandolfi 2007).

The H3.3 chaperone Daxx is associated with the PML-NBs during its transition to the pericentric heterochromatin, via binding to the C-terminus of SUMOylated PML. The accumulation of this complex involves Atrx recruitment and is cell cycle-dependent (Ishov *et al.* 2004). The PML-NBs/Daxx complex associates with Atrx through the binding to Daxx. When the cell undergoes the S phase/cell division, Daxx disassociates from the PML-NBs and accumulates toward the heterochromatin.

PML-NBs are not only required for the localisation of DAXX, but also play a critical role in DAXX transcriptional repression activities. In the absence of Pml, Daxx is concentrated at the condensed chromatin, where genetic transcriptions are repressed, indicating Daxx transcriptional repression activity at these gene sites (Li *et al.* 2000). In the case of increased Pml expression level, Pml recruits Daxx from the condensed chromatin to the PML-NBs, where Daxx transcriptional repression activities are inhibited (Li *et al.* 2000). Moreover, the absence of PML-NBs results in impaired DAXX pro-apoptotic activity, and a diffused nuclear pattern (Zhong *et al.* 2000).

Notably, in acute promyelocytic leukaemia (APL), PML-NBs are disrupted by the oncogene *PML-retinoic acid receptor (RAR)  $\alpha$* , and DAXX is delocalised from the complex. In detail, nearly all APL cases are characterised by the chromosomal translocation between the *PML* gene on chromosome 15 and the *RARA* gene on chromosome 17, and this creates the oncogenic fusion protein PML-RAR $\alpha$ . The PML-NB structure is disrupted in t(15;17) translocated APL cells, and PML is delocalised from the NBs to aberrant

nuclear micro-speckled structures (PML-RAR $\alpha$  bodies). Furthermore, as PML is essential for DAXX localisation into the NBs and its pro-apoptotic activity, loss of Pml in mice results in the delocalisation of Daxx from the PML-NBs in APL cells and in impaired Daxx-induced apoptosis in primary keratinocytes (Zhong *et al.* 2000). These findings suggest that PML and DAXX interaction forms a novel PML-NB-dependent apoptosis pathway, with applications in tumour suppression.

Drane *et al.* have shown that DAXX carries the PML-NBs to H3.3, where the PML-NBs associate with H3.3 for its coupling at the condensed chromatin (Drane *et al.* 2010). These findings suggest that PML may regulate H3.3 loading onto the chromatin, associating with DAXX. In addition, loss of *Pml* in mice led to increased NPC proliferation levels as well as altered composition of the NPC cell subtypes in the developing neocortex (Regad *et al.* 2009). Moreover, *Pml* loss also resulted in impaired cell differentiation and reduced cortical thickness, while a smaller brain was observed (Regad *et al.* 2009). These indicate Pml modulation of neurogenesis during brain development.

#### **1.4 Outstanding questions, hypotheses and aims**

Despite a number of studies reporting the interaction of H3.3 chaperones with epigenetic regulators, little is known about its interactome in the nervous system, particularly in neural progenitor cells, which can act as cells of origin of brain cancer in children and adults. In this chapter, we hypothesise that DAXX interaction with other epigenetic regulators affects and/or regulates H3.3 loading. We cannot exclude the possibility that some of these interactions could affect chromatin in a H3.3-independent manner. The DAXX interactome in neural cells may change upon expression of GBM tumour drivers (e.g. H3.3 mutant proteins) and during oncogenic transformation, thus contributing to the establishment of cancer-associated chromatin changes. More generally, association with other chromatin modifiers can affect DAXX localisation in the genome as well as its ability to load H3.3. With respect to candidate epigenetic regulators that can interact with DAXX, given the interaction between ATRX and non-coding RNA in regulating PRC2 function, it is plausible that DAXX also could interact with RNA and/or RNA-interacting proteins and affect PRC2

complex function. Moreover, other chromatin remodelling factors, for example BRG1/BRM and CHD, are potential DAXX/H3.3-interacting candidates.

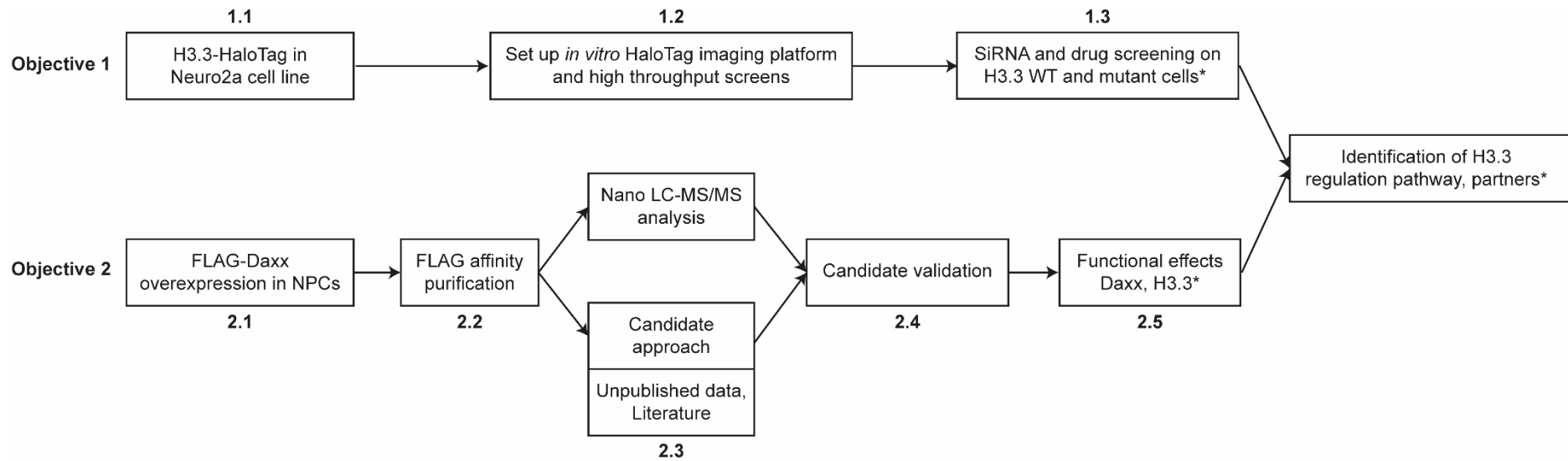
As a complementary and equally unbiased approach, we reasoned that it would be important to develop an imaging platform for visualising H3.3 deposition in the CNS. Through this imaging platform, siRNA and drug screenings can be run to identify novel regulators of H3.3 and its mutants.

## **1.5 Aims**

The main aims of this research are:

- 1) To develop an automated platform for visualising H3.3 loading in a robust mammalian CNS cell line
- 2) To study the H3.3 chaperone Daxx interactome in the CNS

## 1.6 Project Scheme



\*future perspectives

## **Chapter 2**

### **Material and Methods**

## 2. Material and Methods

### 2.1 Materials

#### 2.1.1 Plasmids

Table 2. 1 Plasmids

a/a	Name	Construct	Source
1	HaloTag	G771A Promega, able to produce a fusion protein at its N-terminal	Promega
2	CMV-H3.3-YFP	<i>Drosophila</i> H3.3	Addgene
3	CMV-dH3-YFP	<i>Drosophila</i> H3 (dH3)	Addgene
4	H3.3-HaloTag	<i>Drosophila</i> H3.3 sequence fused at HaloTag N-terminal	Generated
5	dH3-HaloTag	<i>Drosophila</i> H3 sequence fused at HaloTag N-terminal	Generated
6	pLenti-PGK-Neo-DEST w531-1	Lentivector construct plasmid	Addgene
7	pCMV-G	Envelope plasmid of pHIV-dTomato lentivirus	Addgene
8	pCMV-HIV-1	Packaging plasmid of pHIV-dTomato lentivirus	Addgene
9	H3.3-HaloTag-pLenti-PGK-Neo-DEST w531-1	Lentivector construct plasmid with fusion <i>Drosophila</i> H3.3 and HaloTag sequence	Generated by Michod group
10	dH3-HaloTag-pLenti-PGK-Neo-DEST w531-1	Lentivector construct plasmid with fusion <i>Drosophila</i> H3 and HaloTag sequence	Generated by Michod group
11	Gene Art Daxx WT	Mouse Daxx wild type	Salomoni group
12	FLAG-Daxx	FLAG sequence at N-terminal of Daxx sequence in Gene Art Daxx WT plasmid	Generated
13	pHIV-dTomato	Lentivector construct plasmid	Addgene
14	FLAG-Daxx-pHIV-dTomato	pHIV-dTomato with FLAG-Daxx sequence	Generated

## 2.1.2 Primers

### 2.1.2.1 PCR

The PCR primers were generated by and purchased from Invitrogen (Life Technologies). Lyophilized oligos were resuspended in the appropriate volume of sterile nuclease-free H<sub>2</sub>O to yield a stock of 100 μM and were thoroughly mixed by vortexing. The primers were further diluted using sterile nuclease-free H<sub>2</sub>O to a working concentration of 5 μM and stored at -20°C.

**Table 2. 2 Primers for PCR.**

a/a	Gene	Forward (5'-3')	Reverse (5'-3')
1	FLAG-Daxx	AAAGGATCCGCGGCCGCGCCA CCATGGACTACAAGGACGACGA TGACAAGGCCACCGATGACAGC ATCATTGTA	TAAGTTCAACTTC TTCTT
2	H3.3-HaloTag	AAAGAATTGCGCCACCATGGCAC GTACCAAGCAA	AAAGAATTGCGCC CGCTCGCCACG
3	dH3-HaloTag	AAAGAATTGCGCCACCATGGCTC GTACCAAGCAA	AAAGAATTGCGGTG GCGACCGGCGG

### 2.1.2.2 Real-time PCR (qPCR)

The qPCR primers were generated by and purchased from Invitrogen (Life technologies). Lyophilized oligos were resuspended in the appropriate volume of sterile nuclease-free H<sub>2</sub>O to yield a stock of 100 μM and were thoroughly mixed by vortexing. The primers were further diluted using sterile nuclease-free H<sub>2</sub>O to a working concentration of 5 μM and stored at -20°C.

**Table 2. 3 Primers for qPCR.**

a/a	Gene	Forward (5'-3')	Reverse (5'-3')
1	Hira	GGATTCTGGGAAGGTTGTG A	TCATCTCCCCCAGAAGCTAA
2	Daxx	AGCAGTAACTCCGGTAGTA GGAAG	AGGAACGGAACCACCTCAG
3	Gapdh	TCCACCACCCTGTTGCTGTA	ACCACAGTCCATGCCATCAC
4	Actin	TATAAAACCCGGCGGCGCA	TCATCCATGGCGAACTGGTG

### 2.1.3 NPCs and cell lines

E13.5 NPCs: NPCs isolated from E13.5 mouse embryo cortex

HEK293T: Human embryonic kidney 293T cells

NIH3T3: Mouse embryonic fibroblast cells

Neuro2a (ATCC, CCL): Mouse neuroblastoma cells

## 2.1.4 Antibodies

### 2.1.4.1 Antibodies for immunoblotting (western blotting)

**Table 2. 4 Primary antibodies for western blotting.**

a/a	Primary Antibody	Species	Dilution	Category No	Supplier
1	ATRX	Rabbit	1:200	A0308	Santa Cruz
2	$\alpha$ -Tubulin	Mouse	1:30,000	T5168	Sigma
3	$\beta$ -Actin	Mouse	1:5,000	A5441	Sigma
4	Brg-1	Mouse	1:1,000	sc-17796X	Santa Cruz
5	Brm	Rabbit	1:1,000	ab15597	Abcam
6	CHD4/Mi-2 beta	Rabbit	1:1,000	39289	Active Motif
7	CPSF2	Rabbit	1:2,000	NB100-79823	Novus Biologicals
8	DAXX (M-112)	Rabbit	1:500	sc-7152	Santa Cruz
9	EZH2 (AC22)	Mouse	1:1,000	3147	Cell Signalling
10	FLAG	Rabbit	1:5,000	F-7425	Sigma
11	Anti-Histone H3	Rabbit	1:50,000	ab1791	Abcam
12	H3.3	Rabbit	1:1,000	09-838	Millipore
13	Anti-HaloTag	Mouse	1:1,000	G9211	Promega
14	Hira	Mouse	1:20	Homemade: WC119, 19, 15 and 117	Peter Adam's group (University of Glasgow)
15	pH3 (Ser10)	Rabbit	1:500	9716	Cell Signalling
16	NET1	Rabbit	1:1,000	12740-1-AP	Proteintech
17	Human TR4/NR2C2	Mouse	1:500	PP-H0107B-00	R&D Systems
18	SUZ12 (P15)	Goat	1:200	sc-46264	Santa Cruz

**Table 2. 5 Secondary antibodies for western blotting.**

a/a	Secondary Antibody	Dilution	Category No	Supplier
1	Goat Anti-Rabbit IgG, DyLight 800	1:5,000	35571	Thermo Scientific
2	Goat Anti-Mouse IgG, DyLight 680	1:5,000	35518	Thermo Scientific
3	ECL Anti-Rabbit IgG, Horseradish Peroxidase linked whole antibody (from donkey)	1:5,000	NA934V	GE Healthcare UK Limited
4	ECL Anti-Mouse IgG, Horseradish Peroxidase linked whole antibody (from sheep)	1:5,000	NA931V	GE Healthcare UK Limited
5	Polyclonal Rabbit Anti-Goat Immunoglobulins/HRP	1:2,000	P0160	Dako

### 2.1.4.2 Antibodies for immunofluorescence (IF)

**Table 2. 6 Primary antibodies for immunofluorescence studies.**

a/a	Antibody	Species	Dilution	Category No	Supplier
1	HaloTag® R110Direct™ Ligand	N/A	1:1,000	G3221	Promega
2	HaloTag® TMR ligand	N/A	1:1,000	G8251	Promega
3	HaloTag® Oregon Green ligand	N/A	1:200	G2801	Promega
4	DAXX	Mouse	1:100	ab492687	Abcam
5	FLAG	Rabbit	1:1,000	F-7425	Sigma

**Table 2. 7 Secondary antibodies for immunofluorescence studies.**

a/a	Antibody	Dilution	Category No	Supplier
1	Anti-Rabbit IgG Alexa Flour 488 (from goat)	1:1,000	A11008	Life Technologies
2	Anti-Mouse IgG Alexa Flour 568 (from goat)	1:1,000	A11019	Life Technologies

### 2.1.5 siRNA oligonucleotides

The siRNA oligonucleotides were generated by and purchased from ThermoFisher Scientific. The dried oligonucleotides were resuspended in an appropriate volume of RNase-free H<sub>2</sub>O to yield a stock of 100 µM and were thoroughly mixed by vortexing, and stored at -20°C.

**Table 2. 8 siRNA oligonucleotides.**

a/a	siRNA	Category No	Supplier
1	<i>Hira</i> siRNA I	439077/n426232	Thermo Fisher Scientific
2	<i>Hira</i> siRNA II	439077/s67545	Thermo Fisher Scientific
3	<i>Daxx</i> siRNA I	AM16708/61220	Thermo Fisher Scientific
4	<i>Daxx</i> siRNA II	AM16708/160479	Thermo Fisher Scientific
5	<i>Gapdh</i> siRNA	4390849	Thermo Fisher Scientific
6	Scramble siRNA	4390843	Thermo Fisher Scientific

## 2.1.6 Materials for immunoprecipitation (IP)

Table 2. 9 Materials for immunoprecipitation.

a/a	Material	Category No	Supplier
1	Anti-FLAG <sup>®</sup> M2 Affinity Gel	A2220	Sigma
2	Anti-FLAG <sup>®</sup> M2 Magnetic Beads	M8823	Sigma
3	Benzonase nuclease	E1014-5KU	Sigma
4	Tissue grinders/cell homogeniser	k885300/0007	Kimble Chase
5	FLAG peptide	F3290	Sigma
6	Pierce <sup>™</sup> Protein G Plus agarose beads	22851	Thermo Fisher Scientific

## 2.1.7 Buffer Recipes

**5x Polyethylene glycol (PEG) (pH 7.2):** 50 mM PEG, 0.41 M NaCl, and 0.2% 1 M Tris (pH 7.5).

**2X HEPES Buffer (pH 7.05):** 280 mM NaCl, 10 mM KCl, 1.5 mM Na<sub>2</sub>HPO<sub>4</sub>, 12 mM D(+)-Glucose Monohydrate, and 50 mM HEPES.

**1x Tris-acetate-EDTA buffer (TAE):** 40 mM Trisma Base, 0.001% (v/v) Acetic acid, and 1 mM EDTA (pH 8).

**5x Laemmli buffer:** 10% (w/v) SDS, 50% (w/v) Glycerol, 0.125% (w/v) bromophenol blue, 250 mM Tris (pH 6.8), and 2 mM 2-mercaptoethanol.

**1x SDS-PAGE running buffer:** 0.186 M Glycine, 0.02 M Trisma Base, and 0.15% (v/v) SDS.

**1x Transfer buffer:** 0.186 M Glycine; 0.02 M Trisma Base, and 20% (v/v) Methanol.

**Phosphate-buffered saline (PBS):** 137 mM NaCl, 2.7 mM KCl, 8 mM Na<sub>2</sub>HPO<sub>4</sub>, and 2 mM KH<sub>2</sub>PO<sub>4</sub>.

**PBS-Tween 20:** 1x PBS (pH 7.4) supplemented with 0.1% (v/v) Tween 20.

**7% Polyacrylamide gel (18 ml):** 9.0 ml H<sub>2</sub>O, 4.2 ml 30% Acrylamide mix, 4.5 ml 1.5 M Tris (pH 8.8), 90 µl 20% SDS, 180 µl 10% APS, and 18 µl TEMED.

**15% Polyacrylamide gel (20 ml):** 4.7 ml H<sub>2</sub>O, 10.0 ml 30% Acrylamide mix, 5.0 ml 1.5 M Tris (pH 8.8), 100 µl 20% SDS, 200 µl 10% APS, and 8 µl TEMED.

## **2.2 Methods**

### **2.2.1 Molecular biology**

#### **2.2.1.1 Cloning (restriction enzyme digestion and ligation)**

The RT-PCR of the insert fragments were prepared with a mix of 5  $\mu$ l 10 nM forward and reverse primers, 1  $\mu$ l PCR-grade nucleotide mix, 2.5  $\mu$ l 10 $\times$  PCR buffer + MgCl<sub>2</sub>, 100–300 ng template, 0.5  $\mu$ l FastStart Taq DNA Polymerase, and H<sub>2</sub>O to a total volume of 25  $\mu$ l. PCR settings were set according to the PCR fragment size and annealing temperature. The PCR products were electrophoresed on an agarose gel; appropriate-size bands were cut and collected, DNA was extracted and purified, and the PCR products were either used directly for restriction enzyme digestion and ligation or stored at -20°C for future use.

Restriction enzyme digestion was performed on both the insert fragment (PCR product) and the backbone. For the inserts reaction, 2  $\mu$ l 10 $\times$  reaction buffer and 1  $\mu$ l enzyme(s) were mixed with PCR product for a total volume of 20  $\mu$ l. The control reaction mix contained 10  $\mu$ l PCR product and 10  $\mu$ l H<sub>2</sub>O. For the backbone reaction, 3  $\mu$ g plasmid was mixed with 1  $\mu$ l enzyme(s) and 2  $\mu$ l 10 $\times$  reaction buffer. Water was added to increase the total volume to 20  $\mu$ l. The control reaction mix contained 3  $\mu$ g backbone plasmid and water to a total reaction volume of 20  $\mu$ l. The restriction enzyme digestion mix was incubated in a 37°C water bath for 2 hours. After incubation, the backbone was dephosphorylated with alkaline phosphatase in a reaction mixture of 17  $\mu$ l Backbone, 1  $\mu$ l rAPid Alkaline Phosphatase, and 2  $\mu$ l 10 $\times$  buffer for 15 minutes at 37°C, followed by 2-minute inactivation at 75°C. Both the inserts and backbones were electrophoresed on an agarose gel; appropriate-size bands were cut and collected, and DNA was extracted and purified. The 10- $\mu$ l ligation mix was prepared as follows: for the experimental reaction, a mixture of 3.5  $\mu$ l Insert, 0.5  $\mu$ l backbone, 1  $\mu$ l T4 DNA Ligase and 5  $\mu$ l 2 $\times$  Rapid Ligation Buffer were prepared; for the control reaction, a mixture of 3.5  $\mu$ l elution buffer, 0.5  $\mu$ l backbone, 1  $\mu$ l T4 DNA Ligase and 5  $\mu$ l 2 $\times$  Rapid Ligation Buffer were prepared. The ligation mixes were incubated at room temperature for 30 minutes, and the products were used for *Escherichia coli* transformation.

### **2.2.1.2 Transformation**

Top10 Chemical competent cells were thawed on ice and mixed with 10 µl DNA ligation mix. The tubes were mixed by gentle tapping. The cells were incubated on ice for 30 minutes, and heat-shocked for 30 seconds in a 42°C water bath, followed by 2-minute incubation on ice. The cells were then mixed with 250 µl room-temperature S.O.C. medium and shaken at 225 rpm (37°C) for 1 hour. All cells were plated on LB agar plates with the corresponding antibiotic selection. The plates were incubated overnight in a 37°C incubator.

### **2.2.1.3 Miniprep, sequencing, and Maxiprep**

#### 1) Miniprep with JetStar 2.0 plasmid purification kits

Several colonies were picked from the LB agar plates for further culture in 5 ml LB media with antibiotic selection and incubated overnight. Bacterial overnight culture (4 ml) was pelleted by centrifugation at 8,000 rpm for 3 minutes at room temperature (15–25°C). The pellet was resuspended in 250 µl Cell Resuspending Buffer and transferred to a microcentrifuge tube. The same volume of Cell Lysis Buffer (250 µl) was added to the cells and mixed thoroughly by inverting the tube 6 times. The cells were lysed for less than 5 minutes. Neutralisation Buffer (350 µl) was added to the lysate and mixed immediately and thoroughly by inverting the tube 6 times. The samples were centrifuged for 10 minutes at 13,000 rpm. Supernatant (800 µl) was added to a spin column by pipetting and the fluid was spun down by centrifugation for 60 seconds at 13,000 rpm. The flow-through from the column was discarded and the column was washed once with 500 µl Buffer PB. The column was centrifuged again for 60 seconds at 13,000 rpm and the flow-through was discarded. Finally, the column was washed with 750 µl Buffer PE, centrifuged for 60 seconds at 13,000 rpm and the flow-through was discarded. The spin column was centrifuged again at 13,000 rpm to remove all washing buffer. The spin column was then transferred to a clean collection tube and eluted with 20 µl Buffer EB with 1-minute incubation following 1-minute centrifugation at 13,000 rpm. The Miniprep samples were used for DNA sequencing. The extra 1 ml from the mini-culture bacteria was stored at 4°C for further expansion for Maxiprep after sequencing.

## 2) Sequencing

Plasmid sequencing was performed using the Source Bioscience Sanger sequencing service.

## 3) Maxiprep with JetStar 2.0 plasmid purification kits

Equilibration buffer (30 ml) was added to the column for equilibration. The solution in the column was drained by gravity flow. Bacterial overnight culture (200 ml) was pelleted via centrifugation at 12,000  $\times g$  for 3 minutes and medium was aspirated. The cell pellet was resuspended in 10 ml Cell resuspending buffer. The same amount (10 ml) of Lysis buffer was added and mixed by gently inverting the tube. The cells were lysed at room temperature for 5 minutes. Precipitation buffer (10 ml) was then added to the mix, and the tube was immediately inverted 6 times and centrifuged for 10 minutes at room temperature at 13,000  $\times g$ . The supernatant was collected and loaded onto the column, and the solution was drained by gravity flow. The column was washed once with 60 ml Wash buffer; DNA was eluted with 15 ml Elution buffer. The Elution buffer containing DNA was collected in a clean 50 ml tube by gravity flow. Isopropanol (10.5 ml) was mixed into the DNA elute, followed by centrifugation at 4°C for 30 minutes at 13,000  $\times g$ . The supernatant was aspirated, and the DNA pellet was washed once with 5 ml 70% ethanol. The tube was centrifuged again under the same conditions for another 5 minutes. After the supernatant had been aspirated, the pellet was air-dried for 10 minutes and resuspended in 200  $\mu$ l water. The DNA/plasmid was quantified using a NanoDrop spectrophotometer, aliquoted and stored at -20°C.

## 2.2.2 Cell culture

### 2.2.2.1 Calcium phosphate transfection for virus particle production

#### 2.2.2.1.1 Lentiviral production

On day 0 (the day before virus production),  $6 \times 10^6$  HEK293T cells were seeded in a 15-cm dish containing 20 ml complete Dulbecco's modified Eagle's medium (DMEM, 31966-021 Gibco) containing 10% fetal bovine serum (FBS) and 1% penicillin/streptomycin (Pen/Strep) at 37°C. Two cell plates were prepared for each type of viral production. On the morning of the next day, for each viral production, DNA/calcium mix was prepared in 900  $\mu$ l H<sub>2</sub>O with 7.2  $\mu$ g pCMV-G vector, 15.6  $\mu$ g pCMV-HIV-1 vector, 24  $\mu$ g desired

plasmid DNA, and 100  $\mu$ l 2.5 M  $\text{CaCl}_2$ . The DNA/calcium solution was mixed by pipetting up and down 10 times, and equilibrated for 20–30 minutes at room temperature. Meanwhile, 20  $\mu$ l chloroquine was added to the cell culture medium, and the cell plates were incubated in a 37°C incubator for 10 minutes. Pre-warmed 37°C 2x HEPES buffer (1 ml) was added to the DNA/calcium solution, and mixed immediately 5 times by pipetting the solution up and down. The DNA-HEPES mixture was incubated for 1 minute and added to the culture medium. The cell plates were rocked left to right and up and down twice, and incubated at 37°C for 8 hours.

After 8-hour incubation, the transfection medium was replaced with normal culture medium containing Pen/Strep. The cells were incubated at 37°C for 48 hours.

On day 3, the supernatant was collected and centrifuged at 3000  $\times g$  for 15 minutes to remove cells and debris. The supernatant was filtered through a 0.45- $\mu$ m PVDF filter to further eliminate cellular debris. One volume of cold, sterile 5x PEG for every 4 volumes of supernatant was mixed with the supernatant by inverting the tube and was refrigerated overnight. On day 4, the supernatant/PEG mixture was centrifuged at 1500  $\times g$  for 30 minutes at 4°C. The supernatant was aspirated and the residual PEG solution was spun down by centrifugation at 1500  $\times g$  for 5 minutes. All traces of fluid were removed by aspiration, and the lentiviral pellets were resuspended in 1:50 dilution of the original volume in 1x PBS. The lentivirus was aliquoted in PCR Eppendorf tubes (20  $\mu$ l each) and stored at -80°C.

#### **2.2.2.1.2 Lentivirus titration (pHIV-dTomato and FLAG-Daxx-pHIV-dTomato) for dTomato expression**

On the day before titration, 70,000 HEK293T cells per well were plated in a 24-well plate with 500  $\mu$ l DMEM containing 10% FBS. The cells were prepared as follows and were incubated at 37°C overnight:

One well: Count cells prior to transduction

One well: Untransduced control

Six wells for each virus: Serial dilutions

The next day, the cells in one well were counted, and 10-fold serial dilutions of  $10^{-2}$  to  $10^{-7}$  were prepared in 200  $\mu$ l DMEM containing 10% FBS. For the 6

virus transfection wells, the medium was aspirated and replaced with 200  $\mu$ l diluted virus. The cells were incubated at 37°C overnight.

At 24 hours post-transduction, the cell medium was replaced with fresh medium, and incubated for another 48 hours. dTomato expression was visualised under Zeiss Axio Observer Z1 with Apotome, and 3 images were obtained under 10 $\times$  magnification for each well. The dTomato-positive (dTomato<sup>+</sup>) cells were counted versus the total cells.

The counted dTomato<sup>+</sup>/total cell ratio between 5–20% were used to calculate the transduction titre:

$$T = \frac{(P/N)}{(D/V)}$$

T = titre

P = % dTomato<sup>+</sup> cells

N = number of cells at transduction

D = dilution factor

V = volume of viral inoculum

### **2.2.2.1.3 Lentivirus transduction (pHIV-dTomato and FLAG-Daxx-pHIV-dTomato) in NIH3T3 cells and NPCs and cell sorting**

Cells (150,000 per well) were seeded in 6-well plates containing 2 ml DMEM (10% FBS, 1% Pen/Strep) and incubated overnight at 37°C. On the second day, the medium was replaced with fresh medium 1 hour prior to transduction. The volume of virus per well was calculated at multiplicity of infection (MOI) = 7 [MOI; V = (MOI  $\times$  N<sub>cells</sub>/T)]. Empty vector (EV; pHIV-dTomato) and FLAG-Daxx (FLAG-Daxx-pHIV-dTomato) lentiviruses were mixed into the medium and added to the cells for lentiviral transfection, followed by 8-hour incubation at 37°C. After 8 hours, the medium was replaced with fresh medium, and the cells were incubated for another 48 hours.

For the transduced NIH3T3 cells, the cells were imaged after incubation under Zeiss Axio Observer Z1 with Apotome. There were up to 90% dTomato<sup>+</sup> cells versus the total cell number. The cells were collected for immunoblotting examination of FLAG and Daxx expression.

For the transduced NPCs, cell sorting was performed post-transduction. Cells (10  $\times$  10<sup>6</sup> per ml) were prepared for fluorescence-activated cell sorting (FACS).

The dTomato<sup>+</sup> cells were sorted and plated in 24-well plates and T25 flasks for further expansion. The expanded cells underwent immunoblotting for FLAG and Daxx, as well as immunoprecipitation (IP) of FLAG.

#### **2.2.2.1.4 Lentivirus titration (H3.3-HaloTag-pLenti-PGK-Neo-DEST w531-1 and dH3-HaloTag-pLenti-PGK-Neo-DEST w531-1) for neomycin expression<sup>1</sup>**

On the day before titration, 25,000 HEK293T cells per well were plated in 12-well plates in 1 ml DMEM containing 10% FBS. The cells are prepared as follows and were incubated at 37°C overnight:

One well: Untransduced control

Six wells for each virus: Serial dilutions

The next day, 10-fold serial dilutions of virus of 10<sup>-1</sup> to 10<sup>-6</sup> were prepared in DMEM. The cell medium was replaced with 1 ml diluted virus. The cells were incubated at 37°C overnight.

At 24 hours post-transduction, the medium was replaced with fresh medium, and the cells were incubated for another 24 hours. Neomycin G418 (2 mg/ml) was added to the medium, and the medium was changed after 2 days. After another 2 days, the cells were collected and counted.

$$\text{Titre} = \frac{\text{Number of cells in } 10^{-1} \text{ virus treatment}}{\text{Number of cells in no virus treatment} / \text{Number of cells in no neomycin treatment}} \times 100\%$$

#### **2.2.2.1.5 Lentivirus transduction (H3.3-HaloTag-pLenti-PGK-Neo-DEST w531-1 and dH3-HaloTag-pLenti-PGK-Neo-DEST w531-1) in Neuro2a cells and cell sorting<sup>2</sup>**

Neuro2a cells (150,000 per well) were seeded in 6-well plates with 2 ml DMEM (10% FBS, 1% Pen/Strep). On the second day, the medium was replaced with fresh medium 1 hour prior to transduction. The viruses were added to the Neuro2a cells and incubated for 8 hours at 37°C. Then, the medium was replaced with fresh medium, and the cells were incubated for another 48 hours at 37°C. Cells (10 × 10<sup>6</sup> per ml) were prepared for FACS: the cells were labelled with HaloTag fluorescence ligand, and HaloTag-positive cells were

---

<sup>1</sup> The lentiviruses were generated by Michod group at ICH. The following is a description of the standard procedures carried out in our laboratory.

<sup>2</sup> The cells were transduced by Michod group at ICH. The following is a description of the standard procedures carried out in our laboratory.

sorted and plated in 6-cm dishes for further expansion and immunoblotting analysis.

## **2.2.3 Biochemistry**

### **2.2.3.1 Immunoprecipitation (IP)**

#### **2.2.3.1.1 IP optimisation I**

Six million cells were plated on a 10-cm plate at 2 plates for each condition (EV and FLAG-Daxx), and the cells were incubated overnight at 37°C. The next day, the cell medium was aspirated, and the cells were washed once with 5 ml 1× PBS. Lysis buffer (500 µl: 50 mM Tris HCL [pH 7.4], 150 mM NaCl, 1 mM EDTA, 1% Triton X-100 supplemented with 1× cOmplete™ Protease Inhibitor Cocktail [11697498001 Roche], 50 mM sodium fluoride, 1 mM sodium orthovanadate) was added to each plate and incubated on ice for 30 minutes. The cells were then scraped down and collected in 1.5-ml tubes. The cell lysates were centrifuged at 12,000 ×g for 10 minutes at 4°C, the supernatants were collected and the total proteins were quantified via Bradford assay. FLAG beads resin (A2220 Sigma) (40 µl, i.e. 20 µl packed beads) were prepared via 4 washes in 500 µl lysis buffer, each followed by centrifugation at 8200 ×g for 1 minute at 4°C. Protein (500 µg) was added to the beads, and the protein/beads mix volume was topped up to 600 µl by lysis buffer. The protein/beads mix was incubated on a rotator at 4°C for 3 hours. After rotation, the beads were washed with 500 µl lysis buffer 3 times, each followed by centrifugation at 8200 ×g for 1 minute at 4°C. The immunoprecipitated protein was eluted with 45 µl Laemmli buffer (1×) at 95°C for 6 minutes. The supernatant was collected after centrifugation as the IP samples. The samples were stored at -20°C and underwent immunoblotting and silver staining analyses.

#### **2.2.3.1.2 IP optimisation II**

Fifty million fresh cell pellets were collected on ice and washed once with 1× PBS. The cells were then lysed with 500 µl isotonic buffer (20 mM Tris [pH 7.5], 100 mM NaCl, 5 mM MgCl<sub>2</sub>, 10% glycerol, 0.2% NP-40 supplemented with 1× cOmplete™ Protease Inhibitor Cocktail [11697498001 Roche], 50 mM sodium fluoride, 1 mM sodium orthovanadate) and incubated on ice for 10 minutes. The lysate was homogenised 10 times, followed by ice incubation for

10 minutes. This procedure was repeated 5 times until more than 90% of the cells were stained with Trypan blue. The nuclei were spun down by centrifugation at 11,000  $\times g$  for 20 minutes at 4°C. The supernatant was moved to a clean tube and collected as the cytosolic samples. High-salt buffer (500  $\mu$ l: 50 mM Tris [pH 7.5], 400 mM NaCl, 10% glycerol, 0.2% NP-40 supplemented with 1 $\times$  cOmplete™ Protease Inhibitor Cocktail [11697498001 Roche], 50 mM sodium fluoride, 1 mM sodium orthovanadate) was added to the nuclei pellet, followed by 30-minute incubation on ice. The nuclei were sonicated for 15 seconds at 20%, and spun down for 5 minutes at the highest speed at 4°C. The supernatant was saved as the IP input samples and quantified by Bradford assay. FLAG beads (A2220 Sigma) (40  $\mu$ l, i.e. 20  $\mu$ l packed beads) were prepared via 4 washes in 500  $\mu$ l high-salt buffer, each followed by centrifugation at 8200  $\times g$  for 1 minute at 4°C. Nuclear lysate/IP input (500  $\mu$ g) was added to the beads and incubated on a rotator at 4°C for 3 hours. After rotation, the beads were washed with 500  $\mu$ l high-salt buffer 3 times, each followed by centrifugation at 8200  $\times g$  for 1 minute at 4°C. The immunoprecipitated protein was eluted with 45  $\mu$ l Laemmli buffer (1 $\times$ ) at 95°C for 6 minutes. The supernatant was collected after centrifugation as the IP samples. The samples were stored at -20°C and underwent immunoblotting and silver staining analyses.

#### **2.2.3.1.3 IP optimisation III**

1) One hundred million fresh cell pellets were collected on ice and washed once with 1 $\times$  PBS. The cells were lysed with 1 ml isotonic buffer (20 mM Tris [pH 7.5], 100 mM NaCl, 5 mM MgCl<sub>2</sub>, 10% glycerol, 0.2% NP-40 supplemented with protease and phosphatase inhibitors including 1 $\times$  cOmplete™ Protease Inhibitor Cocktail [11697498001 Roche], 50 mM sodium fluoride, 1 mM sodium orthovanadate) and incubated on ice for 10 minutes. The lysate was homogenised 10 times and followed by ice incubation for 10 minutes. This procedure was repeated 10 times until more than 90% of the cells were stained with Trypan blue. The nuclei were spun down by centrifugation at 11,000  $\times g$  for 20 minutes at 4°C. The supernatant was collected as the cytosolic samples. Lysis buffer 1 ml: 50 mM Tris-HCl [pH 7.4], 150 mM NaCl, 1 mM EDTA, 1% Triton X-100 supplemented with 1 $\times$

cOmplete™ Protease Inhibitor Cocktail [11697498001 Roche], 50 mM sodium fluoride, 1 mM sodium orthovanadate) was added to the nuclei pellet and incubated on ice for 30 minutes. The nuclei were sonicated for 10 seconds twice and 5 seconds once at 20%, and centrifuged for 10 minutes at the highest speed at 4°C. The supernatant was saved as nuclear input and quantified by Bradford assay.

The FLAG beads resin (40 µl, i.e. 20 µl packed beads) were washed 4 times in 1 ml lysis buffer and incubated with the IP samples at 4°C on a rotator for 2.5 hours. After rotation, the beads were washed with 1 ml lysis buffer 10 times, 1 minute each, on a rotator at 4°C. Each wash was followed by centrifugation at 8,000 ×g for 1 minute at 4°C. The beads were resuspended in 45 µl Laemmli buffer (1×) and boiled at 95°C for 6 minutes. After 1-minute centrifugation at 8,000 ×g, the supernatants were collected and the samples were analysed by immunoblotting and silver staining.

2) For Coomassie staining, prior to FLAG IP, Pierce™ Protein G Plus agarose beads (22851 Thermo Fisher Scientific) were first used to pre-clear non-specific binding on the FLAG beads. The agarose beads (40 µl) were washed 3 times in 1 ml lysis buffer, each followed by centrifugation at 8,000 ×g for 1 minute at 4°C. Nuclear lysate (1 mg) was added to the Pierce™ Protein G Plus agarose beads, and different conditions were adjusted to the same volume by adding lysis buffer. The agarose beads were incubated with the input samples for 1 hour at 4°C on a rotator. After incubation, the resin was spun down at 8,000 ×g at 4°C. The supernatants were kept as the IP samples.

3) For Co-IP (candidate approach), fourteen million cells were collected. 500 µg nuclear lysate was used for IP. After immunoprecipitation and beads washing steps, the FLAG beads were eluted with 35 µl Laemmli buffer (1×) and boiled at 95°C for 6 minutes, and the elutions were used for immunoblotting analysis.

#### **2.2.3.1.4 IP optimisation IV**

Forty-eight million cells were pelleted down and washed in PBS once. The cells were resuspended in 1 ml Buffer A (10 mM HEPES [pH 7.9], 1.5 mM MgCl<sub>2</sub>, 10 mM KCl supplemented with protease and phosphatase inhibitors

including 1× cOmplete™ Protease Inhibitor Cocktail [11697498001 Roche], 50 mM sodium fluoride, 1 mM sodium orthovanadate). After 10-minute incubation on ice, the cells were pelleted down at 1400 ×g for 5 minutes. The supernatants were removed, and 300 µl of Buffer A supplemented with 0.1% NP-40 was added to the samples. The samples were incubated on ice for 10 minutes with gentle agitation. The nuclei were recovered by centrifugation at 1500 rpm for 5 minutes at 4°C. The supernatant was collected as the cytoplasmic fraction samples. The nuclei were resuspended in 100 µl Buffer B (5 mM HEPES [pH 7.9], 26% glycerol, 1.5 mM MgCl<sub>2</sub>, 0.2 mM EDTA, 250 mM NaCl supplemented with 1× cOmplete™ Protease Inhibitor Cocktail [11697498001 Roche], 50 mM sodium fluoride, 1 mM sodium orthovanadate) for 1 hour on ice with occasional agitation. The lysates were sonicated for 15 seconds twice at 20%. While incubating the nuclei, the FLAG beads resin (40 µl, i.e. 20 µl packed beads) were washed 4 times in 800 µl Buffer BC150 (150 mM KCl, 10% glycerol, 50 mM HEPES [pH 7.9], 0.5 mM EDTA supplemented with 1× cOmplete™ Protease Inhibitor Cocktail [11697498001 Roche], 50 mM sodium fluoride, 1 mM sodium orthovanadate) on ice. The nuclei were spun down at 13,000 rpm at 4°C for 20 minutes, and the supernatants were collected as the nuclear extract samples. Bradford quantification assays were used to quantify the protein. Nuclear extract (1 mg) was added to the FLAG beads, and the sample volume was topped to 600 µl with Buffer BC150. The sample/beads mixes were rotated for 3 hours at 4°C. After rotation, the beads were washed in 1 ml Buffer BC300 (300 mM KCl, 10% glycerol, 50 mM HEPES [pH 7.9] supplemented with 1× cOmplete™ Protease Inhibitor Cocktail [11697498001 Roche], 50 mM sodium fluoride, 1 mM sodium orthovanadate) 4 times at 8,000 ×g at 4°C. The beads were resuspended in 50 µl Laemmli buffer (1×) and boiled at 95°C for 6 minutes. After centrifugation at 8,000 ×g for 1 minute, the supernatant was collected and analysed by immunoblotting and silver staining.

#### **2.2.3.1.5 IP optimisation V**

Sixty million NPCs per condition were collected and washed twice with 1 ml 1× PBS and once with 1 ml hypotonic buffer A (10 mM HEPES [pH 7.9], 10 mM KCl, 1.5 mM MgCl<sub>2</sub> supplemented with protease and phosphatase

inhibitors including 1× cOmplete™ Protease Inhibitor Cocktail [11697498001 Roche], 50 mM sodium fluoride, 1 mM sodium orthovanadate). The cells were pelleted down by low-speed centrifugation at 3000 rpm. Buffer A (300 µl) was added to the cell pellet. The pellet was homogenised about 10 times, and placed on ice incubation for 5 minutes between each homogenisation. This procedure was repeated 15 times until more than 90% of the cells were stained with Trypan blue. The nuclei were collected by centrifugation at 11,000 ×g for 5 minutes at 4°C. The supernatant was collected as the cytosol fraction samples. The nuclei were washed once with 200 µl buffer A to remove the contaminating cytosol proteins, which were collected by centrifugation at 11,000 ×g for 15 minutes. The nuclear extract was prepared by extracting the nuclei 2 consecutive times using 200 µl buffer C each time (20 mM HEPES [pH 7.9], 420 mM NaCl, 25% glycerol, 1.5 mM MgCl<sub>2</sub>, 0.2 mM EDTA supplemented with protease and phosphatase inhibitors including 1× cOmplete™ Protease Inhibitor Cocktail [11697498001 Roche], 50 mM sodium fluoride, 1 mM sodium orthovanadate). In detail, the nuclei were homogenised about 10 times to improve the efficiency of the extraction, and they were rotated in buffer C for 30 minutes at 4°C, followed by high-speed centrifugation, i.e. 15,000 rpm, for 15 minutes. The supernatant was collected as nuclear extract I. The pellets were resuspended with 200 µl buffer C the second incubation. The lysate was passed through a syringe needle 10 times and rotated at 4°C for another 30 minutes. The supernatants were collected as nuclear extract II after centrifugation at 15,000 rpm for 15 minutes. Supernatants I and II were mixed and used as the nuclear extract samples for IP. Bradford assay was performed to quantify the protein. FLAG beads resin (60 µl, i.e. 30 µl packed beads) were washed 3 times with 800 µl IP buffer (20 mM HEPES [pH 7.9], 200 mM NaCl, 10% glycerol supplemented with 1× cOmplete™ Protease Inhibitor Cocktail [11697498001 Roche], 50 mM sodium fluoride, 1 mM sodium orthovanadate). Nuclear sample (250 µg) was added to the beads and the samples were diluted 4-fold with the IP buffer. The protein/beads mix was rotated at 4°C for 2.5 hours. After rotation, the beads were collected and washed with 1 ml IP buffer by centrifugation 10 times, 1 minute each, at 4°C. The beads were eluted with 50 µl Laemmli buffer (1×)

and boiled at 95°C for 6 minutes, and the elutions were used for immunoblotting, silver staining and mass spectrometry (MS) analyses.

#### **2.2.3.1.6 'Mock' IP optimisation V with different protease and phosphatase inhibitors**

Following the Optimisation V protocol, 10 million NPCs per condition were collected for 'mock' IP with buffers supplemented with: 1) 1× cOmplete™ Protease Inhibitor Cocktail (11697498001 Roche), 50 mM sodium fluoride, and 1 mM sodium orthovanadate; 2) 1× cOmplete™ ULTRA EDTA-free Protease Inhibitor Cocktail (05892953001 Roche), 1 µg/ml leupeptin, 50 µg/ml PMSF (phenylmethylsulphonyl fluoride), 50 mM sodium fluoride and 1 mM sodium orthovanadate. The nuclear lysates (30 µg) were incubated at 4°C for 0 hour and 5 hours. Laemmli buffer (5×) was added directly to the cell lysates after the incubation, and Daxx, FLAG, α-tubulin and total H3 were immunoblotted to examine the effects of the change in protease and phosphatase inhibitors.

#### **2.2.3.1.7 IP optimisation V with dithiothreitol (DTT)**

From this experiment onwards, magnetic FLAG beads (M8823 Sigma) were used in the IP optimisations. Following the Optimisation V protocol, 20 million NPCs per condition were collected. All buffers were supplemented with 0.5 mM DTT, 1× cOmplete™ ULTRA EDTA-free Protease Inhibitor Cocktail [05892953001 Roche], 1 µg/ml leupeptin, 50 µg/ml PMSF, 50 mM sodium fluoride and 1 mM sodium orthovanadate. Magnetic FLAG beads resin (40 µl, i.e. 20 µl packed magnetic beads) were used for the IP. 300 µg nuclear lysate was used for IP. After immunoprecipitation and beads washing steps, the magnetic FLAG beads were eluted with 45 µl Laemmli buffer (1×) and boiled at 95°C for 6 minutes, and the elutions were used for immunoblotting analysis.

#### **2.2.3.1.8 Modified IP optimisation V for reduced background and specificity of co-IP proteins**

1) In the first modified Optimisation V, 15 million NPCs per condition were collected. All buffers were supplemented with 0.5 mM DTT, protease and phosphatase inhibitors including 1× cOmplete™ ULTRA EDTA-free Protease Inhibitor Cocktail (05892953001 Roche), 1 µg/ml leupeptin, 50 µg/ml PMSF,

50 mM sodium fluoride and 1 mM sodium orthovanadate. The nuclear cell lysates (200 µg) were pre-cleared with mouse IgG/Protein G Plus agarose beads. Protein G Plus agarose resin (22851 Thermo Fisher Scientific) (60 µl, i.e. 30 µl packed beads) were washed once with 1 ml IP buffer and incubated with 3 µg mouse IgG in 1 ml IP buffer at 4°C with rotation for 1.5 hour. The mouse IgG/Protein G Plus agarose beads were washed twice in 1 ml IP buffer and used for pre-clearing the cell nuclear lysates. The nuclear lysates were pre-cleared for 1 hour at 4°C on a rotator, and the supernatants were collected for FLAG IP. Magnetic FLAG beads resin (M8823 Sigma) (40 µl beads resin, i.e. 20 µl packed beads) were used for FLAG IP. After 2.5-hour rotation, the FLAG beads were washed 10 times, 5 minutes each, on a rotator at 4°C. The beads were then eluted with 60 µl Laemmli buffer (1×) and boiled at 95°C for 6 minutes, and the elutions were used for immunoblotting analysis.

2) In the second modified Optimisation V, 15 million NPCs per condition were collected. All buffers were supplemented with 0.5 mM DTT, 1× cOmplete™ ULTRA EDTA-free Protease Inhibitor Cocktail (05892953001 Roche), 1 µg/ml leupeptin, 50 µg/ml PMSF, 50 mM sodium fluoride and 1 mM sodium orthovanadate. Magnetic FLAG beads resin (M8823 Sigma) (40 µl beads resin, i.e. 20 µl packed beads) were used for the IP. 200 µg nuclear lysate was used for IP. The washing buffer used for the post-IP beads contained the addition of 0.2% Triton X-100. The beads were eluted with 60 µl Laemmli buffer (1×) and boiled at 95°C for 6 minutes, and the elutions were used for immunoblotting analysis.

#### **2.2.3.1.9 IP optimisation VI**

Twenty million NPCs per condition were collected and washed twice in 10 ml cold 1× PBS and once with 4 ml cold Buffer A (10 mM HEPES [pH 7.65], 10 mM MgCl<sub>2</sub>, 10 mM KCl, 0.5 mM DTT supplemented with protease and phosphatase inhibitors including 1× cOmplete™ ULTRA EDTA-free Protease Inhibitor Cocktail [05892953001 Roche], 1 µg/ml leupeptin, 50 µg/ml PMSF, 50 mM sodium fluoride, 1 mM sodium orthovanadate). The cells were resuspended in 4 ml ice-cold Buffer A and incubated on ice for 15 minutes. The cells were lysed to release the nuclei using a 7 ml Dounce homogeniser via 5 strokes with the loose pestle and 10 strokes with the tight pestle. The

dounded cells were centrifuged at 230 ×g at 4°C for 5 minutes and the supernatants were collected as the cytoplasmic fraction samples. The nuclei were washed twice with 5 ml Buffer N (15 mM HEPES [pH 7.65], 1 mM MgCl<sub>2</sub>, 0.5 mM DTT, 250 mM sucrose supplemented with protease and phosphatase inhibitors including 1× cOmplete™ ULTRA EDTA-free Protease Inhibitor Cocktail [05892953001 Roche], 1 µg/ml leupeptin, 50 µg/ml PMSF, 50 mM sodium fluoride, 1 mM sodium orthovanadate) and collected by centrifugation at 2800 ×g for 10 minutes at 4°C. The nuclei were resuspended in 500 µl Buffer B (5 mM HEPES [pH 7.65], 25% glycerol, 5 mM MgCl<sub>2</sub>, 0.2 mM EDTA, 0.5 mM DTT, 250 mM NaCl supplemented with protease and phosphatase inhibitors including 1× cOmplete™ ULTRA EDTA-free Protease Inhibitor Cocktail [05892953001 Roche], 1 µg/ml leupeptin, 50 µg/ml PMSF, 50 mM sodium fluoride, 1 mM sodium orthovanadate). Concentrated 5 M NaCl was mixed dropwise into the nuclei to increase the salt concentration to 300 mM (i.e. 22 µl 5 M NaCl per ml nuclei extract), and 37.5 U Benzonase nuclease was added to the mix. The nuclei extract mix was incubated at 4°C for 2 hours with agitation, and was pelleted with centrifugation at 13,000 rpm for 20 minutes at 4°C. The supernatant was collected as the nuclear extract samples, and the salt concentration was reduced to 150 mM by diluting the extract into Buffer B (5 mM HEPES [pH 7.65], 25% glycerol, 5 mM MgCl<sub>2</sub>, 0.2 mM EDTA, 0.5 mM DTT, supplemented with protease and phosphatase inhibitors including 1× cOmplete™ ULTRA EDTA-free Protease Inhibitor Cocktail [05892953001 Roche], 1 µg/ml leupeptin, 50 µg/ml PMSF, 50 mM sodium fluoride, 1 mM sodium orthovanadate). The nuclear extract samples were incubated at 4°C for 1 hour. BCA assay was performed to quantify the protein.

Magnetic FLAG beads resin (M8823 Sigma) (40 µl beads resin, i.e. 20 µl packed beads) were washed three times with 1 ml Buffer B, and the supernatant was removed. The beads were resuspended with 100 µl Buffer B (5 mM HEPES [pH 7.65], 25% glycerol, 5 mM MgCl<sub>2</sub>, 0.2 mM EDTA, 0.5 mM DTT, 0.01% NP-40, 150 mM NaCl supplemented with protease and phosphatase inhibitors including 1× cOmplete™ ULTRA EDTA-free Protease Inhibitor Cocktail [05892953001 Roche], 1 µg/ml leupeptin, 50 µg/ml PMSF, 50 mM sodium fluoride, 1 mM sodium orthovanadate) and kept on ice until used. The nuclear extract (200 µg) was added to the beads and incubated at

4°C on a rotator for 3 hours. After incubation, the FLAG beads were washed 10 times, 5 minutes each, with Buffer B containing 150 mM NaCl. FLAG peptide (100 µl, F3290 Sigma) (100 µg/ml) was used for FLAG protein elution. The mixture was incubated in a ThermoMixer with gentle shaking (1100 rpm) for 30 minutes at 4°C, and the supernatant was collected with a magnet as the IP elutions. Laemmli buffer (5×) was mixed to the IP elutions, and they were boiled at 95°C for 6 minutes before being analysed by immunoblotting.

#### **2.2.3.1.10 IP optimisation VII (non-denaturing buffer)**

1) Six million HEK293T cells were collected for the first optimisation with non-denaturing buffer. The cells were washed twice with 1 ml 1× PBS, and were pelleted down with centrifugation at 1200 rpm at room temperature. The cells were resuspended in 500 µl non-denaturing buffer (1% IGEPAL CA-630, 20 mM Tris [pH 7.4], 137 mM sodium chloride, 2 mM EDTA [pH 8.0] supplemented with 10 µg/ml aprotinin, 10 µg/ml pepstatin A, 10 µg/ml leupeptin, 1 mM benzamidine-HCl, 50 µg/ml PMSF, 50 mM sodium fluoride, 1 mM sodium orthovanadate) and incubated on ice for 30 minutes. The cells were homogenised 30 times with a Dounce homogeniser, with intervals every 10 times, until more than 90% of the cells were stained with Trypan blue. The cell lysates were collected by centrifuging at 14,000 ×g for 10 minutes at 4°C, and the total proteins were quantified with BCA assay. Magnetic FLAG beads resin (M8823 Sigma) (40 µl beads resin, i.e. 20 µl packed beads) were washed 3 times with 500 µl non-denaturing buffer, and 700 µg lysates were added to the beads for IP. The beads/lysates mixture was incubated on a rotator for 4 hours at 4°C, and washed 10 times in 1 ml non-denaturing buffer. The beads were then eluted with 50 µl Laemmli buffer (2×) and boiled at 95°C for 6 minutes, and the supernatants were collected for immunoblotting analysis.

2) For the second optimisation with non-denaturing buffer, Benzonase nuclease and FLAG peptides (F3290 Sigma) were used, and 6 million HEK293T cells were collected per condition. The cells were washed twice in 1 ml 1× PBS, and pelleted down at 1200 rpm at room temperature. The cells were resuspended in 500 µl non-denaturing buffer (0.5% IGEPAL CA-630, 20 mM Tris [pH 7.4], 137 mM sodium chloride, 1 mM EDTA [pH 8.0] supplemented with 10 µg/ml aprotinin, 10 µg/ml pepstatin A, 10 µg/ml

leupeptin, 1 mM benzamidine-HCl, 50 µg/ml PMSF, 50 mM sodium fluoride, 1 mM sodium orthovanadate) and incubated on ice for 1 hour. Benzonase nuclease (37.5 U) was added to the mixture only in the experimental group. The cells were homogenised 30 times with a Dounce homogeniser, with intervals every 10 times, and incubated on a rotator for 2 hours at 4°C. The supernatants were collected by centrifuging at 14,000 ×g for 10 minutes at 4°C, and quantified with BCA assay. Magnetic FLAG beads resin (M8823 Sigma) (40 µl beads resin, i.e. 20 µl packed beads) were washed three times with 500 µl non-denaturing buffer, and lysates (700 µg) were added to the beads for IP. The beads/lysates mixture was incubated on a rotator for 3 hours at 4°C, and washed 10 times in 1 ml non-denaturing buffer. The beads were eluted with 80 µl FLAG peptides (100 µg/ml) (F3290 Sigma), with gentle shaking at 1100 rpm for 30 minutes at 4°C. The supernatants were collected as the FLAG peptide elutions. Laemmli buffer (5×) was mixed to the FLAG peptide elutions and were boiled at 95°C for 6 minutes. The FLAG peptide-eluted beads were further eluted with 50 µl Laemmli buffer (2×) and boiled at 95°C for 6 minutes, and the supernatants were collected as the Laemmli elutions. The IP-eluted samples were analysed by immunoblotting.

3) For IP of NPCs, 15 million cells were collected per condition. This IP protocol followed the second optimisation protocol above for the HEK293T cells. 1412 µg lysates were used for IP. Post-IP and post-washing FLAG beads were first eluted with FLAG peptides, and then eluted with Laemmli buffer (2×). The supernatants were collected as the FLAG peptide elutions and Laemmli elutions, respectively. The IP beads were also eluted with Laemmli buffer (2×) only, and the supernatants were collected as Laemmli elutions<sup>+</sup>. The IP-eluted samples were analysed by immunoblotting and silver staining.

#### **2.2.3.2 MS sample preparation**

After FLAG IP, the beads were washed 3 times with 1 ml digestion buffer (0.1% Triton X-100, 100 mM TEAB [pH 8–8.5]), and resuspended in 100 µl digestion buffer with 200 ng trypsin (0.1% Triton X-100, 100 mM TEAB [pH 8–8.5], 2 ng/µl trypsin). The beads were incubated in the digestion buffer for 10 minutes at 37°C with gentle shaking at 1100 rpm. The supernatant was collected with centrifugation for 1 minute at 8,000 ×g into 1.5-ml tubes. The IP samples were

then moved to a vacuum centrifuge and evaporated for 2 hours at room temperature.

### **2.2.3.3 siRNA transfection and immunoblotting of Daxx, Hira and Gapdh**

At 24 hours before siRNA transfection, 100,000 Neuro2a cells were seeded in 6-well plates and incubated in 2 ml DMEM (10% FBS, 1% Pen/Strep) at 37°C overnight. *Daxx*, *Hira*, *Gapdh* and Scramble siRNAs were used for the Lipofectamine transfection. For each transfection well, 250 µl Opti-MEM with 30 nM siRNA were mixed with 250 µl Opti-MEM with 5 µl Lipofectamine RNAiMAX (13778075 Thermo Fisher Scientific) at room temperature for 30 minutes, and the medium/siRNA mixture was added gently and evenly onto the cells. The cells were incubated for 24 hours in a 37°C incubator, and the medium was replaced with differentiation medium (DMEM, 2% FBS, 1% Pen/Strep, 20 µM RA). The cells were incubated in the differentiation medium for 48 hours and collected for immunoblotting.

To collect the cells, all cells in the 6-well plates were collected with 1× trypsin (15400054 Gibco) and pelleted down by centrifugation at 1200 rpm. The cell pellets were washed once with 1× PBS, and centrifuged at 1200 rpm at room temperature. The cells were resuspended in 50 µl lysis buffer (0.5% IGEPAL CA-630, 20 mM Tris [pH 7.4], 137 mM NaCl supplemented with protease and phosphatase inhibitors including 1 mM EDTA [pH 8.0], 1 mM sodium orthovanadate, 5 mM sodium fluoride, 10 µg/ml pepstatin A, 10 µg/ml aprotinin, 1 mM benzamidine-HCl, 10 µg/ml leupeptin, 50 µg/ml PMSF) and incubated on ice for 20 minutes. The cell lysates were sonicated at 40% for 4 seconds on ice, and spun in a refrigerated centrifuge at 13,000 rpm for 5 minutes. The supernatants were collected and transferred to fresh pre-chilled tubes as the cell lysate samples. The protein concentrations for each condition was measured with the BCA assay, and 5× Laemmli buffer was added to the protein extracts. The samples were boiled at 95°C for 6 minutes and stored at -20°C until immunoblotted.

## 2.2.3.4 Immunoblotting (western blotting)

### 2.2.3.4.1 Gel electrophoresis, protein transfer and primary antibody incubation

The polyacrylamide gels were freshly made on the day of the electrophoresis corresponding to the size of the protein of interest (FLAG-Daxx and Hira experiments, 7% polyacrylamide gels; H3-HaloTag experiments, 15% polyacrylamide gels). 1× SDS-PAGE running buffer was prepared in the electrophoresis tanks. Samples were added to the polyacrylamide gels. The gels were electrophoresed first at 55 V, and the speed was increased to 95 V. The electrophoresis continued until the ladders were well separated.

**Table 2. 10 Quantity of protein for immunoblotting analyses.**

a/a	Experiment	SDS-PAGE	Sample(s)	Quantity
1	H3.3-HaloTag and dH3-HaloTag chromatin extraction (Figure 3. 5 A)	15%	All	15 µg
2	<i>Hira</i> siRNA downregulation (Figure 3. 12 A and B)	7%	All	30 µg
3	<i>Daxx</i> siRNA downregulation (Figure 3. 13 A and B)	7%	All	15 µg
4	<i>Daxx</i> and <i>Hira</i> siRNA downregulation (Figure 3. 14 A)	7%	All	20 µg
5	FLAG and Daxx overexpression in NIH3T3 cells (Figure 4. 3)	7%	All	40 µg
6	IP optimisation I (Figure 4. 4 A)	7%	IP	19 µl of IP elution (45 µl total)
			Input and Output	40 µg
7	IP optimisation II (Figure 4. 5 A)	7%	IP	20 µl of IP elution (45 µl total)
			Input, Output and Cytosolic	30 µg
8	IP optimisation III (Figure 4. 6 A)	7%	IP	20 µl of IP elution (45 µl total)
			Input, Output and Cytosolic	40 µg

9	IP optimisation IV (Figure 4. 7 A)	7%	IP	20 µl of IP elution (50 µl total)
			Input, Output and Cytosolic	30 µg
10	IP optimisation V (Figure 4. 8 A) and Candidates validation with IP optimisation V (Figure 4. 9 B)	7%	IP	10 µl of IP elution (50 µl total)
			Input, Output and Cytosolic	30 µg
11	Protein degradation (Figure 4. 10 A)	7%	All	10 µg
12	Oxidative stress (Figure 4. 10 B)	7%	IP	36 µl of IP elution (45 µl total)
			Input, Output and Cytosolic	5 µg
13	Reduction of the background and specificity of co-IP (Figure 4. 11 A and B)	7%	IP	20 µl of IP elution (60 µl total)
			Input, Output and Cytosolic	10 µg
14	IP optimisation VI (Figure 4. 12)	7%	IP	50 µl of IP elution (140 µl total)
			Input, Output, Cytosolic, ATRX <sup>+</sup> and ATRX <sup>-</sup>	10 µg
15	IP optimisation VII on HEK293T cells (Figure 4. 13 A and B)	7%	IP (FLAG peptide)	25 µl of IP elution (100 µl total)
			IP (2x Laemmli)	12 µl of IP elution (50 µl total)
			Input, Output, Cytosolic, ATRX <sup>+</sup> and ATRX <sup>-</sup>	30 µg
16	IP optimisation VII on NPCs (Figure 4. 14 A)	7%	IP (FLAG peptide)	25 µl of IP elution (100 µl total)
			IP (2x Laemmli)	12 µl of IP elution (50 µl total)
			Input, Output, Cytosolic, ATRX <sup>+</sup> and ATRX <sup>-</sup>	30 µg
17	Co-IP (candidate approach) (Figure 4. 15)	7%	IP	11 µl of IP elution (35 µl total)
			Input, Output and Cytosolic	20 µg

#### 2.2.3.4.2 Transfer

Immediately after electrophoresis was completed, the polyacrylamide gel was collected from the glass plates. A transfer sandwich was made by stacking the following materials: sponge → 3 layers of paper → membrane →

polyacrylamide gel → 3 layers of paper → sponge. The transfer sandwich was placed into the transfer clasper, and the protein transfer was performed with 65 V at 4°C for 2.5–3 hours. Once the transfer had been completed, the membranes were examined with Ponceau red. The membrane was cut at variable sizes for detecting the different proteins.

#### **2.2.3.4.3 Immunoblotting**

The membranes were incubated twice with PBS–0.1% Tween 20 to wash off the Ponceau red, and blocked with 5% non-fat milk in PBS–0.1% Tween 20 at room temperature for 1 hour with gentle agitation. For FLAG and HaloTag antibodies, the blocking buffer was 5% BSA in PBS–0.1% Tween 20. The antibodies were prepared in 5 ml dilution buffer (the same as blocking buffer) in 50-ml Falcon tubes. The membranes were incubated in the primary antibodies overnight at 4°C.

On the second day, the membranes were washed 3 times in PBS–0.1% Tween 20, 10 minutes each time, with gentle agitation at room temperature, and incubated in the secondary antibodies (in 5% non-fat milk in PBS–0.1% Tween 20) for 1 hour at room temperature. If using the LI-COR imaging system, the membranes were protected from light. The membranes were washed 3 times, 10 minutes each time, and developed with enhanced chemiluminescence (ECL) or the Lycor imaging system.

#### **2.2.3.5 Silver staining**

Silver staining was performed with a Silver Stain Kit (161-0443 Bio-Rad). The polyacrylamide gel was first fixed in Fixative solution I [40% methanol/10% acetic acid (v/v)] for 1 hour at room temperature, with gentle agitation. Fixative solution I was replaced with Fixative solution II [10% ethanol/5% acetic acid (v/v)] for 30 minutes twice at room temperature, with gentle agitation. The gel was then incubated in 1× Oxidizer for 10 minutes. The gel was then washed in deionised water 6 times, 10 minutes each time. The gel was washed in water until the gel turned from yellow to transparent. The gel was then incubated in Silver reagent for 30 minutes, followed by a 2-minute wash in deionized water. The gel was developed with 1× Developer. The gel was first incubated with 1× Developer for 30 seconds, and the solution was replaced twice until the gel was well stained. Development was terminated by incubating the gel in Stop

solution [5% acetic acid (v/v)] for 5 minutes. The gel was then rinsed in deionized water and imaged with the ChemiDoc™ XRS+ System (Bio-Rad).

**Table 2. 11 Quantity of protein for silver staining.**

a/a	Experiment	SDS-PAGE	Sample(s)	Quantity
1	IP optimisation I (Figure 4. 4 B)	7%	All	19 µl of IP elution (45 µl total)
2	IP optimisation II (Figure 4. 5 B)	7%	All	20 µl of IP elution (45 µl total)
3	IP optimisation III (Figure 4. 6 B)	7%	All	20 µl of IP elution (45 µl total)
4	IP optimisation IV (Figure 4. 7 B)	7%	All	20 µl of IP elution (50 µl total)
5	IP optimisation V (Figure 4. 8 B)	7%	All	10 µl of IP elution (50 µl total)
6	IP optimisation VII (Figure 4. 14 B)	7%	IP (FLAG peptide)	25 µl of IP elution (100 µl total)
			IP (2x Laemmli)	12 µl of IP elution (50 µl total)

### 2.2.3.6 Coomassie staining

The polyacrylamide gel was rinsed with 100 ml deionized water 3 times, 5 minutes each time, to remove the SDS and buffer salts. The gel was then stained overnight at room temperature in 20 ml SimplyBlue™ SafeStain (LC6060 Invitrogen) with 2 ml 20% NaCl with gentle shaking. The next day, the gel was washed with 100 ml deionized water for 3 hours, and dried with a gel dryer for 1 hour at 60°C.

### 2.2.3.7 iCLIP (individual nucleotide resolution UV crosslinking and IP)

iCLIP was used to demonstrate whether Daxx is an RNA-associated protein. Five million NPCs for both EV and FLAG-Daxx conditions were collected. The cell plates were washed twice with cold 1× PBS and were UV-crosslinked with 0.15 J/cm<sup>2</sup> 365 nm/254 nm UV light in a Stratalinker 2400. The cells were scraped from the plates with 500 µl PBS, and the cell pellets were collected with centrifugation at 3,000 rpm. The cells were resuspended with 1 ml PBS and stored at -80°C.

To prepare for the FLAG-beads, 50 µl protein G/A Dynabeads (100.02 Dynal) per condition was used. The beads were washed twice with lysis buffer (50 mM Tris-HCl [pH 7.4], 100 mM NaCl, 1% NP-40, 0.1% SDS, 0.5% sodium deoxycholate, +Complete) and resuspended in 50 µl lysis buffer with 5 µg

FLAG antibody. The antibody and beads were rotated at room temperature for 1 hour. After 3 washes in 900  $\mu$ l lysis buffer, the beads were ready to proceed to IP. The cell pellets were resuspended in 1 ml lysis buffer, and the lysates were passed through a 27G needle 10 times. The lysates were treated with a gradient of RNase I (AM2295 Ambion), with 1:1,000, 1:500, 1:100 and 1:25 dilutions. The samples were incubated in RNase I for 3 minutes at 37°C on a shaker at 1,100 rpm, and were transferred into ice immediately. The lysates were centrifuged at 22,000  $\times g$  for 10 minutes at 4°C, and the supernatants were collected and added to the FLAG-coupled beads. The samples were rotated for 5 hours at 4°C. After incubation, the beads were collected and washed 3 times in 900  $\mu$ l high-salt buffer (50 mM Tris-HCl, [pH 7.4], 1 M NaCl, 1 mM EDTA, 1% NP-40, 0.1% SDS, 0.5% sodium deoxycholate). The beads were then resuspended in 8  $\mu$ l PNK mix (0.4  $\mu$ l PNK [NEB], 0.8  $\mu$ l  $^{32}$ P- $\gamma$ -ATP, 0.8  $\mu$ l 10 $\times$  PNK buffer [NEB], 6  $\mu$ l water) and incubated at 37°C for 5 minutes. The hot PNK mix was removed and 20  $\mu$ l 1 $\times$  NuPAGE loading buffer with reducing agent (Invitrogen) was added to the beads. The mix was incubated on a ThermoMixer at 70°C for 10 minutes. The supernatant was collected and loaded on a NuPAGE Bis-Tris gel (Invitrogen), which was run at 180 V for 55 minutes. The protein–RNA complexes were transferred from the gel to a nitrocellulose membrane at 30 V for 1 hour at room temperature in NuPAGE transfer buffer. The membrane was rinsed with PBS buffer once, wrapped in Saran wrap and exposed to film at -80°C overnight. FLAG antibody (G9211 Promega) was used for the FLAG protein immunoblotting to further demonstrate whether RNA is linked with Daxx. The membrane was developed and imaged with the ChemiDoc™ XRS+ System (Bio-Rad).

#### **2.2.3.8 Immunofluorescence (IF)**

On the day before IF, small round cover glasses (13 mm) were placed in the wells of a 24-well plate. The cover glasses were sterilised by dipping in 100% ethanol and flame-treated. The 24-well plate was further sterilised by microwaving for 20 minutes. Cells (50,000 per well) were seeded in the 24-well plate and incubated in 500  $\mu$ l medium overnight at 37°C. The next day, fresh 4% PFA was added to medium (1:1) and incubated at room temperature for 5 minutes. All liquid was aspirated and 4% PFA was added to the cells. The

cells were fixed for another 10 minutes. After fixation, the cells were washed with PBS 3 times, 2 minutes each time. The cells were then permeabilised with PBS/Triton-X (0.5%) for 15 minutes at room temperature. After 5-minute wash with PBS–Tween 20 (0.1%), the cells were blocked with goat serum [5% GS/PBS–Tween 20 (0.1%)] for 1 hour at room temperature. The primary antibodies were diluted in the blocking solution and added to the cells for overnight incubation at 4°C. The cover glasses were placed upside down to ensure the cells were incubated in the antibodies evenly. On day 2, the cover glasses were placed back upwards, and the cells were washed 3 times, 5 minutes each time, with PBS–Tween 20 (0.1%). The cover glasses were incubated in the secondary antibody diluted in 5% GS/PBS–0.1% Tween 20 for 1 hour at room temperature in the dark. After secondary antibody incubation, the cells were washed twice, 5 minutes each time, with PBS–Tween 20 (0.1%). The cover glasses were incubated in DAPI/Hoechst diluted 1:10,000 in PBS in the dark for 15 minutes at room temperature. The cover glasses were then washed in PBS for 5 minutes and rinsed with distilled water, mounted with FluorSave and sealed on glass slides. The cells were dried overnight at 4°C and then imaged with Zeiss Axio Observer Z1 with Apotome.

#### **2.2.3.9 Chromatin extraction for HaloTag and histone proteins**

Ten million Neuro2a cells (untransduced, H3.3-HaloTag– and dH3-HaloTag–transduced) were collected for chromatin extraction. The cell pellets were washed once with 1× PBS, resuspended in 200 µl Lysis buffer (10 mM HEPES [pH 7.4], 10 mM KCl, 0.05% NP-40 supplemented with protease and phosphatase inhibitors including 1 mM sodium orthovanadate, 5 mM sodium fluoride, 5 µM trichostatin A [TSA]) and incubated on ice for 20 minutes. The nuclei were collected by centrifugation at 14,000 rpm at 4°C for 10 minutes, and the supernatants were saved as the cytoplasmic protein samples. The nuclei were washed once with lysis buffer and were centrifuged again at 14,000 rpm at 4°C for 10 minutes. The nuclei were resuspended in 200 µl low-salt buffer (10 mM Tris-HCl [pH 7.4], 0.2 mM MgCl<sub>2</sub> supplemented with protease and phosphatase inhibitors including 1 mM sodium orthovanadate, 5 mM sodium fluoride, 5 µM TSA) with 1% Triton X-100, and incubated on ice for 15 minutes. The lysates were centrifuged at 14,000 rpm for 10 minutes at

4°C, and the supernatants were collected as nucleoplasmic protein samples. The pellets containing the chromatin were resuspended in 200 µl 0.2N HCl and incubated on ice for 20 minutes. The supernatants containing the acid-soluble proteins were collected and neutralised with 200 µl 1 M Tris-HCl (pH 8). Laemmli buffer (5x) was added to the protein samples. The samples were then boiled at 95°C for 6 minutes, and stored at -20°C for immunoblotting.

## **2.2.4 Function assay: HaloTag imaging assay**

### **2.2.4.1 H3.3/dH3-HaloTag Lipofectamine transfection on HEK293T cells and HaloTag live imaging**

On the day before transfection, 30,000 HEK293T cells per well were plated in a 6-well plate with 2 ml DMEM (10% FBS, 1% Pen/Strep) overnight at 37°C. The next day, 150 µl Opti-MEM (31985062 Gibco) was mixed with 9 µl and 12 µl Lipofectamine as the Lipofectamine mix. Opti-MEM (350 µl) was mixed with 7 µg plasmids (H3.3-HaloTag/dH3-HaloTag) as the DNA mix. The transfection mix, comprising a 1:1 Lipofectamine mix (150 µl) and DNA mix (150 µl), was prepared and incubated for 5 minutes at room temperature. The transfection mix (250 µl) was added to each transfection well and incubated overnight at 37°C. The medium was replaced with fresh Opti-MEM and the cells were incubated for a further 2 days. On day 4, DMEM (10% FBS, 1% Pen/Strep) was added to the cells. The cells were used for HaloTag live cell labelling with Direct110 FluroLigand. In detail, 5x Ligand was prepared 1:200 in DMEM, and one-fifth of the medium was replaced with a 5x Ligand/DMEM mix. The cells were incubated overnight at 37°C, and imaged under Zeiss Axio Observer Z1 with Apotome for 488 GFP in fresh DMEM.

### **2.2.4.2 Preliminary examinations of the HaloTag imaging assay**

300,000 Neuro2a cells were seeded on laminin-coated cover slips in 6-cm dishes and incubated in 3 ml DMEM (10% FBS, 1% Pen/Strep) at 37°C overnight. On the second day, the medium was removed and replaced with differentiation medium (DMEM containing 2% FBS, 1% Pen/Strep, 20 µM RA) and incubated at 37°C for 48 hours.

The cells were first quenched with HaloTag<sup>®</sup> Oregon Green<sup>®</sup> (1:1,000) in the differentiation medium overnight. The cells were rinsed once in DMEM and

incubated in 1:1,000 HaloTag<sup>®</sup> TMR Ligand for 0.5, 3, 6 and 9 hours in the differentiation medium. Once the incubation was completed, the cover slips with Neuro2a cells were washed gently with 1× PBS and permeabilised with 0.1% Triton X-100 in PBS for 10 minutes at room temperature. The cover slips were then washed once with 1× PBS before fixation with 4% PFA/PBS for 15 minutes. The cover slips were washed again with 1× PBS and placed upside down on glass slides, mounted with Fluoroshield Mounting Medium with DAPI (ab104139) and sealed with nail polish. The cells were then analysed under an epifluorescence microscope.

#### **2.2.4.3 Cell number and plate coating for high-content screens**

Between 1,000 and 7,000 Neuro2a cells were seeded in 384-well plates (CUSG77540 Perkin Elmer) with a Multidrop Combi Reagent Dispenser (Thermo Fisher Scientific). Each well contained 70 µl growth medium (DMEM containing 10% FBS and 1% Pen/Strep), and the cells were seeded for 24 hours before differentiation. The growth medium was replaced with differentiation medium (DMEM containing 2% FBS, 1% Pen/Strep, 20 µM RA), and incubated at 37°C for 48 hours. The cells were observed under a bright field microscope for the best density; 4,000 cells per well was determined as the initial seeding number for the 384-well plates.

Various coating methods were tested on the 384-well plates, including Vitronectin XF (07180 STEMCELL), poly-L-lysine (0413 ScienCell), poly-D-lysine (A-003-E EMD Millipore) and collagen/fibronectin (C5533/F1141 Sigma). Cells (4,000 per well) were seeded onto differently coated surfaces in the 384-well plates in 70 µl growth medium (DMEM containing 10% FBS and 1% Pen/Strep). Following the differentiation protocol, after 72 hours, the cells grown on the poly-D-lysine (10 µg/ml)-coated surfaces were the most evenly distributed, and no multilayer formation was observed.

#### **2.2.4.4 Mitotic index (pH3 staining) with automated platform**

The 384-well plates were first coated with 10 µl per well poly-D-lysine (10 µg/ml) for up to 2 days. On the day of cell seeding, the coated plates were washed 3 times with sterile water (100 µl per well). Neuro2a cells (1,000 and 4,000) were seeded in the 384-well plates in 70 µl DMEM (10% FBS, 1% Pen/Strep) and incubated at 37°C overnight. On the second day, the medium

in the wells containing 4,000 cells was replaced with differentiation medium (DMEM, 2% FBS, 1% Pen/Strep, 20  $\mu$ M RA) and incubated for 48 hours. On day 4, both differentiated and undifferentiated cells were fixed with 100  $\mu$ l 4% PFA in PBS for 15 minutes at room temperature. The cells were washed once with PBS and permeabilised with 100  $\mu$ l 0.5% Triton X-100 for 10 minutes. Next, the cells were blocked with 50  $\mu$ l 1% BSA in 0.5% Triton X-100 in PBS at room temperature for 30 minutes and incubated with 1:500 pH3 antibody (9716 Cell Signalling) in blocking buffer for 2 hours in the dark at room temperature. Then, the cells were washed once with 100  $\mu$ l blocking buffer. Hoechst was diluted 1:2,500 in 100  $\mu$ l PBS per well and added to the cells. The cells were stained with Hoechst for 10 minutes in the dark at room temperature and washed twice in 100  $\mu$ l 1 $\times$  PBS, then imaged and analysed with CellVoyager CV6000 (Yokogawa).

#### **2.2.4.5 EdU staining on differentiated versus G1-inhibited Neuro2a cells<sup>3</sup>**

The 384-well plates were first coated with poly-D-lysine (10  $\mu$ g/ml) for up to 2 days, and the coated plates were washed 3 times with sterile water on the day of the cell seeding. Neuro2a cells (1,000 and 4,000) were seeded in the 384-well plates in DMEM (10% FBS, 1% Pen/Strep) and incubated at 37°C overnight. On the second day, the medium in the wells containing 4,000 cells were replaced with differentiation medium (DMEM containing 2% FBS, 1% Pen/Strep, 20  $\mu$ M RA) or G1/cyclin-dependent kinase (CDK) 4/6 inhibition medium (DMEM containing 2% FBS, 1% Pen/Strep, 0.25  $\mu$ M CDK 4/6 inhibitor). The cells were incubated for 48 hours, and 10  $\mu$ M EdU (C10340 Invitrogen) was added to the cells by replacing half of the cell medium with 20  $\mu$ M EdU. After 2-hour incubation, the cells were fixed with 3.7% PFA/PBS for 15 minutes at room temperature. The cells were washed twice with 3% BSA in PBS, and permeabilised with 0.5% Triton X-100 for 20 minutes. Next, the cells were washed twice with 3% BSA/PBS and incubated in Click-iT<sup>®</sup> reaction cocktail (Click-iT EdU Alexa Flour 647 Imaging Kit) for 30 minutes in the dark at room temperature. Then, the cells were washed once with 3% BSA/PBS, and Hoechst was diluted 1:2,500 in 100  $\mu$ l PBS per well and added to the cells.

---

<sup>3</sup> This was carried out by the Laboratory Automation Technologies group at DZNE, Bonn.

The cells were stained with Hoechst for 10 minutes in the dark at room temperature and washed twice in 100  $\mu$ l 1 $\times$  PBS. The cells were then imaged and analysed with CellVoyager CV6000 (Yokogawa).

#### **2.2.4.6 Batch preparation of H3.3-HaloTag and dH3-HaloTag overexpression Neuro2a cells for high-content screens**

The earliest batch of Neuro2a frozen stock was thawed in T75 flasks (159910 Thermo Fisher Scientific) with 10 ml DMEM (10% FBS, 1% Pen/Strep), and the cells were collected and expanded in T175 flasks with 30 ml DMEM (10% FBS, 1% Pen/Strep). Two days later, the cells in the T175 flasks were collected as Passage (-2), and 10 vials of 2 million Passage (-2) cells for each condition were stored in freezing medium (DMEM, 10% FBS, 1% Pen/Strep, 10% DMSO) in liquid nitrogen. The rest of the Passage (-2) cells in the T175 flasks were expanded twice in DMEM (10% FBS, 1% Pen/Strep). After 2 passages, the cells were collected as Passage 0, and frozen stocks were made. Around 60 frozen vials, at 2 million cells per vial, were produced as Passage 0 and stored in the freezing medium in liquid nitrogen.

#### **2.2.4.7 H3 deposition on H3.3-HaloTag and dH3-HaloTag overexpression Neuro2a cells: High-content screening setup with automated technologies**

One vial of Passage 0 stock containing 2 million H3.3-HaloTag and dH3-HaloTag expression Neuro2a cells were thawed in the T75 flasks with 10 ml DMEM (10% FBS, 1% Pen/Strep), and the cells were incubated at 37°C for 2 days. The cells were collected on day 3 and expanded once more in the T175 flasks in 30 ml DMEM (10% FBS, 1% Pen/Strep) at 37°C for 3 days. Meanwhile, 384-well plates were coated with 10  $\mu$ l per well poly-D-lysine (10  $\mu$ g/ml) for up to 2 days at 4°C in the dark.

On the day of cell seeding (Day 1), the poly-D-lysine-coated 384-well plates were washed 3 times with 100  $\mu$ l per well sterile water. Cells (4,000) were seeded in each well in 70  $\mu$ l DMEM (10% FBS, 1% Pen/Strep) using a Multidrop Combi Reagent Dispenser (Thermo Scientific Fisher), and cultured at 37°C for 24 hours. On Day 2, the cell medium was replaced with 70  $\mu$ l differentiation medium (DMEM, 2% FBS, 1% Pen/Strep, 20  $\mu$ M RA) and incubated at 37°C for 24 hours. On Day 3, 70  $\mu$ l 5  $\mu$ M (1:200) Quench Oregon

Green HaloTag ligand in the differentiation medium (DMEM, 2% FBS, 1% Pen/Strep, 20  $\mu$ M RA) was added to the cells. The cells were incubated with the ligand for overnight/16 hours. On Day 4, the cells were washed gently in 70  $\mu$ l fresh differentiation medium 3 times, and 50  $\mu$ l 5  $\mu$ M (1:1,000) Pause TMR HaloTag ligand in the differentiation medium (DMEM, 2% FBS, 1% Pen/Strep, 20  $\mu$ M RA) was added to the cells. The cells were incubated with the ligand for between 30 minutes and 96 hours.

The 384-well plates with quenched and the paused cells were collected and placed on the Biomek NX<sup>P</sup> Automated Workstation loaded with 96 tips (P10330-32 717251). The wells were washed with 80  $\mu$ l 1 $\times$  PBS 3 times and permeabilised with 80  $\mu$ l 0.1% Triton X-100/PBS for 5 minutes. The cells were washed gently with 80  $\mu$ l PBS once and with 100  $\mu$ l PBS twice, and nuclei staining and fixation were performed in 40  $\mu$ l 1:2,500 Hoechst in 4% PFA/PBS for 20 minutes in the dark at room temperature. The cells were imaged and analysed with CellVoyager CV6000 (Yokogawa).

#### **2.2.4.8 qPCR of siRNA-transfected Neuro2a cells**

At 24 hours before siRNA transfection, 100,000 Neuro2a cells were seeded in 6-well plates and incubated in 2 ml DMEM (10% FBS, 1% Pen/Strep) at 37°C overnight. *Daxx*, *Hira*, *Gapdh* and Scramble siRNAs were used for the Lipofectamine transfection. For each transfection well, 250  $\mu$ l Opti-MEM with the desired concentration of siRNA was mixed with 250  $\mu$ l Opti-MEM and 5  $\mu$ l Lipofectamine RNAiMAX (13778075 Thermo Fisher Scientific) at room temperature for 30 minutes, and the transfection mix was gently and evenly added onto the cell medium. The cells were incubated for 24 hours in a 37°C incubator, and the medium was removed and replaced with differentiation medium (DMEM containing 2% FBS, 1% Pen/Strep, 20  $\mu$ M RA). The cells were incubated in the differentiation medium for 48 hours, and were prepared for the RNA extraction as follows.

A RNeasy Plus Kit (74134 Qiagen) was used for extracting RNA from the Neuro2a cells. The collected cell pellets were resuspended and homogenised in 350  $\mu$ l Buffer RLT (1%  $\beta$ -mercaptoethanol). The homogenised lysates were transferred to a gDNA eliminator spin column in a 2-ml collection tube. After centrifugation for 30 seconds at 8,000  $\times g$ , the flow-through was collected and

mixed with 350 µl 70% ethanol. Up to 700 µl sample was transferred to the RNeasy spin columns placed in the 2-ml collection tubes, and the samples were centrifuged for 15 seconds at 8,000 ×g. The flow-throughs were discarded and 700 µl Buffer RW1 was added to the spin columns and centrifuged for 15 seconds at 8,000 ×g. Again, the flow-throughs were discarded and 500 µl Buffer RPE was added to the spin columns and centrifuged for 15 seconds at 8,000 ×g. The columns were washed again with Buffer RPE and spun for 2 minutes at 8,000 ×g. The columns were placed in new 1.5-ml collection tubes, and 30 µl RNase-free water was added directly to the spin column membrane. The RNA samples were collected by centrifuging the columns for 1 minute at 8,000 ×g. The samples were stored at -80°C for cDNA reverse transcription (RT).

A High-Capacity cDNA RT Kit (4368814 Applied Biosystems) was used for the cDNA RT. Each 10 µl 2× RT master mix was prepared by mixing 2 µl 10× RT Buffer, 0.8 µl 25× dNTPMix (100 mM), 2 µl 10× RT random primers, 1 µl MultiScribe™ Reverse Transcriptase and 4.2 µl nuclease-free H<sub>2</sub>O. Nuclease-free H<sub>2</sub>O (10 µl) containing 500 µg RNA was mixed with 10 µl 2× RT master mix to a total reaction volume of 20 µl. The cDNA RT reaction mix was placed in a thermal cycler, and the program conditions were set as follows:

	Lid	Step 1	Step 2	Step 3	Step 4
Temperature (°C)	25	25	37	85	4
Time (minutes)	-	10	120	5	∞

After the cDNA RT, the PCR tubes were kept on ice and mixed with 30 µl nuclease-free H<sub>2</sub>O. SYBR™ Green PCR Master Mix 2× (4309155 Applied Biosystems) was used for the qPCR. The qPCR mix was prepared by mixing 1 µl primer mix, 2 µl sample cDNA, 7 µl H<sub>2</sub>O and 10 µl 2× SYBR™ Green PCR Master Mix. The qPCR programme was performed in a 7500 Fast Real-Time PCR System (Applied Biosystems) as follows: 50°C for 2 minutes; 95°C for 10 minutes; 95°C for 15 seconds (40 cycles); and 60°C for 1 minute. The relative abundance of gene expression for *Daxx*, *Hira* and *Gapdh* were normalised to actin (*ACTB*) mRNA, and the calculation was generated using the 2<sup>-ΔΔCt</sup> method in the qPCR programme.

## **Chapter 3**

# **Visualisation of H3.3 Loading for High-content Screening**

## **3. Visualisation of H3.3 Loading for High-content Screening**

### **3.1 Background**

#### **3.1.1 Visualisation of H3.3 loading**

To identify novel regulatory pathways controlling H3.3 deposition in the CNS, we need a powerful tool to visualise its deposition. Via the establishment of the H3.3 loading visualisation assay, we will be able to observe whether and how the selected candidates affect the deposition of H3.3. This project was carried out in collaboration with Michod Group at ICH, London and Phillip Group at DZNE, Bonn.

#### **3.1.2 High-content screening analysis**

The H3.3 visualisation platform is adapted for high-content analysis of drug/compound screening. The advantages of high-content screening include rapid unbiased acquisition of a large number of cells, relevant and robust view of heterogeneity within a population, statistically relevant sampling, and robust analysis algorithms. During the establishment of the high-content screening, time-saving and unbiased procedures were performed with the assistance of robotised automation.

#### **3.1.3 Neuro2a cells and their differentiation**

Neuro2a cells are a fast-growing neuroblastoma cell line with neuronal stem cell/amoeboid-like morphology. They are widely used in studies, including those on neurite outgrowth, neurotoxicity, and signalling pathways, amongst others. Studies involving Neuro2a cells benefit from their rapid growth rate and easy manipulation. They are often studied in their differentiated form, in which, a neuron-like morphology is presented. Neuro2a cells are easily expanded, providing a robust visualisation platform for the establishment of the HaloTag imaging assay for high-content screening in the CNS.

The literature review showed that differentiation methods apparently vary among research papers. Retinoic acid (RA) plays critical roles in nervous system development, including neuronal patterning and neurite outgrowth (Clagett-Dame *et al.* 2006), and it is generally used for Neuro2a cell differentiation. In this study, Neuro2a cells were differentiated with DMEM

containing 2% FBS and 20  $\mu$ M RA for 48 hours (Riboni *et al.* 1995, Yanaka *et al.* 2007).

### **3.1.4 HaloTag system and H3.3 deposition**

HaloTag protein is a modified bacterial haloalkane dehalogenase that forms a covalent bond with the synthetic HaloTag ligand (Los *et al.* 2008), with its binding being rapid, specific, stable and irreversible. The HaloTag ligand comprises a chloroalkane linker that could be attached to a variety of molecules allowing comprehensive protein analyses using a single generic construct (England *et al.* 2015). Similar to the other traditional tagging systems, the technology has wide application possibilities, including protein isolation and purification, protein functional analysis and protein–protein/DNA interaction studies, among others (Figure 3. 1). The HaloTag visualisation system was constructed following two steps: development of the 48-KDa variant H3.3-HaloTag and canonical dH3-HaloTag fusion proteins, and visualisation with the HaloTag specific ligand. This technique can be used for cellular imaging of both live and fixed cells *in vitro*, as well as for *in vivo* visualisation using 2-photon microscopy. Notably, HaloTag enables monitoring of H3.3 deposition via ratiometric analysis, which other tags (e.g. SNAP-tag) cannot perform.

The HaloTag sequence is fused at the C-terminus of H3.3 and dH3, where the histones are folded and incorporated into the chromatin (Figure 1. 2). We demonstrated here for the first time the ability of the HaloTag system could be applied in histone deposition studies, and that fusing HaloTag at the C-terminus of histones does not interfere with their loading/eviction onto/from the chromatin *in vitro*.

H3.3 differs from the canonical H3 by only one amino acid in the histone tail and 3 amino acids (comparing to H3.1)/4 amino acids (comparing to H3.2) in the histone folding region, but their expression and function vary significantly (Szenker *et al.* 2011). Canonical H3 expression is restricted to the S phase, while H3.3 is expressed throughout the cell cycle (Tagami *et al.* 2004, Szenker *et al.* 2011). During the establishment of the H3.3 deposition imaging assay, dH3 was considered the negative control for the deposition, as it would neither

be deposited onto nor evicted from the chromatin in the differentiated/growth-arrested Neuro2a cells.

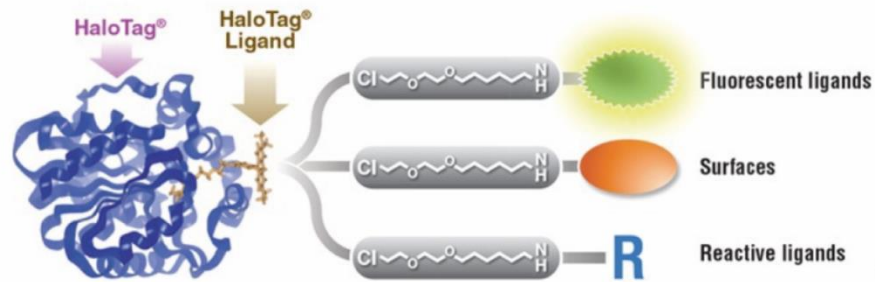


**Figure 3. 1: The HaloTag imaging platform.** Representation of the HaloTag system. HaloTag protein forms a covalent bond with the HaloTag ligand. Each ligand contains a binding group and functional moiety, such as fluorescent molecules for intracellular or extracellular purposes, surface ligand for protein immobilisation with resins or slides, and reactive ligand for imaging purposes. (Figure adapted from England *et al.* 2015.)

### 3.1.5 Quench-chase-pause analysis

The quench-chase-pause protocol enables the recording and visualisation of H3.3 deposition changes. (Figure 3. 2). Old/already incorporated histones were labelled with Oregon Green HaloTag ligand, and newly loaded histones were labelled with TMR HaloTag ligand. During H3.3 deposition, we expected the red pause signal to reach the maximum level of intensity, as all old histones would be replaced by new histones, while the intensity of the green quench signal would decrease to the minimum level. On the other hand, from the negative condition dH3-HaloTag, as canonical H3 are only deposited in the S phase, we expected that the red pause signal intensity would not change significantly, and the green quench signal would remain at the minimum level in the differentiated/growth-arrested Neuro2a cells.

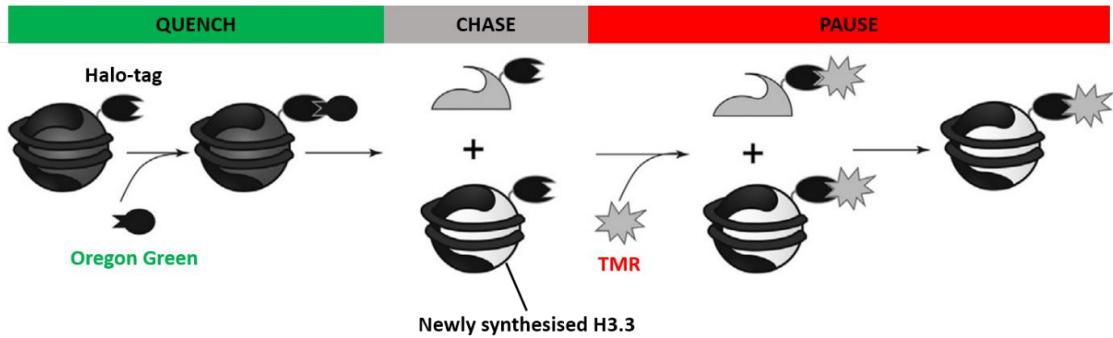


**Figure 3. 2: HaloTag imaging platform of H3.3 deposition into the nucleosome.** Existing H3.3 in the nucleosome were quenched with the Oregon Green HaloTag ligand. The cells were chased. Meanwhile, more H3.3 were newly synthesised and incorporated into the chromatin. These newly loaded H3 were paused with the TMR HaloTag ligand. The old and new incorporation exchange of H3.3 was visualised through the green and red fluorescence signals from the ligands. (Figure modified based on Clément *et al.* 2016.)

## 3.2 Results

### 3.2.1 Construction of expression vectors (H3.3/dH3-HaloTag and H3.3/dH3-pLenti-PGK-Neo-DEST)

As the functional region of the H3.3 and dH3 proteins are at the N-terminus, the HaloTag sequence was fused at the C-terminus of H3.3 and dH3 (Figure 3. 3). The fusion sequence of H3.3/dH3-HaloTag was then cloned into the lentiviral vector pLenti-PGK-Neo-DEST (w531-1) to produce the H3.3/dH3-HaloTag lentiviral construct.<sup>4</sup>

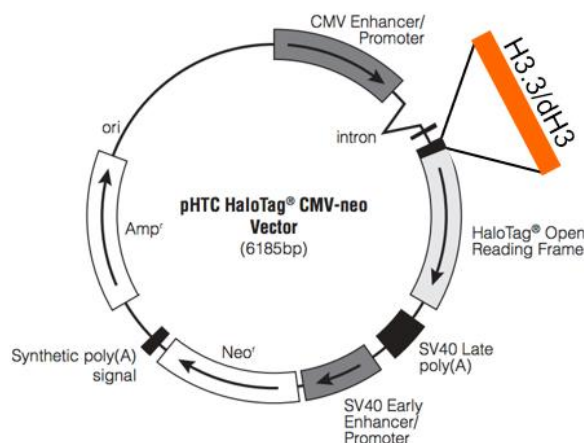


**Figure 3. 3: H3.3- and dH3-HaloTag construct.** Re-constructed pHTC HaloTag CMV-neo Vector with H3.3 or dH3 sequence inserted at the HaloTag N-terminus. (Figure modified based on Promega.)

<sup>4</sup> This was carried out by Michod group at ICH, London.

### 3.2.2 H3.3/dH3-HaloTag Lipofectamine transfection on HEK293T cells, and HaloTag live imaging

Once the H3.3-HaloTag and dH3-HaloTag constructs were produced (Figure 3. 3), Lipofectamine transfection was performed in HEK293T cells for exogenous HaloTag overexpression. The transfected cells were labelled with the HaloTag® R110Direct™ Ligand and imaged live in GFP for HaloTag expression. As a result, both the H3.3-HaloTag– and dH3-HaloTag–transfected HEK293T cells were HaloTag-positive (Figure 3. 4).

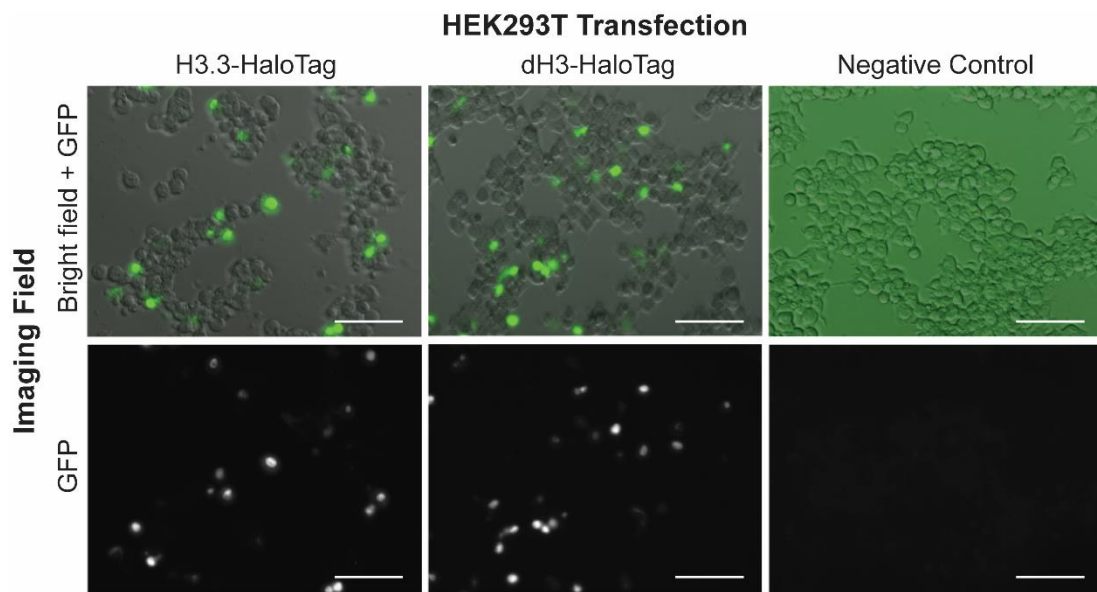


**Figure 3. 4: HEK293T HaloTag live cell imaging.** Pictures show live cell imaging on the H3.3-HaloTag and dH3-HaloTag Lipofectamine-transfected HEK293T cells with the HaloTag® R110Direct™ Ligand. Negative control is untransfected cells. Images were acquired with Zeiss Axio Observer Z1 with Apotome. Scale bar = 100 µm.

### 3.2.3 H3.3-HaloTag and dH3-HaloTag overexpression in Neuro2a cells

The lentiviral constructs were produced and used for transducing H3.3/dH3-HaloTag into Neuro2a cells.<sup>5</sup> Both the endogenous H3.3 (15 KDa) and exogenous H3.3-HaloTag fusion protein (48 KDa) were shown via H3.3 immunoblotting (Figure 3. 5 A). Notably, the membrane blotted with the H3.3 antibody demonstrated non-specific binding at under 55 KDa (\*) (Figure 3. 5 A). It was unsurprising that dH3 was also visualised by the H3.3 antibody, as the two histones differ by only a few amino acids (Figure 3. 5 A). In addition,

<sup>5</sup> This was carried out by Michod group at ICH, London.

HaloTag IF demonstrated specific signals from the H3.3– and dH3–HaloTag transduced Neuro2a cells (Figure 3. 5 B).

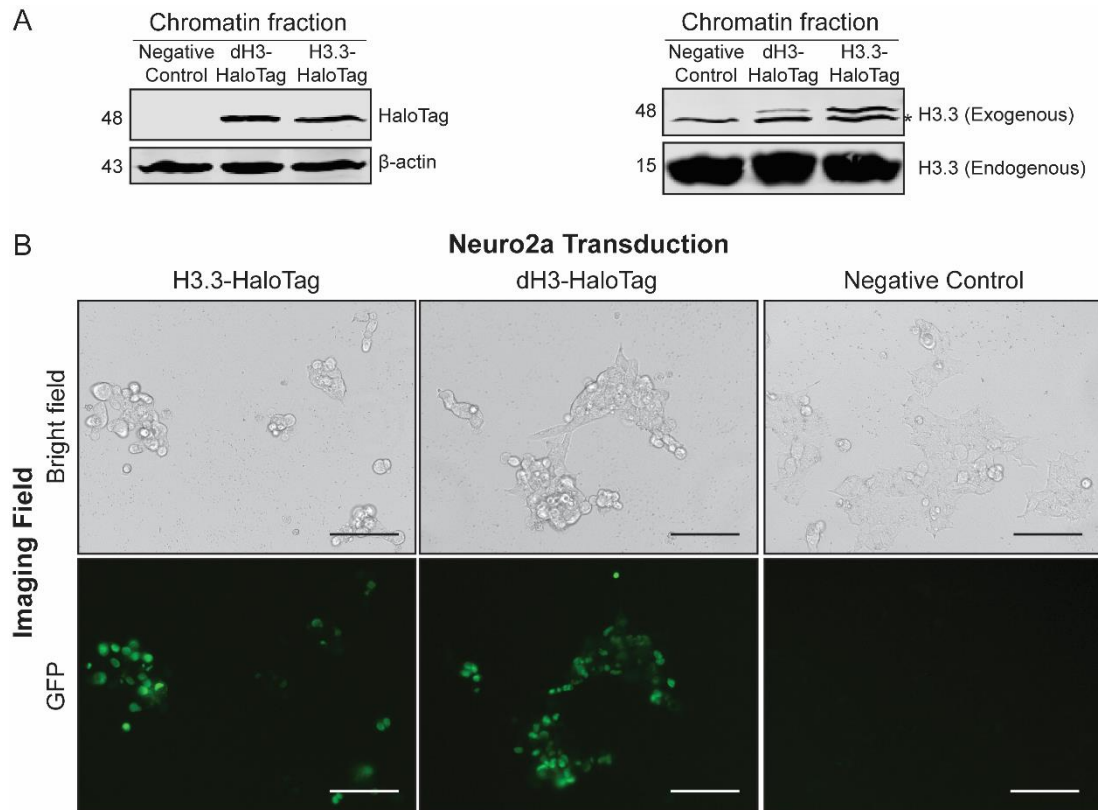


**Figure 3. 5: Chromatin extraction and IF of H3.3-HaloTag– and dH3-HaloTag–transduced Neuro2a cells. (A)** Immunoblotting of HaloTag, H3.3 and  $\beta$ -actin on the chromatin fraction of H3.3-HaloTag– and dH3-HaloTag–transduced Neuro2a cells. \* Represents the non-specific binding of H3.3 antibody. Negative control is untransduced cells. **(B)** Pictures show the GFP IF of the transduced Neuro2a cells labelled with the HaloTag ligand Oregon Green. Negative control is untransduced cells. Images were acquired with an epifluorescence microscope. Scale bar = 100  $\mu$ m.

### 3.2.4 Neuro2a cell differentiation and growth arrest

Neuro2a cells were cultured in complete DMEM for 24 hours before differentiation. RA (20  $\mu$ M) was used as the differentiation treatment. The cells were cultured in differentiation medium for 48 hours before they were used for HaloTag assay analyses. Compared with undifferentiated Neuro2a cells, the differentiated cells exhibited neuron-like morphology, and axon extension was observed (Figure 3. 6 A).

As H3 is specifically phosphorylated during mitosis, pH3 was examined in the differentiated versus undifferentiated Neuro2a cells (Figure 3. 6 B). Around 4% of the total counted Neuro2a cells were pH3-positive, of which around 0.5%

were differentiated cells and about 3.5% were undifferentiated cells (Figure 3.6 B, Left). The mitotic index of the differentiated cells was about 5 times lower than that of the undifferentiated cells (Figure 3.6 B, Right), indicating that the differentiated cells were indeed growth-arrested.

In the following sections, the experiments were performed on differentiated Neuro2a cells. The detailed protocols have been described in the Material and Methods, Section 2.2.4.

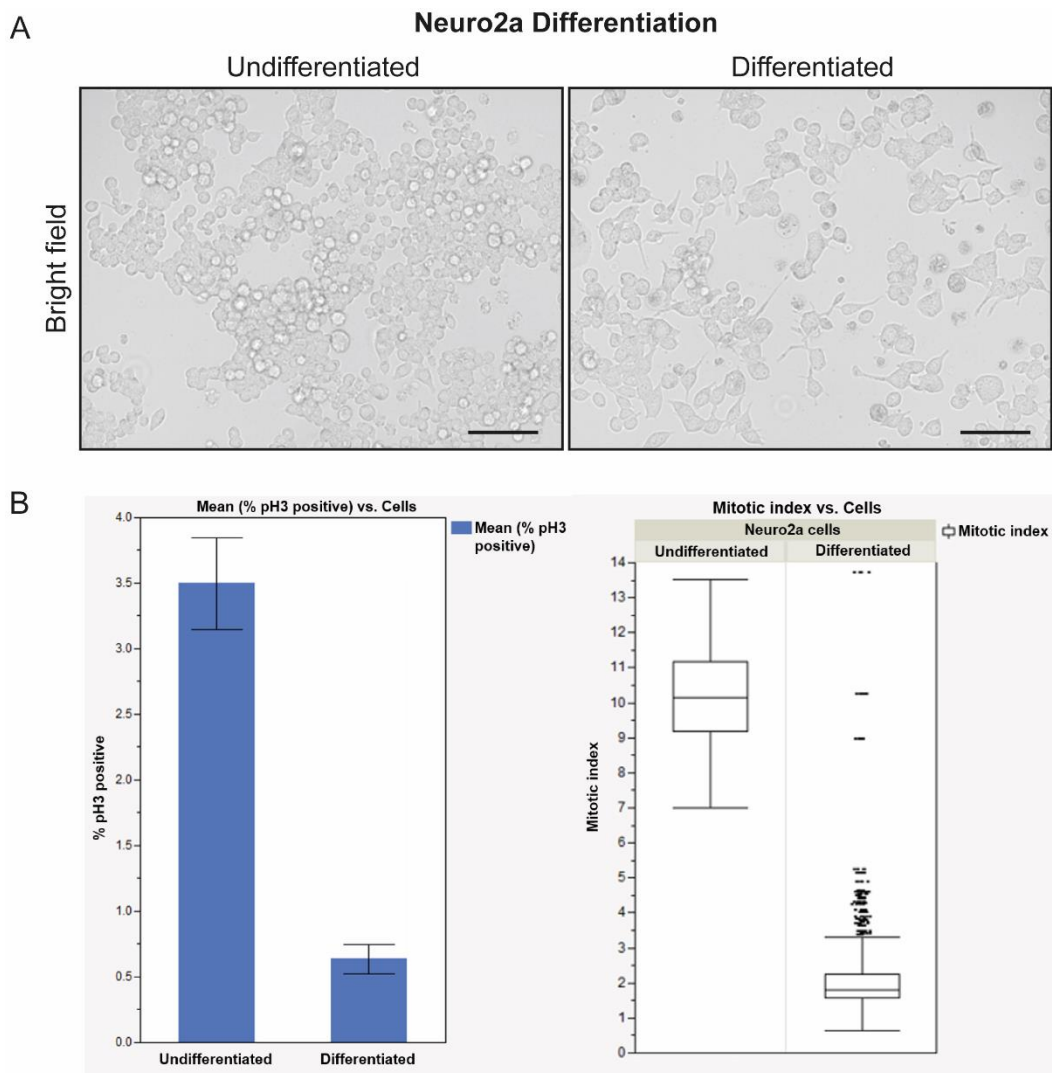


**Figure 3. 6: Neuro2a cell differentiation and pH3 expression. (A)** Pictures show morphology of undifferentiated and differentiated Neuro2a (N2a) cells. Images were acquired with a bright field microscope. Scale bar = 100  $\mu$ m. **(B) (Left)** The expression level of pH3 in differentiated and undifferentiated Neuro2a cells. **(Right)** The mitotic index of differentiated and undifferentiated Neuro2a cells.<sup>6</sup>

<sup>6</sup> These graphs were produced by the Laboratory Automation Technologies group at DZNE, Bonn.

### **3.2.5 H3.3 and dH3 loading in Neuro2a cells: HaloTag fluorescence imaging assay**

The HaloTag ligands, Oregon Green and TMR, were applied to H3.3-HaloTag- and dH3-HaloTag-transduced Neuro2a cells. The Oregon Green ligand was used for quenching histone deposition, and the TMR ligand was used for pausing histone deposition. The TMR control (pause-only) showed that the signal was exclusive in the red channel; no cross-channel leakage was observed (Figure 3. 7 A and B). The cells were quenched with the Oregon Green ligand, chased for 4 time points: 0, 3, 6, and 9 hours, and paused with the TMR ligand. Signal intensities differed between the time points and the fluorescence channels (Figure 3. 7 A and B). Quantification analysis of the corrected total cell fluorescence (CTCF) demonstrated changes in the intensities, representing changes in the deposited and evicted histones (Figure 3. 7 C). The CTCF analysis showed that the intensity of both the green signal (quench) and the red signal (pause) increased during the 9-hour chase period in the H3.3-HaloTag overexpression Neuro2a cells (Figure 3. 7 C). In the dH3-HaloTag overexpression Neuro2a cells, CTCF analysis showed a decreased green signal (quench) while the red signal remained unchanged in the 9-hour chase period (Figure 3. 7 C).

The quench-chase-pause experiment was duplicated, in which an Oregon Green control (quench-only) was included (Figure 3. 8 A). The results from the TMR ligand control were consistent with the experiment in Figure 3. 7, and the Oregon Green ligand control experiment showed no leakage of green signals to the red channel (Figure 3. 8 A, B and C). Similar findings were observed from CTCF analysis of the H3.3-HaloTag overexpression Neuro2a cells, in which the intensity of both the green signal (quench) and the red signal (pause) increased during the 9-hour chase period (Figure 3. 8 D). CTCF analysis of the dH3-HaloTag overexpression Neuro2a cells also demonstrated a similar result as in its duplicate experiment above (Figure 3. 8 D versus Figure 3. 7 C).

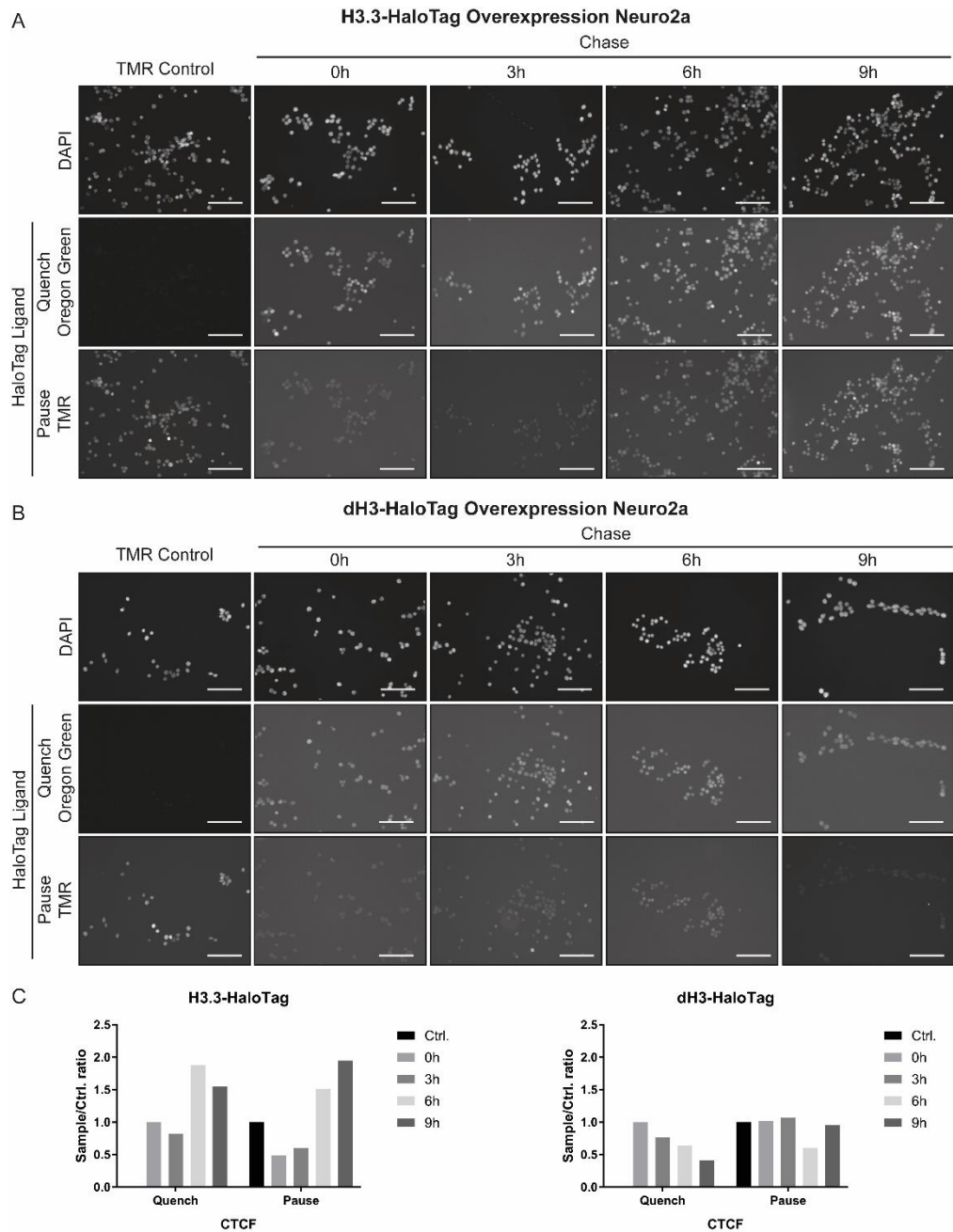
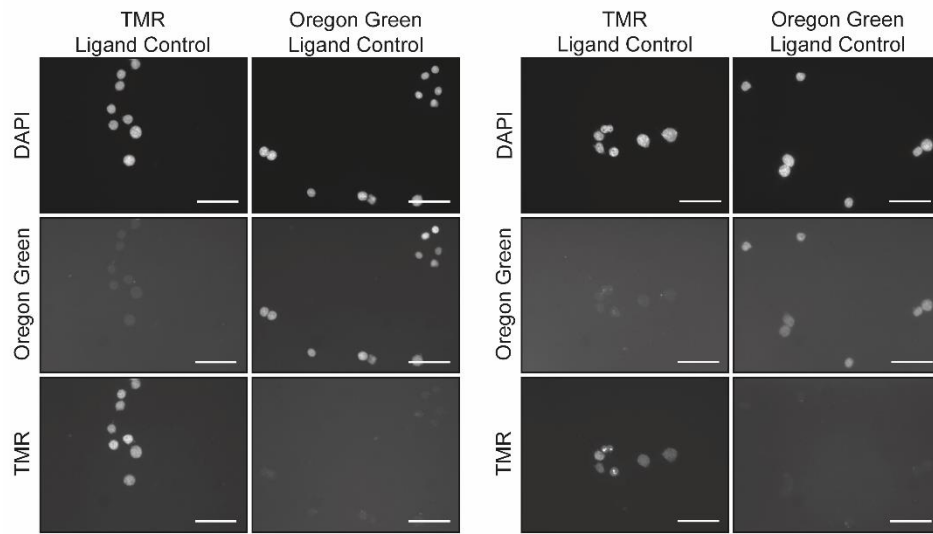
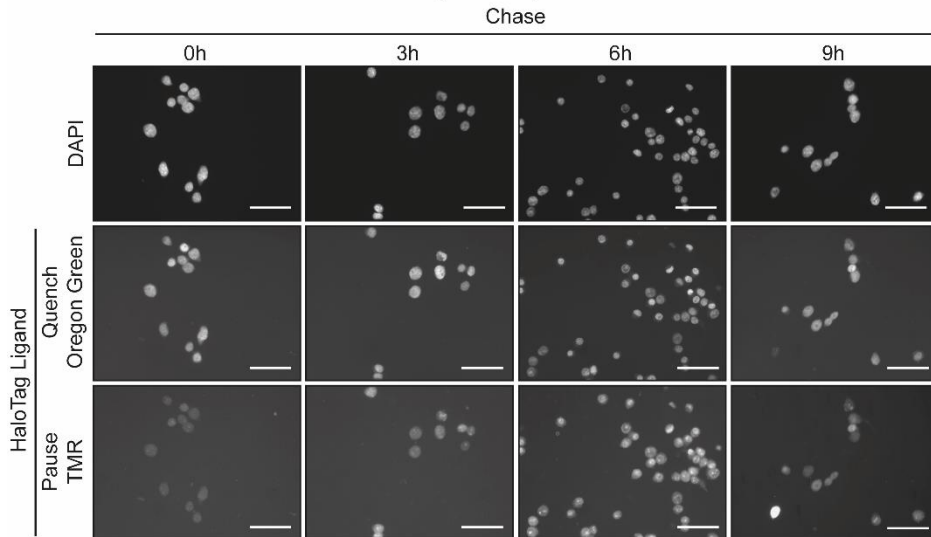


**Figure 3. 7: HaloTag IF of quench-chase-pause in H3.3/dH3-HaloTag overexpression Neuro2a cells. (A)** Images show H3.3-HaloTag overexpression Neuro2a cells quenched with the Oregon Green HaloTag ligand; chased for 0, 3, 6 and 9 hours; and paused with the TMR HaloTag ligand. The nuclei were labelled with DAPI. For the red channel control, the cells were only labelled with the TMR HaloTag ligand. **(B)** Images show the dH3-HaloTag overexpression Neuro2a cells quenched with the Oregon Green HaloTag ligand; chased for 0, 3, 6 and 9 hours; and paused with the HaloTag TMR ligand. The nuclei were labelled with DAPI. For the red channel control, the cells were only labelled with the TMR HaloTag ligand. **(C)** CTCF quantification of HaloTag signals at the pause time points 0, 3, 6 and 9 hours. The expression levels of the Oregon Green HaloTag signal were normalised to the 0-hour signal. The expression levels of the TMR HaloTag signal were normalised to the TMR control signal. Images were acquired with an epifluorescence microscope. Scale bar = 200  $\mu$ m.

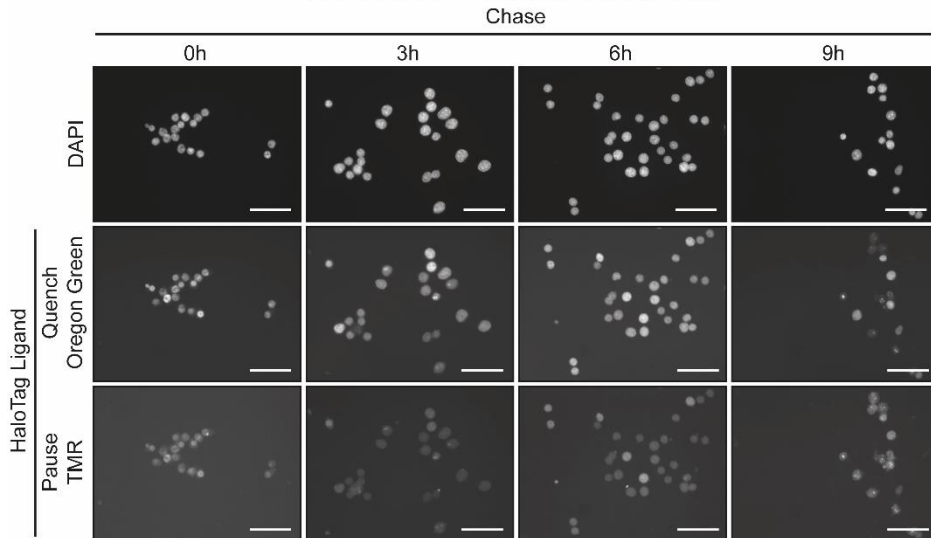
**A H3.3-HaloTag Overexpression Neuro2a      dH3-HaloTag Overexpression Neuro2a**



**B H3.3-HaloTag Overexpression Neuro2a**



**C dH3-HaloTag Overexpression Neuro2a**



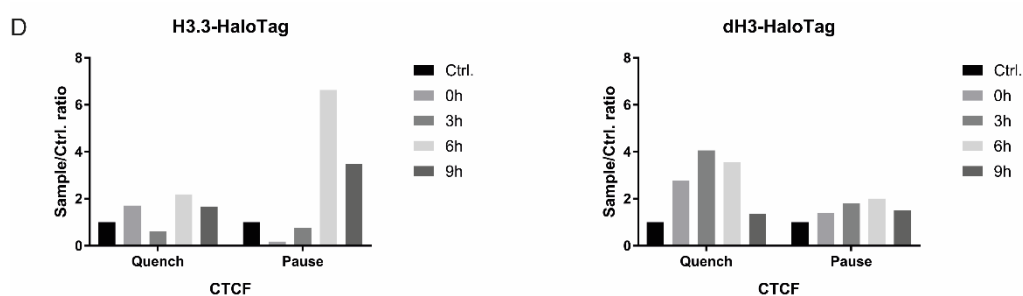


**Figure 3. 8: HaloTag IF of quench-chase-pause in H3.3/dH3-HaloTag overexpression Neuro2a cells (duplicate).** (A) H3.3/dH3-HaloTag overexpression Neuro2a cells labelled with either red-only or green-only HaloTag ligand as the red or green channel control, respectively. The nuclei were labelled with DAPI. (B) H3.3-HaloTag overexpression Neuro2a cells were quenched with Oregon Green HaloTag ligand; chased for 0, 3, 6 and 9 hours; and paused with the HaloTag TMR ligand. The nuclei were labelled with DAPI. (C) dH3-HaloTag overexpressing Neuro2a cells were quenched with the Oregon Green HaloTag ligand; chased for 0, 3, 6 and 9 hours; and paused with the HaloTag TMR ligand. The nuclei were labelled with DAPI. (D) CTCF quantification of HaloTag signals at the pause time points 0, 3, 6 and 9 hours. Expression levels of the Oregon Green HaloTag signal were normalised to the Oregon Green control signal. Expression levels of the TMR HaloTag signal were normalised to the TMR control signal. Images were acquired with an epifluorescence microscope. Scale bar = 100  $\mu$ m.

### 3.2.6 Establishment of H3.3 deposition assay for high-content compound/drug screening

Before establishing the histone deposition assay with the automated platform for high-content screening, the H3.3/dH3-HaloTag overexpression Neuro2a cells were first examined as quality control. This included examining the percentage of cells expressing the HaloTag protein, and the percentage of cells labelled with the HaloTag fluorescence ligand (Figure 3. 9 A). We found that all HaloTag-transduced cells were labelled with the HaloTag fluorescence ligand, i.e. all the Neuro2a cells were HaloTag-positive (Figure 3. 9 A).

Compared with nuclear staining (Hoechst), the intensity of the HaloTag signal was more evenly distributed (Figure 3. 9 B). Moreover, the mean intensity of the HaloTag fluorescence ligand was lower than that of the Hoechst signal by 0.02 points (Figure 3. 9 B, Top). There was no cross-channel contamination between the blue (Hoechst) and green channels (HaloTag Oregon Green ligand) (Figure 3. 9 B, Bottom).

Although altered morphology and reduced mitotic index were observed (Section 3.2.4), the level of Neuro2a cell growth arrest was examined as part

of the quality control. Here, the growth rate of Neuro2a cells treated and differentiated with G1-inhibitor and RA, respectively, were analysed (Figure 3. 10 A). In detail, the undifferentiated Neuro2a cell number varied between 100 and 1,250, and the mean value was >1,100 cells per well (Figure 3. 10 A). Compared with the undifferentiated cells, the cell counts of the Neuro2a cells treated with G1-inhibitor and differentiated with RA among the cell wells were more concentrated (Figure 3. 10 A). Moreover, the mean cell number of the RA-differentiated Neuro2a cells was only 25 cells higher than that of the cells treated with G1-inhibitor (Figure 3. 10 A). Consistent results were observed from the EdU staining, in which the proportion of the dividing cells in the RA-differentiated condition was about 10% higher than that of the G1-inhibited condition (Figure 3. 10 B).

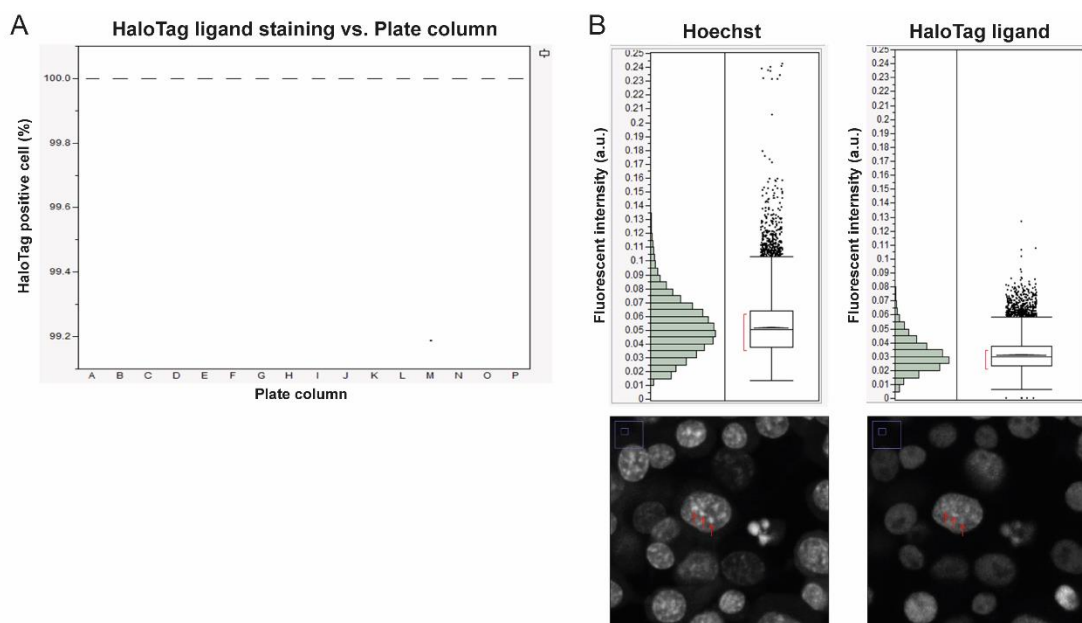


**Figure 3. 9: *In vitro* HaloTag expression in transduced Neuro2a cells, and the HaloTag imaging assay.**<sup>7</sup> **(A)** Proportion of cells positive for HaloTag staining in HaloTag-transduced Neuro2a cells. **(B) (Top)** Intensity distribution of nuclear staining (Hoechst) and HaloTag ligand staining in HaloTag-transduced Neuro2a cells. **(Bottom)** The two images are examples of nuclear and HaloTag staining in the transduced Neuro2a cells corresponding to the top left and right graphs, respectively. Red arrows highlight DAPI-stained nucleus and its corresponding location in the HaloTag ligand channel. Images were acquired with CellVoyager CV6000 (Yokogawa) confocal microscope.

<sup>7</sup> These graphs were produced by the Laboratory Automation Technologies group at DZNE, Bonn.

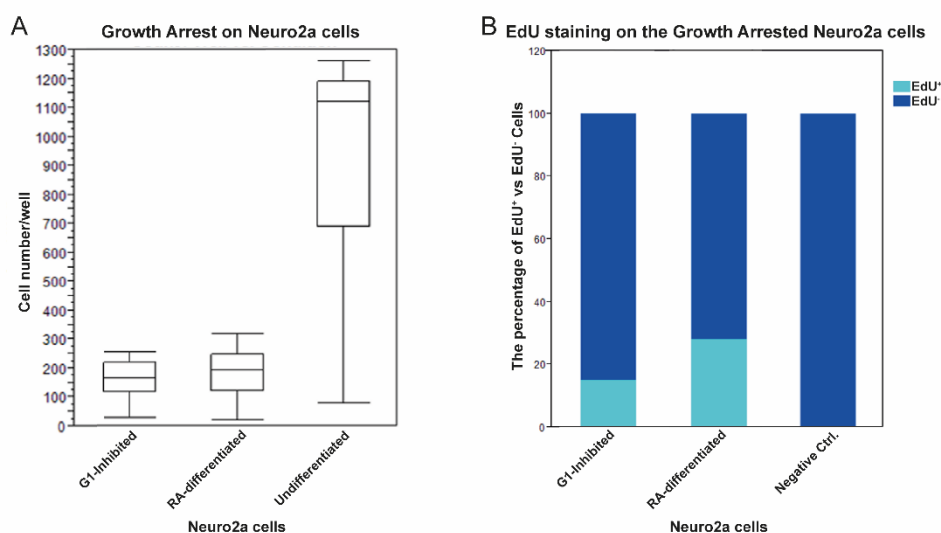


**Figure 3. 10: Analysis of cell growth arrest and EdU staining.**<sup>8</sup> **(A)** The number of cells among the G1-inhibited, RA-differentiated and undifferentiated Neuro2a cells. **(B)** The percentage of EdU-positive cells among G1-inhibited and RA-differentiated Neuro2a cells. The negative control was Neuro2a cells without EdU staining.

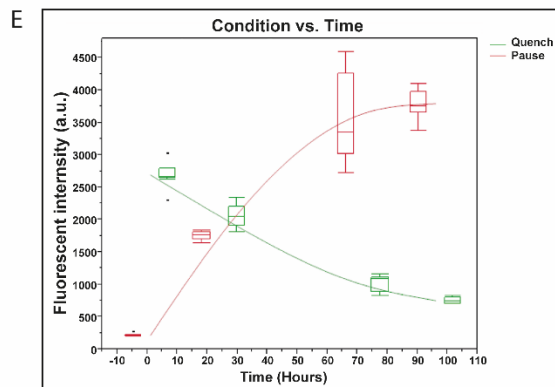
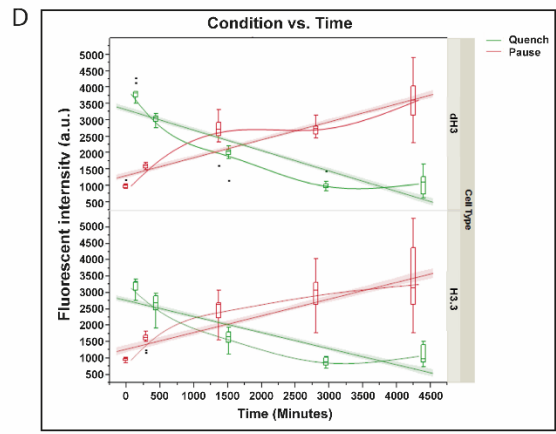
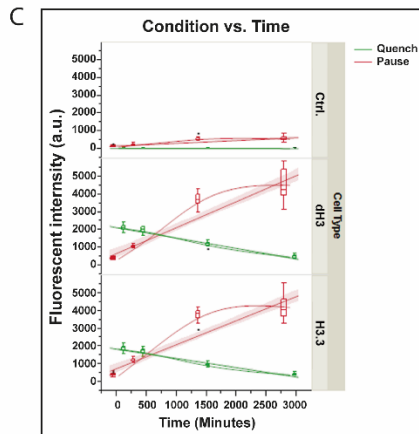
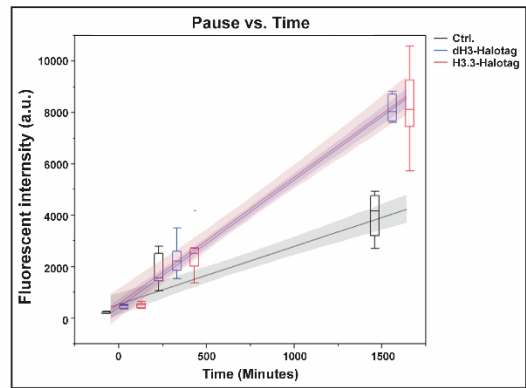
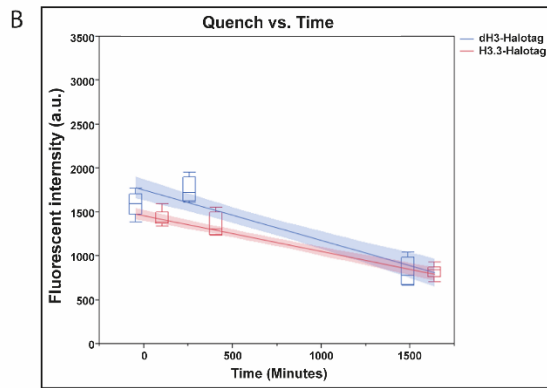
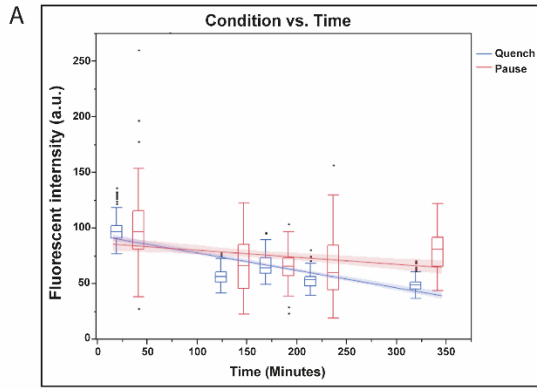
Following quality control analysis, H3.3 deposition visualisation with the HaloTag fluorescence ligand was examined. Although the preliminary experiment in Section 3.2.5 showed increased H3.3 deposition during the 9-hour quench-chase-pause, neither the quench nor the pause exhibited altered intensity during the observed time (0–6 hours) (Figure 3. 11 A).

Next, the observation time of the quench-chase-pause was increased to 26 hours (Figure 3. 11 B). Consequently, the quench signals (old histones) were decreased between 6 and 26 hours of the chase period, and the pause signals (new histones) were increased during the 26-hour chase period in both the H3.3-HaloTag and dH3-HaloTag overexpression Neuro2a cells (Figure 3. 11 B).

To examine the complete turnover duration of H3.3 eviction–deposition in the chromatin, the observation time of the quench-chase-pause was extended to 48 hours and 72 hours (Figure 3. 11 C and D, respectively). Although changes in quench/pause signal intensity were visualised (Figure 3. 11 F), neither 48 nor 72 hours were sufficient for H3.3/dH3 to complete the eviction–deposition cycle.

<sup>8</sup> This experiment was carried out and the graphs were produced by the Laboratory Automation Technologies group at DZNE, Bonn.

In the end, the quench and pause signals reached their minimum and maximum intensities, respectively, at 96 hours (Figure 3. 11 E), indicating that the turnover time of H3.3 eviction–deposition requires 96 hours.



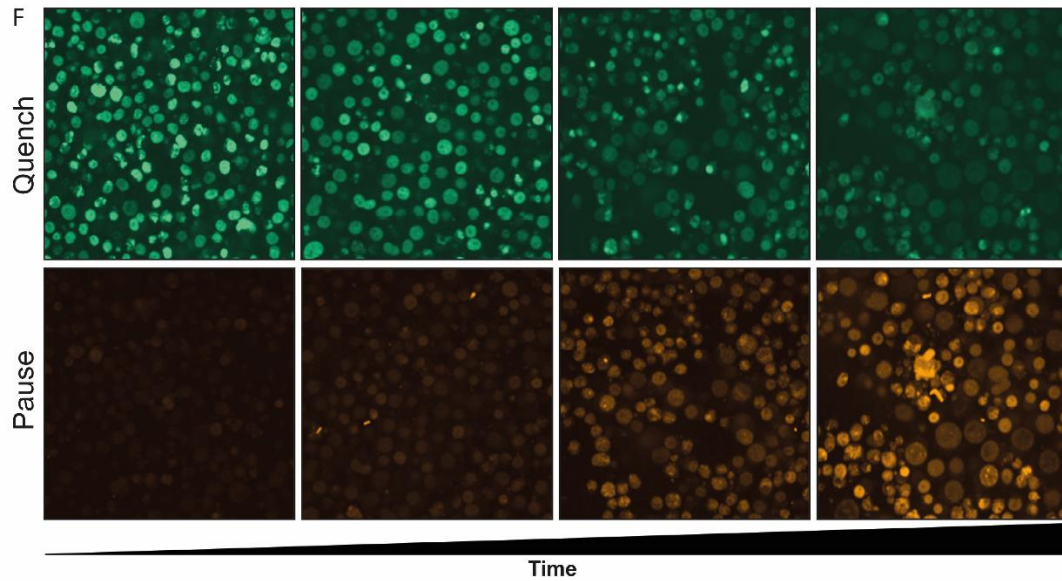


**Figure 3. 11: H3.3/dH3-HaloTag deposition assay in differentiated Neuro2a cells. The quench-chase-pause assay visualises and quantifies H3.3/dH3 eviction and incorporation from and into the chromatin.<sup>9</sup> (A)** H3.3-HaloTag overexpression Neuro2a cells were quenched with the Oregon Green HaloTag ligand; chased for 0, 2.5, 3, 3.5 and 6 hours; and paused with the HaloTag TMR ligand. **(B)** H3.3-HaloTag and dH3-HaloTag overexpression Neuro2a cells were quenched with the Oregon Green HaloTag ligand; chased for 0, 6 and 26 hours; and paused with the HaloTag TMR ligand. **(Left)** The eviction of H3.3 and dH3 from the chromatin. **(Right)** The deposition of H3.3 and dH3 on the chromatin. The control group was untransfected Neuro2a cells. **(C)** H3.3-HaloTag and dH3-HaloTag overexpression Neuro2a cells were quenched with the Oregon Green HaloTag ligand; chased for 0, 6, 24 and 48 hours; and paused with the HaloTag TMR ligand. The control group was untransfected Neuro2a cells. **(D)** H3.3-HaloTag and dH3-HaloTag overexpression Neuro2a cells were quenched with the Oregon Green HaloTag ligand; chased for 0, 6, 24, 48 and 72 hours; and paused with the HaloTag TMR ligand. **(E)** H3.3-HaloTag overexpression Neuro2a cells were quenched with the Oregon Green HaloTag ligand; chased for 0, 24, 72 and 96 hours; and paused with the HaloTag TMR ligand. **(F)** Images of Oregon Green (Quench) and TMR (Pause) at 0–48 hours from H3.3-HaloTag overexpression Neuro2a cells. Images were acquired with CellVoyager CV6000 (Yokogawa) confocal microscope.

<sup>9</sup> The graphs A–E were produced by the Laboratory Automation Technologies group at DZNE, Bonn.

### 3.2.7 Single downregulation of Hira and Daxx with RNAi

As Daxx and Hira are the two main H3.3 deposition chaperones, Daxx and Hira single and double downregulations in Neuro2a cells are established here. These conditions will be considered the negative controls in *de novo* H3.3 loading, and will be performed with the high-content drug/compound screening.

siRNA was used for downregulating the Hira and Daxx proteins in the H3.3-HaloTag and dH3-HaloTag overexpression Neuro2a cells. As Neuro2a cell differentiation takes place over 48 hours (Section 3.2.4), the cells were transfected 24 hours before differentiation. Therefore, the cells were differentiated when the transfection reagents had been completely washed out.

First, the downregulation transfection with gradient *Hira* siRNA concentrations was examined. The cells were also transfected with *Gapdh* and Scramble siRNA as the transfection positive and negative control, respectively. The immunoblotting quantification showed that *Hira* RNAi was most effective at 72 hours post-transfection in the H3.3-HaloTag overexpression Neuro2a cells, where Hira was downregulated by 50% (Figure 3. 12 A). At 72 hours post-transfection, Hira downregulation was maintained despite the *Hira* siRNA concentration being increased (Figure 3. 12 A and B). Moreover, *Gapdh* downregulation (positive control) was most effective at 72 hours post-transfection, with a reduction rate of over 75% (Figure 3. 12 A and B). Daxx expression in the *Hira* siRNA transfection cells was monitored. Notably, the Daxx expression level was increased by almost 50% and 20% at 72 hours post-transfection in the H3.3-HaloTag and dH3-HaloTag overexpression Neuro2a cells, respectively (Figure 3. 12 A and B).

The downregulation with 30 nM *Daxx* siRNA was then examined (Figure 3. 13). At 72 hours post-transfection, Daxx was downregulated by about 50%, and *Gapdh* was downregulated by about 75% (Figure 3. 13 A). Notably, although the Hira expression level in the dH3-HaloTag overexpression Neuro2a cells was unaffected by the Daxx downregulation, that of the H3.3-HaloTag overexpression Neuro2a cells was increased by 20% (Figure 3. 13 B).

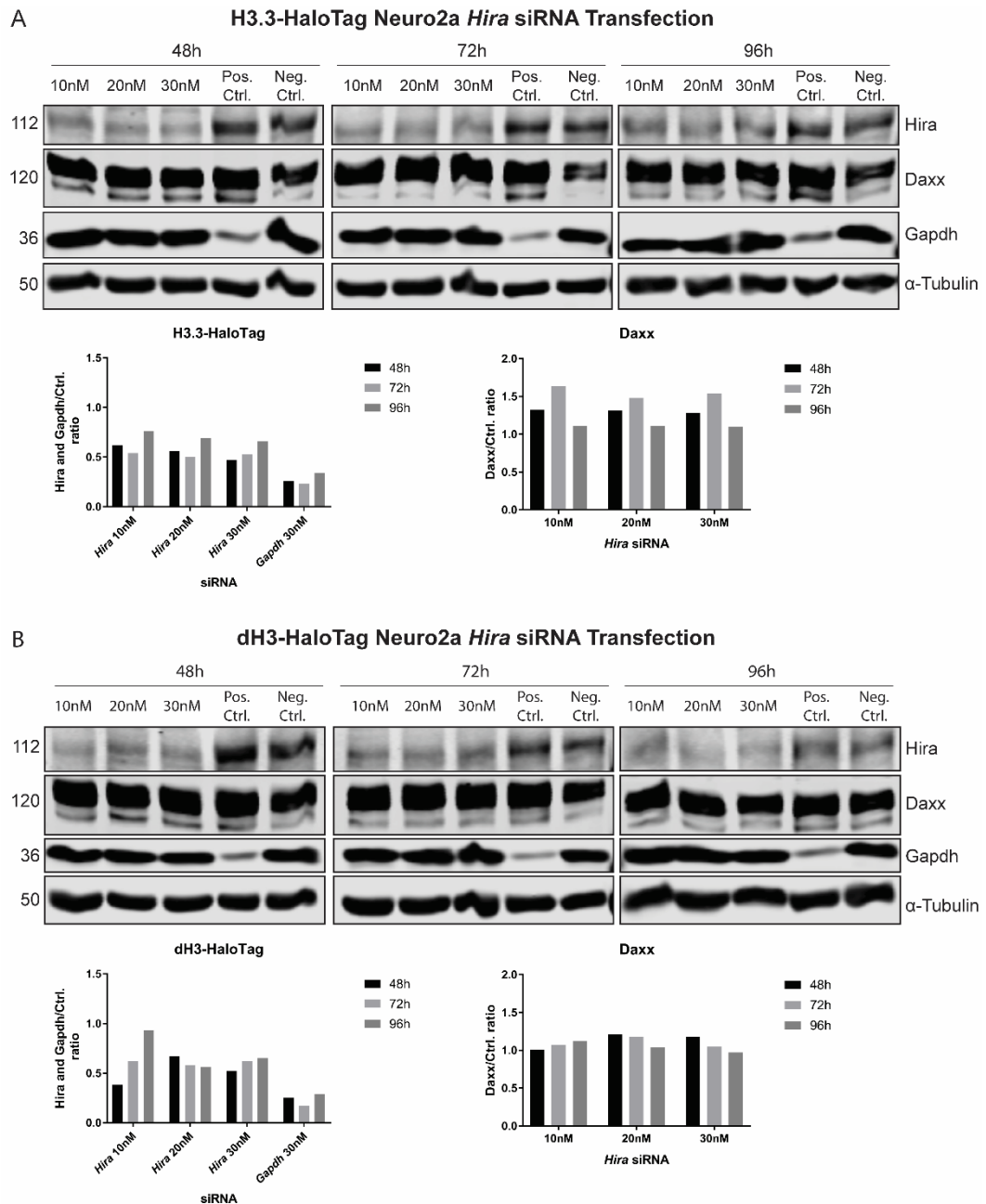


**Figure 3. 12: *Hira* siRNA downregulation in the H3.3/dH3-HaloTag overexpression Neuro2a cells. (A)** Immunoblotting of Hira, Daxx, Gapdh and  $\alpha$ -tubulin in H3.3-HaloTag overexpression Neuro2a cells. The cells were treated with 10 nM, 20 nM or 30 nM *Hira* siRNA and collected 48, 72 or 96 hours post-transfection. The positive control was cells treated with 30 nM *Gapdh* siRNA. The negative control was cells treated with 30 nM Scramble siRNA. The histogram shows the immunoblotting expression quantification for Hira, Gapdh and Daxx normalised to the negative control. **(B)** Immunoblotting of Hira, Daxx, Gapdh and  $\alpha$ -tubulin in dH3-HaloTag overexpression Neuro2a cells. The cells were treated with 10 nM, 20 nM or 30 nM *Hira* siRNA and collected 48, 72 or 96 hours post-transfection. The positive control was cells treated with 30 nM *Gapdh* siRNA. The negative control was cells treated with 30 nM Scramble siRNA. The histogram shows the immunoblotting expression quantification for Hira, Gapdh and Daxx normalised to the negative control.

### Neuro2a *Daxx* siRNA (30nM) 72h Post-transfection

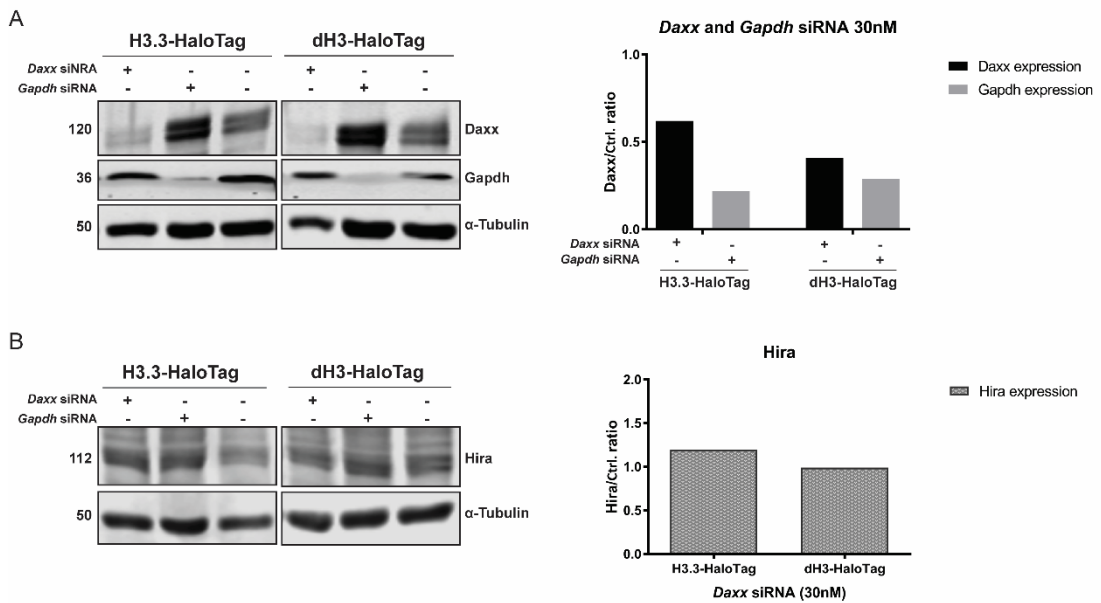


**Figure 3.13: *Daxx* siRNA downregulation in H3.3/dH3-HaloTag overexpression Neuro2a cells. (A) (Left)** Immunoblotting of Daxx, Gapdh and  $\alpha$ -tubulin in H3.3-HaloTag and dH3-HaloTag overexpression Neuro2a cells. The cells were treated with 30 nM *Daxx* and collected 72 hours post-transfection. Cells treated with 30 nM *Gapdh* siRNA were the positive control. Cells treated with 30 nM Scramble siRNA were the negative control. **(Right)** The histogram shows the immunoblotting expression quantification for Daxx and Gapdh normalised to the negative control. **(B) (Left)** Immunoblotting of Hira and  $\alpha$ -tubulin in H3.3-HaloTag and dH3-HaloTag overexpression Neuro2a cells. The cells were treated with 30 nM *Daxx* siRNA and collected 72 hours post-transfection. Cells treated with 30 nM *Gapdh* siRNA were the positive control. Cells treated with 30 nM Scramble siRNA were the negative control. **(Right)** The histogram shows the immunoblotting expression quantification for Hira normalised to the negative control.

#### 3.2.8 Hira and Daxx double downregulation with RNAi

Double downregulation of Daxx and Hira was first performed in the H3.3-HaloTag overexpression Neuro2a cells. Daxx was downregulated by 90% by *Daxx* single siRNA transfection and by 55% by *Daxx/Hira* double siRNA transfection (Figure 3.14 A). However, there were strong background signals on the immunoblotting membrane blotted with the HIRA antibody (Figure 3.14 A). We speculate that the Hira antibody did not perform well, possibly due to handling during transport of the antibody to Germany or due to change of batch of the homemade antibody.

Therefore, the experiment was repeated, and qPCR was used to analyse the mRNA expression of *Daxx* and *Hira* in the siRNA-transfected Neuro2a cells. *Hira* mRNA was downregulated (by 50%) only in the *Hira* siRNA transfection

H3.3-HaloTag overexpression Neuro2a cells (Figure 3. 14 B, Left). However, Hira expression was increased in all other conditions, including the *Daxx* siRNA-only transfection (Figure 3. 14 B, Left).

As qPCR analysis showed that *Hira* siRNA downregulation was not efficient, increased *Hira* siRNA treatments at 40 nM and 50 nM were tested. Transfection with 40 nM or 50 nM *Hira* siRNA resulted in similar levels of *Hira* mRNA downregulation, ranging between 70% and 80% (Figure 3. 15, Left). *Hira* downregulation with 30 nM *Hira* siRNA transfection was ~10% and ~80% in the H3.3-HaloTag and dH3-HaloTag overexpression Neuro2a cells, respectively.

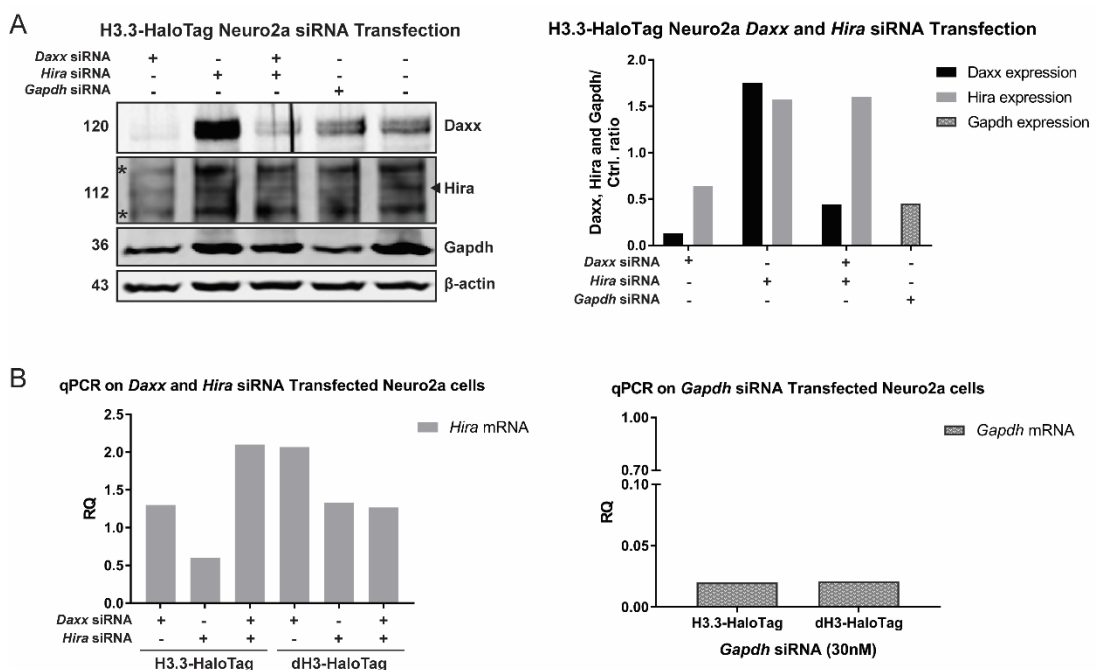


**Figure 3. 14: *Daxx* and *Hira* siRNA downregulation in H3.3/dH3-HaloTag overexpression Neuro2a cells. (A) (Left)** Immunoblotting of *Daxx*, *Hira*, *Gapdh* and  $\beta$ -actin in H3.3-HaloTag overexpression Neuro2a cells. The cells were treated with 30 nM *Daxx* siRNA, 30 nM *Hira* siRNA, or 30 nM *Daxx* and 30 nM *Hira* siRNA. The cells were collected 72 hours post-transfection. Cells treated with 30 nM *Gapdh* siRNA were the positive control. Cells treated with 30 nM Scramble siRNA were the negative control. **(Right)** The histogram shows the immunoblotting expression quantification for *Daxx*, *Hira* and *Gapdh* normalised to the negative control. Arrowhead indicates the *Hira* protein immunoblotting signal. \* Represents non-specific binding of *Hira* antibody. **(B)** qPCR analysis of *Daxx*, *Hira* and *Gapdh* in H3.3-HaloTag and dH3-HaloTag overexpression Neuro2a cells normalised to the negative control. RQ = relative quantification.

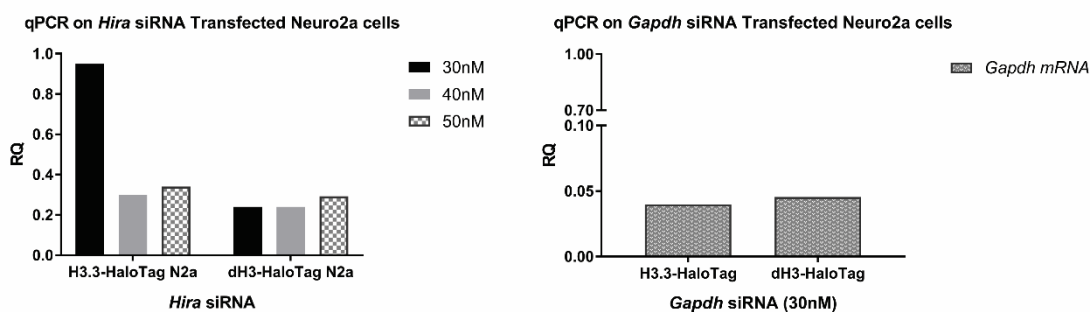


**Figure 3. 15: *Hira* siRNA downregulation in H3.3/dH3-HaloTag overexpression Neuro2a cells. (Left)** qPCR analysis of *Hira* in H3.3-HaloTag and dH3-HaloTag overexpression Neuro2a cells. The cells were treated with 30 nM, 40 nM and 50 nM *Hira* siRNA. **(Right)** qPCR analysis of *Gapdh* in H3.3-HaloTag and dH3-HaloTag overexpression Neuro2a cells. The cells were treated with 30 nM *Gapdh* siRNA. The cell lysates were collected 72 hours post-treatment. Quantification was normalised to cells treated with 50 nM Scramble siRNA (negative control). RQ = relative quantification.

The double siRNA transfection was repeated, in which increased, i.e. 50 nM, *Hira* siRNA was used for downregulating *Hira*. The *Daxx* siRNA downregulated the expression of *Daxx* (Figure 3. 16, Top left). Notably, in the double siRNA transfection conditions, *Daxx* downregulation in the dH3-HaloTag overexpression Neuro2a cells was around 50% less effective than that in the H3.3-HaloTag overexpression Neuro2a cells (Figure 3. 16, Top left). In addition, *Hira* was downregulated by around 50% in the single *Hira* siRNA transfection cells (Figure 3. 16, Top right). However, in the double siRNA transfection conditions, *Hira* mRNA level was increased almost 50 times in the H3.3-HaloTag overexpression Neuro2a cells (Figure 3. 16, Top right). Meanwhile, *Hira* mRNA level in the dH3-HaloTag overexpression Neuro2a cells was increased by almost 2 times (Figure 3. 16, Top right).

We speculate that the *Daxx* downregulation may interfere with the *Hira* downregulation and/or activate a cell defensive mechanism, thus leading to the boosted *Hira* mRNA level.

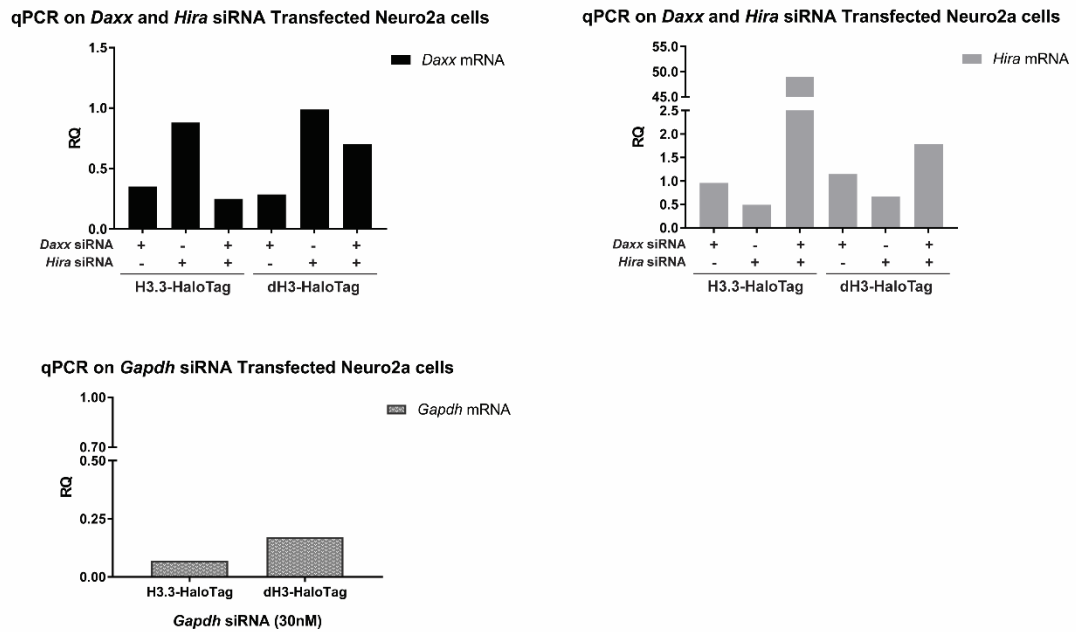


**Figure 3. 16: *Daxx* and *Hira* siRNA downregulation in H3.3/dH3-HaloTag overexpression Neuro2a cells.** H3.3-HaloTag and dH3-HaloTag overexpression Neuro2a cells were treated with 30 nM *Daxx* siRNA and 50 nM *Hira* siRNA, or 30 nM *Daxx* and 50 nM *Hira* siRNA. **(Top left)** qPCR analysis of *Daxx* in H3.3-HaloTag and dH3-HaloTag overexpression Neuro2a cells. **(Top right)** qPCR analysis of *Hira* in H3.3-HaloTag and dH3-HaloTag overexpression Neuro2a cells. **(Bottom)** qPCR analysis of *Gapdh* in H3.3-HaloTag and dH3-HaloTag overexpression Neuro2a cells. The cells were treated with 30 nM *Gapdh* siRNA. The cell lysates were collected 72 hours post-treatment. Quantification was normalised to cells treated with 50 nM Scramble siRNA (negative control). RQ = relative quantification.

### **3.3 Discussion**

This chapter focused on the development of the H3.3 chromatin-incorporation imaging assay in Neuro2a cells. The visualisation assay was also adapted to the robotised automation platform for use in high-content/drug screening.

#### **3.3.1 HaloTag imaging assay for H3.3 deposition**

##### **3.3.1.1 Generation of H3.3/dH3-HaloTag overexpression Neuro2a cells**

During the generation of the H3.3-HaloTag and dH3-HaloTag overexpression Neuro2a cells, HaloTag immunoblotting showed the expected 48-KDa H3-HaloTag fusion protein (Figure 3. 5 A). Only H3.3 was immunoblotted, as there are no suitable *Drosophila* H3 antibodies. Given that dH3 only differs from H3.3 by 5 amino acids, non-specific binding was expected. *Drosophila* H3 immunoblotting should be performed once the antibody is available. In addition, the immunoblotting results suggest that the H3.3-HaloTag fusion protein was indeed expressed in the Neuro2a cells. Meanwhile, IF confirmed that all Neuro2a cells were transduced with H3.3/dH3-HaloTag, and confirmed the specificity of the HaloTag ligand (Figure 3. 9).

##### **3.3.1.2 RA differentiation of Neuro2a cells**

Even though neuronal-like morphology with elongated neurites was observed in the RA-treated Neuro2a cells (Figure 3. 6), Neuro2a cell differentiation was validated via pH3 staining (i.e. the mitotic index) analysis and EdU staining (Figure 3. 6 and Figure 3. 10). The expression level of pH3 was significantly reduced in the differentiated Neuro2a cells, and the percentage of the dividing cells (EdU) among the RA-differentiated Neuro2a cells was as low as that of the G1-inhibited Neuro2a cells (Figure 3. 10 B).

##### **3.3.1.3 Quench-chase-pause assay**

Preliminary examinations of the HaloTag imaging assay were performed using the traditional IF method, with cells plated on coverslips and imaged with an epifluorescence microscope. The results obtained from the differentiated Neuro2a cells indicated a significant increase in H3.3 chromatin deposition at 6 hours and 9 hours post-quinching, whereas dH3 generally remained unchanged (Figure 3. 7 and Figure 3. 8). However, when the visualisation protocol was applied with the robotised automation platform, there was no indication of the increased H3.3 deposition at 6 hours (Figure 3. 11 A). This

could be because: 1) a limited number of Neuro2a cells were quantified on a coverslip, while the robotised automation imaging platform quantified cells in up to 384 wells; 2) as the Neuro2a cells are easily detached, cells were lost during the manual laboratory procedures (e.g. medium change, detergent exchange and washes on the coverslips). The automated platform avoided this.

Significantly, the deposition of H3.3 and dH3 was boosted between 6 and 26 hours, which meant that the newly produced H3.3 and dH3 were replacing the evicted old histones (Figure 3. 11 B). It is also noteworthy that not only was H3.3 incorporated onto the chromatin, dH3 was also loaded onto the chromatin. The chase time was extended to 48 and 72 hours (Figure 3. 11 C and D). Both the quench and pause signals apparently reached the bottom and top thresholds, respectively, after 72 hours. However, it appeared that the longer the chase duration, the less concentrated the intensity levels. In addition, in the growth-arrested Neuro2 cells, the deposition patterns for dH3 and H3.3 were identical.

Eventually, H3.3 deposition at up to 96 hours showed an overlapping but more concentrated intensity of pause signal compared to that at 72 hours, indicating that all 'available' H3.3 slots on the nucleosome were replaced with the newly produced histone (Figure 3. 11 E). The results also suggest that complete turnover of H3.3 requires about 96 hours.

The establishment of high-content analysis of the HaloTag imaging assay provides a method for visualising the deposition of H3.3 for functional biology study. This would also provide a powerful tool in the application to therapeutic development in, but not limited to, brain tumour and neurodegeneration diseases. Via the visualisation assay, the deposition pattern of mutant H3.3 cells reportedly found in glioblastomas can be studied; last but not least, drugs specifically targeting the deposition of mutant H3.3 can be identified and developed.

#### **3.3.1.4 Canonical H3 deposition**

It has been widely reported that canonical H3 are only expressed during the S-phase, and is loaded onto the chromatin in a DNA synthesis-dependent manner (Tagami *et al.* 2004, Szenker *et al.* 2011). The dH3-HaloTag

overexpression Neuro2a cells were produced with the original intention of being used as the negative control for H3.3 loading onto the chromatin. The differentiated Neuro2a cells provide a platform where the cells are growth-arrested, from which H3.3 deposition onto the chromatin could be studied. However, in this study, the canonical H3 displayed the same deposition pattern as H3.3 in the growth-arrested Neuro2a cells. As the RA-differentiated cells had a higher EdU<sup>+</sup> count compared to the G1-inhibited condition (Figure 3. 10), it was suspected that some of the RA-treated Neuro2a cells were still under division; However, the deposition pattern of dH3 was almost identical to that of H3.3 (Figure 3. 11), suggesting this was possibly not the case here.

The data here challenges the commonly accepted idea that canonical H3 loading onto the chromatin is limited to the S-phase. It suggests a more comprehensive coupling of canonical H3 deposition during DNA synthesis events. Notably, canonical H3 deposition out of S-phase has also been reported by Polo *et al.* during their study on H3.1 incorporation by its chaperone CAP-1 at DNA damage repair sites in HeLa cells (Polo *et al.* 2006). In addition, Shi *et al.* have also suggested that H3.1 may under certain circumstances (nor specified in the paper) be deposited into the chromatin during interphase in a DNA replication-independent manner in *Arabidopsis* (Shi *et al.* 2011).

### **3.3.2 Downregulation of Hira and Daxx**

The single siRNA downregulation of the H3.3 chaperones Hira and Daxx was successful in the differentiated Neuro2a cells. At 72 hours after *Hira* siRNA treatment (30 nM siRNA), Hira expression was downregulated by around 50%, and did not affect normal expression of Daxx in the cells (Figure 3. 12). Daxx proteins were also downregulated by *Daxx* siRNA (30 nM), which caused downregulation of about 50%, while Hira expression was increased by 20% in the H3.3-HaloTag overexpression Neuro2a cells (Figure 3. 14).

However, the double downregulation of Daxx and Hira was not as efficient. The downregulation of Hira in the *Daxx* siRNA-treated cells resulted in increased *Hira* expression regardless of the *Hira* siRNA concentration. This might indicate that *Daxx* siRNA interferes with *Hira* siRNA in double siRNA transfection, or that *Hira* was increased *in vitro* due to the loss of *Daxx* as a

cellular defence mechanism. Further analysis is required to determine the reason behind this. For example, a different *Hira* siRNA can be examined in Daxx and Hira double downregulation, and Hira can be downregulated in Daxx knockout neuronal cells.

## **Chapter 4**

### **H3.3 Chaperone Binding Partners in NPCs**

## 4. H3.3 Chaperone Binding Partners in NPCs

### 4.1 Background

#### 4.1.1 Choice of model: neural progenitor cells

In this study, NPCs were used as it is a neural cell system and can be kept in self-renewal mode or differentiated to main neuronal and glial subtypes in a temporal fashion. NPCs from mouse embryos prenatal embryonic day 13.5 (E13.5) were used for identifying the H3.3 chaperone Daxx binding partner, as E13.5 is the peak stage of mouse embryonic neurogenesis.

#### 4.1.2 Identifying H3.3 regulatory pathways in neural cells

As discussed above, DAXX is a H3.3 chaperone and plays a crucial role in H3.3 deposition onto the chromatin (Goldberg *et al.* 2010, Michod *et al.* 2012). While gain-of-function mutations in H3.3 have been identified in human GBM samples and other tumours (Khuong-Quang *et al.* 2012, Schwartzentruber *et al.* 2012, Sturm *et al.* 2012, Wu *et al.* 2012, Behjati *et al.* 2013), loss-of-function DAXX and ATRX mutations co-occur with H3.3 mutations and also with several H3.3 unmutated neoplasms (Heaphy *et al.* 2011, Liu *et al.* 2014). In addition, DAXX may also play a role in chromatin remodelling and transcription at least partially independent from its ability to load H3.3 (Li *et al.* 1992, Pluta *et al.* 1998, Hollenbach *et al.* 1999). Critically, DAXX have been shown to regulate chromatin remodelling and transcription in neurons, with implications for neuronal plasticity, brain function and ageing. In this respect, H3.3 loading is required for lifespan extension in worms, suggesting that it plays a protective role during ageing (Piazzesi *et al.* 2016).

To identify the Daxx interactomes, we used the co-IP technique to pull down the potential Daxx-interacting/binding partners with FLAG-tag. The FLAG-tag protein is a short and hydrophilic 8–amino acid peptide DYKDDDDK. It is fused on the N-terminus of DAXX protein, close to the binding sites of H3.3 (aa183-417) (Lewis *et al.* 2010) and its known interacting partner ATRX (aa55-144) (Tang *et al.* 2004) (Figure 4. 1). Due to its hydrophilic nature, the FLAG-tag is located on the surface of the fusion protein, therefore it can be easily accessed by the FLAG antibody during IP. Additionally, given its small size, it does not obstruct the functional domains of Daxx.

## Daxx



**Figure 4. 1: Schematic presentation of the DAXX domain map.** Functional domains are highlighted with coloured boxes (Red: ATRX binding domain; Green: H3.3 binding domain). FLAG-tag is cloned at the N-terminus of Daxx.

In detail, the FLAG-Daxx sequence was cloned into a dTomato lentiviral construct. The FLAG-Daxx overexpression NPCs were produced via lentiviral transfection. To develop the most efficient FLAG-Daxx pull-down system, the FLAG IP protocol first had to be established by optimising the salt concentration and buffer composition. The efficiency of the IP was examined via immunoblotting and silver staining. The immunoblotting demonstrated the overexpression of the FLAG-Daxx fusion protein and the efficiency of FLAG IP. Silver staining indicated the total proteins eluted from the FLAG beads, including Daxx and its interaction partners. Successful Daxx co-IP was determined by whether there was Atrx presence, as Atrx is a known Daxx co-function partner. The negative control of the FLAG-Daxx overexpression cells were cells transduced with dTomato lentivirus only (i.e. EV). The negative control group in each IP experiment was constructed following the same procedure as the experiment group, but the cell lysates were replaced with the same volume of lysis buffer only.

### 4.1.3 Mass spectrometry

MS analysis was performed once the IP protocol (Protocol V, Section 4.2.3.1) had been established. Specifically, FLAG-Daxx was co-immunoprecipitated with its known interactome Atrx, and unique protein bands with low background were observed via silver staining.

Nanoscale liquid chromatography coupled to tandem MS (nano-LC-MS/MS) is an improved LC-MS/MS technique with high sensitivity that allows the analysis of peptide mixtures under sample-limited situations. Gaspari and Cuda established a nano-LC-MS/MS technique that allows the analysis of peptides from enzymatic digestion of complex protein mixtures (Gaspari and Cuda 2011). In this study, FLAG beads with FLAG-Daxx and its potential associating

proteins were digested into short peptides with trypsin (cleaved at lysine and arginine residues), and these protein peptides were analysed with MS by Gaspari's group at University of Catanzaro in Italy. Proteins that were significantly scored from the analysis had higher potential as Daxx binding partners and were selected for further validation.

## **4.2 Results**

### **4.2.1 Generating FLAG-Daxx and FLAG-Daxx-pHIV-dTomato constructs, and FLAG-Daxx overexpression in NPCs**

The FLAG-tag was fused at the N-terminus of *Daxx* in the Gene Art *Daxx* WT plasmid. The fused *FLAG-Daxx* sequence was then inserted into the lentiviral construct pHIV-dTomato. The lentiviruses was generated with the EV (pHIV-dTomato) and FLAG-Daxx (FLAG-Daxx-pHIV-dTomato) lentiviral vectors and were titrated with HEK293T cells. These lentiviruses were used to infect the HIN3T3 cells and mouse NPCs (mNPCs).

The pHIV-dTomato and FLAG-Daxx-pHIV-dTomato lentiviruses were first tested on NIH3T3 cells. As a result, the virus transduction rate indicated by dTomato fluorescent signal was about 90% (Figure 4. 2 A). The FLAG and Daxx protein expression levels were examined with IF (Figure 4. 2 B).

Furthermore, whole cell lysates were extracted for immunoblotting of the FLAG and Daxx expression levels. The expression of FLAG protein was observed in the FLAG-Daxx condition, while the FLAG signal in the EV condition was non-specific (Figure 4. 3 A). Daxx expression was about 9-fold higher in the FLAG-Daxx-transduced cells than in the EV-transduced cells (Figure 4. 3 A). After the above analysis on the transduced NIH3T3 cells, the same infection protocol was applied to the mNPCs, and the dTomato-positive cells were collected via FACS (Figure 4. 3 B).

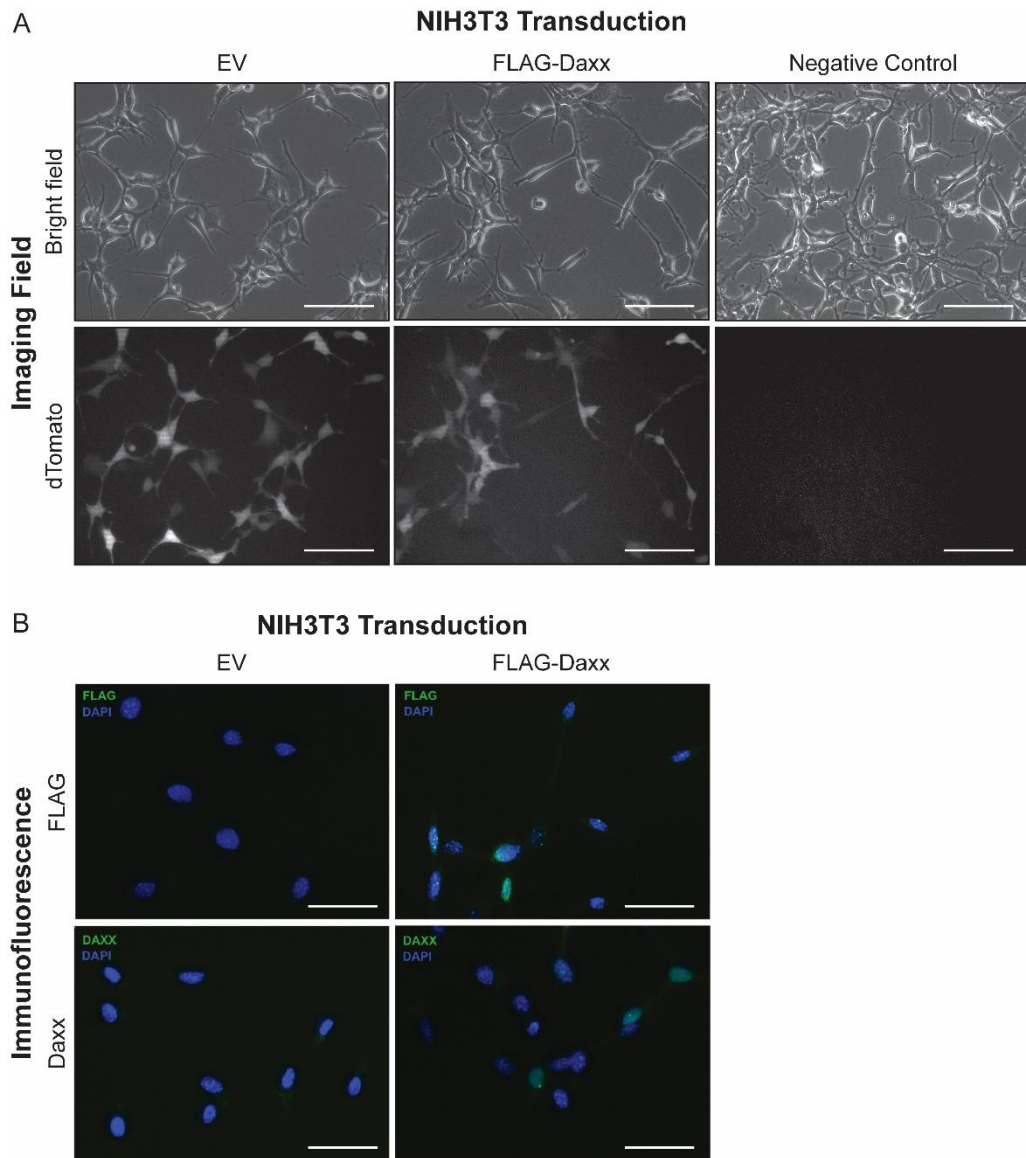


**Figure 4. 2: NIH3T3 lentiviral transduction, and IF of FLAG/Daxx expression. (A)** The EV- and FLAG-Daxx–transduced NIH3T3 cells in bright field (top) and the same field cells in dTomato (bottom). The negative control condition was the untransduced cells. Images were acquired with Zeiss Axio Observer Z1 with Apotome. Scale bar = 10  $\mu$ m **(B)** IF of FLAG and Daxx on EV- and FLAG-Daxx–transduced NIH3T3 cells. Images were acquired with Zeiss Axio Observer Z1 with Apotome. Scale bar = 10  $\mu$ m.

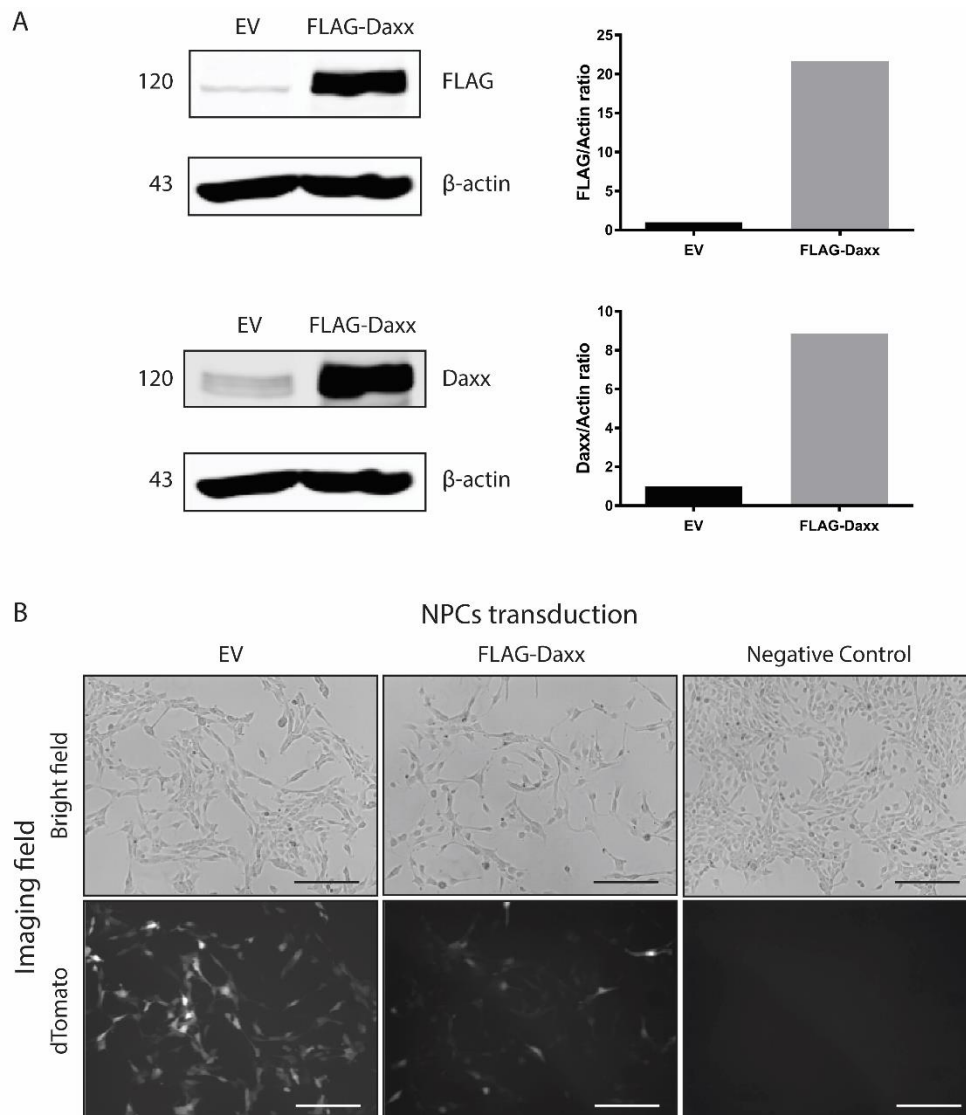


**Figure 4. 3: FLAG/Daxx overexpression in NIH3T3 cells and the transduction of mNPCs.** (A) Immunoblotting of FLAG and Daxx in EV- and FLAG-Daxx–transduced NIH3T3 cells. The protein expression levels were normalised to  $\beta$ -actin. (B) Transduced mNPCs. The negative control condition was the untransduced cells. Images were acquired with Zeiss Axio Observer Z1 with Apotome. Scale bar = 10  $\mu$ m.

## **4.2.2 Initial optimisation of FLAG-IP in FLAG-Daxx overexpression mNPCs**

### **4.2.2.1 Optimisation I (IP on whole cell lysate)**

The first FLAG-Daxx IP optimisation was performed on whole cell lysates. The proteins were extracted in lysis buffer containing 150 mM salt. The detailed protocol is described in the Material and Methods, Section 2.2.3.1.1. Daxx was overexpressed >6 times more in the FLAG-Daxx conditions than in the EV conditions (Figure 4. 4 A). Almost all of the FLAG-Daxx exogenous proteins were immunoprecipitated from the input samples (Figure 4. 4 A). Moreover, the known Daxx binding partner Atrx was co-immunoprecipitated from the FLAG-Daxx condition (Figure 4. 4 A). Interestingly, the expression of Atrx was increased by about 3-fold in the whole cell lysates of the FLAG-Daxx overexpression cells (Figure 4. 4 A).

Silver staining showed one specific band of <130 KDa, which was presumably the Daxx protein (Figure 4. 4 B).

These results suggest that the NPCs overexpressed the transduced FLAG-Daxx fusion protein, and the exogenous Daxx protein was bound with its interacting partner Atrx *in vitro*.

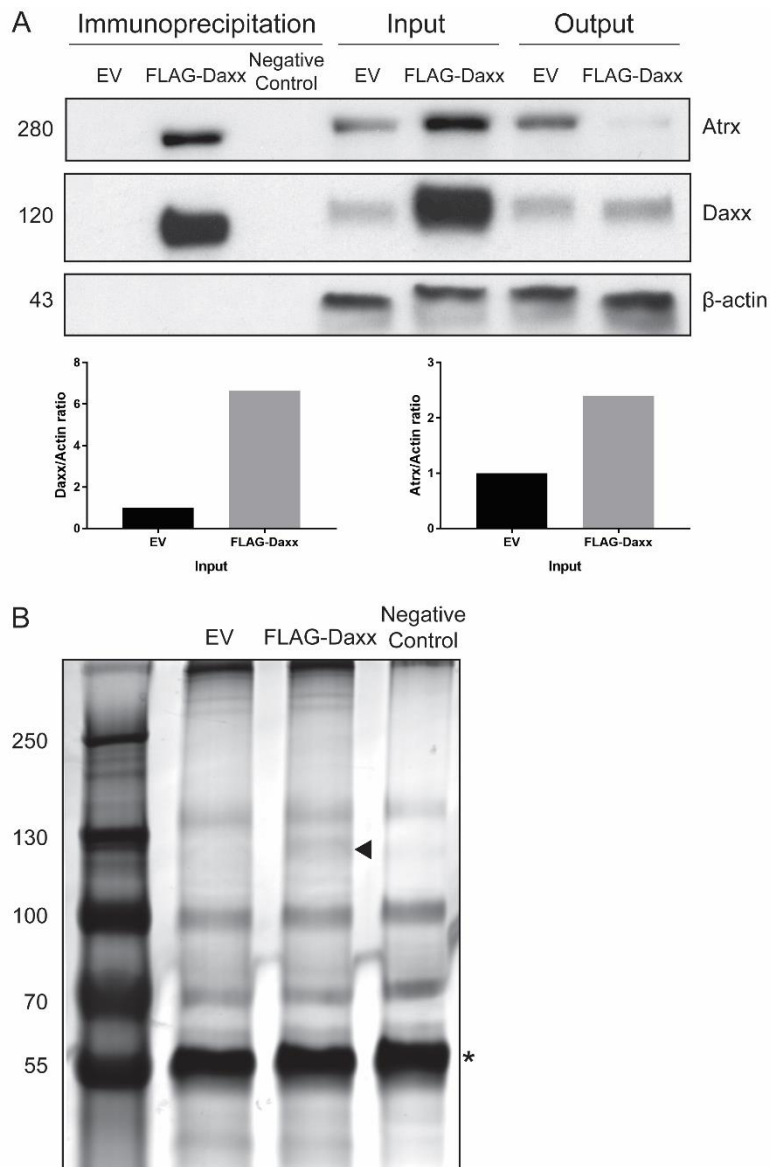


**Figure 4. 4: Immunoblotting and silver staining analyses of FLAG IP by Optimisation I on whole cell lysate. (A)** Co-IP of whole protein lysate of EV- and FLAG-Daxx–transduced mNPCs. Daxx is overexpressed in the input sample of the FLAG-Daxx condition. Atrx and Daxx proteins are shown in the FLAG-Daxx IP sample. The bottom two graphics are the quantification of Daxx and Atrx in the EV and FLAG-Daxx input samples. The protein expression levels are normalised to  $\beta$ -actin. **(B)** Silver staining of the IP samples. The arrowhead indicates Daxx protein (120 KDa). \* Represents the heavy chain of FLAG antibody eluted from the FLAG beads.

#### **4.2.2.2 Optimisation II (IP of nuclear extracts with high-salt buffer)**

As the majority of Daxx protein expression is localised in the nucleus, the IP protocol with nuclear extraction was tested on the NPCs. The cytosol and the nucleus were separated, and the nucleus was extracted with 400 mM salt buffer. The detailed protocol is described in the Material and Methods, Section 2.2.3.1.2.

The immunoblotting results show that the nuclear extract was isolated from the cytosolic proteins, and the histone proteins were extracted. The FLAG IP was successful, but no co-immunoprecipitated Atrx was shown (Figure 4. 5 A). Silver staining of the IP samples did not visualise the heavy chain or light chain of the FLAG antibody (Figure 4. 5 B). However, the Daxx protein band, sized at <130 KDa, was shown in the FLAG-Daxx condition (Figure 4. 5 B).

The loss of the co-IP proteins was very likely due to the high salt in the nuclear lysis buffer. The high salt in the lysis buffer damaged the protein–protein link between Daxx and Atrx, and potentially disrupted Daxx interaction with other interacting partners. In addition, more bait (FLAG-Daxx) was required for improved FLAG IP from the input.

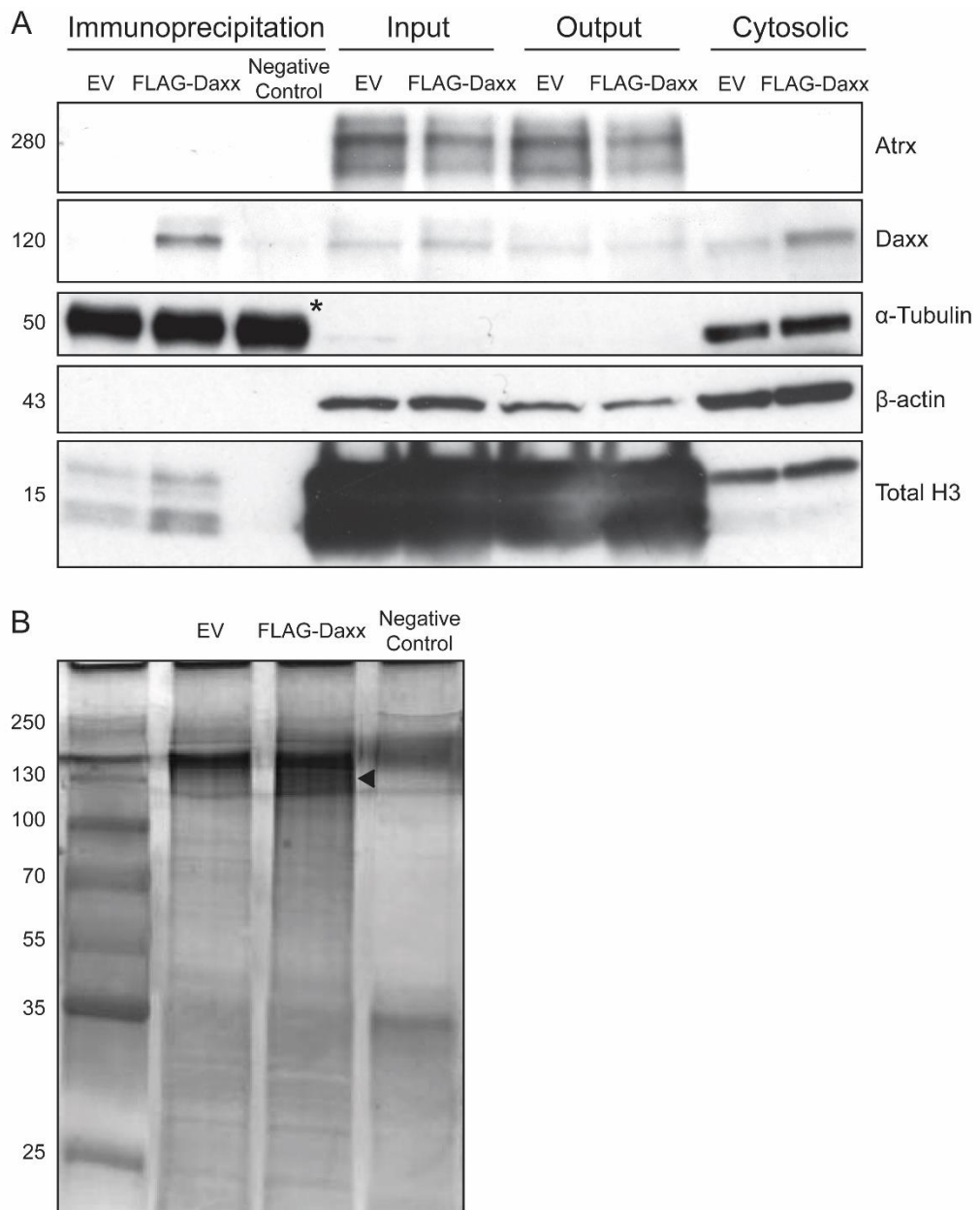


**Figure 4. 5: Immunoblotting and silver staining of FLAG IP from Optimisation II of nuclear extracts. (A)** Co-IP of the nuclear lysates of EV- and FLAG-Daxx-transduced mNPCs. The images show the immunoblotting of Atrx, Daxx,  $\alpha$ -tubulin,  $\beta$ -actin and total H3. \* Represents the heavy chain of FLAG antibody eluted from the FLAG beads. **(B)** Silver staining of the IP samples. Arrowhead indicates Daxx protein.

#### **4.2.2.3 Optimisation III (IP of nuclear extracts with pre-clearing, low-salt buffer and stringent washes)**

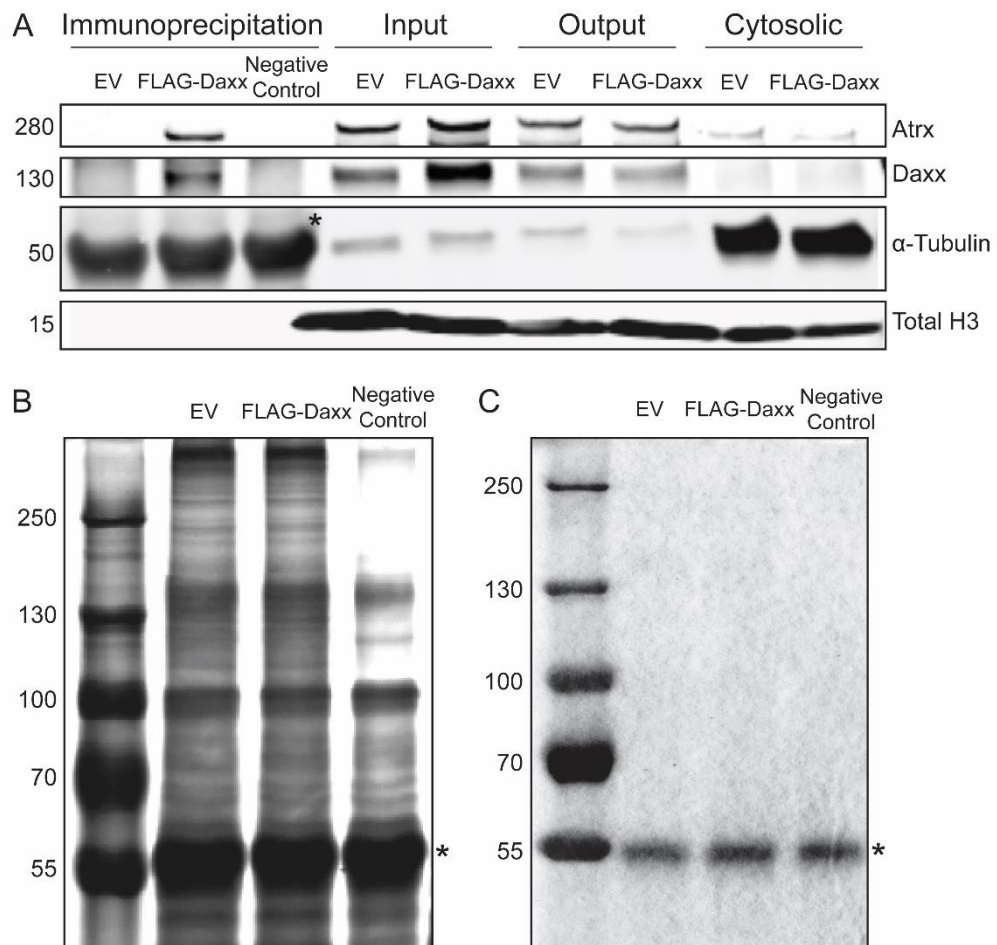
The results from Optimisation II suggested that 400 mM salt in the lysis buffer was too harsh for the FLAG IP, and an increased amount of cell lysate was needed. In Optimisation III, the salt concentration of the nuclear extraction buffer was reduced to 150 mM. Moreover, increased washing steps were performed on the post-IP FLAG beads in response to the increased background signals. The detailed protocol is described in the Material and Methods, Section 2.2.3.1.3, 1).

Figure 4. 6 A shows that the immunoblotting demonstrated clean separation of the nuclear extract from the cytosolic proteins. The protein Daxx was present only in the nuclear extract samples (Figure 4. 6 A). Moreover, the FLAG-Daxx protein was immunoprecipitated with the FLAG beads, and Atrx was co-immunoprecipitated with Daxx (Figure 4. 6 A).

However, silver staining of the IP samples showed significant background signals, indicating that increased washes of the post-IP beads was not efficient for reducing the non-specific protein binding (Figure 4. 6 B).

Therefore, to minimise the background binding, the nuclear protein lysates were pre-cleared with mouse IgG/Protein G Plus agarose beads before IP. The detailed protocol is described in the Material and Methods, Section 2.2.3.1.3, 2). The IP samples were analysed with Coomassie staining, as it is less sensitive than silver staining and might eliminate some background signals. Unfortunately, Coomassie staining did not reveal any protein bands apart from the heavy chains of the FLAG antibody (Figure 4. 6 C).

Overall, these results imply that the salt concentration was yet too mild to reduce the non-specific protein binding on the FLAG agarose beads.



**Figure 4. 6: Immunoblotting and silver staining of FLAG IP from Optimisation III.** (A) Co-IP of the nuclear extract of EV- and FLAG-Daxx-transduced mNPCs. Images show the immunoblotting of Atrx, Daxx,  $\alpha$ -tubulin and total H3. (B) Silver staining of the IP samples. (C) Coomassie staining of the IP samples. \* Represents the heavy chain of FLAG antibody eluted from the FLAG beads.

#### **4.2.2.4 Optimisation IV (IP with 300mM salt washing buffer)**

Optimisation IV was designed to determine whether an increased salt concentration of the washing buffer would reduce the non-specific protein binding onto the FLAG beads. The same salt concentration of 150 mM was maintained in the IP buffer, while the salt concentration in the washing buffer was increased to 300 mM. The detailed protocol is described in the Material and Methods, Section 2.2.3.1.4.

Almost no FLAG-Daxx protein was immunoprecipitated from the nuclear lysate, and no Atrx co-IP was indicated (Figure 4. 7 A). Moreover, the presence of cytosolic protein in the nuclear extract suggested that the nucleus/cytosol separation was not efficient (Figure 4. 7 A). In addition, faint signals were observed from the silver staining, and the signal patterns of the EV and FLAG-Daxx were nearly identical (Figure 4. 7 B).

These results suggest that the protocol with 300 mM salt washing buffer interfered with the binding of FLAG-Daxx protein to the FLAG beads, which also affected the co-IP of the interacting partners.

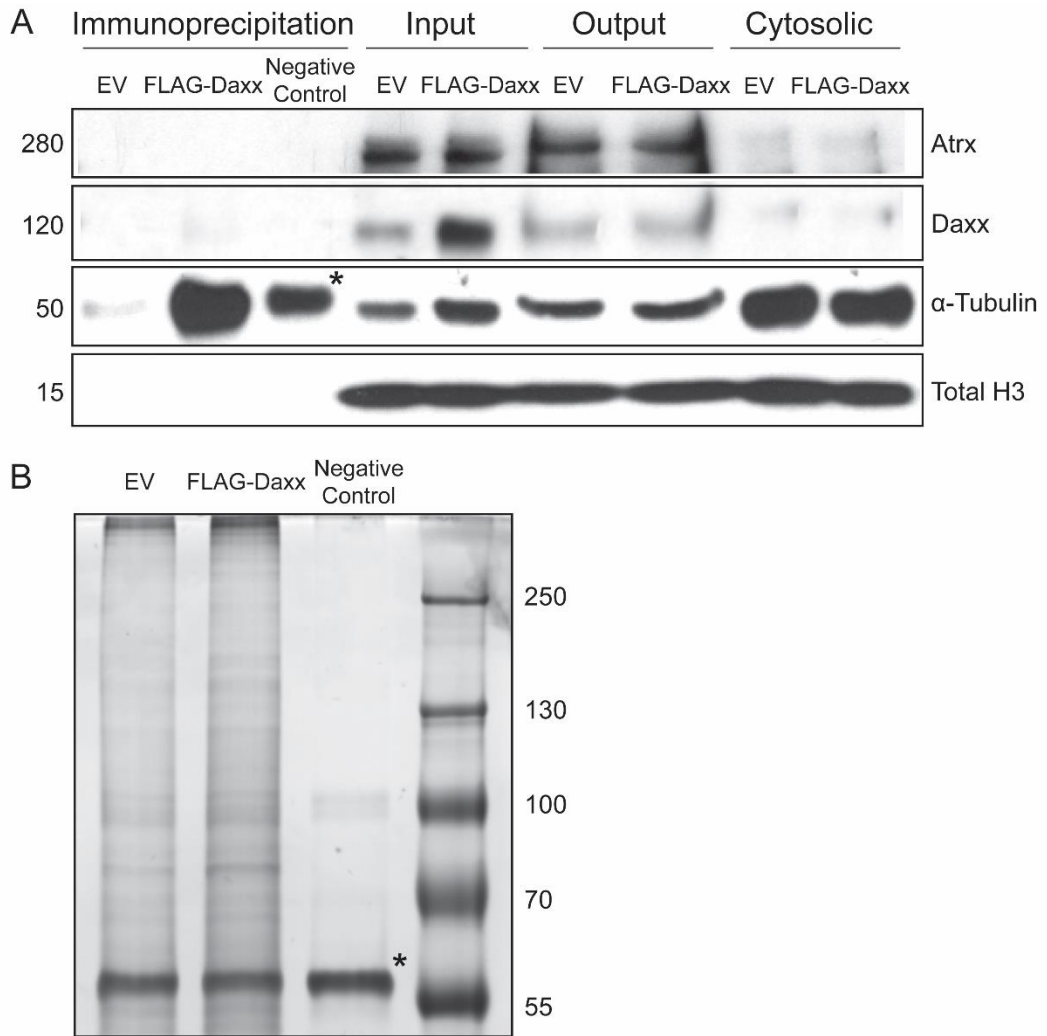


**Figure 4. 7: Immunoblotting and silver staining of FLAG IP from Optimisation IV. (A)** Co-IP of the nuclear extract of EV- and FLAG-Daxx–transduced mNPCs. Images show the immunoblotting of Atrx, Daxx,  $\alpha$ -tubulin and total H3. **(B)** Silver staining of the IP samples. \* Represents the heavy chain of FLAG antibody eluted from the FLAG beads.

### **4.2.3 Optimised FLAG-IP in FLAG-Daxx-overexpression mNPCs and MS analysis**

#### **4.2.3.1 FLAG-IP of the nuclear extract of FLAG-Daxx overexpression mNPCs (Optimisation V protocol)**

The fifth optimisation protocol (optimisation V) yielded improved IP results. The detailed protocol is described in the Material and Methods, Section 2.2.3.1.5. First, the immunoblotting results demonstrated that the overexpressed FLAG protein was specifically detected in the FLAG-Daxx-transduced NPCs (Figure 4. 8 A). The FLAG protein was bound to the FLAG IP beads and was immunoprecipitated from the nuclear lysate (Figure 4. 8 A). The Atrx protein was also co-immunoprecipitated along with the FLAG-Daxx fusion protein (Figure 4. 8 A). Notably, silver staining revealed at least four specific protein bands in the FLAG-Daxx overexpression sample (Figure 4. 8 B).

Overall, the IP results from this protocol met the sample requirements for the MS analysis, as the immunoprecipitated FLAG-Daxx fusion protein (the bait) was sufficient to pull-down its interacting protein complex (Figure 4. 8 A). However, it should be noted that the output samples suggested that the proteins were degraded during the IP (Figure 4. 8 A). In addition, the presence of the cytosolic protein  $\alpha$ -tubulin indicated incomplete separation of nuclear extracts from the cytosol (Figure 4. 8 A), but this did not affect the IP efficiency.

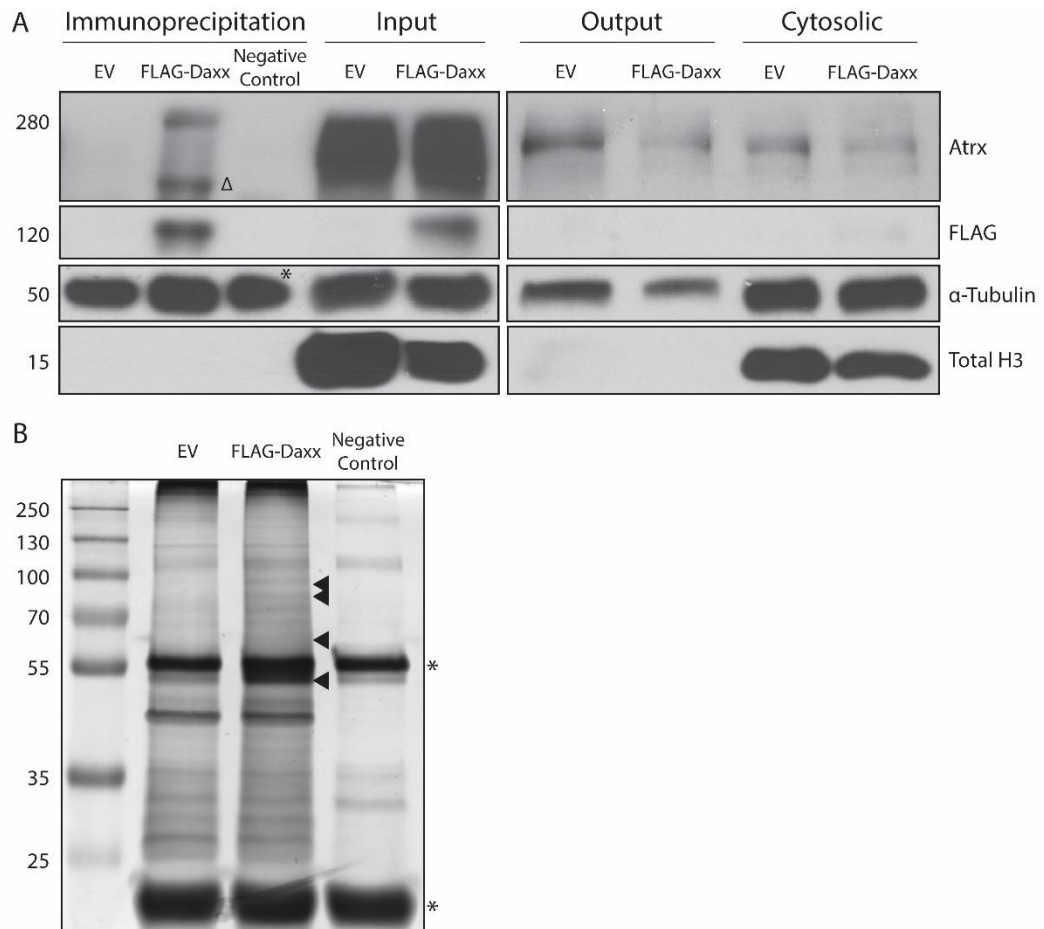


**Figure 4. 8: Immunoblotting and silver staining of FLAG IP with Optimisation V.** **(A)** Co-IP of the nuclear extract of EV- and FLAG-Daxx–transduced mNPCs. Images show the immunoblotting of Atrx, FLAG, α-tubulin and total H3. **(B)** Silver staining of the IP samples. Arrowheads indicate the unique bands on the FLAG-Daxx sample in comparison to the EV sample. \* Represents the heavy chain (55 KDa) and the light chain (25 KDa) of the FLAG antibody eluted from the FLAG beads. Δ Represents the non-specific binding of the Atrx immunoblotting antibody.

#### **4.2.3.2 Mass spectrometry analysis**

MS analysis was performed on the IP samples obtained from the Optimisation V protocol (duplicate experiment). The detailed MS sample preparation protocol is described in the Material and Methods, Section 2.2.3.2. The post-IP FLAG beads were digested partially and sent to our collaborator, i.e. Gaspari's group at the University of Catanzaro in Italy, where the samples were processed with full digestion and the protein peptides were identified with nano-LC-MS/MS.

Four percent of the full tryptic digestion was submitted for the initial test run, and around 10,000 of 30,000 MS/MS events matched the mouse proteins tryptic peptides, meaning that the signal obtained from the IP was sufficient. Later on, full MS analysis was performed. Consequently, 1604 proteins were identified from the mass spectrum; 308 proteins obtained peptide-spectrum matches (PSM) ratio (FLAG-Daxx/EV) scores of  $\geq 2.0$ , and these proteins were considered hit interactors. Atrx, the known Daxx binding partner, obtained a ratio value of 2.8, and H3 (including H3.3) obtained a ratio value of 2.24. Table 4. 1 shows the identified proteins with PSM ratio of  $\geq 10.0$ . These proteins were considered significantly enriched in the FLAG-Daxx sample, and are more likely to be true hits as Daxx interaction partners.

**Table 4. 1: Identified proteins from MS with PSM ratio  $\geq 10.0$** 

Identified proteins	PSM ratio
Death domain-associated protein 6 [DAXX_MOUSE]	57.01
Netrin-1 [NET1_MOUSE]	42.72
Nuclear receptor subfamily 2 group C member 2 [NR2C2_MOUSE]	40.94
Cleavage and polyadenylation specificity factor subunit 2 [CPSF2_MOUSE]	32.76
Alpha-amylase 1 [AMY1_MOUSE]	30.72
Pre-mRNA-splicing factor CWC22 homolog [CWC22_MOUSE]	24.46
Putative ATP-dependent RNA helicase DHX57 [DHX57_MOUSE]	23.65
Putative ATP-dependent RNA helicase DHX30 [DHX30_MOUSE]	20.69
Perilipin-2 [PLIN2_MOUSE]	20.36
Nuclear-interacting partner of ALK [NIPA_MOUSE]	20.26
Signal-induced proliferation-associated 1-like protein 1 [SI1L1_MOUSE]	19.38
Integrator complex subunit 1 [INT1_MOUSE]	19.30
GA-binding protein alpha chain [GABPA_MOUSE]	17.31
40S ribosomal protein S24 [RS24_MOUSE]	14.91
Bifunctional coenzyme A synthase [COASY_MOUSE]	13.78
Pre-mRNA 3' end processing protein WDR33 [WDR33_MOUSE]	12.19
Histone H1.2 [H12_MOUSE]	10.33

#### 4.2.3.3 Validation of top hits Net1, Nr2c2 and Cpsf2

The top three protein hits from the MS analysis were validated via immunoblotting. The same immunoblotting membrane from Optimisation V (Figure 4. 8 A) was immunoblotted with CPSF2, NET1 and NR2C2 antibodies. Cpsf2 and Nr2c2 were identified in the FLAG-Daxx nuclear extract IP sample (Figure 4. 9), indicating that they were true hits. However, we could not exclude Net1 as a Daxx-interacting partner, as the immunoblotting antibody did not perform well (Figure 4. 9). Net1 should be further analysed in the future with a working antibody for mNPCs.

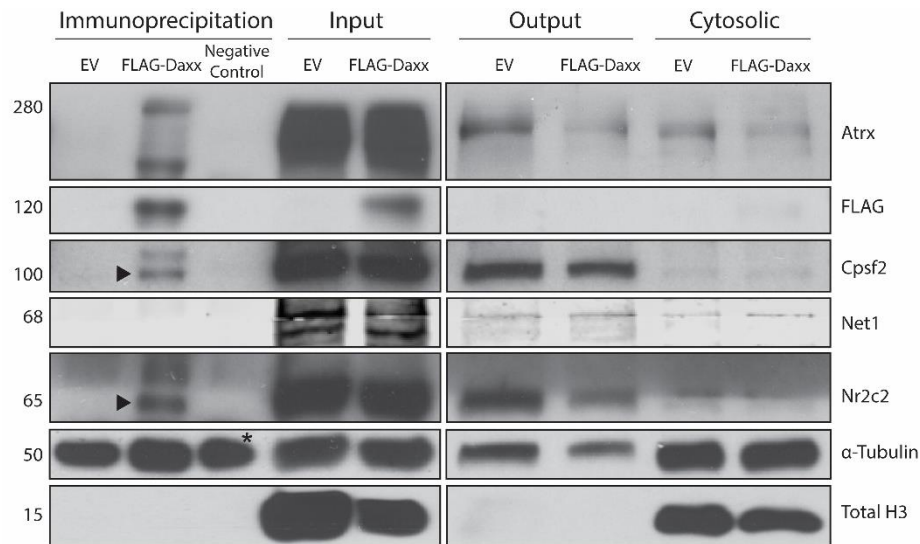


**Figure 4. 9: Validation of Net1, Nr2c2 and Cpsf2.** Images show immunoblotting of Cpsf2, Net1 and Nr2c2 on the immunoblotting membrane in Figure 4. 8 A. Arrowheads indicate the specific protein signals of Cpsf2 and Nr2c2. \* Represents the heavy chain (55 KDa) of FLAG antibody eluted from the FLAG beads. **Note:** The Net1 immunoblotting antibody (12740-1-AP) is currently off-shelf because it is being tested by Proteintech. We did not exclude Net1 as a Daxx interactome although it is shown negative here.

#### **4.2.4 Attempts to optimise IP**

Although the MS analysis identified several Daxx-interacting candidates, further improvement of the protocol was needed. These included: 1) Improving separation of the nuclear extraction from the cytosolic extraction; 2) Solving the issue of protein loss in output samples; 3) Reducing the background from the FLAG IP beads.

To achieve this, magnetic FLAG-beads (M8823 Sigma) were used to reduce the non-specific binding. The protocol and buffers were adjusted to overcome the issues from Optimisation V, and a different elution method was tested.

##### **4.2.4.1 Protein degradation and oxidative stress**

One of the potential reasons for protein loss in the output/post-IP samples is protein degradation. Thus, additional protease inhibitors, including a different PMSF and leupeptin were added to the buffers throughout the 'mock' IP procedure. The detailed protocol is described in the Material and Methods, Section 2.2.3.1.6. However, regardless of the incubation duration, there was a sharp reduction in the overall protein concentrations in the output samples (Figure 4. 10 A), suggesting that the loss of the output proteins from this protocol was not due to the degradation of the proteins or that degradation occurred also in the presence of additional protease inhibitors.

The other potential reason for the protein loss was oxidative stress. The detailed protocol is described in the Material and Methods, Section 2.2.3.1.7. Therefore, IP buffers containing DTT were tested.

However, the presence of DTT in the buffers did not aid the protein preservation in the output samples (Figure 4. 10 B). In addition, the proteins/FLAG beads were 'stickier', as more background binding appeared in the EV condition. Interestingly, unlike the results from Optimisation V (Figure 4. 9), the histone proteins were preserved in the output samples, and were pulled down together with the beads in the IP samples non-specifically (Figure 4. 10 B).

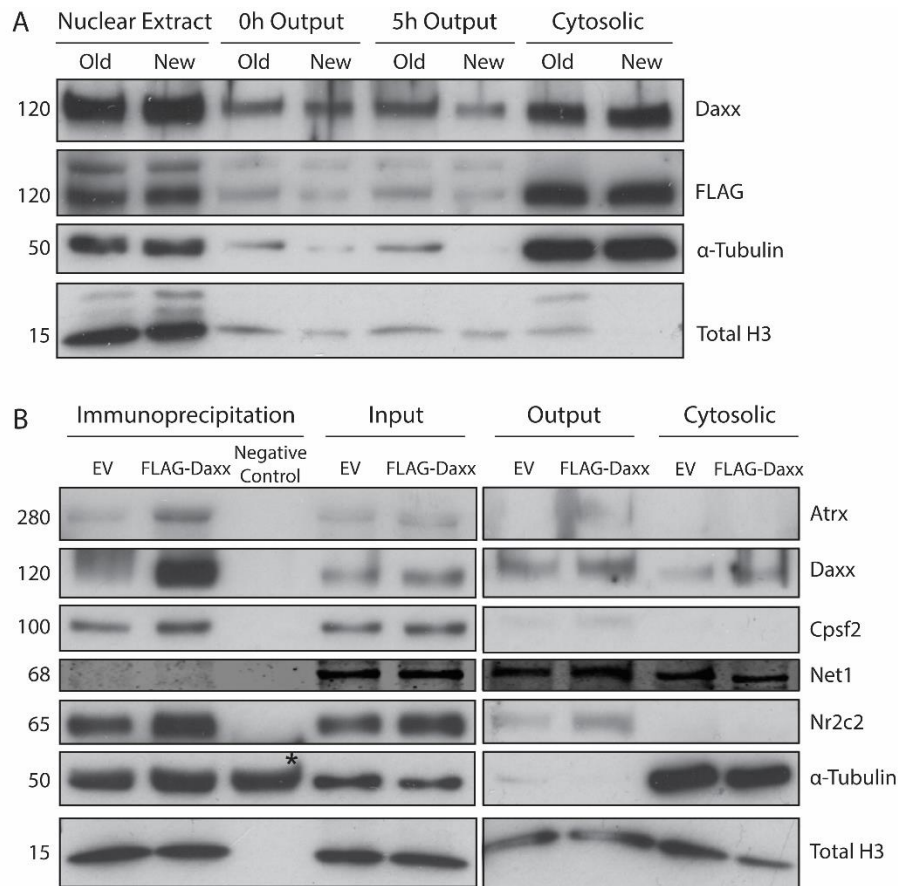


**Figure 4. 10: Protein degradation and oxidative stress. (A)** FLAG-Daxx–transduced mNPCs lysed in buffers containing protease inhibitors. The protein lysates were incubated in the IP buffer for 0 hour and 5 hours. **Old:** ‘Mock’ IP with buffers supplemented with 1x cOmplete™ Protease Inhibitor Cocktail, 50 mM sodium fluoride, and 1 mM sodium orthovanadate. **New:** ‘Mock’ IP with buffers supplemented with 1x cOmplete™ ULTRA EDTA-free Protease Inhibitor Cocktail, 1 µg/ml leupeptin, 50 µg/ml PMSF, 50 mM sodium fluoride, and 1 mM sodium orthovanadate. **(B)** Co-IP (with 0.5 mM DTT) on the nuclear extract of EV- and FLAG-Daxx–transduced mNPCs. Images show the immunoblotting of Atrx, Daxx, Cpsf2, Net1, Nr2c2, α-tubulin and total H3. \* Represents the heavy chain (55 KDa) of FLAG antibody eluted from the FLAG beads.

#### **4.2.4.2 Background reduction**

The following experiments were designed to yield more stringent washes as well as to reduce the background staining from DTT: 1) cell lysates were pre-cleared with mouse IgG/Protein G Plus agarose beads to remove the 'sticky proteins' (Figure 4. 11 A); 2) 0.2% Triton X-100 was added to the washing buffer for more stringent washes. The detailed protocol is described in the Material and Methods, Section 2.2.3.1.8.

Consequently, pre-clearing the nuclear lysates with the mouse IgG/Protein G Plus agarose beads before IP indeed prevented most of the non-specific binding to the FLAG magnetic beads, as the non-specific proteins were bound to the pre-clear agarose beads (Figure 4. 11 A). However, no Atrx was observed in the FLAG-Daxx IP sample (Figure 4. 11 A).

On the other hand, Triton X-100 in the washing buffer did not improve the background signals in the IP samples, as the non-specific proteins still bound to the FLAG magnetic beads (Figure 4. 11 B).

It can be summarised here that despite our attempts, the protein loss in the output samples remained substantially unchanged. Notably, the additive DTT somehow strengthened the bound between the protein and the IP beads, thus worsening the background binding. Efforts were made by washing the beads in a more stringent washing buffer (0.2% Triton X-100) but returned little success. Furthermore, although pre-clearing the proteins with the agarose beads improved the situation, the connection between the Daxx protein and its interacting partners was lost during the process.

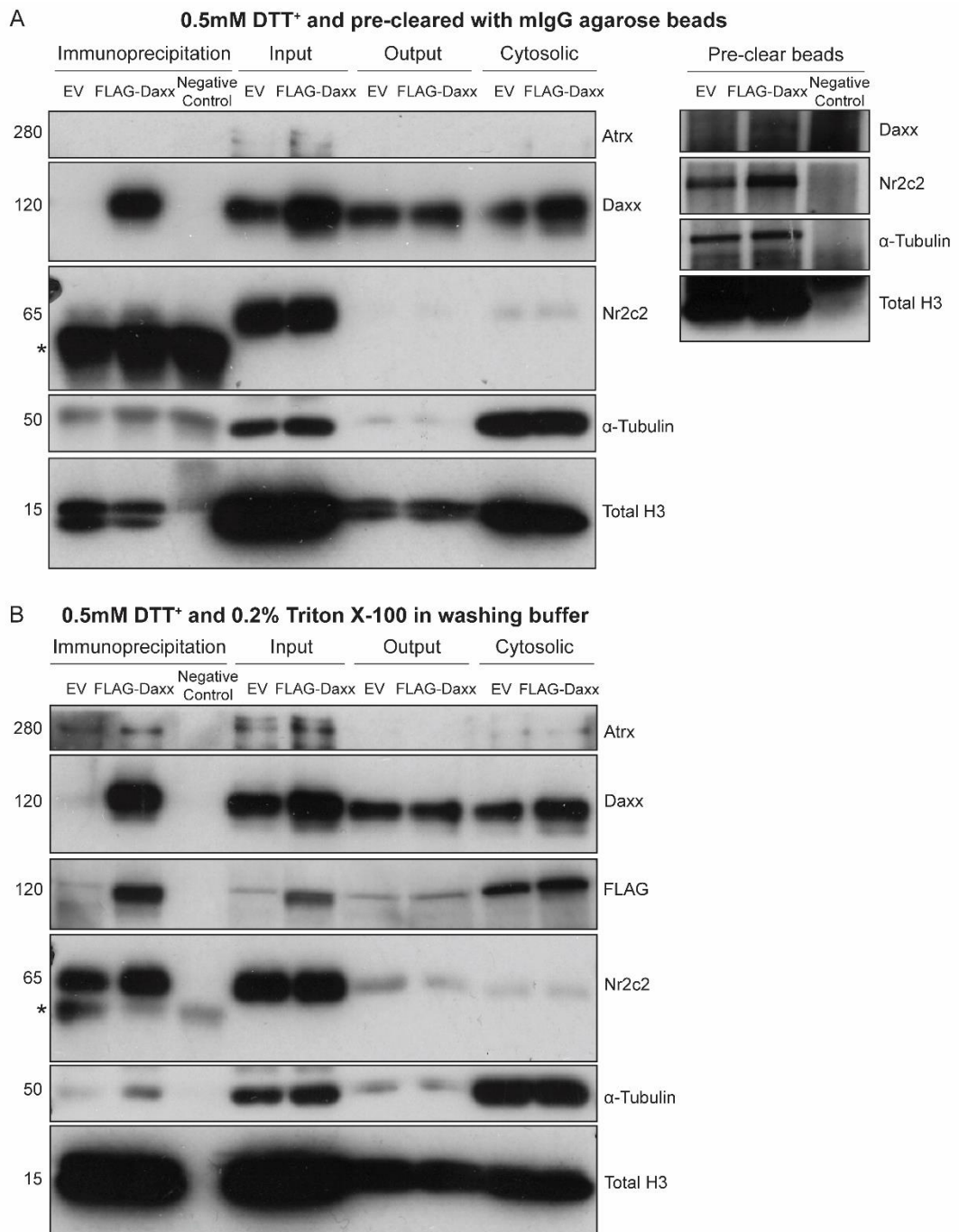


**Figure 4. 11: Reduction of the background and specificity of co-IP proteins. (A)** Co-IP of the nuclear extract of EV- and FLAG-Daxx–transduced mNPCs. The protein lysates were pre-cleared with mouse IgG/Protein G Plus agarose beads. The IP and washing buffers contained 0.5 mM DTT. Images show the immunoblotting of Atrx, Daxx, Nr2c2,  $\alpha$ -tubulin and total H3. Images on the right are the immunoblotting of the elutions from the pre-clearing beads. **(B)** Co-IP of the nuclear extract of EV- and FLAG-Daxx–transduced mNPCs. The IP buffer contained 0.5 mM DTT, and the washing buffer contained 0.5 mM DTT and 0.2% Triton X-100. Images show the immunoblotting of Atrx, Daxx, FLAG, Nr2c2,  $\alpha$ -tubulin, total H3 and FLAG. \* Represents the heavy chain (55 KDa) of FLAG antibody eluted from the FLAG beads.

#### 4.2.4.3 Optimisation VI (Elution with FLAG peptides)

Steen Ooi's group at the UCL Cancer Institute have also been working on the FLAG-fused protein IP of nuclear extracts from NPCs. Notably, in their protocol (described in the Material and Methods, Section 2.2.3.1.9), FLAG proteins were eluted with FLAG peptides (competitive elution) instead of Laemmli sample buffer.

This protocol greatly improved the separation of the nuclear extracts from the cytosolic proteins as compared with optimisation V (Figure 4. 12). Importantly, no significant protein degradation was observed in the output samples (Figure 4. 12). There was no signal interference from the FLAG antibody heavy chain, as the FLAG beads were eluted via FLAG peptide competition (Figure 4. 12). However, the FLAG-Daxx protein IP was less efficient, and not all the FLAG-Daxx fusion proteins were immunoprecipitated from the nuclear lysates (Figure 4. 12). Moreover, no co-immunoprecipitated Atrx was observed from the FLAG-Daxx overexpression cell lysates (Figure 4. 12).

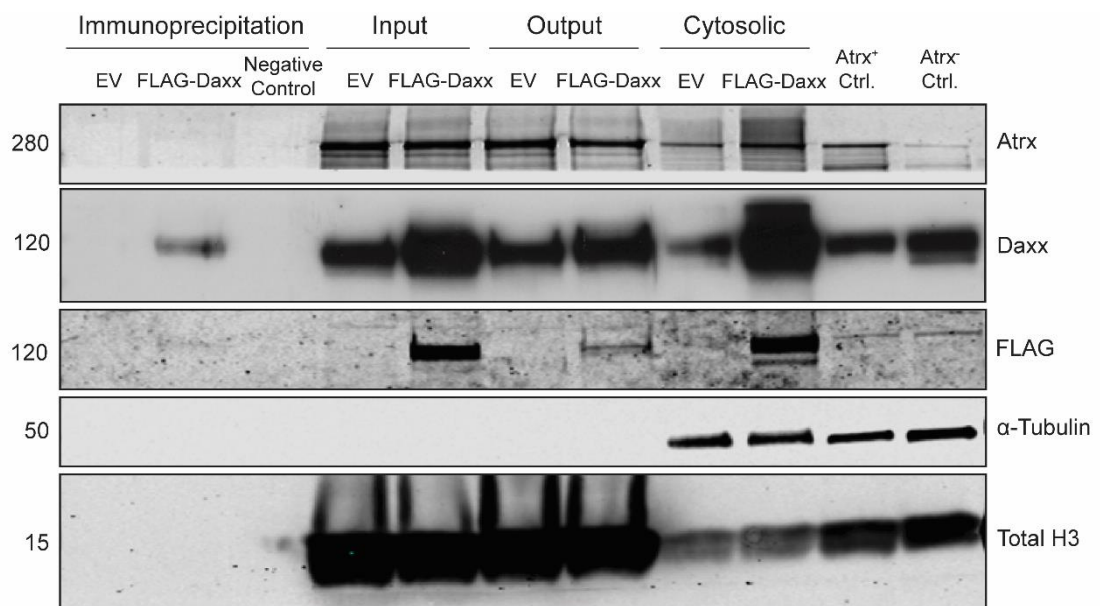


**Figure 4. 12: Immunoblotting of FLAG IP from Optimisation VI.** Co-IP of on the nuclear extract of EV- and FLAG-Daxx-transduced mNPCs. Images show the immunoblotting of Atrx, Daxx, FLAG, α-tubulin and total H3. Atrx<sup>+</sup> represents the protein lysate from wild-type mNPCs. Atrx<sup>-</sup> represents the protein lysate from Atrx knockout mNPCs.

#### **4.2.4.4 Optimisation VII (IP with non-denaturing buffer)**

One of the advantages of non-denaturing buffer is that it does not contain denaturants or components that might interfere with antibody binding or protein–protein interactions. The IP protocol using non-denaturing buffer extracts whole cell lysates, including the cytosolic proteins and nuclear extracts. This buffer was modified based on the non-denaturing lysis buffer recipe from Abcam, and the detailed protocol is described in the Material and Methods, Section 2.2.3.1.10.

This was first tested on the HEK293T cells overexpressing EV and FLAG-Daxx [protocol described in the Material and Methods, Section 2.2.3.1.10, 1)]. Figure 4. 13 A shows that FLAG-Daxx was immunoprecipitated from the whole cell lysates of the FLAG-Daxx overexpression condition, and Atrx was co-immunoprecipitated. The cytosol proteins did not experience any protein degradation (Figure 4. 13 A). However, the FLAG-Daxx elution by the FLAG peptides was not complete, as more FLAG-Daxx proteins were eluted with the Laemmli buffer (arrowheads in Figure 4. 13 A). It was also worth noting that most of the histone proteins (total H3) were not extracted from the cells.

We suspect that the histones were ‘trapped’ with the chromatin, and were pelleted down and discarded with the cell debris during the lysing procedure. Therefore, Benzonase nuclease was added to the lysis buffer to aid the extraction of proteins from chromatin [protocol described in the Material and Methods, Section 2.2.3.1.10, 2)]. Little improvement in the histone protein extraction was observed (Figure 4. 13 B). However, there was an increased signal of Atrx co-IP (Figure 4. 13 B). The FLAG elution was unaffected, and the FLAG-Daxx elution by the FLAG peptides was not thorough (Figure 4. 13 B).

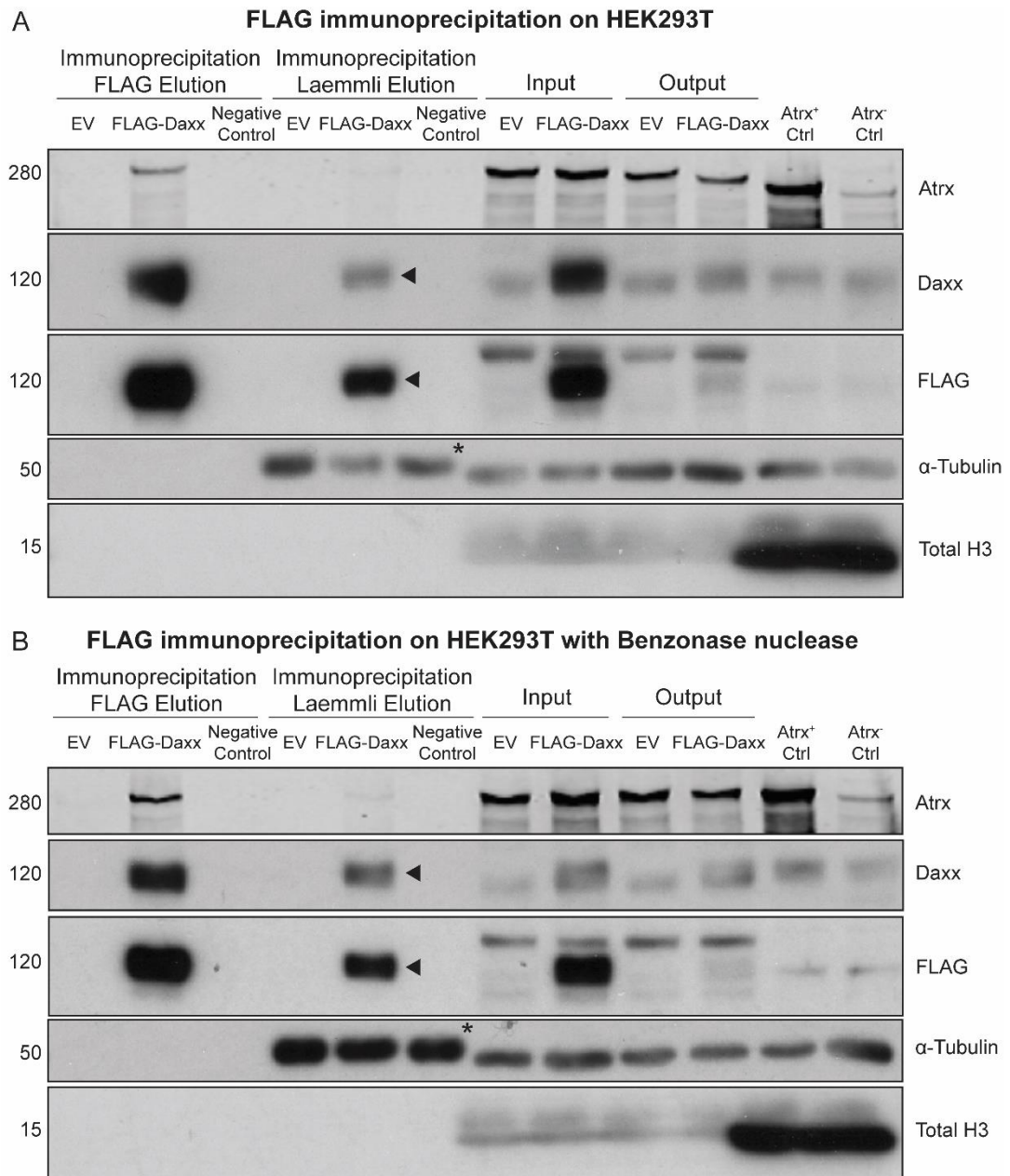


**Figure 4. 13: Immunoblotting of FLAG IP from Optimisation VII on HEK293T cells eluted with FLAG peptides followed by Laemmli buffer. (A) Co-IP of the nuclear extract of EV- and FLAG-Daxx-transduced HEK293T cells. Images show the immunoblotting of Atrx, Daxx, FLAG,  $\alpha$ -tubulin and total H3. Arrowheads indicate the FLAG and Daxx proteins eluted with Laemmli buffer. (B) Co-IP of the nuclear extract of EV and FLAG-Daxx conditions with Benzonase nuclease (37.5 U) in lysis buffer. The images show the immunoblotting of Atrx, Daxx, FLAG,  $\alpha$ -tubulin and total H3. Atrx<sup>+</sup> represents the protein lysate from wild-type cells. Atrx<sup>-</sup> represents the protein lysate from Atrx knockout cells. \* Represents the heavy chain (55 KDa) of FLAG antibody eluted from the FLAG beads.**

The IP protocol with non-denaturing buffer was applied to the FLAG-Daxx overexpression mNPCs [protocol described in the Material and Methods, Section 2.2.3.1.10, 3)], and similar immunoblotting results were obtained as from the HEK293T cells (Figure 4. 14 A versus Figure 4. 13 B). Not all of the FLAG-Daxx protein was eluted with the FLAG peptides, as more FLAG-Daxx proteins were eluted with the Laemmli buffer from the beads (Figure 4. 14 A). No protein degradation was shown in the samples. Atrx was co-immunoprecipitated in the FLAG-Daxx condition (Figure 4. 14 A). Notably, the histone proteins/DNA-associating proteins, indicated by the total H3, were extracted with the Benzonase nuclease-containing lysis buffer (Figure 4. 14 A). Moreover, no co-IP from the Daxx potential binding partners was identified (Figure 4. 14 A).

Silver staining of the FLAG peptides-eluted IP samples did not indicate any unique protein band in the FLAG-Daxx condition, nor from the samples further eluted with Laemmli buffer (Figure 4. 14 B). Importantly, several distinct protein bands were shown in the FLAG-Daxx IP samples eluted with Laemmli buffer only (Figure 4. 14, Immunoprecipitation Laemmli Elution<sup>+</sup>).

We can conclude here that IP with non-denaturing buffer is indeed an appropriate protocol for studying Daxx interactome in the NPCs. It resolves the protein instability issue in the post-IP samples in Optimisation V (Figure 4. 8). The whole cell lysates, including the chromatin proteins, were extracted with the aid of the Benzonase nuclease. Although the FLAG peptide elution method helps to exclude the heavy and light chains of the FLAG beads and yields cleaner immunoblotting and silver staining, the elution efficiency is not as good as elution with Laemmli buffer. More importantly, silver staining showed unique protein bands with the IP sample eluted with Laemmli buffer, suggesting that it would benefit more from the Laemmli buffer elution method.

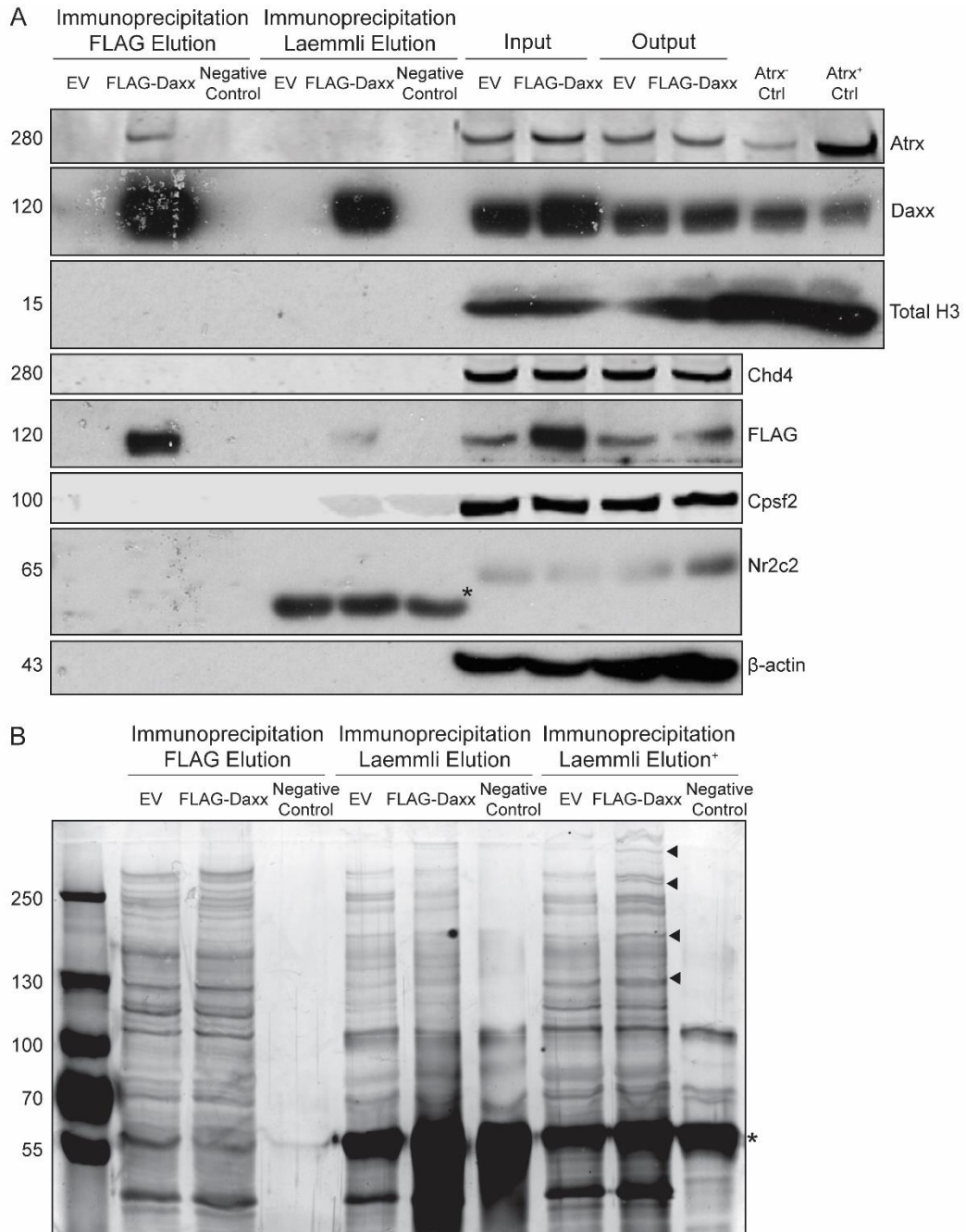


**Figure 4. 14: Immunoblotting and silver staining of FLAG IP from Optimisation VII eluted with FLAG peptides and Laemmli buffer. (A)** Co-IP of the nuclear extract of EV- and FLAG-Daxx–transduced mNPCs eluted with FLAG peptides followed by Laemmli buffer. The lysis buffer contained Benzonase nuclease. Images show the immunoblotting of Atrx, Daxx, total H3, Chd4, FLAG, Cpsf2, Nr2c2 and β-actin. Atrx<sup>+</sup> corresponds to protein lysate from wild-type cells. Atrx<sup>-</sup> corresponds to protein lysate from Atrx knockout cells. **(B)** Silver staining of the IP samples from Optimisation VII eluted with FLAG peptides followed by Laemmli buffer and eluted with Laemmli buffer only (\*). Arrowheads indicate the unique bands in FLAG-Daxx condition versus EV condition. \* Represents the heavy chain (55 KDa) of FLAG antibody eluted from FLAG beads.

## 4.2.5 Candidate approach

### 4.2.5.1 Analysis of candidate chromatin regulators for their ability to interact with Daxx

Parallel to the unbiased MS approach (Section 4.2.3), we decided to use a candidate approach. As discussed in the Introduction, Section 1.2.4 and 1.2.5, Chd4, Brm, Brg1, Ezh2 and Suz12 are epigenetic regulators that interact with Daxx-associated epigenetic regulators. The candidate approach was carried out with Optimisation III, which was prior to the MS analysis. The detailed protocol is described in the Material and Methods, Section 2.2.3.1.3, 3). From the immunoblots, none of the protein candidates were co-immunoprecipitated in the FLAG-Daxx overexpression mNPC lysate (Figure 4. 15).

If there had been more time, I would examine these candidate chromatin regulators with the IP protocols in Optimisation V and Optimisation VII.

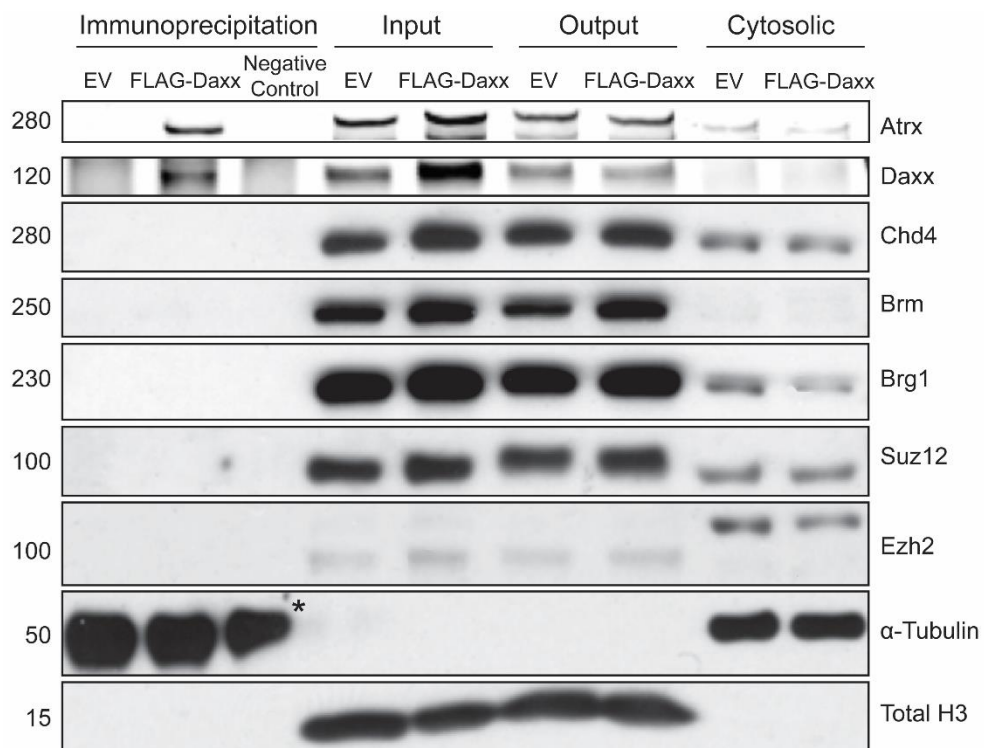


**Figure 4. 15: Co-IP (candidate approach).** Co-IP of the nuclear extract of EV- and FLAG-Daxx–transduced mNPCs. The cell lysates were obtained using Optimisation III. Images show the immunoblotting of Chd4, Brm, Brg1, Suz12, Ezh2, α-tubulin and Total H3. The immunoblotting of Atrx and Daxx are from Figure 4. 6. \* Represents the heavy chain of FLAG antibody eluted from the FLAG beads.

#### 4.2.5.2 iCLIP: Daxx association with RNA

H3.3 has been reported to be recruited through an RNA-mediated mechanism at the activated transcription site (Newhart *et al.* 2013). Sarma's group has suggested an interaction between ATRX and non-coding RNAs in the regulation of PRC2 function (Sarma *et al.* 2014). In addition, association between ATRX and noncoding RNA TERRA have been identified in cancer cells with ALT, in which loss of ATRX leads to disrupted ALT and triggers cell apoptosis (Zou *et al.* 2003). As DAXX forms a partnership with ATRX during H3.3 loading, we reasoned that it could also interact with RNA directly or indirectly. To test this, we performed iCLIP on FLAG-Daxx overexpression NPCs to determine whether Daxx interacts with RNA. This assay was run in collaboration with Richard Jenner's group at the UCL Cancer Institute. The detailed protocol is described in the Material and Methods, Section 2.2.3.7.

The iCLIP results barely suggested direct RNA binding on the FLAG-Daxx protein, as the RNA–protein signals were not clearly shown even when treated with 1:25 RNase I (Figure 4. 16 A). Therefore, the iCLIP membrane was analysed with immunoblotting for FLAG (Figure 4. 16 B). If Daxx was bound to RNAs, we would observe protein bands >120 KDa, as the binding to RNAs would increase the size of the FLAG-Daxx protein. However, no such indication was observed (Figure 4. 16 B). In addition, although strong RNA-binding signal was observed in the positive control group (RNA-binding protein FUS), the negative control group (IgG) was also positive for RNA-binding (Figure 4. 16 A).

Therefore, we cannot conclude that DAXX does not bind to any RNA. First, this protocol should be improved: as the negative control group (IgG) was not negative (Figure 4. 16 A). If the time of the project allowed, I would have tried to solve this technical problem before studying further on Daxx interaction with RNA. Further optimisation of the buffer components should be performed in the future.

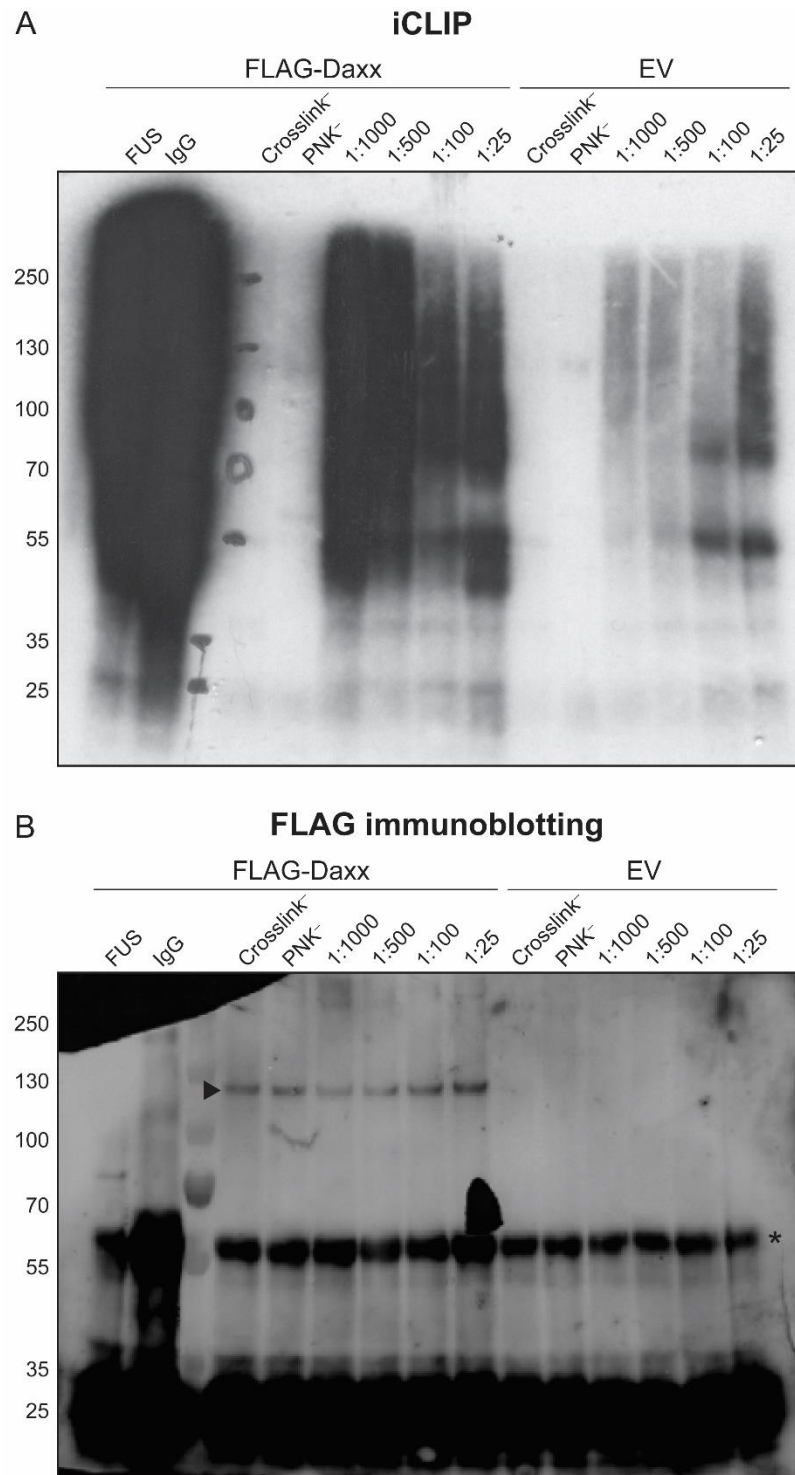


**Figure 4. 16: FLAG iCLIP on FLAG-Daxx– and EV–transduced mNPCs. (A)** Autoradiograph showing potential RNAs that cross-linked and immunoprecipitated with the FLAG-Daxx protein. The RNA–protein samples were digested with RNase I diluted to between 1:1000 and 1:25. FUS was the positive control and IgG was the negative control. **(B)** FLAG immunoblotting on the iCLIP membrane. Arrowhead indicates the FLAG protein at 120 KDa. \* Represents the heavy chain of FLAG antibody eluted from the FLAG Dynabeads.

## 4.3 Discussion

### 4.3.1 Daxx binding partners in mNPCs: Identifying the best FLAG-Daxx IP protocol

A total of 7 FLAG IP protocols were tested on the mNPCs. The first protocol, Optimisation I, analysed FLAG-Daxx overexpression and FLAG IP in whole cell lysates (Section 4.2.2.1). With this protocol, complete immunodepletion of exogenous FLAG-Daxx with FLAG agarose beads was achieved. Notably, the co-IP of the known Daxx functioning partner Atrx was present in the FLAG-Daxx condition, suggesting that the overexpressed Daxx protein is indeed correctly assembled *in vitro* and bound to the endogenous Atrx.

As DAXX is a nuclear protein, we decided to isolate nuclear extracts to increase our chances of identifying Daxx nuclear interactors. First, high-salt (400 mM) lysis buffer was used for the nuclear extraction and bead washes (Optimisation II, Section 4.2.2.2). As protein–protein interactions are highly salt-dependent, the 400 mM salt concentration disrupted the link between Daxx and Atrx.

The salt concentration in Optimisation III was reduced to 150 mM. As expected, the decreased concentration maintained the Daxx-Atrx interaction (Section 4.2.2.3). However, the low salt in the washing buffer was insufficiently stringent to remove non-specific binding from the FLAG agarose beads.

Therefore, a higher salt concentration of 300 mM was tested on the mNPCs in Optimisation IV (Section 4.2.2.4). The background in the silver staining was significantly reduced. This demonstrated the benefit of using a high-salt washing buffer to achieve reduced non-specific protein binding levels. Nevertheless, the FLAG-Daxx IP was negatively affected, likely due to the IP buffers, and the binding of FLAG-Daxx to the FLAG beads was weakened.

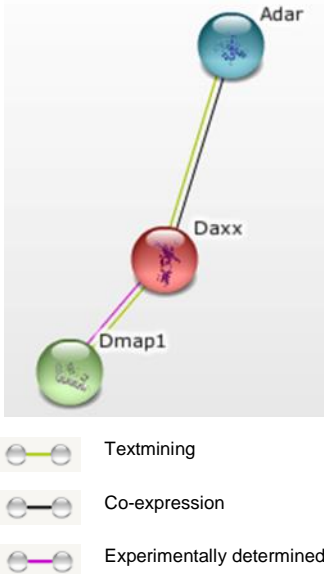
In Optimisation V (Section 4.2.3.1), the nuclear proteins were extracted in 420 mM salt extraction buffer, and the FLAG IP beads were washed with 200 mM salt washing buffer. Notably, FLAG-Daxx protein was immunoprecipitated with the FLAG beads, and Atrx was co-immunoprecipitated. Although the loss of output proteins was observed from the IP, the silver staining of the IP samples was clear, and multiple unique protein bands were observed in the FLAG-Daxx

condition. The experiment was duplicated and the samples were analysed with MS.

#### **4.3.2 Mass Spectrometry analysis and Daxx interaction candidates**

Two proteins, Dmap1 (DNA methyltransferase 1-associated protein 1) and Adar (double-stranded RNA-specific adenosine deaminase; adenosine deaminases that act on RNA), identified from the MS (with PSM ratio  $\geq 4.0$ ), have been previously reported as Daxx-associated proteins (Muromoto *et al.* 2004) (Table 4. 2). Adar obtained an enrichment ratio of 4.64 from the nano-LC-MS/MS analysis. Biological function studies have shown that Adar catalyses the hydrolytic deamination of adenosine to inosine in the double-stranded RNA (A-to-I RNA editing) and affects gene expression and function (St Laurent *et al.* 2013, Sakurai *et al.* 2014). It initiates mRNA translation by changing the codons, thus altering the protein sequence and activity of the encoded protein. It also regulates pre-mRNA splicing by altering the splice site recognition sequences, and alters RNA stability by changing the sequences involved in nuclease recognition (St Laurent *et al.* 2013, Sakurai *et al.* 2014). On the other hand, Dmap1 gained an enrichment ratio of 5.93. Biological function studies have shown its involvement in transcriptional repression activity, and it can repress transcription independently (Rountree *et al.* 2000, Muromoto *et al.* 2004). It targets the replication foci by binding directly from its N-terminus throughout the S-phase. Importantly, it also initiates DAXX-mediated repression of glucocorticoid receptor-dependent transcription (Rountree *et al.* 2000, Muromoto *et al.* 2004).

**Table 4. 2: Identified Daxx-associated proteins with PSM ratio  $\geq 4.0$  (STRING: Known and Predicted Protein–Protein Interactions)**

Protein name	Biological process	
<b>Adar</b>	Cell differentiation Metabolic process Regulation of biological process Transport Response to stimulus Cell organization and biogenesis Defence response	
<b>Dmap1</b>	Regulation of biological process Metabolic process Response to stimulus Cell organization and biogenesis	

From MS analysis, the higher the PSM ratio, the more enriched a protein is in the FLAG-Daxx sample, and is more likely to be a candidate of Daxx interactor. Here I discuss the top three candidates, i.e. Net1, Nr2c2 and Cpsf2, from the MS analysis.

#### 4.3.2.1 Net1 (PSM ratio score 42.72)

NET1 (neuroepithelial cell transforming 1) is part of the family of Rho guanine nucleotide exchange factors (Rho GEFs). The Rho GTPases control many cellular processes, such as cell survival, gene expression and cell migration. NET1 is an unusual member of the Rho GEFs family, as it is localised in the nucleus because of its multiple nuclear localisation signal (NLS) sequence at its N-terminus.

It has been suggested that NET1 can shuttle in and out of the nucleus and control the activation of Rho in the nucleus by changing its subcellular localisation. NET1 is overexpressed in a number of human cancers, as the truncation at its N-terminus leads to its delocalisation from the nucleus to the cytoplasm, thus activating its oncogenic feature (Schmidt 2002, Menon *et al.* 2013). Moreover, NET1 contributes to the activation of nuclear RhoA and RhoB in response to cell ionizing radiation and DNA damage, leading to

apoptosis (Dubash *et al.* 2011, Srougi and Burridge 2011). Although the validation was not conclusive, as no immunoblot signal was observed in the FLAG-Daxx IP condition, we cannot exclude NET1 as a Daxx-interacting candidate, until a more suitable antibody is found.

#### **4.3.2.2 Nr2c2 (PSM ratio score 40.94)**

NR2C2 is also known as TR4 (testicular orphan nuclear receptor 4). It is a transcription factor and can bind to the AGGTCA DNA sequence motifs in the promoters of its target genes. NR2C2 is widely expressed in both embryonic and adult tissues, suggesting that it is involved in various developmental and physiological pathways. More importantly, it is widely expressed in the neural tissues, including the forebrain and spinal cord, during embryonic development (Young *et al.* 1997), suggesting a potential role of Nr2c2 in neurogenesis. In detail, the absence of Nr2c2 in mice *in vivo* results in defects in postnatal growth, and female mice have reduced fertility and severe defects in maternal behaviour (Collins *et al.* 2004). These findings demonstrate an essential role of Nr2c2 in the various physiological functions associated with early embryonic development as well as reproduction. Moreover, the lack of Nr2c2 leads to changes in cerebellar cortex lamination, resulting in disrupted granule cell proliferation during cerebellar development (Chen *et al.* 2008). Another Nr2c2 knockout study indicated the essential function of Nr2c2 in osteoblast differentiation and calcification during osteoporosis (Lin *et al.* 2012). In that study, Nr2c2 bound directly to the promoter region of the osteocalcin gene, and induced gene expression at transcriptional level in a dose-dependent manner. Interestingly, Nr2c2 has been identified as a tumour suppressor during prostate tumorigenesis, in which it modulates the activation of the DNA damage/repair system—ATM (Ataxia Telangiectasia Mutated) expression—at transcriptional level (Lin *et al.* 2014).

Notably, despite the findings on the significant roles of Nr2c2 during early development and adulthood maintenance, its binding ligand remain unclear. We showed here that Nr2c2 was immunoprecipitated along with FLAG-Daxx, suggesting that Daxx could be a ligand of Tr4 related to the neurogenesis pathways.

#### 4.3.2.3 Cpsf2 (PSM ratio score 32.76)

CPSF2 (cleavage and polyadenylation specificity factor 2) is a component of the multi-subunit CPSF complex, which catalyses the cleavage step of the mRNA 3' end formation. Polyadenylation of mRNA by poly(A) polymerase (PAP) requires specificity factors and their recognition sequences. The CPSF complex recognises the upstream core AAUAAA element, in conjunction with CtsF (cleavage stimulation factor), thus recognises the U/GU-rich downstream core element. This serves as a platform for the assembly of enzymatic components onto the pre-mRNA substrates. Cleavage factor I and II (CFI and CFII) are also required for generating the 3' end of the transcript, which is subsequently polyadenylated by PAP (Sagawa *et al.* 2011). The CPSF complex consists of subunits 160 KDa, 100 KDa, 73 KDa, 30 KDa, hFip1 and symplekin; CPSF2 is the 100-KDa subunit (Bienroth *et al.* 1993, Shi *et al.* 2009).

However, CPSF2 may not act as an essential factor among the CPSF subunits (Schonemann *et al.* 2014), with studies suggesting its roles in other aspects. In detail, CPSF2 is required for the assembly of endonuclease activity that cleaves the histone pre-mRNA (maturation of pre-mRNA) together with CPSF73 (Kolev *et al.* 2008). CPSF2 forms a complex with THOC5, a member of the transcription/export complex, to the 3' UTR of the THOC5-targeting genes during the modulation of immediate early gene transcription. CPSF2 is also a co-factor of RBFOX2, an RNA-binding protein. Together with SYMPK, the CPSF2/RBFOX2 complex promotes either exon inclusion or exclusion in alternative splicing regulation of the precursor mRNAs. Moreover, the CPSF/SYMPK complex is a co-factor of NOVA2 as well as the heterologous nuclear ribonucleoprotein A1 during the regulation of alternative splicing (Misra *et al.* 2015).

A knockdown study of CPSF2 showed increased cellular invasion in thyroid cancer cells, while decreased CPSF2 expression is linked to more aggressive papillary thyroid cancer (Nilubol *et al.* 2014). These indicate the significance of CPSF2 in tumour development and invasion. Significantly, we show that Cpsf2 is immunoprecipitated along with FLAG-Daxx. This indicates that Daxx might interact with RNAs via its binding partners Atrx and Cpsf2.

### 4.3.3 Graphical representation of LC-MS/MS results

The proteins presented in Figure 4. 17 were identified from the LC-MS/MS analysis, and had a PSM ratio of  $\geq 4.0$ . The protein analysis here is based on the biological database and web resource of known and predicted protein–protein interactions (STRING). The proteins involved in regulating DNA-templated transcription are highlighted in red. Notably, the ribosomal proteins normally considered background in MS analysis were considered actual hits here, as they obtained high PSM ratio scores. Moreover, CHD2 had a score of 4.66, indicating it is likely connected to Daxx. The detailed protein candidates with a PSM ratio of  $\geq 4.0$  are listed in Appendix I.

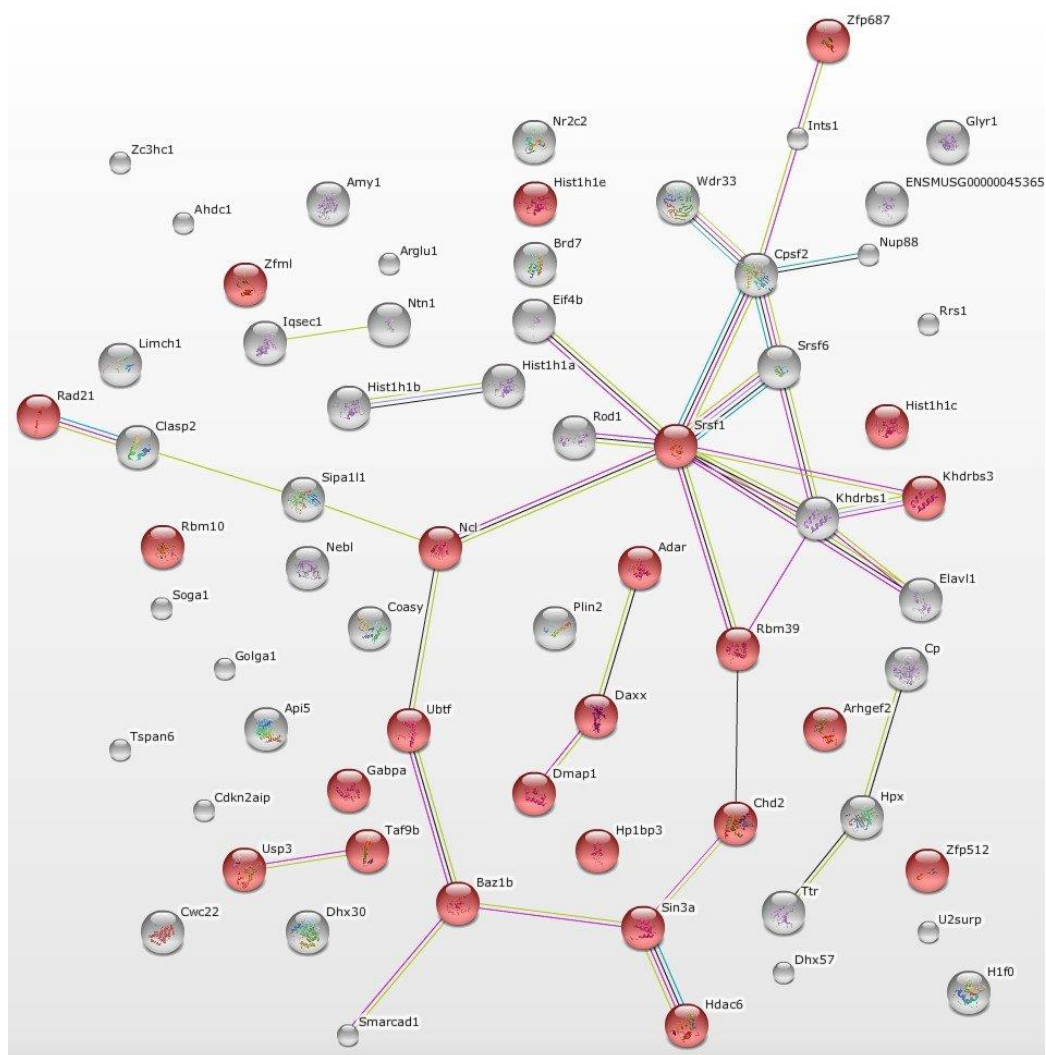


**Figure 4. 17: MS analysis identified candidates Daxx-associated proteins with PSM ratio  $\geq 4.0$  (STRING).** The proteins labelled in red are involved in the regulation of DNA-templated transcription. **Associations:** Blue – from curated databases; Purple – experimentally determined; Yellow – textmining; Black – co-expression. **Note:** The size of the nodes is unrelated to the MS score of the proteins, and ribosome proteins are not presented here.

#### 4.3.4 Further optimisations of FLAG-Daxx IP

The magnetic FLAG beads were used in further optimisations of the IP protocol, as they perform better in terms of purity specificity as compared to agarose FLAG beads. In addition, the protocol in Optimisation V required improvement to overcome the loss of proteins during the IP. It was suspected that the protein loss was caused by protein degradation and oxidative stress. Unfortunately, the improved buffer recipe with change of protease and phosphatase inhibitors and DTT did not prevent protein loss in the output/post-IP samples.

Finally, IP with non-denaturing buffer in Optimisation VII was tested on the NPCs, and no significant protein loss was observed during the IP. Interestingly, the FLAG peptides could elute the FLAG-Daxx proteins from the FLAG beads, but the FLAG elution was not absolute and no specific protein bands were observed in the silver stain. On the other hand, the FLAG beads eluted with Laemmli buffer worked better than FLAG peptide elution, and silver staining showed unique protein bands in the FLAG-Daxx condition.

In conclusion, two co-IP protocols have been developed in this project on mNPCs for application on Daxx interactome identification. Several Daxx binding partners have already been validated from IP using the first protocol (Optimisation V). If my PhD project timeline had allowed, I would have continued working on the following experiments: 1) Functional analysis of the validated DAXX interaction partners, including their knockdown/knockout impacts *in vitro* and *in vivo*, in relation to the DAXX cellular mechanisms as well as H3.3 deposition. 2) More top hits from the MS analysis to be validated via immunoblotting from the experiment duplicates, followed by functional analysis of the validated proteins. On the other hand, the protocol in Optimisation VII benefits from its non-denaturing feature, and novel protein bands were shown from the silver staining. Notably, the different buffer components and salt concentrations would result in altered protein–protein interactions, which could explain why CPSF2 was not co-immunoprecipitated with FLAG-Daxx here. If there had been more time, I would perform MS analysis of these samples, and: 1) The top hits would be validated, and their function in relation to DAXX would be analysed. 2) The identified potential DAXX-interacting partners could also be compared with that from Optimisation

V, and any overlapping candidates would be further studied. In addition, the co-IP protocols developed in this project can be applied in other nuclear protein interactome studies, potentially in other neuronal cells including neural stem cells and glioma cells. More importantly, using the co-IP protocols, the potentially altered DAXX interactomes in the neural cells carrying the oncogenic transformed H3.3 (K27M or G34R/V mutation) can be studied.

#### **4.3.5 Candidate approach (immunoblotting and iCLIP)**

As elaborated above, several chromatin-remodelling factors were examined to determine whether they are Daxx-associating proteins. Unfortunately, with the adapted protocols, no association was found between Daxx and the selected protein candidates. Nevertheless, we cannot rule out these proteins, as the IP analysis of the protein–protein connections depends greatly on the salt concentration. It is also possible that these proteins associate with Daxx in an indirect manner.

Moreover, although the iCLIP results indicated that Daxx is not an RNA-associated protein, we cannot be certain of this here, as MS analysis identified the ribosomal proteins and pre-mRNA processing proteins as potential Daxx interactomes. In addition, this experiment should be repeated, as we expect the IgG negative control to be negative. Therefore, further optimisation should be performed to achieve an improved outcome that indicates the connection of DAXX or its interacting partners to RNAs.

## **Chapter 5**

### **Conclusions and Future Research**

## 5 Conclusions and Future Research

### 5.1 Conclusions

Recent studies in our group and others have shown the importance of H3.3 in chromatin remodelling and transcriptional regulation. In particular, H3.3 turnover on chromatin has been suggested to play an important role in regulating transcriptional identity and cell plasticity. Moreover, H3.3 driver mutations have been identified in paediatric brainstem (K27M) and cerebral hemisphere (G34R/V) GBM. H3.3 accumulates on chromatin during ageing and plays a significant pro-survival role in lifespan extension in nematodes. Finally, it has been suggested that a lack of H3.3 promotes the development of several psychiatric disorders as well as neurodegenerative diseases.

The H3.3 deposition chaperone DAXX is required for H3.3 deposition at the pericentric heterochromatin and telomeres in a replication-independent manner. Our group has demonstrated the involvement of Daxx in the activity-dependent regulation of H3.3 loading at immediate early gene regulatory regions in neurons, and that Daxx may regulate H3.3 incorporation in downstream calcium signalling.

The key question in this study is whether and how we can modulate H3.3 loading. Insights into H3.3 regulatory mechanisms could provide new tools for modulating H3.3 loading in cancer as well as ageing.

We took dual approach: on one hand, we developed a H3.3 deposition visualisation assay that will allow us to compound screen for the H3.3 modulation factors (Chapter 3). On the other hand, we used a biochemical approach to identify candidate interactors in the regulatory pathway of H3.3 deposition (Chapter 4).

For the high content/drug screening analysis of H3.3 deposition, a robust visualisation platform with Halo-tagged H3.3 in Neuro2a cells was developed via the cutting-edge automated platform. Notably, during the establishment of the imaging assay, it was demonstrated that the turnover time for old–new H3.3 and dH3 in the growth-arrested Neuro2a cells was 96 hours. Significantly, dH3-HaloTag demonstrated identical loading patterns as H3.3-HaloTag, suggesting that the canonical H3 is also deposited when the cells are in growth arrest. Further analysis should be performed at different cell cycle stages and

in various cell types. The established visualisation assay will be applied in compound screening for H3.3 modulation factors, thus identifying and developing drugs specifically targeting the deposition of mutant H3.3.

A FLAG affinity purification system was established on Daxx, and was adapted using a number of IP protocol optimisations. MS analysis revealed 101 proteins with PSM scores  $\geq 4.0$ . The top two Daxx-interacting candidates, Nr2c2 and Cpsf2, were verified via IP-immunoblotting, linking Daxx to neurogenesis as well as RNA processing. In addition, MS/MS analysis showed a top score for Net1, but no immunoblotting antibody is commercially available for its validation. If Net1 were validated, it would suggest that Daxx interacts with Net1 during its programmed cell death process. The finding of Daxx-interacting partners, which have not been previously reported, not only suggests its novel functions in cellular processing, but also provides key insights in future exploration of Daxx functional studies including in brain tumour and age-related diseases.

Overall, through this work, we were able to identify novel and potentially targetable regulatory mechanisms of H3.3 loading with implications for cancer treatment and the amelioration of age-associated tissue dysfunction and disease.

## 5.2 Future research

During the development of the H3.3 imaging assay, the unexpected finding of the canonical H3 chromatin loading patterns has challenged the commonly acknowledged 'fact' that this histone is only incorporated during the S phase. Further studies should be carried out in cell growth arrest at different cell cycle stages, as well as in various cell types. Significantly, the established visualisation assay will be applied in compound screening for H3.3-interacting partners, for the eventual purpose of developing pharmaceutical treatments for tumour and psychology-related diseases.

Currently, the high-content/drug screening platform is undergoing further optimisation, and the PI3K/mTOR inhibitors have been recently applied to the cells with the visualisation platform. In addition to the application of the HaloTag system *in vitro*, this system can also be applied *in vivo*. For example, HaloTag can be electroporated *in utero* to the brain area of interest, and the HaloTag expression would be examined via visualisation on tissue slides or *in vivo* 2-photon microscopy.

The finding of Daxx-interacting partners, which has not been previously reported, not only suggests its novel functions in cellular processing, but also provides key insights into future exploration of Daxx functional studies. These include, but are not limited to, brain tumour and age-related diseases. Moreover, the two Daxx-interacting partners identified in this research are currently under further investigation by our group. The *in vitro* and *in vivo* functional analysis of these candidates will be performed in the future, and more top scored MS/MS candidates would be validated.

I believe that this work will provide a window of opportunity for targeting H3.3 deposition via modulation of H3.3 chaperones. More generally, it will increase our understanding of fundamental mechanisms regulating chromatin structure and function in physiological processes and human disease. In addition, this study has the potential to pave the way for drug discovery aimed at targeting the cancer epigenome, with implications for brain cancer, neurodegeneration diseases as well as bone neoplasms.

## Bibliography

- Ahmad, K. and Henikoff, S., 2002. The Histone Variant H3.3 Marks Active Chromatin by Replication-Independent Nucleosome Assembly. *Molecular Cell*, 9 (6), 1191–1200.
- Albig, W. and Doenecke, D., 1997. The human histone gene cluster at the D6S105 locus. *Human Genetics*, 101 (3), 284–294.
- Banaszynski, L.A., Wen, D., Dewell, S., Whitcomb, S.J., Lin, M., Diaz, N., Elsässer, S.J., Chapgier, A., Goldberg, A.D., Canaani, E., Rafii, S., Zheng, D., and Allis, C.D., 2013. Hira-Dependent Histone H3.3 Deposition Facilitates PRC2 Recruitment at Developmental Loci in ES Cells. *Cell*, 155 (1), 107–120.
- Banks, D.D. and Gloss, L.M., 2004. Folding mechanism of the (H3-H4)<sub>2</sub> histone tetramer of the core nucleosome. *Protein Science*, 13 (5), 1304–1316.
- Bano, D., Piazzesi, A., Salomoni, P., and Nicotera, P., 2017. The histone variant H3.3 claims its place in the crowded scene of epigenetics. *Aging*, 9 (3), 602–614.
- Banumathy, G., Somaiah, N., Zhang, R., Tang, Y., Hoffmann, J., Andrade, M., Ceulemans, H., Schultz, D., Marmorstein, R., and Adams, P.D., 2009. Human UBN1 is an ortholog of yeast Hpc2p and has an essential role in the HIRA/ASF1a chromatin-remodeling pathway in senescent cells. *Molecular and cellular biology*, 29 (3), 758–770.
- Becker, P.B. and Workman, J.L., 2013. Nucleosome Remodeling and Epigenetics. *Cold Spring Harbor Perspectives in Biology*, 5 (9), a017905–a017905.
- Behjati, S., Tarpey, P.S., Presneau, N., Scheipl, S., Pillay, N., Van Loo, P., Wedge, D.C., Cooke, S.L., Gundem, G., Davies, H., Nik-Zainal, S., Martin, S., McLaren, S., Goody, V., Goodie, V., Robinson, B., Butler, A., Teague, J.W., Halai, D., Khatri, B., Myklebost, O., Baumhoer, D., Jundt, G., Hamoudi, R., Tirabosco, R., Amary, M.F., Futreal, P.A., Stratton, M.R., Campbell, P.J., and Flanagan, A.M., 2013. Distinct H3F3A and H3F3B driver mutations define chondroblastoma and giant cell tumor of bone. *Nature Genetics*, 45 (12), 1479–1482.
- Bender, S., Tang, Y., Lindroth, A.M., Hovestadt, V., Jones, D.T.W., Kool, M., Zapatka, M., Northcott, P.A., Sturm, D., Wang, W., Radlwimmer, B., Højfeldt, J.W., Truffaux, N., Castel, D., Schubert, S., Ryzhova, M., Şeker-Cin, H., Gronych, J., Johann, P.D., Stark, S., Meyer, J., Milde, T., Schuhmann, M.,

- Ebinger, M., Monoranu, C.-M., Ponnuswami, A., Chen, S., Jones, C., Witt, O., Collins, V.P., von Deimling, A., Jabado, N., Puget, S., Grill, J., Helin, K., Korshunov, A., Lichter, P., Monje, M., Plass, C., Cho, Y.-J., and Pfister, S.M., 2013. Reduced H3K27me3 and DNA Hypomethylation Are Major Drivers of Gene Expression in K27M Mutant Pediatric High-Grade Gliomas. *Cancer Cell*, 24 (5), 660–672.
- Bernardi, R. and Pandolfi, P.P., 2007. Structure, dynamics and functions of promyelocytic leukaemia nuclear bodies. *Nature Reviews Molecular Cell Biology*, 8 (12), 1006–1016.
- Bienroth, S., Keller, W., and Wahle, E., 1993. Assembly of a processive messenger RNA polyadenylation complex. *The EMBO journal*, 12 (2), 585–594.
- Bodai, L., Pardi, N., Ujfaludi, Z., Bereczki, O., Komonyi, O., Balint, E., and Boros, I.M., 2007. Daxx-like protein of Drosophila interacts with Dmp53 and affects longevity and Ark mRNA level. *The Journal of biological chemistry*, 282 (50), 36386–93.
- Bonet-Costa, C., Vilaseca, M., Diema, C., Vujatovic, O., Vaquero, A., Omeñaca, N., Castejón, L., Bernués, J., Giralt, E., and Azorín, F., 2012. Combined bottom-up and top-down mass spectrometry analyses of the pattern of post-translational modifications of Drosophila melanogaster linker histone H1. *Journal of Proteomics*, 75 (13), 4124–4138.
- Boyer, L.A., Plath, K., Zeitlinger, J., Brambrink, T., Medeiros, L.A., Lee, T.I., Levine, S.S., Wernig, M., Tajonar, A., Ray, M.K., Bell, G.W., Otte, A.P., Vidal, M., Gifford, D.K., Young, R.A., and Jaenisch, R., 2006. Polycomb complexes repress developmental regulators in murine embryonic stem cells. *Nature*, 441 (7091), 349–353.
- Bracken, A.P., Pasini, D., Capra, M., Prosperini, E., Colli, E., and Helin, K., 2003. EZH2 is downstream of the pRB-E2F pathway, essential for proliferation and amplified in cancer. *The EMBO journal*, 22 (20), 5323–5335.
- Brown, Z.Z., Müller, M.M., Jain, S.U., Allis, C.D., Lewis, P.W., and Muir, T.W., 2014. Strategy for ‘detoxification’ of a cancer-derived histone mutant based on mapping its interaction with the methyltransferase PRC2. *Journal of the American Chemical Society*, 136 (39), 13498–13501.
- Buscarlet, M., Krasteva, V., Ho, L., Simon, C., Hébert, J., Wilhelm, B., Crabtree,

- G.R., Sauvageau, G., Thibault, P., and Lessard, J. a., 2014. Essential role of BRG, the ATPase subunit of BAF chromatin remodeling complexes, in leukemia maintenance. *Blood*, 123 (11), 1720–1728.
- Campos, E.I., Fillingham, J., Li, G., Zheng, H., Voigt, P., Kuo, W.-H.W., Seepany, H., Gao, Z., Day, L.A., Greenblatt, J.F., and Reinberg, D., 2010. The program for processing newly synthesized histones H3.1 and H4. *Nature structural & molecular biology*, 17 (11), 1343–1351.
- Cao, K., Lailier, N., Zhang, Y., Kumar, A., Uppal, K., Liu, Z., Lee, E.K., Wu, H., Medrzycki, M., Pan, C., Ho, P.Y., Cooper, G.P., Dong, X., Bock, C., Bouhassira, E.E., and Fan, Y., 2013. High-resolution mapping of h1 linker histone variants in embryonic stem cells. *PLoS genetics*, 9 (4), e1003417.
- Chan, K.-M., Fang, D., Gan, H., Hashizume, R., Yu, C., Schroeder, M., Gupta, N., Mueller, S., James, C.D., Jenkins, R., Sarkaria, J., and Zhang, Z., 2013. The histone H3.3K27M mutation in pediatric glioma reprograms H3K27 methylation and gene expression. *Genes & development*, 27 (9), 985–990.
- Chang, H.Y., Nishitoh, H., Yang, X., Ichijo, H., and Baltimore, D., 1998. Activation of Apoptosis Signal-Regulating Kinase 1 (ASK1) by the Adapter Protein Daxx. *Science*, 281 (5384), 1860–1863.
- Chen, Y.T., Collins, L.L., Chang, S.S., and Chang, C., 2008. The roles of testicular orphan nuclear receptor 4 (TR4) in cerebellar development. *Cerebellum*, 7 (1), 9–17.
- Cheung, N.-K. V, Zhang, J., Lu, C., Parker, M., Bahrami, A., Tickoo, S.K., Heguy, A., Pappo, A.S., Federico, S., Dalton, J., Cheung, I.Y., Ding, L., Fulton, R., Wang, J., Chen, X., Becksfort, J., Wu, J., Billups, C.A., Ellison, D., Mardis, E.R., Wilson, R.K., Downing, J.R., and Dyer, M.A., 2012. Association of age at diagnosis and genetic mutations in patients with neuroblastoma. *Jama*, 307 (10), 1062–1071.
- Cheung, W.L., Ajiro, K., Samejima, K., Kloc, M., Cheung, P., Mizzen, C.A., Beeser, A., Etkin, L.D., Chernoff, J., Earnshaw, W.C., and Allis, C.D., 2003. Apoptotic phosphorylation of histone H2B is mediated by mammalian sterile twenty kinase. *Cell*, 113 (4), 507–517.
- Chow, C.-M., Georgiou, A., Szutorisz, H., Maia e Silva, A., Pombo, A., Barahona, I., Dargelos, E., Canzonetta, C., and Dillon, N., 2005. Variant histone H3.3 marks

- promoters of transcriptionally active genes during mammalian cell division. *EMBO reports*, 6 (4), 354–360.
- Chu, C.-S., Hsu, P.-H., Lo, P.-W., Scheer, E., Tora, L., Tsai, H.-J., Tsai, M.-D., and Juan, L.-J., 2011. Protein Kinase A-mediated Serine 35 Phosphorylation Dissociates Histone H1.4 from Mitotic Chromosome. *THE JOURNAL OF BIOLOGICAL CHEMISTRY*, 286 (41), 35843–35851.
- Clagett-Dame, M., McNeill, E.M., and Muley, P.D., 2006. Role of all-trans retinoic acid in neurite outgrowth and axonal elongation. *Journal of Neurobiology*, 66 (7), 739–756.
- Clément, C., Vassias, I., Ray-Gallet, D., and Almouzni, G., 2016. Functional Characterization of Histone Chaperones Using SNAP-Tag-Based Imaging to Assess De Novo Histone Deposition. *Methods in Enzymology*, 573, 97–117.
- Collins, L.L., Lee, Y.-F., Heinlein, C. a, Liu, N.-C., Chen, Y.-T., Shyr, C.-R., Meshul, C.K., Uno, H., Platt, K. a, and Chang, C., 2004. Growth retardation and abnormal maternal behavior in mice lacking testicular orphan nuclear receptor 4. *Proceedings of the National Academy of Sciences of the United States of America*, 101 (42), 15058–15063.
- Cook, A.J.L., Gurard-Levin, Z.A., Vassias, I., and Almouzni, G., 2011. A specific function for the histone chaperone NASP to fine-tune a reservoir of soluble H3-H4 in the histone supply chain. *Molecular cell*, 44 (6), 918–927.
- Costanzi, C. and Pehrson, J.R., 1998. Histone macroH2A1 is concentrated in the inactive X chromosome of female mammals. *Nature*, 393 (6685), 599–601.
- Couldrey, C., Carlton, M.B., Nolan, P.M., Colledge, W.H., and Evans, M.J., 1999. A retroviral gene trap insertion into the histone 3.3A gene causes partial neonatal lethality, stunted growth, neuromuscular deficits and male sub-fertility in transgenic mice. *Human molecular genetics*, 8 (13), 2489–2495.
- Creppe, C., Janich, P., Cantariño, N., Noguera, M., Valero, V., Musulén, E., Douet, J., Posavec, M., Martín-Caballero, J., Sumoy, L., Di Croce, L., Benitah, S.A., and Buschbeck, M., 2012. MacroH2A1 regulates the balance between self-renewal and differentiation commitment in embryonic and adult stem cells. *Molecular and cellular biology*, 32 (8), 1442–1452.
- Czermin, B., Melfi, R., McCabe, D., Seitz, V., Imhof, A., and Pirrotta, V., 2002. Drosophila enhancer of Zeste/ESC complexes have a histone H3

- methyltransferase activity that marks chromosomal Polycomb sites. *Cell*, 111 (2), 185–196.
- Daujat, S., Zeissler, U., Waldmann, T., Happel, N., and Schneider, R., 2005. HP1 Binds Specifically to Lys 26 -methylated Histone H1.4, whereas Simultaneous Ser Phosphorylation Blocks HP1 Binding. *THE JOURNAL OF BIOLOGICAL CHEMISTRY*, 280 (45), 38090–38095.
- Daury, L., Chailleux, C., Bonvallet, J., and Trouche, D., 2006. Histone H3.3 deposition at E2F-regulated genes is linked to transcription. *EMBO reports*, 7 (1), 66–71.
- Deb, G., Thakur, V.S., and Gupta, S., 2013. Multifaceted role of EZH2 in breast and prostate tumorigenesis: Epigenetics and beyond. *Epigenetics*, 8 (5), 464–476.
- Dhar, S., Gursoy-Yuzugullu, O., Parasuram, R., and Price, B.D., 2017. The tale of a tail: histone H4 acetylation and the repair of DNA breaks. *Philosophical transactions of the Royal Society of London. Series B, Biological sciences*, 372 (1731), 2016.0284.
- Drane, P., Ouararhni, K., Depaux, A., Shuaib, M., and Hamiche, A., 2010. The death-associated protein DAXX is a novel histone chaperone involved in the replication-independent deposition of H3.3. *Genes Dev*, 24 (12), 1253–1265.
- Dubash, A.D., Guilluy, C., Srougi, M.C., Boulter, E., BurrIDGE, K., and García-Mata, R., 2011. The small GTPase RhoA localizes to the nucleus and is activated by Net1 and DNA damage signals. *PloS one*, 6 (2), e17380.
- Elsaesser, S.J. and Allis, C.D., 2010. HIRA and Daxx constitute two independent histone H3.3-containing predeposition complexes. *Cold Spring Harbor Symposia on Quantitative Biology*, 75, 27–34.
- Elsässer, S.J., Huang, H., Lewis, P.W., Chin, J.W., Allis, C.D., and Patel, D.J., 2012. DAXX envelops a histone H3.3–H4 dimer for H3.3-specific recognition. *Nature*, 491 (7425), 560–565.
- England, C.G., Luo, H., and Cai, W., 2015. HaloTag technology: a versatile platform for biomedical applications. *Bioconjugate chemistry*, 26 (6), 975–986.
- Ernst, T., Chase, A.J., Score, J., Hidalgo-Curtis, C.E., Bryant, C., Jones, A. V, Waghorn, K., Zoi, K., Ross, F.M., Reiter, A., Hochhaus, A., Drexler, H.G., Duncombe, A., Cervantes, F., Oscier, D., Boulwood, J., Grand, F.H., and

- Cross, N.C.P., 2010. Inactivating mutations of the histone methyltransferase gene EZH2 in myeloid disorders. *Nature Genetics*, 42 (8), 722–726.
- Fan, Y., Nikitina, T., Morin-Kensicki, E.M., Zhao, J., Magnuson, T.R., Woodcock, C.L., and Skoultschi, A.I., 2003. H1 linker histones are essential for mouse development and affect nucleosome spacing in vivo. *Molecular and cellular biology*, 23 (13), 4559–4572.
- Feng, J., Fouse, S., and Fan, G., 2007. Epigenetic regulation of neural gene expression and neuronal function. *Pediatric Research*, 61 (5 PART 2 SUPPL.), 58–63.
- FMarzluff, W., 2005. Metazoan replication-dependent histone mRNAs: a distinct set of RNA polymerase II transcripts. *Current Opinion in Cell Biology*, 17 (3), 274–280.
- Fyodorov, D. V, Zhou, B.-R., Skoultschi, A.I., and Bai, Y., 2017. Emerging roles of linker histones in regulating chromatin structure and function. *Nature Reviews Molecular Cell Biology*, 19 (3), 192–206.
- Gaspari, M. and Cuda, G., 2011. Nano LC–MS/MS: A Robust Setup for Proteomic Analysis. *In: Methods in molecular biology (Clifton, N.J.)*. 115–126.
- Gatta, R. and Mantovani, R., 2010. Single nucleosome ChIPs identify an extensive switch of acetyl marks on cell cycle promoters. *Cell Cycle*, 9 (11), 2149–2159.
- Gatta, R. and Mantovani, R., 2011. NF-Y affects histone acetylation and H2A.Z deposition in cell cycle promoters. *Epigenetics*, 6 (4), 526–534.
- Gibbons, R.J., 2005. Histone modifying and chromatin remodelling enzymes in cancer and dysplastic syndromes. *Human molecular genetics*, 14 Spec No (1), R85-92.
- Goldberg, A.D., Banaszynski, L.A., Noh, K.-M., Lewis, P.W., Elsaesser, S.J., Stadler, S., Dewell, S., Law, M., Guo, X., Li, X., Wen, D., Chapgier, A., DeKaveler, R.C., Miller, J.C., Lee, Y.-L., Boydston, E.A., Holmes, M.C., Gregory, P.D., Grealley, J.M., Rafii, S., Yang, C., Scambler, P.J., Garrick, D., Gibbons, R.J., Higgs, D.R., Cristea, I.M., Urnov, F.D., Zheng, D., and Allis, C.D., 2010. Distinct factors control histone variant H3.3 localization at specific genomic regions. *Cell*, 140 (5), 678–691.
- Grewal, S.I.S. and Elgin, S.C.R., 2002. Heterochromatin: new possibilities for the

- inheritance of structure. *Current opinion in genetics & development*, 12 (2), 178–187.
- Hake, S.B. and Allis, C.D., 2006. Histone H3 variants and their potential role in indexing mammalian genomes: The “H3 barcode hypothesis”. *Proceedings of the National Academy of Sciences*, 103 (17), 6428–6435.
- Hake, S.B., Garcia, B.A., Duncan, E.M., Kauer, M., Dellaire, G., Shabanowitz, J., Bazett-Jones, D.P., Allis, C.D., and Hunt, D.F., 2006. Expression Patterns and Post-translational Modifications Associated with Mammalian Histone H3 Variants. *NUMBER 1 JOURNAL OF BIOLOGICAL CHEMISTRY*, 281 (1), 559–568.
- Hall, J.M. and Cole, R.D., 1986. Mechanisms of H1<sup>o</sup> Accumulation in Mouse Neuroblastoma Cells Differ with Different Treatments. *THE JOURNAL OF BIOLOGICAL CHEMISTRY*, 261 (11), 5168–5174.
- Happel, N., Schulze, E., and Doenecke, D., 2005. Characterisation of human histone H1x. *Biol. Chem.*, 386 (6), 541–551.
- Harada, A., Okada, S., Konno, D., Odawara, J., Yoshimi, T., Yoshimura, S., Kumamaru, H., Saiwai, H., Tsubota, T., Kurumizaka, H., Akashi, K., Tachibana, T., Imbalzano, A.N., and Ohkawa, Y., 2012. Chd2 interacts with H3.3 to determine myogenic cell fate. *The EMBO Journal*, 31 (13), 2994–3007.
- Hargreaves, D.C. and Crabtree, G.R., 2011. ATP-dependent chromatin remodeling: genetics, genomics and mechanisms. *Cell Research*, 21 (3), 396–420.
- Heaphy, C.M., de Wilde, R.F., Jiao, Y., Klein, A.P., Edil, B.H., Shi, C., Bettgowda, C., Rodriguez, F.J., Eberhart, C.G., Hebbar, S., Offerhaus, G.J., McLendon, R., Rasheed, B.A., He, Y., Yan, H., Bigner, D.D., Oba-Shinjo, S.M., Marie, S.K.N., Riggins, G.J., Kinzler, K.W., Vogelstein, B., Hruban, R.H., Maitra, A., Papadopoulos, N., and Meeker, A.K., 2011. Altered telomeres in tumors with ATRX and DAXX mutations. *Science (New York, N. Y.)*, 333 (6041), 425.
- Henikoff, S., Furuyama, T., and Ahmad, K., 2004. Histone variants, nucleosome assembly and epigenetic inheritance. *Trends in Genetics*, 20 (7), 320–326.
- Hergeth, S.P. and Schneider, R., 2015. The H1 linker histones: multifunctional proteins beyond the nucleosomal core particle. *EMBO Reports*, 16 (11), 1439–1453.

- Ho, L., Ronan, J.L., Wu, J., Staahl, B.T., Chen, L., Kuo, A., Lessard, J., Nesvizhskii, A.I., Ranish, J., and Crabtree, G.R., 2009. An embryonic stem cell chromatin remodeling complex, esBAF, is essential for embryonic stem cell self-renewal and pluripotency. *Proceedings of the National Academy of Sciences of the United States of America*, 106 (13), 5181–5186.
- Hödl, M. and Basler, K., 2009. Transcription in the absence of histone H3.3. *Current biology : CB*, 19 (14), 1221–1226.
- Hoek, M. and Stillman, B., 2003. Chromatin assembly factor 1 is essential and couples chromatin assembly to DNA replication in vivo. *Proceedings of the National Academy of Sciences of the United States of America*, 100 (21), 12183–12188.
- Hohmann, A.F. and Vakoc, C.R., 2014. A rationale to target the SWI/SNF complex for cancer therapy. *Trends in genetics : TIG*, 30 (8), 356–363.
- Hollenbach, A.D., McPherson, C.J., Mientjes, E.J., Iyengar, R., and Grosveld, G., 2002. Daxx and histone deacetylase II associate with chromatin through an interaction with core histones and the chromatin-associated protein Dek. *Journal of cell science*, 115 (Pt 16), 3319–3330.
- Hollenbach, A.D., Sublett, J.E., McPherson, C.J., and Grosveld, G., 1999. The Pax3-FKHR oncoprotein is unresponsive to the Pax3-associated repressor hDaxx. *The EMBO journal*, 18 (13), 3702–3711.
- Huang, H., Yu, Z., Zhang, S., Liang, X., Chen, J., Li, C., Ma, J., and Jiao, R., 2010. Drosophila CAF-1 regulates HP1-mediated epigenetic silencing and pericentric heterochromatin stability. *Journal of Cell Science*, 123 (16), 2853–2861.
- Huang, S., Litt, M., and Felsenfeld, G., 2005. Methylation of histone H4 by arginine methyltransferase PRMT1 is essential in vivo for many subsequent histone modifications. *Genes & development*, 19 (16), 1885–1893.
- Ishov, A.M., Vladimirova, O. V, Maul, G.G., Sullivan, K.F., and Sullivan, K., 2004. Heterochromatin and ND10 are cell-cycle regulated and phosphorylation-dependent alternate nuclear sites of the transcription repressor Daxx and SWI/SNF protein ATRX. *Journal of cell science*, 117 (Pt 17), 3807–3820.
- Jackson, J.D., Falciano, V.T., and Gorovsky, M.A., 1996. A likely histone H2A.F/Z variant in *Saccharomyces cerevisiae*. *Trends in Biochemical Sciences*, 21 (12), 466–467.

- Jenuwein, T. and Allis, C.D., 2001. Translating the Histone Code. *Science*, 293 (5532), 1074–1080.
- Kallappagoudar, S., Yadav, R.K., Lowe, B.R., and Partridge, J.F., 2015. Histone H3 mutations-a special role for H3.3 in tumorigenesis? *Chromosoma*, 124 (2), 177–189.
- Kamakaka, R.T. and Biggins, S., 2005. Histone variants: deviants? *Genes & development*, 19 (3), 295–310.
- Kamieniarz, K., Izzo, A., Dundr, M., Tropberger, P., Ozretic, L., Kirfel, J., Scheer, E., Tropel, P., Wisniewski, J.R., Tora, L., Viville, S., Buettner, R., and Schneider, R., 2012. A dual role of linker histone H1.4 Lys 34 acetylation in transcriptional activation. *Genes & development*, 26 (8), 797–802.
- Kapoor, A., Goldberg, M.S., Cumberland, L.K., Ratnakumar, K., Segura, M.F., Emanuel, P.O., Menendez, S., Vardabasso, C., LeRoy, G., Vidal, C.I., Polsky, D., Osman, I., Garcia, B.A., Hernando, E., and Bernstein, E., 2010. The histone variant macroH2A suppresses melanoma progression through regulation of CDK8. *Nature*, 468 (7327), 1105–1109.
- Kasinsky, H.E., Lewis, J.D., Dacks, J.B., and Ausió, J., 2001. Origin of H1 linker histones. *FASEB journal : official publication of the Federation of American Societies for Experimental Biology*, 15 (1), 34–42.
- Kato, S., Inoue, K., and Youn, M.-Y., 2010. Emergence of the osteo-epigenome in bone biology. *IBMS BoneKEy*, 7 (9), 314–324.
- Kehle, J., Beuchle, D., Treuheit, S., Christen, B., Kennison, J. a, Bienz, M., and Müller, J., 1998. dMi-2, a hunchback-interacting protein that functions in polycomb repression. *Science (New York, N. Y.)*, 282 (December), 1897–1900.
- Khuong-Quang, D.-A., Buczkowicz, P., Rakopoulos, P., Liu, X.-Y., Fontebasso, A.M., Bouffet, E., Bartels, U., Albrecht, S., Schwartzenuber, J., Letourneau, L., Bourgey, M., Bourque, G., Montpetit, A., Bourret, G., Lepage, P., Fleming, A., Lichter, P., Kool, M., von Deimling, A., Sturm, D., Korshunov, A., Faury, D., Jones, D.T., Majewski, J., Pfister, S.M., Jabado, N., and Hawkins, C., 2012. K27M mutation in histone H3.3 defines clinically and biologically distinct subgroups of pediatric diffuse intrinsic pontine gliomas. *Acta Neuropathologica*, 124 (3), 439–447.
- Kim, K., Jeong, K., Kim, H., Choi, J., Lu, W., Stallcup, M., and An, W., 2012.

- Functional interplay between p53 acetylation and H1.2 phosphorylation in p53-regulated transcription. *Oncogene*, 31 (39), 4290.
- Kim, K., Lee, B., Kim, J., Choi, J., Kim, J.-M., Xiong, Y., Roeder, R.G., and An, W., 2013. Linker Histone H1.2 Cooperates with Cul4A and PAF1 to Drive H4K31 Ubiquitylation-Mediated Transactivation. *Cell Reports*, 5 (6), 1690–1703.
- Kleer, C.G., Cao, Q., Varambally, S., Shen, R., Ota, I., Tomlins, S.A., Ghosh, D., Sewalt, R.G.A.B., Otte, A.P., Hayes, D.F., Sabel, M.S., Livant, D., Weiss, S.J., Rubin, M.A., and Chinnaiyan, A.M., 2003. EZH2 is a marker of aggressive breast cancer and promotes neoplastic transformation of breast epithelial cells. *Proceedings of the National Academy of Sciences of the United States of America*, 100 (20), 11606–11611.
- Ko, T.Y., Kim, J.I., Park, E.S., Mun, J.M., and Park, S.D., 2018. The Clinical Implications of Death Domain-Associated Protein (DAXX) Expression. *The Korean Journal of Thoracic and Cardiovascular Surgery*, 51 (3), 187–194.
- Kolev, N.G., Yario, T.A., Benson, E., and Steitz, J.A., 2008. Conserved motifs in both CPSF73 and CPSF100 are required to assemble the active endonuclease for histone mRNA 3'-end maturation. *EMBO reports*, 9 (10), 1013–1018.
- Konev, A.Y., Tribus, M., Park, S.Y., Podhraski, V., Lim, C.Y., Emelyanov, A. V., Vershilova, E., Pirrotta, V., Kadonaga, J.T., Lusser, A., and Fyodorov, D. V., 2007. CHD1 motor protein is required for deposition of histone variant H3.3 into chromatin in vivo. *Science (New York, N.Y.)*, 317 (5841), 1087–1090.
- Kornberg, R.D., 2005. Mediator and the mechanism of transcriptional activation. *Trends in Biochemical Sciences*, 30 (5), 235–239.
- Koschmann, C., Calinescu, A.-A., Nunez, F.J., Mackay, A., Fazal-Salom, J., Thomas, D., Mendez, F., Kamran, N., Dzaman, M., Mulpuri, L., Krasinkiewicz, J., Doherty, R., Lemons, R., Brosnan-Cashman, J.A., Li, Y., Roh, S., Zhao, L., Appelman, H., Ferguson, D., Gorbunova, V., Meeker, A., Jones, C., Lowenstein, P.R., and Castro, M.G., 2016. ATRX loss promotes tumor growth and impairs nonhomologous end joining DNA repair in glioma. *Science Translational Medicine*, 8 (328), 328ra28.
- Lee, T.I., Jenner, R.G., Boyer, L.A., Guenther, M.G., Levine, S.S., Kumar, R.M., Chevalier, B., Johnstone, S.E., Cole, M.F., Isono, K., Koseki, H., Fuchikami, T., Abe, K., Murray, H.L., Zucker, J.P., Yuan, B., Bell, G.W., Herbolzheimer, E.,

- Hannett, N.M., Sun, K., Odom, D.T., Otte, A.P., Volkert, T.L., Bartel, D.P., Melton, D.A., Gifford, D.K., Jaenisch, R., and Young, R.A., 2006. Control of developmental regulators by Polycomb in human embryonic stem cells. *Cell*, 125 (2), 301–313.
- Lepack, A.E., Bagot, R.C., Peña, C.J., Loh, Y.-H.E., Farrelly, L.A., Lu, Y., Powell, S.K., Lorsch, Z.S., Issler, O., Cates, H.M., Tamminga, C.A., Molina, H., Shen, L., Nestler, E.J., Allis, C.D., and Maze, I., 2016. Aberrant H3.3 dynamics in NAc promote vulnerability to depressive-like behavior. *Proceedings of the National Academy of Sciences*, 113 (44), 12562–12567.
- Lewis, P.W., Elsaesser, S.J., Noh, K.-M., Stadler, S.C., and Allis, C.D., 2010. Daxx is an H3.3-specific histone chaperone and cooperates with ATRX in replication-independent chromatin assembly at telomeres. *Proceedings Of The National Academy Of Sciences (Of The United States Of America)*, 107 (32), 14075–14080.
- Lewis, P.W., Müller, M.M., Koletsky, M.S., Cordero, F., Lin, S., Banaszynski, L.A., Garcia, B.A., Muir, T.W., Becher, O.J., and Allis, C.D., 2013. Inhibition of PRC2 Activity by a Gain-of-Function H3 Mutation Found in Pediatric Glioblastoma, 340 (May), 857–861.
- Li, E., Bestor, T.H., and Jaenisch, R., 1992. Targeted mutation of the DNA methyltransferase gene results in embryonic lethality. *Cell*, 69 (6), 915–926.
- Li, H., Cai, Q., Wu, H., Vathipadiekal, V., Dobbin, Z.C., Li, T., Hua, X., Landen, C.N., Birrer, M.J., Sánchez-Beato, M., and Zhang, R., 2012. SUZ12 promotes human epithelial ovarian cancer by suppressing apoptosis via silencing HRK. *Molecular cancer research : MCR*, 10 (11), 1462–1472.
- Li, H., Leo, C., Zhu, J., Wu, X., O’Neil, J., Park, E.J., and Chen, J.D., 2000. Sequestration and inhibition of Daxx-mediated transcriptional repression by PML. *Molecular and cellular biology*, 20 (5), 1784–1796.
- Lin, S.-J., Ho, H.-C., Lee, Y.-F., Liu, N.-C., Liu, S., Li, G., Shyr, C.-R., and Chang, C., 2012. Reduced osteoblast activity in the mice lacking TR4 nuclear receptor leads to osteoporosis. *Reproductive biology and endocrinology : RB&E*, 10 (43).
- Lin, S.-J., Lee, S.O., Lee, Y.-F., Miyamoto, H., Yang, D.-R., Li, G., and Chang, C., 2014. TR4 nuclear receptor functions as a tumor suppressor for prostate

- tumorigenesis via modulation of DNA damage/repair system. *Carcinogenesis*, 35 (6), 1399–1406.
- Lindroth, A.M. and Plass, C., 2013. Recurrent H3.3 alterations in childhood tumors. *Nature Genetics*, 45 (12), 1413–1414.
- Liu, X., McEachron, T. a, Schwartzentruber, J., and Wu, G., 2014. Histone H3 mutations in pediatric brain tumors. *Cold Spring Harbor perspectives in biology*, 6 (4), a018689.
- Los, G. V., Encell, L.P., McDougall, M.G., Hartzell, D.D., Karassina, N., Zimprich, C., Wood, M.G., Learish, R., Ohana, R.F., Urh, M., Simpson, D., Mendez, J., Zimmerman, K., Otto, P., Vidugiris, G., Zhu, J., Darzins, A., Klaubert, D.H., Bulleit, R.F., and Wood, K. V., 2008. HaloTag: A Novel Protein Labeling Technology for Cell Imaging and Protein Analysis. *ACS Chemical Biology*, 3 (6), 373–382.
- Lu, X., Wontakal, S.N., Emelyanov, A. V, Morcillo, P., Konev, A.Y., Fyodorov, D. V, and Skoultchi, A.I., 2009. Linker histone H1 is essential for Drosophila development, the establishment of pericentric heterochromatin, and a normal polytene chromosome structure. *Genes & development*, 23 (4), 452–465.
- Luger, K., Mäder, A.W., Richmond, R.K., Sargent, D.F., and Richmond, T.J., 1997. Crystal structure of the nucleosome core particle at 2.8 Å resolution. *Nature*, 389 (6648), 251–260.
- Luger, K., Suto, R.K., Clarkson, M.J., and Tremethick, D.J., 2000. Crystal structure of a nucleosome core particle containing the variant histone H2A.Z. *Nature Structural Biology*, 7 (12), 1121–1124.
- MacAlpine, D.M. and Almouzni, G., 2013. Chromatin and DNA replication. *Cold Spring Harbor perspectives in biology*, 5 (8), a010207.
- Mansfield, R.E., Musselman, C. a, Kwan, A.H., Oliver, S.S., Garske, A.L., Davrazou, F., Denu, J.M., Kutateladze, T.G., and Mackay, J.P., 2011. Plant homeodomain (PHD) fingers of CHD4 are histone H3-binding modules with preference for unmodified H3K4 and methylated H3K9. *The Journal of Biological Chemistry*, 286 (13), 11779–11791.
- Margueron, R. and Reinberg, D., 2011. The Polycomb complex PRC2 and its mark in life. *Nature*, 469 (7330), 343–349.

- Maze, I., Wenderski, W., Noh, K.-M., Bagot, R.C., Tzavaras, N., Purushothaman, I., Elsässer, S.J., Guo, Y., Ionete, C., Hurd, Y.L., Tamminga, C.A., Halene, T., Farrelly, L., Soshnev, A.A., Wen, D., Rafii, S., Birtwistle, M.R., Akbarian, S., Buchholz, B.A., Blitzler, R.D., Nestler, E.J., Yuan, Z.-F., Garcia, B.A., Shen, L., Molina, H., and Allis, C.D., 2015. Critical Role of Histone Turnover in Neuronal Transcription and Plasticity. *Neuron*, 87 (1), 77–94.
- McKenzie Duncan, I., 1982. Polycomblike: A gene that appears to be required for the normal expression of the bithorax and antennapedia gene complexes of *Drosophila melanogaster*. *Genetics*, 102 (1), 49–70.
- Mei, Q., Huang, J., Chen, W., Tang, J., Xu, C., Yu, Q., Cheng, Y., Ma, L., Yu, X., and Li, S., 2017. Regulation of DNA replication-coupled histone gene expression. *Oncotarget*, 8 (55), 95005–95022.
- Meneghini, M.D., Wu, M., and Madhani, H.D., 2003. Conserved Histone Variant H2A.Z Protects Euchromatin from the Ectopic Spread of Silent Heterochromatin. *Cell*, 112 (5), 725–736.
- Menon, S., Oh, W., Carr, H.S., and Frost, J.A., 2013. Rho GTPase-independent regulation of mitotic progression by the RhoGEF Net1. *Molecular biology of the cell*, 24 (17), 2655–2667.
- Michaelson, J.S., Bader, D., Kuo, F., Kozak, C., and Leder, P., 1999. Loss of Daxx, a promiscuously interacting protein, results in extensive apoptosis in early mouse development. *Genes & development*, 13 (15), 1918–1923.
- Michod, D., Bartesaghi, S., Khelifi, A., Bellodi, C., Berliocchi, L., Nicotera, P., and Salomoni, P., 2012. Calcium-Dependent Dephosphorylation of the Histone Chaperone DAXX Regulates H3.3 Loading and Transcription upon Neuronal Activation. *Neuron*, 74 (1), 122–135.
- Minsky, N., Shema, E., Field, Y., Schuster, M., Segal, E., and Oren, M., 2008. Monoubiquitinated H2B is associated with the transcribed region of highly expressed genes in human cells. *Nature Cell Biology*, 10 (4), 483–488.
- Misra, A., Ou, J., Zhu, L.J., and Green, M.R., 2015. Global Promotion of Alternative Internal Exon Usage by mRNA 3' End Formation Factors. *Molecular Cell*, 58 (5), 819–831.
- Mito, Y., Henikoff, J.G., and Henikoff, S., 2007. Histone Replacement Marks the Boundaries of cis-Regulatory Domains. *Science*, 315 (5817), 1408–1411.

- Müller, J., Hart, C.M., Francis, N.J., Vargas, M.L., Sengupta, A., Wild, B., Miller, E.L., O'Connor, M.B., Kingston, R.E., and Simon, J.A., 2002. Histone methyltransferase activity of a Drosophila Polycomb group repressor complex. *Cell*, 111 (2), 197–208.
- Muromoto, R., Sugiyama, K., Takachi, A., Imoto, S., Sato, N., Yamamoto, T., Oritani, K., Shimoda, K., and Matsuda, T., 2004. Physical and Functional Interactions between Daxx and DNA Methyltransferase 1-Associated Protein, DMAP1. *The Journal of Immunology*, 172 (5), 2985–2993.
- Nakanishi, S., Lee, J.S., Gardner, K.E., Gardner, J.M., Takahashi, Y., Chandrasekharan, M.B., Sun, Z.-W., Osley, M.A., Strahl, B.D., Jaspersen, S.L., and Shilatifard, A., 2009. Histone H2BK123 monoubiquitination is the critical determinant for H3K4 and H3K79 trimethylation by COMPASS and Dot1. *The Journal of Cell Biology*, 186 (3), 371–377.
- Newhart, A., Rafalska-Metcalf, I.U., Yang, T., Joo, L.M., Powers, S.L., Kossenkov, A. V, Lopez-Jones, M., Singer, R.H., Showe, L.C., Skordalakes, E., and Janicki, S.M., 2013. Single cell analysis of RNA-mediated histone H3.3 recruitment to a cytomegalovirus promoter-regulated transcription site. *The Journal of biological chemistry*, 288 (27), 19882–19899.
- Nilubol, N., Boufraquech, M., Zhang, L., and Kebebew, E., 2014. Loss of CPSF2 expression is associated with increased thyroid cancer cellular invasion and cancer stem cell population, and more aggressive disease. *The Journal of clinical endocrinology and metabolism*, 99 (7), E1173-1182.
- Novikov, L., Park, J.W., Chen, H., Klerman, H., Jalloh, A.S., and Gamble, M.J., 2011. QKI-mediated alternative splicing of the histone variant MacroH2A1 regulates cancer cell proliferation. *Molecular and cellular biology*, 31 (20), 4244–4255.
- Olave, I., Wang, W., Xue, Y., Kuo, A., and Crabtree, G.R., 2002. Identification of a polymorphic, neuron-specific chromatin remodeling complex. *Genes & development*, 16 (19), 2509–2517.
- Pan, W.-W., Zhou, J.-J., Liu, X.-M., Xu, Y., Guo, L.-J., Yu, C., Shi, Q.-H., and Fan, H.-Y., 2013. Death domain-associated protein DAXX promotes ovarian cancer development and chemoresistance. *The Journal of biological chemistry*, 288 (19), 13620–13630.

- Pathania, M., De Jay, N., Maestro, N., Harutyunyan, A.S., Nitarska, J., Pahlavan, P., Henderson, S., Mikael, L.G., Richard-Londt, A., Zhang, Y., Costa, J.R., Hébert, S., Khazaei, S., Ibrahim, N.S., Herrero, J., Riccio, A., Albrecht, S., Ketteler, R., Brandner, S., Kleinman, C.L., Jabado, N., and Salomoni, P., 2017. H3.3K27M Cooperates with Trp53 Loss and PDGFRA Gain in Mouse Embryonic Neural Progenitor Cells to Induce Invasive High-Grade Gliomas. *Cancer cell*, 32 (5), 684–700.e9.
- Pchelintsev, N., McBryan, T., Rai, T., VanTuyn, J., Ray-Gallet, D., Almouzni, G., and Adams, P., 2013. Placing the HIRA Histone Chaperone Complex in the Chromatin Landscape. *Cell Reports*, 3 (4), 1012–1019.
- Pehrson, J.R. and Fried, V.A., 1992. MacroH2A, a core histone containing a large nonhistone region. *Science*, 257 (5075), 1398–1400.
- Piazzesi, A., Papić, D., Bertan, F., Salomoni, P., Nicotera, P., and Bano, D., 2016. Replication-Independent Histone Variant H3.3 Controls Animal Lifespan through the Regulation of Pro-longevity Transcriptional Programs. *Cell Reports*, 17 (4), 987–996.
- Pluta, A.F., Earnshaw, W.C., and Goldberg, I.G., 1998. Interphase-specific association of intrinsic centromere protein CENP-C with HDaxx, a death domain-binding protein implicated in Fas-mediated cell death. *Journal of Cell Science*, 111 (Pt 14), 2029–2041.
- Polo, S.E., Roche, D., and Almouzni, G., 2006. New Histone Incorporation Marks Sites of UV Repair in Human Cells. *Cell*, 127 (3), 481–493.
- Qiu, Z. and Ghosh, A., 2008. A Calcium-Dependent Switch in a CREST-BRG1 Complex Regulates Activity-Dependent Gene Expression. *Neuron*, 60 (5), 775–787.
- Quivy, J.-P., Grandi, P., and Almouzni, G., 2001. Dimerization of the largest subunit of chromatin assembly factor 1: importance in vitro and during Xenopus early development. *The EMBO Journal*, 20 (8), 2015–2027.
- Rai, T.S., Puri, A., McBryan, T., Hoffman, J., Tang, Y., Pchelintsev, N.A., van Tuyn, J., Marmorstein, R., Schultz, D.C., and Adams, P.D., 2011. Human CABIN1 Is a Functional Member of the Human HIRA/UBN1/ASF1a Histone H3.3 Chaperone Complex. *Mol. Cell. Biol.*, 31 (19), 4107–4118.
- Raisner, R.M. and Madhani, H.D., 2006. Patterning chromatin: form and function for

- H2A.Z variant nucleosomes. *Current Opinion in Genetics & Development*, 16 (2), 119–124.
- Ray-Gallet, D. and Almouzni, G., 2010. Nucleosome dynamics and histone variants. *Essays in biochemistry*, 48 (1), 75–87.
- Ray-Gallet, D., Woolfe, A., Vassias, I., Pellentz, C., Lacoste, N., Puri, A., Schultz, D.C., Pchelintsev, N.A., Adams, P.D., Jansen, L.E.T., and Almouzni, G., 2011. Dynamics of histone H3 deposition in vivo reveal a nucleosome gap-filling mechanism for H3.3 to maintain chromatin integrity. *Molecular cell*, 44 (6), 928–941.
- Regad, T., Bellodi, C., Nicotera, P., and Salomoni, P., 2009. The tumor suppressor Pml regulates cell fate in the developing neocortex. *Nature Neuroscience*, 12 (2), 132–140.
- Reisman, D.N., Sciarrotta, J., Wang, W., Funkhouser, W.K., and Weissman, B.E., 2003. Loss of BRG1/BRM in Human Lung Cancer Cell Lines and Primary Lung Cancers: Correlation with Poor Prognosis. *Cancer Research*, 63 (919), 560–566.
- Riboni, L., Prinetti, A., Bassi, R., Caminiti, A., and Tettamanti, G., 1995. A mediator role of ceramide in the regulation of neuroblastoma Neuro2a cell differentiation. *The Journal of biological chemistry*, 270 (45), 26868–26875.
- Ricketts, M.D., Frederick, B., Hoff, H., Tang, Y., Schultz, D.C., Singh Rai, T., Grazia Vizioli, M., Adams, P.D., and Marmorstein, R., 2015. Ubinuclein-1 confers histone H3.3-specific-binding by the HIRA histone chaperone complex. *Nature Communications*, 6 (1), 7711.
- Ringrose, L. and Paro, R., 2004. Epigenetic Regulation of Cellular Memory by the Polycomb and Trithorax Group Proteins. *Annual Review of Genetics*, 38 (1), 413–443.
- Rountree, M.R., Bachman, K.E., and Baylin, S.B., 2000. DNMT1 binds HDAC2 and a new co-repressor, DMAP1, to form a complex at replication foci. *Nature genetics*, 25 (3), 269–277.
- Sagawa, F., Ibrahim, H., Morrison, A.L., Wilusz, C.J., and Wilusz, J., 2011. Nucleophosmin deposition during mRNA 3' end processing influences poly(A) tail length. *The EMBO journal*, 30 (19), 3994–4005.

- Sakurai, M., Ueda, H., Yano, T., Okada, S., Terajima, H., Mitsuyama, T., Toyoda, A., Fujiyama, A., Kawabata, H., and Suzuki, T., 2014. A biochemical landscape of A-to-I RNA editing in the human brain transcriptome. *Genome research*, 24 (3), 522–534.
- Saratsis, A.M., Kambhampati, M., Snyder, K., Yadavilli, S., Devaney, J.M., Harmon, B., Hall, J., Raabe, E.H., An, P., Weingart, M., Rood, B.R., Magge, S.N., MacDonald, T.J., Packer, R.J., and Nazarian, J., 2014. Comparative multidimensional molecular analyses of pediatric diffuse intrinsic pontine glioma reveals distinct molecular subtypes. *Acta neuropathologica*, 127 (6), 881–895.
- Sarma, K., Cifuentes-Rojas, C., Ergun, A., Rosario, A. del, Jeon, Y., White, F., Sadreyev, R., and Lee, J.T., 2014. ATRX Directs Binding of PRC2 to Xist RNA and Polycomb Targets. *Cell*, 159 (4), 869–883.
- Schenk, R., Jenke, A., Zilbauer, M., Wirth, S., and Postberg, J., 2011. H3.5 is a novel hominid-specific histone H3 variant that is specifically expressed in the seminiferous tubules of human testes. *Chromosoma*, 120 (3), 275–285.
- Schmidt, A., 2002. The Rho Exchange Factor Net1 Is Regulated by Nuclear Sequestration. *Journal of Biological Chemistry*, 277 (17), 14581–14588.
- Schonemann, L., Kuhn, U., Martin, G., Schafer, P., Gruber, A.R., Keller, W., Zavolan, M., and Wahle, E., 2014. Reconstitution of CPSF active in polyadenylation: recognition of the polyadenylation signal by WDR33. *Genes Dev*, 28 (21), 2381–2393.
- Schwartz, Y.B., Kahn, T.G., Nix, D.A., Li, X.-Y., Bourgon, R., Biggin, M., and Pirrotta, V., 2006. Genome-wide analysis of Polycomb targets in *Drosophila melanogaster*. *Nature Genetics*, 38 (6), 700–705.
- Schwartzentruber, J., Korshunov, A., Liu, X.-Y., Jones, D.T.W., Pfaff, E., Jacob, K., Sturm, D., Fontebasso, A.M., Quang, D.-A.K., Tönjes, M., Hovestadt, V., Albrecht, S., Kool, M., Nantel, A., Konermann, C., Lindroth, A., Jäger, N., Rausch, T., Ryzhova, M., Korbel, J.O., Hielscher, T., Hauser, P., Garami, M., Klekner, A., Bogner, L., Ebinger, M., Schuhmann, M.U., Scheurle, W., Pekrun, A., Frühwald, M.C., Roggendorf, W., Kramm, C., Dürken, M., Atkinson, J., Lepage, P., Montpetit, A., Zakrzewska, M., Zakrzewski, K., Liberski, P.P., Dong, Z., Siegel, P., Kulozik, A.E., Zapatka, M., Guha, A., Malkin, D., Felsberg, J., Reifenberger, G., von Deimling, A., Ichimura, K., Collins, V.P., Witt, H.,

- Milde, T., Witt, O., Zhang, C., Castelo-Branco, P., Lichter, P., Faury, D., Tabori, U., Plass, C., Majewski, J., Pfister, S.M., and Jabado, N., 2012. Driver mutations in histone H3.3 and chromatin remodelling genes in paediatric glioblastoma. *Nature*, 482 (7384), 226–231.
- Shi, L., Wang, J., Hong, F., Spector, D.L., and Fang, Y., 2011. Four amino acids guide the assembly or disassembly of Arabidopsis histone H3.3-containing nucleosomes. *Proceedings of the National Academy of Sciences of the United States of America*, 108 (26), 10574–10578.
- Shi, Y., Di Giammartino, D.C., Taylor, D., Sarkeshik, A., Rice, W.J., Yates, J.R., Frank, J., and Manley, J.L., 2009. Molecular Architecture of the Human Pre-mRNA 3' Processing Complex. *Molecular Cell*, 33 (3), 365–376.
- Sporn, J.C., Kustatscher, G., Hothorn, T., Collado, M., Serrano, M., Muley, T., Schnabel, P., and Ladurner, A.G., 2009. Histone macroH2A isoforms predict the risk of lung cancer recurrence. *Oncogene*, 28 (38), 3423–3428.
- Srougi, M.C. and Burrige, K., 2011. The nuclear guanine nucleotide exchange factors Ect2 and Net1 regulate RhoB-mediated cell death after DNA damage. *PloS one*, 6 (2), e17108.
- St Laurent, G., Tackett, M.R., Nechkin, S., Shtokalo, D., Antonets, D., Savva, Y. a, Maloney, R., Kapranov, P., Lawrence, C.E., and Reenan, R. a, 2013. Genome-wide analysis of A-to-I RNA editing by single-molecule sequencing in *Drosophila*. *Nature structural & molecular biology*, 20 (11), 1333–1339.
- Stahl, B.T. and Crabtree, G.R., 2013. Creating a neural specific chromatin landscape by npBAF and nBAF complexes. *Curr Opin Neurobiol.*, 23 (6), 903–913.
- Stargell, L.A., Bowen, J., Dadd, C.A., Dedon, P.C., Davis, M., Cook, R.G., Allis, C.D., and Gorovsky, M.A., 1993. Temporal and spatial association of histone H2A variant hv1 with transcriptionally competent chromatin during nuclear development in *Tetrahymena thermophila*. *Genes & development*, 7 (12B), 2641–2651.
- Sturm, D., Witt, H., Hovestadt, V., Khuong-Quang, D.-A., Jones, D.T.W., Konermann, C., Pfaff, E., Tönjes, M., Sill, M., Bender, S., Kool, M., Zapatka, M., Becker, N., Zucknick, M., Hielscher, T., Liu, X.-Y., Fontebasso, A.M., Ryzhova, M., Albrecht, S., Jacob, K., Wolter, M., Ebinger, M., Schuhmann,

M.U., van Meter, T., Frühwald, M.C., Hauch, H., Pekrun, A., Radlwimmer, B., Niehues, T., von Komorowski, G., Dürken, M., Kulozik, A.E., Madden, J., Donson, A., Foreman, N.K., Drissi, R., Fouladi, M., Scheurlen, W., von Deimling, A., Monoranu, C., Roggendorf, W., Herold-Mende, C., Unterberg, A., Kramm, C.M., Felsberg, J., Hartmann, C., Wiestler, B., Wick, W., Milde, T., Witt, O., Lindroth, A.M., Schwartzentruber, J., Faury, D., Fleming, A., Zakrzewska, M., Liberski, P.P., Zakrzewski, K., Hauser, P., Garami, M., Klekner, A., Bogнар, L., Morrissy, S., Cavalli, F., Taylor, M.D., van Sluis, P., Koster, J., Versteeg, R., Volckmann, R., Mikkelsen, T., Aldape, K., Reifenberger, G., Collins, V.P., Majewski, J., Korshunov, A., Lichter, P., Plass, C., Jabado, N., and Pfister, S.M., 2012. Hotspot Mutations in H3F3A and IDH1 Define Distinct Epigenetic and Biological Subgroups of Glioblastoma. *Cancer Cell*, 22 (4), 425–437.

Sudarsanam, P., Iyer, V.R., Brown, P.O., and Winston, F., 2000. Whole-genome expression analysis of *snf/swi* mutants of *Saccharomyces cerevisiae*. *Proceedings of the National Academy of Sciences of the United States of America*, 97 (7), 3364–3369.

Szenker, E., Lacoste, N., and Almouzni, G., 2012. A Developmental Requirement for HIRA-Dependent H3.3 Deposition Revealed at Gastrulation in Xenopus. *Cell Reports*, 1 (6), 730–740.

Szenker, E., Ray-Gallet, D., and Almouzni, G., 2011. The double face of the histone variant H3.3. *Cell Research*, 21 (3), 421–434.

Tachiwana, H., Kagawa, W., Osakabe, A., Kawaguchi, K., Shiga, T., Hayashi-Takanaka, Y., Kimura, H., and Kurumizaka, H., 2010. Structural basis of instability of the nucleosome containing a testis-specific histone variant, human H3T. *Proceedings of the National Academy of Sciences*, 107 (23), 10454–10459.

Tagami, H., Ray-Gallet, D., Almouzni, G., and Nakatani, Y., 2004. Histone H3.1 and H3.3 complexes mediate nucleosome assembly pathways dependent or independent of DNA synthesis. *Cell*, 116 (1), 51–61.

Talasz, H., Sarg, B., and Lindner, H.H., 2009. Site-specifically phosphorylated forms of H1.5 and H1.2 localized at distinct regions of the nucleus are related to different processes during the cell cycle. *Chromosoma*, 118 (6), 693–709.

Tamura, T., Smith, M., Kanno, T., Dasenbrock, H., Nishiyama, A., and Ozato, K.,

2009. Inducible Deposition of the Histone Variant H3.3 in Interferon-stimulated Genes. *Journal of Biological Chemistry*, 284 (18), 12217–12225.
- Tang, J., Wu, S., Liu, H., Stratt, R., Barak, O.G., Shiekhattar, R., Picketts, D.J., and Yang, X., 2004. A Novel Transcription Regulatory Complex Containing Death Domain-associated Protein and the ATR-X Syndrome Protein. *Journal of Biological Chemistry*, 279 (19), 20369–20377.
- Tang, M.C.W., Jacobs, S.A., Mattiske, D.M., Soh, Y.M., Graham, A.N., Tran, A., Lim, S.L., Hudson, D.F., Kalitsis, P., O'Bryan, M.K., Wong, L.H., and Mann, J.R., 2015. Contribution of the Two Genes Encoding Histone Variant H3.3 to Viability and Fertility in Mice. *PLOS Genetics*, 11 (2), e1004964.
- Tatton-Brown, K., Hanks, S., Ruark, E., Zachariou, A., Duarte, S.D.V., Ramsay, E., Snape, K., Murray, A., Perdeaux, E.R., Seal, S., Loveday, C., Banka, S., Clericuzio, C., Flinter, F., Magee, A., McConnell, V., Patton, M., Raith, W., Rankin, J., Splitt, M., Strenger, V., Taylor, C., Wheeler, P., Temple, K.I., Cole, T., Childhood Overgrowth Collaboration, T.C.O., Douglas, J., and Rahman, N., 2011. Germline mutations in the oncogene EZH2 cause Weaver syndrome and increased human height. *Oncotarget*, 2 (12), 1127–33.
- Taylor, G.C.A., Eskeland, R., Hekimoglu-Balkan, B., Pradeepa, M.M., and Bickmore, W.A., 2013. H4K16 acetylation marks active genes and enhancers of embryonic stem cells, but does not alter chromatin compaction. *Genome research*, 23 (12), 2053–2065.
- Tvardovskiy, A., Schwämmle, V., Kempf, S.J., Rogowska-Wrzesinska, A., and Jensen, O.N., 2017. Accumulation of histone variant H3.3 with age is associated with profound changes in the histone methylation landscape. *Nucleic acids research*, 45 (16), 9272–9289.
- Valdés-Mora, F., Gould, C.M., Colino-Sanguino, Y., Qu, W., Song, J.Z., Taylor, K.M., Buske, F.A., Statham, A.L., Nair, S.S., Armstrong, N.J., Kench, J.G., Lee, K.M.L., Horvath, L.G., Qiu, M., Ilinykh, A., Yeo-Teh, N.S., Gallego-Ortega, D., Stirzaker, C., and Clark, S.J., 2017. Acetylated histone variant H2A.Z is involved in the activation of neo-enhancers in prostate cancer. *Nature Communications*, 8 (1), 1346.
- Venkatesh, S. and Workman, J.L., 2015. Histone exchange, chromatin structure and the regulation of transcription. *Nature Reviews. Molecular Cell Biology*, 16 (3), 178–189.

- Venneti, S., Garimella, M.T., Sullivan, L.M., Martinez, D., Huse, J.T., Heguy, A., Santi, M., Thompson, C.B., and Judkins, A.R., 2013. Evaluation of Histone 3 Lysine 27 Trimethylation (H3K27me3) and Enhancer of Zest 2 (EZH2) in Pediatric Glial and Glioneuronal Tumors Shows Decreased H3K27me3 in H3F3A K27M Mutant Glioblastomas. *Brain Pathology*, 23 (5), 558–564.
- Vujatovic, O., Zaragoza, K., Vaquero, A., Reina, O., Bernués, J., and Azorín, F., 2012. Drosophila melanogaster linker histone dH1 is required for transposon silencing and to preserve genome integrity. *Nucleic acids research*, 40 (12), 5402–5414.
- Wenderski, W. and Maze, I., 2016. Histone turnover and chromatin accessibility: Critical mediators of neurological development, plasticity, and disease. *BioEssays : news and reviews in molecular, cellular and developmental biology*, 38 (5), 410–419.
- Widom, J., 1998. Chromatin structure: Linking structure to function with histone H1. *Current Biology*, 8 (22), R788-791.
- Wu, G., Broniscer, A., McEachron, T. a, Lu, C., Paugh, B.S., Becksfors, J., Qu, C., Ding, L., Huether, R., Parker, M., Zhang, J., Gajjar, A., Dyer, M. a, Mullighan, C.G., Gilbertson, R.J., Mardis, E.R., Wilson, R.K., Downing, J.R., Ellison, D.W., Zhang, J., and Baker, S.J., 2012. Somatic histone H3 alterations in pediatric diffuse intrinsic pontine gliomas and non-brainstem glioblastomas. *Nature Genetics*, 44 (3), 251–253.
- Wu, H. and Sun, Y.E., 2006. Epigenetic Regulation of Stem Cell Differentiation. *Pediatric Research*, 59 (S4), 21R–25R.
- Yamaguchi, H. and Hung, M.C., 2014. Regulation and role of EZH2 in cancer. *Cancer Research and Treatment*, 46 (3), 209–222.
- Yanaka, N., Nogusa, Y., Fujioka, Y., Yamashita, Y., and Kato, N., 2007. Involvement of membrane protein GDE2 in retinoic acid-induced neurite formation in Neuro2A cells. *FEBS Letters*, 581 (4), 712–718.
- Youn, H.D., Sun, L., Prywes, R., and Liu, J.O., 1999. Apoptosis of T cells mediated by Ca<sup>2+</sup>-induced release of the transcription factor MEF2. *Science (New York, N.Y.)*, 286 (5440), 790–793.
- Young, W.J., Smith, S.M., and Chang, C., 1997. Induction of the intronic enhancer of the human ciliary neurotrophic factor receptor (CNTFRalpha) gene by the

- TR4 orphan receptor. A member of steroid receptor superfamily. *J Biol Chem*, 272 (5), 3109–3116.
- Yuen, Benjamin T. K., P.S.K., 2013. Histone H3.3 mutations: a variant path to cancer. *Cancer Cell*, 24 (5), 567–574.
- Zahnow, C. a. and Baylin, S.B., 2010. Epigenetic Networks and miRNAs in Stem Cells and Cancer. *Molecular Cell*, 39 (5), 661–663.
- Zheng, Y., John, S., Pesavento, J.J., Schultz-Norton, J.R., Schiltz, R.L., Baek, S., Nardulli, A.M., Hager, G.L., Kelleher, N.L., and Mizzen, C.A., 2010. Histone H1 phosphorylation is associated with transcription by RNA polymerases I and II. *THE JOURNAL OF CELL BIOLOGY*, 189 (3), 407–415.
- Zhong, S., Salomoni, P., Ronchetti, S., Guo, A., Ruggero, D., and Pandolfi, P.P., 2000. Promyelocytic leukemia protein (PML) and Daxx participate in a novel nuclear pathway for apoptosis. *The Journal of experimental medicine*, 191 (4), 631–640.
- Zhou, Z., Gao, J., Popovic, R., Wolniak, K., Parimi, V., Winter, J.N., Licht, J.D., and Chen, Y.-H., 2015. Strong expression of EZH2 and accumulation of trimethylated H3K27 in diffuse large B-cell lymphoma independent of cell of origin and EZH2 codon 641 mutation. *Leukemia & Lymphoma*, 56 (10), 2895–2901.
- Zou, L., Elledge, S.J., Jeitany, M., Wakimoto, H., Bryll, A.R., Ganem, N.J., Bersani, F., Pineda, J.R., Suvà, M.L., Benes, C.H., Haber, D.A., Boussin, F.D., and Zou, L., 2003. Sensing DNA damage through ATRIP recognition of RPA-ssDNA complexes. *Science (New York, N.Y.)*, 300 (5625), 1542–8.

## Appendix I: Identified proteins from MS with PSM ratio $\geq 4.0$

Identified proteins	PSM Ratio
Death domain-associated protein 6 [DAXX_MOUSE]	57.01
Netrin-1 [NET1_MOUSE]	42.72
Nuclear receptor subfamily 2 group C member 2 [NR2C2_MOUSE]	40.94
Cleavage and polyadenylation specificity factor subunit 2 [CPSF2_MOUSE]	32.76
Alpha-amylase 1 [AMY1_MOUSE]	30.72
Pre-mRNA-splicing factor CWC22 homolog [CWC22_MOUSE]	24.46
Putative ATP-dependent RNA helicase DHX57 [DHX57_MOUSE]	23.65
Putative ATP-dependent RNA helicase DHX30 [DHX30_MOUSE]	20.69
Perilipin-2 [PLIN2_MOUSE]	20.36
Nuclear-interacting partner of ALK [NIPA_MOUSE]	20.26
Signal-induced proliferation-associated 1-like protein 1 [SI1L1_MOUSE]	19.38
Integrator complex subunit 1 [INT1_MOUSE]	19.30
GA-binding protein alpha chain [GABPA_MOUSE]	17.31
40S ribosomal protein S24 [RS24_MOUSE]	14.91
Bifunctional coenzyme A synthase [COASY_MOUSE]	13.78
Pre-mRNA 3' end processing protein WDR33 [WDR33_MOUSE]	12.19
Histone H1.2 [H12_MOUSE]	10.33
Ribosome biogenesis regulatory protein homolog [RRS1_MOUSE]	9.83
Histone H1.5 [H15_MOUSE]	9.53
Histone H1.4 [H14_MOUSE]	9.49
Histone H1.1 [H11_MOUSE]	9.47
60S ribosomal protein L35a [RL35A_MOUSE]	8.26
60S acidic ribosomal protein P2 [RLA2_MOUSE]	7.87
60S ribosomal protein L6 [RL6_MOUSE]	7.82
Putative oxidoreductase GLYR1 [GLYR1_MOUSE]	7.59
Hemopexin [HEMO_MOUSE]	7.58
60S ribosomal protein L14 [RL14_MOUSE]	7.54
Zinc finger protein 512 [ZN512_MOUSE]	7.48
60S ribosomal protein L7 [RL7_MOUSE]	7.47

40S ribosomal protein S16 [RS16_MOUSE]	7.34
60S ribosomal protein L21 [RL21_MOUSE]	7.24
Ig gamma-1 chain C region secreted form [IGHG1_MOUSE]	7.09
60S ribosomal protein L18 [RL18_MOUSE]	7.08
60S ribosomal protein L7a [RL7A_MOUSE]	7
Histone H1.0 [H10_MOUSE]	6.84
60S ribosomal protein L8 [RL8_MOUSE]	6.77
Putative RNA-binding protein 15B [RB15B_MOUSE]	6.76
Nucleolin [NUCL_MOUSE]	6.7
Protein SOGA1 [SOGA1_MOUSE]	6.68
60S ribosomal protein L30 [RL30_MOUSE]	6.6
60S ribosomal protein L10a [RL10A_MOUSE]	6.41
60S ribosomal protein L18a [RL18A_MOUSE]	6.41
Ig kappa chain C region [IGKC_MOUSE]	6.35
60S ribosomal protein L27 [RL27_MOUSE]	6.31
Serine/arginine-rich splicing factor 1 [SRSF1_MOUSE]	6.27
60S ribosomal protein L15 [RL15_MOUSE]	6.24
IQ motif and SEC7 domain-containing protein 1 [IQEC1_MOUSE]	6.22
Ubiquitin carboxyl-terminal hydrolase 3 [UBP3_MOUSE]	6.08
Arginine and glutamate-rich protein 1 [ARGL1_MOUSE]	5.97
Ceruloplasmin [CERU_MOUSE]	5.97
Polypyrimidine tract-binding protein 3 [PTBP3_MOUSE]	5.94
DNA methyltransferase 1-associated protein 1 [DMAP1_MOUSE]	5.93
Serine/arginine-rich splicing factor 6 [SRSF6_MOUSE]	5.93
60S ribosomal protein L13a [RL13A_MOUSE]	5.73
60S ribosomal protein L3 [RL3_MOUSE]	5.64
Double-strand-break repair protein rad21 homolog [RAD21_MOUSE]	5.58
Nucleolar transcription factor 1 [UBF1_MOUSE]	5.58
60S ribosomal protein L26 [RL26_MOUSE]	5.55
60S ribosomal protein L12 [RL12_MOUSE]	5.54
60S ribosomal protein L29 [RL29_MOUSE]	5.51
60S ribosomal protein L4 [RL4_MOUSE]	5.45

60S ribosomal protein L28 [RL28_MOUSE]	5.38
60S ribosomal protein L32 [RL32_MOUSE]	5.32
KH domain-containing, RNA-binding, signal transduction-associated protein 3 [KHDR3_MOUSE]	5.26
Transthyretin [TTHY_MOUSE]	5.22
Bromodomain-containing protein 7 [BRD7_MOUSE]	5.21
Rho guanine nucleotide exchange factor 2 [ARHG2_MOUSE]	5.18
Tetraspanin-6 [TSN6_MOUSE]	5.14
40S ribosomal protein S25 [RS25_MOUSE]	5.13
CLIP-associating protein 2 [CLAP2_MOUSE]	5.1
AT-hook DNA-binding motif-containing protein 1 [AHDC1_MOUSE]	5.06
KH domain-containing, RNA-binding, signal transduction-associated protein 1 [KHDR1_MOUSE]	5.02
U2 snRNP-associated SURP motif-containing protein [SR140_MOUSE]	4.93
60S ribosomal protein L13 [RL13_MOUSE]	4.93
Transcription initiation factor TFIID subunit 9B [TAF9B_MOUSE]	4.9
60S ribosomal protein L36 [RL36_MOUSE]	4.81
40S ribosomal protein S18 [RS18_MOUSE]	4.71
Zinc finger protein 638 [ZN638_MOUSE]	4.67
Chromodomain-helicase-DNA-binding protein 2 [CHD2_MOUSE]	4.66
Golgin subfamily A member 1 [GOGA1_MOUSE]	4.66
Double-stranded RNA-specific adenosine deaminase [DSRAD_MOUSE]	4.64
RNA-binding protein 10 [RBM10_MOUSE]	4.59
60S ribosomal protein L27a [RL27A_MOUSE]	4.58
ELAV-like protein 1 [ELAV1_MOUSE]	4.54
LIM zinc-binding domain-containing Nebulette [LNEBL_MOUSE]	4.52
SWI/SNF-related matrix-associated actin-dependent regulator of chromatin subfamily A containing DEAD/H box 1 [SMRCD_MOUSE]	4.52
Apoptosis inhibitor 5 [API5_MOUSE]	4.5
Tyrosine-protein kinase BAZ1B [BAZ1B_MOUSE]	4.48
Eukaryotic translation initiation factor 4B [IF4B_MOUSE]	4.45
LIM and calponin homology domains-containing protein 1 [LIMC1_MOUSE]	4.41

RNA-binding protein 39 [RBM39_MOUSE]	4.4
Heterochromatin protein 1-binding protein 3 [HP1B3_MOUSE]	4.39
40S ribosomal protein S5 [RS5_MOUSE]	4.39
Histone deacetylase 6 [HDAC6_MOUSE]	4.38
60S ribosomal protein L37a [RL37A_MOUSE]	4.38
60S ribosomal protein L35 [RL35_MOUSE]	4.3
Paired amphipathic helix protein Sin3a [SIN3A_MOUSE]	4.29
Zinc finger protein 687 [ZN687_MOUSE]	4.29
CDKN2A-interacting protein [CARF_MOUSE]	4.28
60S ribosomal protein L34 [RL34_MOUSE]	4.2
Nuclear pore complex protein Nup88 [NUP88_MOUSE]	4.12